Universidade do Minho
Escola de Engenharia

Sara Maria Marques de Oliveira

Novel 3D scaffolds modified with nanostructured polymeric coatings or micro/nanofibers for tissue engineering applications

Outubro de 2014

Universidade do Minho
Escola de Engenharia

Sara Maria Marques de Oliveira

Novel 3D scaffolds modified with nanostructured polymeric coatings or micro/nanofibers for tissue engineering applications

Tese de Doutoramento
Doutoramento em Bioengenharia

Trabalho Efetuado sob a orientação do
Professor Doutor João Filipe Colardelle da Luz Mano
e do
Professor Doutor Rui Luís Gonçalves Reis

Outubro de 2014

STATEMENT OF INTEGRITY

I hereby declare having conducted my thesis with integrity. I confirm that I have not used plagiarism or any form of falsification of results in the process of the thesis elaboration.

I further declare that I have fully acknowledged the Code of Ethical Conduct of the University of Minho.

University of Minho, 28/10/2014

Full name: Ana Maria Marques de Oliveira

Signature: Ana Oliveira

À minha mãe, Maria

Às minhas irmãs, Susana e Inês

E à minha outra metade, Alexandre

"I know quite certainly that I have no special gift. Curiosity, obsession and dogged endurance have brought me my ideas."

Albert Einstein

Acknowledgments

Seems like only two days ago I was on my first day at 3B's Research Group. Today, I want to acknowledge all the people that somehow contributed to my personal and scientific development during this 4 year journey, and to the accomplishment of this thesis. It has been a great opportunity to push myself further.

Firstly, I want to thanks to Professor João Mano for his supervision. His contagious enthusiasm for new ideas makes him a very innovative and inspiring scientist to work with. I am truly appreciative of the opportunity I had to grow as a scientist under his tutelage.

I would also like to express my gratitude towards Professor Rui Reis, director of 3B's Research Group, for his co-supervision, scientific input and his contribution to my development and motivation. His energy and dedication were always a great inspiration.

To my co-workers, colleagues and co-authors Tiago Silva, Vitor E. Santo, Rogério Pirraco, Manuela Gomes and Alexandra Marques thank you for all your help, hard-work and guidance through the development of our works together. I learned much from you and I am greatly thankful.

Specially to Tiago, Vítor and Rogério that so many times shared with me our little victories in the lab, supporting and motivating me in all the up and downs. Thank you for everything.

Prof. Claudio Migliaresi, Prof. Antonella Motta and Dr. Devid Maniglio thank you so much for the warm welcome I received in Trento. I learned immensely from my experience there and with you.

I want to thank Paula Sol for the surreal moments we have shared "fighting" for/with our old friend B. and brainstorming about how to solve those technical issues.

Diana R., Daniel R. and Pedro B., thank you for clarifying all my little doubts about PCR.

I could not forget to thanks to the MT and IT teams that always gave me support whenever I needed. Thank you for being always available.

I would like to acknowledge to Miguel O. and Vítor C. for the support with the micro-CT. Specially to Miguel, for the enthusiasm in the work we started and which I expect we can continue exploring.

Ivo, thanks for always being available to take care of our samples.

To every one of my friends and colleagues at 3Bs, thank you for the times together, for the friendship when it was need and good times we shared together. I sincerely hope we can continue to share many moments together. Specially Mariana O., thanks for our friendship with almost a decade, it will always be treasured.

Um grande obrigada à minha mãe, irmãs e Alexandre, por todo o apoio e amor incondicional. Vocês são a minha força motriz, e a vós dedico esta tese.

Portuguese Foundation for Science and Technology is gratefully acknowledged for fellowships of S.M.O. (SFRH/BD/70107/2010).

Novel 3D scaffolds modified with nanostructured polymeric coatings or micro/nanofibers for tissue engineering applications

Abstract

Designing 3D constructs with adequate properties to instruct and guide cells is one of the major focuses of tissue engineering. The features influencing cell viability, the mechanical load bearing capability and cell instruction are distributed along the nano and macro scale of the construct. This calls on new methodologies integrating bottom-up and top-down approaches, known as integrative, for the development of controlled multiscale 3D constructs. The main goal of this thesis is to develop new multiscale and cell instructive constructs by using an integrative approach and cost-effective natural resources. Using a Bioplotter™, top-down polycaprolactone (PCL) constructs with controlled geometry were prepared. Layer-by-layer assembling (LbL) was chosen as the bottom-up methodology so that a tunable incorporation of instructive polymers/proteins could be achieved. First, this combination of techniques was explored as a way to create coatings and nano/micro fibrils on the prototyped scaffolds, adding new cell-anchorage points and a potential system to modulate cell behavior. The sequential use of rapid prototyping, LbL and freeze-drying allowed the creation of nanocoatings and/or fibrils inside the 3D scaffolds using alginate and chitosan polyelectrolytes (PEs). Those structures could be selectively added by controlling the LbL parameters. Once the concept was proven, the more adequate biochemistry that could be introduced with the LbL step was investigated. Inspired by the natural extracellular matrix (ECM), different marine-origin sulfated and aminated PEs, were selected: carrageenans (Car's) and chitosan (Chi), respectively. Thus, thin coatings with controlled sulfur and nitrogen content were prepared on polycaprolactone 2D surfaces, physicochemically characterized and their effect on osteoblast-like cells studied. Biomineralization increased with the presence of the coatings being significantly higher on ιCar/Chi. This suggested the sulfate groups interact positively with molecules involved in the osteoblastic activity. Consequently, the potential of those PEs for the incorporation of human platelet lysate (PL – source of multiple growth factors, GFs) was investigated: in 2D, on human adipose derived stem cells (hASCs) and human umbilical vein cord endothelial cells (HUVECs), in short-term cultures; and in 3D, for long-term cultures, to investigate the osteogenic differentiation of hASCs. These PEs allowed different degrees of growth factors (GFs) to be incorporated, where iota-Car showed the ability to highly incorporate all the GFs quantified. The sulfated PEs/PL coatings were shown to be efficient in promoting morphological changes, serum-free adhesion and proliferation of high passage hASCs (P>5). The more sulfated nanocoatings activated HUVECs, inducing the formation of tube-like structures and pro-angiogenic gene expressions. Moreover, the ιCar/PL/ιCar/Chi coatings and fibrillar structures, created into PCL constructs, induced the osteogenic differentiation of hASCs. In the absence of dexamethasone (osteogenic inducer), 10 tetralayers with PL induced hASCs into the osteoblastic lineage, while with 30 (or without PL) this did not occur, which emphasized the importance of a controlled PL incorporation. LbL is a suitable method to tune the incorporation of PL and tune its instruction on several cell types. Moreover, the proposed integrative and sequential approach promise new osteoinductive multiscale 3D construct, and nanocoatings for several tissue engineering applications (e.g., cell expansion and angiogenesis).

Novas estruturas porosas 3D modificadas com revestimentos ou micro/nano fibras nano-estruturadas e poliméricas para aplicações em engenharia de tecidos

Resumo

O design de estruturas 3D com propriedades adequadas para instruir e guiar células é um dos maiores focos em engenharia de tecidos. As características que influenciam a viabilidade celular, propriedades mecânicas, e instrução celular, distribuem-se ao longo da escala nano e micro dessa estrutura. Isto apela a novas metodologias, designadas integrativas, que integram abordagens bottom-up e top-down, para o desenvolvimento de estruturas 3D controladas e multi-escala. O objectivo desta tese é o desenvolvimento de novas estruturas 3D instrutivas e multi-escala, recorrendo a uma abordagem integrativa e a recursos naturais. Foram preparadas estruturas 3D top-down de policaprolactona (PCL) com geometria controlada com a Bioplotter™. A técnica de montagem camada-a-camada (CaC) foi utilizada como método bottom-up para permitir uma incorporação controlada de polímeros/proteínas instrutivas. A combinação dessas técnicas foi explorada para criar revestimentos e nano/micro fibrilas no interior do PCL 3D, de forma a adicionar novos pontos de adesão e um sistema passível de modelar o comportamento celular. O uso sequencial da Bioplotter™, CaC e liofilização permitiu a criação desses estruturas dentro do PCL 3D, com os polieletrólitos (PEs) de quitosano e alginato. Uma vez demonstrado o conceito, passou a ser investigada uma bioquímica mais adequada a ser introduzido. Inspirados pela matriz extracelular (MEC), foram usados polielectrólitos sulfatados e aminados de origem marinha: carrageninas (Cars) e quitosano (Qui). Assim, revestimentos finos, com conteúdo de enxofre e azoto controlado, foram preparados em superfícies de policaprolactona, físico-quimicamente caracterizados, e o seu efeito em osteoblastos estudado. Com esses revestimentos a biomineralização aumentou, sendo maior em ι-Car/Qui. Isto sugeriu que os grupos sulfato devem interagir positivamente com moléculas envolvidas na atividade osteoblástica. Consequentemente, o potencial desses PEs para incorporar lisados de plaquetas humanos (LP – fonte de vários factores de crescimento, FCs) foi investigado: em 2D - em células estaminais humanas do tecido adiposo (hASCs), e em células endoteliais da veia do cordão umbilical humano (HUVECs), em culturas de curto termo; e em 3D, em culturas de longo termo, para investigar a diferenciação osteogénica das hASCs. Esses PEs permitiram a incorporação de FCs a diferentes níveis, onde a ιCar mostrou a capacidade de incorporar grandes quantidades de todos os FCs quantificados. Os revestimentos de PE/LP sulfatados mostraram-se eficazes em promover alterações morfológicas, adesão celular sem soro e a proliferação de hASCs de alta passagem (P>5). Os mais sulfatados ativaram as HUVECs, induzindo a formação de estruturas celulares semelhantes a tubos e a expressão de genes pró-angiogénicos. Adicionalmente, os revestimentos e fibrilas de ιCar/LP/ιCar/Qui no PCL 3D induziram a diferenciação das hASCs. Na ausência de dexametasona, apenas 10 tetra-camadas com LP induziram a diferenciação das hASCs na linhagem osteoblástica, o que enfatiza a importância de uma incorporação de LP controlada. CaC é um método adequado para a incorporação de LP, e para controlar a sua capacidade de instruir diversas células. A abordagem sequencial e integrativa proposta promete novas estruturas 3D multi-escala e osteo-indutoras, assim como revestimentos para diversas aplicações em engenharia de tecidos (p.e., expansão celular e angiogénese).

Table of Contents

List of Abbreviations and Acronyms

#

κ, k carrageenan
ι, iota carrageenan
λ, lambda carrageenan
2D, two-dimensional
3D, three-dimensional

A

AFM, Atomic Force Microscope
AGPT-1, Angiopoietin-1
Alg, Alginate
ALP, Alkaline Phosphatase
ARS, Alizarin Red S
AT, Antibiotic/Antimycotic

B

BMP, Bone Morphogenetic Protein
BSA, Bovine Serum Albumin

C

CaP, Calcium Phosphate
Car, Carrageenan
cDNA, complementary DNA
Chi, Chitosan
CO_2, Carbon Dioxide
Col, Collagen

D

DAPI, 4,6-diamino-2-phenylindole
Dex, Dexamthasone
DMEM, Dulbecco's Modified Eagle's Medium
DMSO, Dimethyl Sulfoxide
dsDNA, double stranded DNA

E

ECGS, Endothelial Cell Growth Supplement
ECM, Extracellular Matrix
EDS, Energy Dispersive Spectroscopy
EGF, Epidermal Growth Factor
ELISA, Enzyme-Linked Immunosorbent Assay

F

FBS, Fetal Bovine Serum
FGF, Fibroblast Growth Factor
FGFR2, Fibroblast Growth Factor Receptor 2
FITC, Fluorescein Isothiocyanate

G

GAG, Glycosaminoglycan
GAPDH, Glyceraldehyde-3-phosphate dehydrogenase
GF, Growth Factor

H

Hep, Heparin
Hier, Hierarchical
hASCs, human Adipose derived Stem Cells
HCl, hydrochloric acid
HUVECs, Human Umbilical Vein Endothelial Cells

I

IGF, Insulin-like Growth Factor
IL, Interleukin

L

LbL, Layer-by-Layer

M

MEM, Minimum Essential Medium
Micro-CT, Micro-Computed Tomography
MMP, Matrix Metalloproteinase
mRNA, messenger RNA

N

NaOH, Sodium Hydroxide
NaCl, Sodium Cloride

O

OD, Optical Density
ORO, Oil Red O

P

PBS, Phosphate Buffered Saline
PCL, Polycaprolactone
PDGF, Platelet Derived Growth Factor
PEI, Poly (ethylenimine)
PE, Polyelectrolyte
PEM, Polyelectrolyte Multilayer
PF4, Platelet Factor 4

PG, Proteoglycan
PI, Propidium Iodide
PL, Platelet Lysate
pNp, p-Nitrophenol
pNpp, p-Nitrophenyl Phosphate
PPP, Platelet Poor Plasma
PPARy2, Peroxisome proliferator-activated receptor y2
PRP, Platelet Rich Plasma

Q
QCM-D, Quartz Crystal Microbalance with Dissipation

R
R_a, average roughness
R_q, Root mean square roughness
r, recombinant
RGD, Arginine-Glycine-Aspartic Acid
ROI, Region of Interest
RP, Rapid Prototyping
RT-PCR, Reverse Transcriptase Polymerase Chain Reaction
Runx2, Runt-related transcription factor 2

S
SaOs-2, human osteosarcoma osteoblast-like cells
SBF, Simulated Body Fluid
SD, Sulfation Degree
SEM, Scanning Electron Microscopy
SOST, sclerostin

T
TCPS, Tissue Culture Polystyrene
TE, Tissue Engineering
TGF, Transforming Growth Factor
TNF, Transforming Necrosis Factor
Tris,

U
UV, UltraViolet

V
VEGF, Vascular Endothelial Growth Factor
VEGFR2, Vascular Endothelial Growth Factor Receptor 2
Vn, Vitronectin
vWF, von Willebrand Factor

W
WCA, Water Contact Angle

X
XPS, X-ray Photoelectron Spectroscop

List of Figures

List of Tables

List of Publications

The work performed under the PhD work results in the publications listed below.

International Peer-Reviewed Journal

1. Sara M. Oliveira, Tiago H. Silva, Rui L. Reis, João F. Mano. *Hierarchical fibrillar scaffolds obtained by non-conventional layer-by-layer electrostatic self-assembly*. Advanced Healthcare Materials. 2013

2. Sara M. Oliveira, Tiago H. Silva, Rui L. Reis, João F. Mano. *Nanocoatings containing sulfated polysaccharides prepared by Layer-by-Layer as models to study cell-materials interactions*, Journal of Materials Chemistry B, 2013.

3. Sara M. Oliveira, Vítor E. Santo, Manuela E. Gomes, Reis R.L. and João F. Mano, *Layer-by-Layer Assembled Cell Instructive Nanocoatings containing Platelet Lysate*, submitted, 2014.

4. Sara M. Oliveira, Rogério P. Pirraco, Vítor E. Santo, Alexandra P. Marques, Manuela E. Gomes, Rui L. Reis, João F. Mano, *Pro-Angiogenic nanocoatings containing Platelet Lysate*, submitted 2014.

5. Sara M. Oliveira, Rui L. Reis, João F. Mano, *Assembling human Platelet Lysate into Multiscale 3D Scaffolds for Bone Tissue Engineering*, submitted, 2014.

6. Sara M. Oliveira, Rui L. Reis, João F. Mano, *Towards the Design of Multiscale/Instructive 3D Tissue Engineering Constructs: current approaches and trends*, submitted 2014.

Comunications In International Conferences

Oral presentations

1. Sara M. Oliveira, Rui L. Reis, João F. Mano, *Hierarchical Structuring of 3D Prototyped Scaffolds With human Platelet's Lysates and Marine-Origin Polysaccharides Induce and Improve Biomineralization of human Adipose Derived Stem Cells*, Tissue Engineering and Regenerative Medicine International Society - European Chapter (TERMIS EU), Genova (Italy), 2014.

2. Sara M. Oliveira, Rui L. Reis, João F. Mano, *Patient-Customizable Scaffolds with Nano/Microenvironments Rich in Human Platelet's Lysate and Marine-Origin Polysaccharides for Bone Formation Induction*, 26th Annual Conference of the European Society for Biomaterials (ESB), Liverpool, 2014.

Poster Communications

1. Sara M. Oliveira, Rogério P. Pirraco, Alexandra P. Marques, Rui L. Reis, João F. Mano, *Layer-by-Layer Assembled Nanocoatings of Human Platelet's Lysate and Marine-Origin Polysaccharides Trigger Pro-Angiogenic Behaviour*, Tissue Engineering and Regenerative Medicine International Society - European Chapter (TERMIS EU), Genova (Italy), 2014.

2. Sara M. Oliveira, Rogério P. Pirraco, Vítor E. Santo, Manuela E. Gomes, Alexandra P. Marques, Rui L. Reis, João F. Mano, *Regeneration: Building Up the Cell Instructive Matrix*, 4rd MIT-Portugal Program Conference: New Frontiers for a sustainable prosperity; University of Coimbra, Portugal, 2014.

3. Sara M. Oliveira, Tiago H. Silva, Rui L. Reis, João F. Mano, *Hierarchical scaffolds obtained by non-conventional layer-by-layer electrostatic self-assembly*, 3rd TERMIS World Congress, Vienna, 2012.

4. Sara M. Oliveira, Tiago H. Silva, Rui L. Reis, João F. Mano, *Novel 3D Scaffolds with Nanostructured Coatings or Micro Nanofibers for Tissue Engineering*, 3rd MIT Portugal Program Conference, University of Minho, Braga, 2012.

5. Sara M. Oliveira, Tiago H. Silva, Rui L. Reis, João F. Mano, *Novel approach to create hybrid and hierarchical scaffolds aimed for tissue regeneration*, TERM STEM, Guimarães, Portugal, 2012.

6. Sara M. Oliveira, Tiago H. Silva, Rui L. Reis, João F. Mano, *Polysaccharide-based nanostructured multilayers with distinct sulfated and aminated composition to improve cells response and biomineralization*, TERM STEM, Porto, Portugal, 2013.

7. Sara M. Oliveira, Tiago H. Silva, Rui L. Reis, João F. Mano, *Sulfonic Layer-by-Layer Nanocoatings Made Of Marine-Origin Polysaccharides As Models For Cell-GAGs-like Interactions*, TERMIS EU 2013, 2013.

Others

Patents

1. Sara M. Oliveira, Rui L. Reis, João F. Mano, *Layer-by-layer with platelet's derivatives and uses thereof*, Provisional Patent Request nº107657, Priority Date: 23 May 2014.

Structure of the Thesis

This thesis is divided into 7 sections comprising 8 chapters. The main body of chapters I, III, IV, V, VI and VII are based on the published or submitted manuscripts which have resulted from the research developed in the scope of this thesis. A general introduction and a section with the materials and methods precede those chapters. In the final section there are general conclusions and the future perspectives.

Section 1 is the state of the art regarding the main goal of the thesis. Chapter 1's purpose is to point out the major keys for the development of a 3D construct. The importance of multiscale and instructive controlled 3D constructs, their main multiscale features and the current approaches for their preparation are reviewed.
In section 2, Chapter II details the materials, methods and techniques used during the course of the work developed in this thesis. The intent is a more comprehensive and detailed description of the rationale of the developed methods.

The beginning of the research is described in Chapter III (section 3), where the concept of using an integrative and sequential approach to create fibrils and coatings inside 3D structures is outlined and proven.

In section 4 and 5, the effect of several 2D combinations of polyelectrolytes/proteins was evaluated in association with different cells types, in order to narrow-down the properties of the biochemistry to be included in the 3D structures.
In chapter IV, of section 4, the study of the effect of several sulfated multilayers (composed by chitosan and different carrageenans) on the biomineralization of osteoblast-like cells is presented.
In section 5, the same polyelectrolytes previously described were used to incorporate growth factors from platelet lysate into the multilayers. In Chapter V the effect of such nanocoatings' combinations on human adipose derived stem cells behavior is characterized. Additionally, in Chapter VI, the instructive capability of these nanocoatings was also tested with human endothelial cells.

In the Chapter VII, in section 6, a combination of polyelectrolytes and platelet lysate was chosen and transposed onto the 3D structures, using the approach defined in Chapter III. The ability of those multiscale 3D constructs to trigger the osteogenic differentiation of human adipose derived stem cells was studied.
In the final section of this thesis (Section 7), chapter VIII includes the major general conclusions and consequent future research perspectives.

SECTION 1

STATE OF THE ART

CHAPTER I

TOWARDS THE DESIGN OF 3D MULTISCALE/INSTRUCTIVE TISSUE ENGINEERING CONSTRUCTS: CURRENT APPROACHES AND TRENDS

CHAPTER I*

Towards the Design of 3D Multiscale/Instructive Tissue Engineering Constructs: current approaches and trends

I.1. Abstract

The design of 3D constructs with adequate properties to instruct and guide cells both *in vitro* and *in vivo* is one of the major focuses of tissue engineering. Successful tissue regeneration depends on the favorable crosstalk between the construct, cells and the host tissue so that a balanced matrix production and degradation is achieved. Herein, the major occurring nano/micro-environment properties and events in normal and regenerative tissue are reviewed. These have been inspiring the selection or synthesis of instructive cues to include into the 3D constructs. We further highlight the importance of a multi-scale understanding of the range of properties that can be designed on the constructs. Lastly, we overview the current and developing tissue-engineering approaches for the preparation of 3D constructs: top-down, bottom-up and integrative. The developing bottom-up and integrative approaches present a higher potential for the design of constructs with multiscale features and higher biochemistry control than top-down strategies, and are the main focus of this review.

Keywords: scaffolds, construct, multiscale, instructive, integrative, bottom-up, top-down, building-blocks, nano, biomaterials, nanobiomaterials

*This chapter is based on the following publication:

Oliveira SM, Silva TH, Reis RL, Mano JF, Towards the Design of 3D Multiscale/Instructive Tissue Engineering Constructs: current approaches and trends, submitted, 2014.

I.2. Introduction

Tissue engineering aims to restore the loss of tissue and organ's functionality resulting from injury, aging or disease.[1] Biomaterials, cells and bioactive factors, are commonly considered the key elements needed for the preparation of 3D tissue engineered constructs for the regeneration of those damaged tissues.[2, 3] Controlled 3D constructs comprising biomaterials and bioactive factors act primarily as supportive and informative platforms that guide cell behavior. Their physicochemical properties affect cell adhesion, proliferation, differentiation and matrix synthesis. Upon implantation, their properties also dictate host tissue response: inflammatory and immune response.[4] Moreover, the cellular and matrix compositions of the injured tissue will influence the cell responses in the construct. The further crosstalk between the construct and the host tissue will thus define the provisional micro/nano-environment, dictating cell behavior and consequently tissue fate: failed healing, repair or regeneration – Figure I.1.[5]

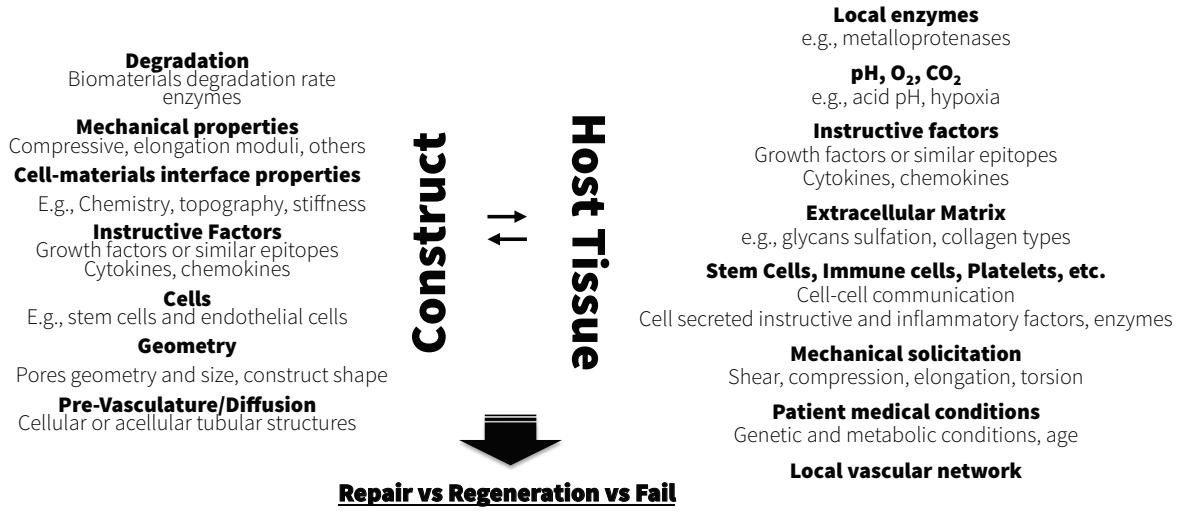

Figure I.1. Successful tissue regeneration depends on favorable crosstalk and multidirectional instructions between the construct and the host tissue implying a balanced matrix production and degradation.

This repairing/regenerative micro/nano-environment is regulated by several cell types, matrix proteins, growth factors and cytokines. Only an adequate balance between new matrix deposition and matrix degradation allows the achievement of a successfully regenerated tissue that is identical to the original one.

Tissue engineering has focused on the design of constructs to promote the regeneration of several types of tissues, e.g.: skin[6], cartilage[7], bone[8], tendon[9], and cardiac tissue[10].

The ideal construct features have been evolving with increasing understanding of cell-materials interactions both *in vitro* and *in vivo*.[3, 11] The intent of the current paradigm of the construct is to provide instructive cues for cellular activation and guidance. Besides demanding an adequate cell instruction regarding migration, proliferation and differentiation, the ideal construct also requires, e.g., nutrients and metabolites diffusion, and patient-customization. The design of constructs fulfilling a list of requirements is still very challenging. It demands the management and understanding of multiple variables that are distributed along all length-scales and affect cell behavior *in vitro* and *in vivo*. Processing techniques are still evolving and promise increasing control on the multiscale and spatial-temporal features of the constructs. Herein, we begin summarizing the

major occurring events and features in the normal and regenerative cell environment (niche) since they are the basis and latest design inspirations for instructive biomaterials. We highlight the importance of a multi-scale understanding of the range of properties that can be included on the constructs. Lastly, we overview the current and expected tissue engineering approaches for the preparation of 3D constructs: top-down, bottom-up and integrative approaches.

I.3. Stem niche and regeneration as inspirations for cell instruction

The stem cell niches are dynamic and complex structures where diverse biochemical, physical, metabolic, inflammatory, and cellular-derived cues bi-directionally and reciprocally interact with the several local cells and stem cells – Table I.1. They are responsible for modulating stem cell behavior, which is crucial for the maintenance of tissue homeostasis.[12-16] The ability of the stem cells to self-renew and differentiate is orchestrated by the spatiotemporal presentation of those cues and the dialogs occurring with several cell types. Both niches and tissues are multiscale and complex systems where smaller units interact originating larger cellular structures. The secreted factors, the physical cues, the extracellular matrix and other cells interact with the cell surface receptors at the nanoscale creating meso, micro and macro's complex structures that are hierarchically and spatially organized.[12, 17] Among the multitude of surface receptors, cells present super-families of integrins, cadherins, receptor tyrosine kinase, selectins, proteoglycans and immunoglobulins. The type, density and stability of the consequently activated/co-activated receptors trigger specific intracellular events defining cell fate at very different extents, such as: survival, motility, polarity, proliferation, cytoskeleton organization, cell-cell interactions and gene-expression.[18-27]

Table I.1. Categories of physicochemical cues in stem cells niches that affect cell behavior, and some examples of extracellular cues-cell receptor interactions.[12, 28] ICAM, intercellular Adhesion Molecule; VCAM, vascular cell adhesion molecule.

Cue Category	Ligands/Cue	Cell Receptors/Effect
Secreted Factors	Chemokine Growth factors	Chemokine receptors Tyrosine kinase receptors
Extracellular Matrix	Fibronectin	Integrins α4β1, α4β7, αVβ3, αVβ6, αIIbβ3, αvβ1, α5β1, α8β1.
	Collagen	Integrins α10β1, α2β1, α1β1, α11β1.
	Vitronectin	Integrins αvβ5, αvβ3, α8β1, αIIbβ3.
Physical	Topography Stiffness/Elasticity	Alters formation of focal adhesion points and cytoskeleton contraction
Hypoxia and metabolic	O_2, pH, Ca_{2+}, Glucose	Calcium Receptors, glucose transporters.
Cellular	Tissue specific-cells, stem cells, immune cells, nerve cells, endothelial cells	Chaderins (N, N2, P, E), ICAM, VCAM, integrins (e.g. αVβ3 with CD31 in endothelial cell)

The nature of the niche is considerer specific for each stem cell type, although the same type of environment features are capable of directing other stem cell niches or other cell type behavior, *in vivo* and *in vitro*. Therefore, understanding the normal and regenerative stem cell niche can enlighten and inspire the design of

instructive constructs.

Upon tissue injury, immune cells, and others migrate, triggering the healing cascade or an immune response. The healing cascade consists of four major integrated and overlapping phases: hemostasis; inflammation; proliferation and repair; and tissue remodeling or resolution – Figure I.2.[29-31]

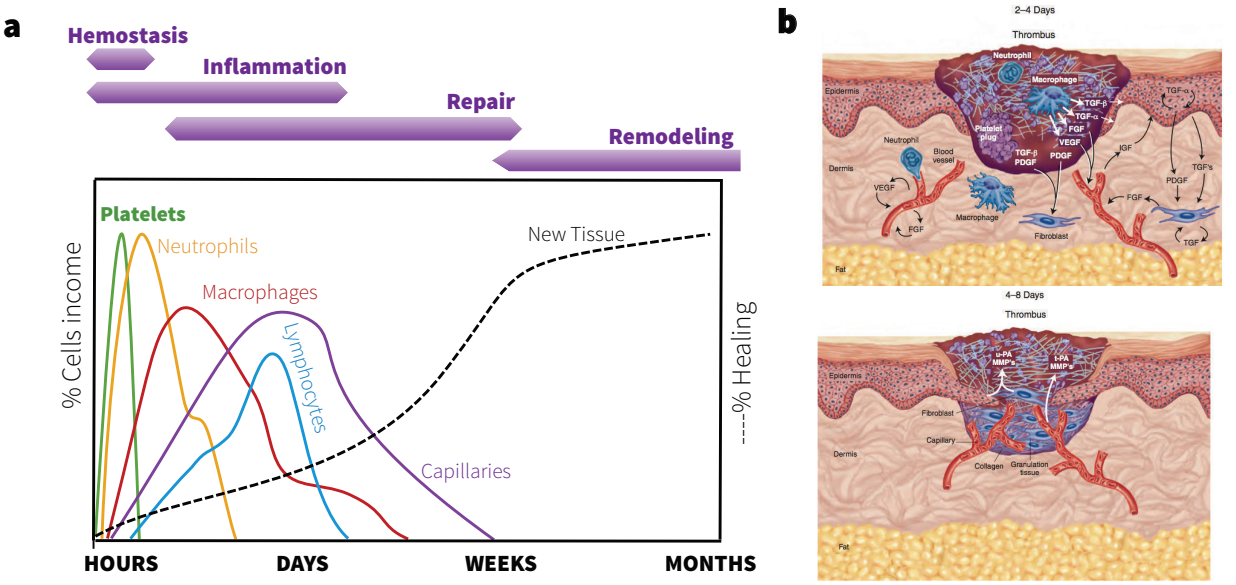

Figure I.2. a) General phases involved in the healing cascade triggered by a tissue injury (based on [29, 32-34]). b) Illustration of a cutaneous wound reproduced from[34]: top - crosstalk between the clot and the surrounding tissue in the inflammatory phase; bottom - and in the remodeling phase. Several bioactive factors have multiple effects and multiple sources. FGF, fibroblast growth factor; IGF, insulin-like growth factor; TGF, transforming growth factor; PDGF, platelet-derived growth factor; VEGF, vascular endothelial growth factor; MMPs, matrix metalloproteinases; t-PA, tissue plasminogen activator; u-PA, urokinase-type plasminogen activator.

The temporary micro/nano-environment of each stage is regulated by several cell types, matrix proteins, growth factors (GFs) and cytokines – Table I.1. Extreme changes are known to happen in the physical, biochemical, bioactive factors content, cell-cell communication and extracellular matrix polysaccharides or proteins patterns, during the normal and efficient healing cascade.[35] The failure, or prolongation, in one phase might result in a delayed or impaired healing. This may be caused by low stem cells availability, aging, continued activation of inflammatory cells, excessive pro-inflammatory MMP, excessive proliferation and matrix synthesis, among others.[35-39] The repair process may only restore some of the structures of the original tissue and involves scar formation. Only an adequate balance between new matrix deposition and matrix degradation, during the heading, allows a successful regenerated tissue identical to the original one to be achieved.

An injury causes vascular endothelium disruption, exposing the collagen layer and other elements that activate platelets. Nowadays, platelets are recognized as major players in the healing cascade, tissue repair and regeneration.[40-42] Besides maintaining the blood vessels integrity by adhering, aggregating and forming a pro-coagulant fibrin surface (hemostasis), platelets initiate the healing process. Once activated, the substances released from the platelet's granules (dense granules, lysosomes and α-granules) are responsible for triggering the healing cascade. For instance, α-granules contain many instructive GFs, such as: vascular

endothelial growth factor (VEGF), fibroblast growth factor (FGF), transforming growth factor β, (TGF β), epidermal growth factor and insulin-like growth factor (IGF). Besides their role in hemostasis, platelets play important anti and pro-inflammatory roles and their releaseates also participate in the other healing stages.[5, 40, 43-46] In the early phase, adherent platelets interact with endothelial cells, monocytes and neutrophils promoting the secondary recruitment of neutrophils. They activate neutrophils and endothelial cells inducing the production of inflammatory cytokines. Platelets are potent instructive cells, and actually have been inspiring and used as source of multiple instructive proteins for the preparation of new constructs for several tissue-engineering applications.[47, 48] Similarly to platelets, other cells involved in the healing cascade play important roles by secreting similar or other instructive compounds such as the leukocytes and other granulocytes – Table I.2.

The specific nature of the extracellular matrix of the tissue also regulates the GFs and other bioactive proteins distribution, type, and stability.[20, 49, 50] GFs are presented either in soluble form, or mainly electrostatically bound to the negatively charged glycosaminoglycans (GAGs). GAGs present various molecular arrangements and different sulfation degrees and are usually linked to a small protein core, forming proteoglycans.[50-52] Furthermore, the nature of the major cell and proteins types forming the extracellular matrix of the tissues shows certain specificity – Table I.3.

Table I.2. Major cell types involved on the healing of injured tissues and their respective function and participating phases adapted from [5, 46, 53, 54].

Cell	Phase	Function
Platelets	Hemostasis Inflammation Repair Remodeling	Major players in hemostasis. Granules release cytokines, chemokines, GFs, clotting agents, proteases and inflammation mediators. Facilitate adhesion, coagulation, vasoconstriction, repair and clot resorption. Their activation attract and activates several cells
Leukocytes	Inflammation	Granulocytes (neutrophils, basophils, eosinophils) and agranulocytes (lymphocytes monocytes and macrophages) are immune system cells involved in the foreign-body reaction. Basophils, e.g., release heparin, histamine, proteases, and chondroitin. The type of leukocytes recruited is controlled by local chemokines. Granulocytes are recruited form bone marrow within the first day and are responsible for the degradation of unviable tissue releasing their granules content. Neutrophils can secrete products that stimulate monocytes and macrophages.
Mast cells	Hemostasis	Resident cells that contains granules rich in histamine and heparin
Resident cells	Hemostasis Inflammation Repair Remodeling	Tissue resident cells such as resident macrophages and stem cells release healing mediators in the early and long-term response
Macrophages	Inflammation Repair Remodeling	Arrive at the injury site shortly after neutrophils where persist for days or longer. Release cytokines, chemokines and GFs. Participate in the phagocytosis of debris and on the development of granulation tissue
Fibroblast, pericytes, smooth muscles cells	Inflammation Repair	These cells are recruited by locally released GFs and extracellular matrix degradation products. In the case of skin, these cells are responsible for matrix synthesis, wound strength and contraction and tissue remodeling
Endothelial cells	Hemostasis Inflammation Repair	This cells form capillaries upon GFs instruction, which are essential for nutrients, gas, metabolites diffusion and for the influx of inflammatory cells

Table I.3. Tissue expression of extracellular matrix molecules adapted from [5] and other extracellular characteristics. Fibrillar collagens (I, II, III, V, XI), network-forming collagen (IV, VIII, X), non-fibrillar collagens (VI, IX, XII, XV, XVIII), anchoring (VII, XVII).

Tissue or fluid	Primary mesoderm cell	Prominent collagen types	Noncollagen proteins	GAGs and PGs	Others
Plasma	-	-	Albumin, Fibronectin, fibrinogen, vitronectin	Hyaluronic acid	Red and white blood cells, platelets
Dermis	Fibroblast	I, II, V, VI, XII	Fibronectin, elastin, fibrillin	Hyaluronic acid, decorin, biglycan, fibromodulin	Stratified and vascularized tissue
Muscle	Muscle cell/Fibroblasts	I, III, V, VI, VIII, XII	Fibronectin, elastin, fibrillin	Aggrecan, biglycan, decorin, fibromodulin	Soft tissue with oriented actin and myosin filaments
Tendon	Fibroblast	I, III, V, VI, XII	Fibronectin, tenascin (myotendon junction), elastin, fibrillin	Decorin, biglycan, fibromodulin, lumican, versican	Bone-muscle connection. Mostly collagen type I forms fiber bundles
Ligament	Fibroblast	I, III, V, VI	Fibonectin, elastin, fibrillin	Decorin, biglycan, versican	Bone-bone connection. Mostly parallel array of collagen fibers closely packed
Cornea	Fibroblast	I, III, V, VI, XII	-	Limican, keratocan, mimecan, biglycan, decorin	Avascular and transparent stratified tissue
Cartilage	Chondrocyte	II, IX, VI, VIII, XI, X (hypertrophic chondrocytes)	Anchorin CII, fibronectin, tenascin	Hyaluronic acid, aggrecan, biglycan, decorin, fibromodulin, limican, perlecan (minor)	Flexible, Avascular and ECM rich in PGs and elastins
Bone	Osteocyte	I, V	Osteocalcin, osteopontin, bone sialoprotein, osteonectin	Decorin, fibromodulin, biglycan	Rigid and hard, Vascular containing 50-70% is calcium phosphate. Long bones contain medullar cavity
Basement membranes	Epithelial, endothelial, adipocytes, Schwann cell, muscle cells, pericyte	IV, XV, XVIII	Laminin, nidogen/entactin	Heparan sulfate, proteoglycans, perlecan	Nano-stratified membrane surrounding cells or cellular structures

Both the specific nature of the extracellular matrix and the healing cascade have been inspiring the development of cell instructive tissue engineered constructs. Overall, those inspired instructive cues have been incorporated into biomaterials and 3D constructs by: i) the incorporation of human or recombinant GFs, or analogues moieties; ii) the incorporation of ECM-tissue specific compounds, or analogues moieties; iii) the use of co/multi-cultures or cell-cell contacts analogues; and iv) the use of immunomodulatory biomaterials. The presentation and incorporation of GFs into biomaterials is commonly made by recourse to release systems or surface modification techniques [14,101,102] More translational developments in this area have been hindered by the high cost of recombinant GFs. Thereby, platelets derivatives have attracted immense attention as a human source of multiple GFs and other bioactive molecules demonstrating huge mitogenic, immunomodulatory and differentiation potential. [41, 42, 44-46, 55-60]

Engraftment of small peptides mimicking the bioactive epitopes of natural ECM molecules, have also shown promising results.[61] Frequently, those moieties play important roles during the tissue morphogenesis. For example, the peptide with the sequence of Asp-Gly-Glu-Ala (DGEA), which is derived from collagen type I, has

been shown to induce an early-commitment of human mesenchymal stem cells towards the osteogenic lineage.[62, 63] The peptide Glu-Glu-Glu (EEE), which is inspired in the acidic residues of non-collagenous matrix proteins such as osteocalcin and osteopontin, has been shown to promote a more mature osteogenic differentiation than the DGEA.[64]

The combination of different cell types is another approach to obtain a closer representation of the complex cross-talk that occurs in the natural tissue.[65] Addition of another cell-type producer of bioactive factors allows a different scheme of interactions, promoting paracrine, autocrine routes and cell-contact dependent effects. Several studies have shown synergistic effects upon the use of co-culture systems or even stem cell differentiation.[66-68]

Biomaterials for immunomodulation are one of the keys to instruct cell behavior upon implantation and promote the long-term functionality of the constructs.[4, 36, 69] The surgical procedure always initiates an inflammatory response and may elicit an adaptive immune reaction towards the constructs surface that should be controlled. Immunomodulatory biomaterials allow control of the tissue response at the implant site regarding primarily cell adhesion and/or cellular activations. An indirect modulation controls immune cells adhesion and activation, consequently indirectly inducing specific GF secretion. On the other hand, on a direct approach, specific singling molecules are included in the biomaterial.[4] Controlling hydrophilicity[70] and fouling properties[71], topography/roughness[72, 73], adhesion sites (e.g., RGD)[74, 75], incorporation of anti-inflammatory mediators [76, 77], self-protein inhibitors[78] and GFs[79-81], and the use of cells with immunomodulatory properties[82, 83] are the common applied strategies.

Currently is technically limitative to fully reconstruct the whole complexity and nature the healing/regeneration events into a tissue-engineered construct. Full understanding of the events occurring in the regenerative niche of each tissue can give a huge contribute on the selection of the most efficient instructive cues. The balanced use of those naturally occurring stimulatory keys, as an integrative part of the biomaterial, may prove very efficient in guiding and instructing cell behavior, modulating the healing cascade and the immune response.

I.4. Multiscale Construct Design Features

Designing the construct features for *in vitro* cell fate control and, simultaneous, adequate *in vivo* performance, is one of the main focuses in tissue engineering.[84-86] According to the processing approach used for the construct preparation, the best scale working range varies: top-down approaches are more adequate for macro-micro scale and bottom-up approaches allow higher micro-nano scale control, while full scale range might be controlled using integrative approaches. Thereby, different approaches offer different control degrees on the final properties of the scaffolds. Nonetheless, multiple variables must be considered, independently of the 3D construct processing approach. Besides the mechanical properties, and immune reaction, the type and spatial-temporal distribution of the construct properties will guide and instruct cell behavior, namely: cell adhesion, cell viability, proliferation, differentiation, matrix production and degradation.

According to their major function and scale range, the general construct design features can be categorized as: i) geometry; ii) cell-anchorage; iii) release-system; iv) cellularity; v) topographical cues; and vi) biochemical cues– Figure I.3. The scale definition considered is: macro (>100mm), sub-macro (100mm – 100μm), micro (100μm – 1μm), sub-micro or meso (1μm – 100 nm), nano (<100nm).

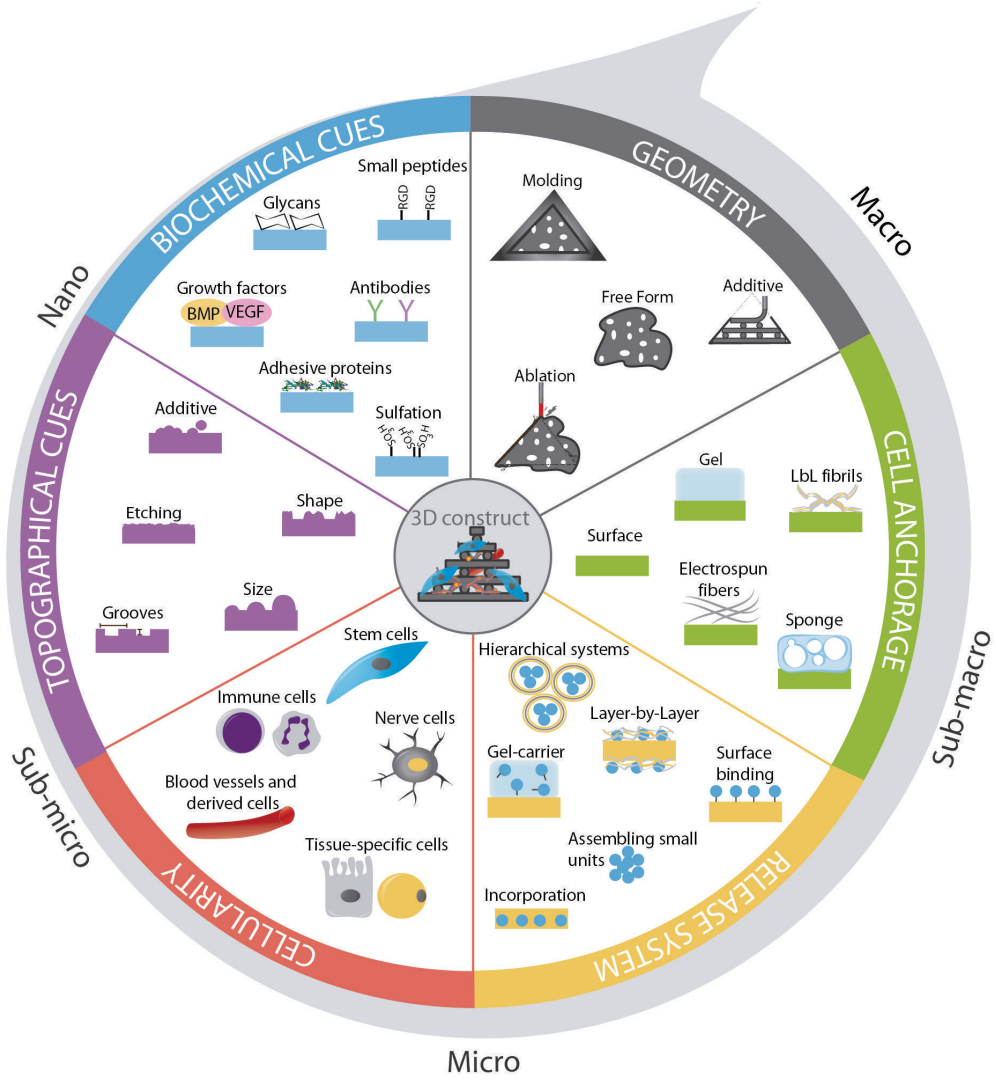

Figure I.3. General 3D construct's features categorized according to their major function and length scale-range: geometry, cell-anchorage, release system, cellularity, topographical cues and biochemical cues.

I.4.1. Geometry – macro, sub-macro

The geometry of the construct has, generally, to be tailored according to the implantation site request, in order to fill the tissue's void space and support the site's mechanical demands. Additive[87-89], ablation[90] and molding[91-93] technologies, based on previous three dimensional patient data acquisition (e.g., by x-ray microtomography or magnetic resonance imaging), allow the preparation of geometry-specific 3D constructs. On the other hand, some applications do not demand specific geometries or high mechanical strength. In such cases, combinations of materials, cells and bioactive factors are usually injected filling the void spaces.[94-96] Shaping the material frequently affects the bulk mechanical properties of the construct. For instance, scaffolds

prepared by rapid prototyping show different compression moduli according to the alignment[97] or the distance between struts[98]. Nonetheless, computer assisted design technologies offer the possibility to simulate and optimize the inner geometry (strut alignment, pore size, pore geometry and interconnectivity) in order to enhance the mechanical performance, by using finite element analysis and CAD design tools.[99-101] Those micro features, pore geometry[102, 103], pore size[104-106] and porosity[107], also affect oxygen perfusion, the removal of cell metabolites, cell seeding efficiency and tissue growth rate, making them very important features regarding cell viability and growth. Additionally, those micro-properties also influence the invasion of inflammatory and immune cells, the ingrowth of blood vessels or other cells from the host tissue.[107-109]

I.4.2. Cell-anchorage – sub-macro, micro, sub-micro, nano

The cell-anchorage defines elements supporting the adhesion of the cells at a lower scale than the geometry of the construct. Depending on the technique used to shape the materials or, e.g., depending on the subsequent/simultaneous incorporation of gels[110, 111], sponges[112, 113], micro/nano-fibers or fibrillar structures[114], the anchorage points, and the pores' micro-properties, can be tailored. Introducing anchorage points within the pores is also a way to increase cell surface growth area/volume and alter the spatial distribution of the tissue growth. Moreover, their physical properties (e.g. stiffness/elasticity and adhesion area) will affect cell morphology by altering the cytoskeletal organization and contractibility, which can guide stem cell differentiation into specific lineages.[115, 116]

I.4.3. Release systems – micro, sub-micro, nano

The incorporation of release systems in the constructs is considered an essential tool for the temporal or spatial-temporal controlled delivery of instructive or pharmaceutical compounds.[117-121] Some examples of release system of interest in tissue engineering relate to the delivery of one or multiple compounds such as GFs[122-125], dexamethasone[126-128], gentamicin[129, 130], ketoprofen[131, 132] and platelet derivatives[133-136]. Typically, a release-system, or simple compounds, is included by the simple combination with the materials prior to the 3D construction[133, 137], or is incorporated afterwards, using surface modification techniques (e.g., by layer-by-layer assembling[138] or adsorption[47]) or impregnation (e.g. supercritical fluid CO_2[139]).[140] In combination with smart materials (e.g., poly (N-isopropylacrylamide)), these systems can be triggered in a controlled manner, for instance by temperature[141], pH[141] and light stimuli[142].[143, 144] Besides being interesting for the development of smart release systems, stimuli responsive materials have been shown to provide variations in the biochemistry (e.g., wettability) affecting cell adhesion[145] or mineralization[146].[147]

I.4.4. Cellularity – micro

For cellular tissue engineered approaches, the type of cells seeded on the constructs has major percussions on

new tissue formation. According to the source tissue or donor, stem cells possess different differentiation potentials.[148-151] Moreover, the seeding of more than one cell type (i.e. co/multiple cell culture), and the ratio between those cells, allows different crosstalk to occur. The presence of other cells will affect the nano/micro-environment, e.g., by creating a new profile of cell-secreted cytokines and GFs. [66-68] Additionally, variables such as cellular density can affect cell growth[152-154] and differentiation[155-158].

I.4.5. Topographical cues – micro, sub-micro, nano

The construct nano/micro-topography and roughness (and biochemistry) are the primary mediators of the fast adsorption of proteins from the surrounding media (e.g., serum media or plasma), which further mediates the cell adhesion process.[159-163] Controlling these features can synergistically improve cell behavior. As has been shown, designing specific surfaces grooves and patterns can induce specific cell shapes[164-166] or alignments[167-169] that alter cytoskeleton contractibility guiding cell differentiation. Well-controlled topographical cues, patterns and surface biochemistries can be easily prepared in 2D. However, the transposition of those features to 3D is still a major challenge. Surface properties design and surface engineering techniques have been extensively reviewed elsewhere.[49, 84-86, 170-173]

I.4.6. Biochemical cues - nano

At the nanoscale, the surface biochemistry instructs cell behavior by directly mediating the adsorption of surrounding proteins to the construct, and the binding/activation of cell surface receptors – Table I.1. The biochemical cues, such as: GFs[174-176], extracellular matrix proteins[177-179] (e.g., collagen and fibronectin), functional groups[180-182] (e.g. sulfation), small peptides[183-185] (e.g., -RGD), cell contacts[186, 187] (e.g., cell-cell interactions or functional groups mimicking cells contact) will trigger specific singling pathways in the cell and define their fate. A controlled design of the biochemistry is commonly made recurring to nanotechnologies and surface modification methods, such as: layer-by-layer assembling[188-192] and antibody mediated binding[193, 194].

Despite most features might be easily allocated to a length scale or range scale, their properties can be intimately related with other features. A classical example is the case of roughness-wettability.[163, 195, 196] Introducing nano/micro-roughness in a construct in the first instance may represent a higher surface area available for cell growth. Nevertheless, the altered roughness might also change the surface wettability into values that are not as favorable for cell adhesion/growth.[197, 198] Whether the ability of a surface to be wet is altered, its profile of protein adsorption will also change (e.g., type, conformation and density of proteins). Consequently, the communication between cell and the constructs at the cell receptor level can be significantly altered.[199]

I.5. Differentiation biases and aging

Regenerative success is intricately dependent on all the interactions that cells are subjected to during *in vitro* culture, the interaction with the construct and the *in vivo* implantation. Besides the crucial roles of the properties considered in most of the research conducted in tissue engineering, there are others affecting mostly the cellular phenotype and genotype quality. Those features concern issues such as cell senescence, aging and differentiation biases.

Most of the commonly used *in vitro* expansion platforms are not adequate and damage cell telomeres, causing cell senescence, aging, reduction of differentiation potential and differentiation biases.[200-202] The conditions used for stem cell expansion can alter the lineage fate. Moreover, it has been reported that stem cells have mechanical memory of previous culture conditions.[203] Also, it has been shown that the chemistry of the surface used to expand stem cells does affect their *in vivo* regeneration capability[204], as well as, the tendency for a certain lineage differentiation.[205] Another example of the biases lineage-commitment is the tendency of mesenchymal stem cells to undergo aging, telomere shortening, and spontaneous low quality osteogenic differentiation upon regular culture expansion.[203, 206] To overcome those issues, besides recurring to telomerase activators, e.g., geometrical, topographical and physical cues can be used to alter cytoskeleton contractibility, guiding stem cell lineage specification, and reducing the biases.[115, 116, 207, 208] There is still an urgent need to develop and spread anti-aging, anti-biases procedures, new 2D/3D expansion substrates and constructs, to improve specificity, cellular performance and tissue regeneration.

I.6. Tissue Engineering Approaches

3D constructs can be prepared using top-down, bottom-up or integrative approaches. Those approaches, based on construction units with different length-scales, allow varied degrees of control of the final properties. With top-down approaches, well-defined constructs, where multiscale control is not a demand, can be prepared, whereas bottom-up allow higher control at the nano/micro scale. On the other hand, integrative approaches emerge as a combination of both top-down and bottom-up approaches, promising constructs with properties and features controlled over the entire scale range. Bottom-up and integrative approaches present higher potential for the design of constructs with multiscale features and high biochemistry control than top-down, being more focused in this review.

I.6.1. Top-down approach

In top-down approaches, the small-scale features of the constructs are indirectly explored with techniques providing higher control over the micro/macro scale. Top-down constructs have been produced recurring to several processing techniques, such as: freeze-drying[209-211], solvent-casting[212-215], electrospinning[216-218], rapid prototyping[219-221] and supercritical fluids[222]. Classic tissue engineering strategies comprise those well-defined scaffolds, with tailored physical and bioactive properties, that are the templates for cells to populate, remodel

and create the appropriate extracellular matrix. They present pores and mechanical properties that can be controlled to some extent, for instance, by controlling the inner geometry and the nature of the materials, respectively. Few techniques, e.g. rapid prototyping, allow a precise and computer assisted design of the inner geometry and simultaneous construct shape. All different kinds of materials and blends (i.e. natural and synthetic polymers and proteins, ceramics and metals) have been used to prepare 3D constructs, however they frequently lack instructive cues. To improve cell behavior on such structures, usually the scaffolds are prepared combining different top-down techniques[223, 224] or are subjected to further functionalization requiring integrative approaches[114, 189, 225]. For instance, electrospinning and 3D printing can be combined to prepare hierarchical scaffold with dual scale fibers: the printed micro-struts combined with electrospun nano/microfibers.[226, 227] The electrospun fibers increase cell-anchorage points and seeding efficiency[218] and can promote cell alignment[228].

I.6.2. Bottom-up approach

Bottom-up methodologies comprising the assembling of micro/nanoscopic-defined building blocks into larger scale structures. The chance to control the construct over several length-scales makes this approach more attractive for matrices engineering than the top-down approach. This approaches promise new opportunities to mimic a tissue microstructure and the spatial organization of multiple cell types.[61] The most commonly used building blocks comprise cells, cell aggregates/spheroids, nano/microparticles, tubes, layers, fibers and gels. The development of methodologies to produce, functionalize and assemble those small units is the major challenge – Figure I.4. Currently, there are three general alternatives to assemble the units: i) randomly; ii) mediated by an external force; and iii) specifically assembled.

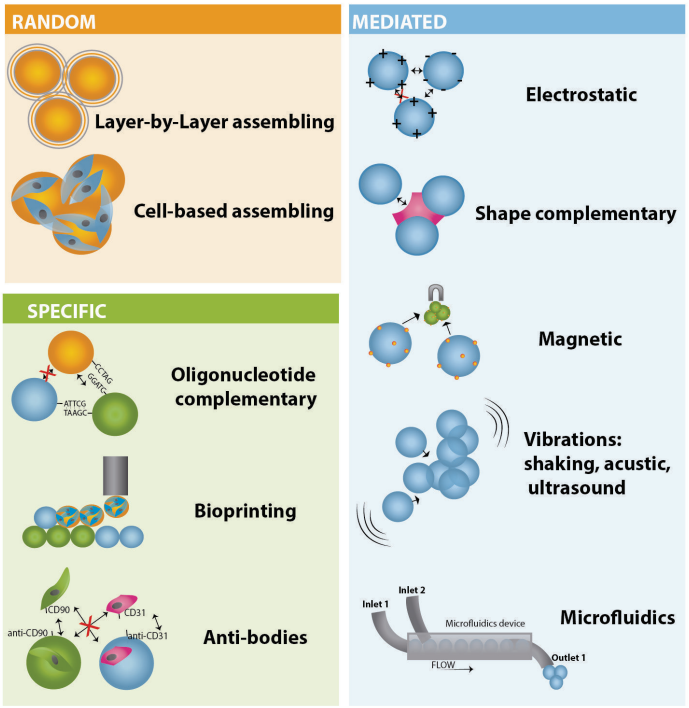

Figure I.4. Current strategies employed for the bottom-up assembling of small units: random, mediated and specific.

I.6.2.1. Random assembling

Layer-by-layer assembling (LbL) is a simple and random bottom-up assembling method based on the alternated deposition of polyelectrolytes with different charges.[190, 229, 230] Using LbL, multilayered structures can be created around the units, binding and stabilizing the entire set and forming a scaffold[231], temporary templates to produce high porous foams [232, 233] or hierarchical capsules[234, 235]. Such extension of the LbL methodology towards the fabrication of 3D structures is an example of the application of this technology in the biomedical field.[236]

It has also been shown that the building blocks can be unspecifically assembled by cells which colonize their surfaces, consolidating the construct.[237-239] The presentation of cell-recognizable moieties on the surface can accelerate this cell-based assembling. For instance, chitosan microparticles functionalized with a mitogenic GF (PDGF) have shown a stable and faster assembling, within 12 hours, than in the absence of PDGF.[194]

Scaffold free technologies represent another derivation of the bottom-up approach. Cells grown on thermoresponsive culture dishes are retrieved as a confluent monolayer, containing the extracellular matrix proteins, by decreasing the local temperature. [145, 240, 241] These cell sheets can be consecutively stacked on top of each other to produce thicker and more complex tissues. A reported alternative is based on consecutive cell seeding on top of confluent cell layers previously coated with proteins.[242, 243] The preparation of thick cell-constructs and their low load-bearing capability are the major challenges in using such technology in tissue engineering.

I.6.2.2. Mediated assembling

The assembling of small units can be guided by external stimuli, allowing control over their spatial organization to a certain extent. For example, the successful attachment of gels surfaces, with the same charge using silica particles, has been demonstrated. [244-246] Through electrostatic interactions at the particles-gel interface, and cohesion forces in the particles layer, two gel-surfaces can be attached. The adhesion force, mediated by the particles, can reach 20 kPa as opposed to 1.5 kPa when using an oppositely charged polyelectrolyte solution.[244-246] Hydrogel units composed by materials presenting opposite charges can also be assembled by electrostatic attraction.[247] However, to promote the electrostatic binding, the distance among the units has to be decreased, e.g. by direct positioning[244], by shaking [247] or using acoustic waves [248]. Alternatively, it has been shown that template gels can be successively dipped onto oppositely charged micro-gel colloid to form multilayered-like constructs.[249] Moreover, the use of shape complementary building blocks allows the formation of lock-and-key shaped assemblies mediated by electrostatic interaction or surface tension.[247, 250] In alternative, magnetic nanoparticles can be incorporated into cells[251, 252] and biomaterial units[253-255] and further 3D organized recurring to an external magnetic field.

I.6.2.3. Specific assembling

While the alternatives for the unspecific 3D assembling of building block are many, the current available

methods to design 3D constructs with specific spatial organizations are yet limited and more complex.

Microfluidic technologies have been proposing promising tools for the assembly, for example, of small gel units mostly by mediated assembling. By controlling the inlets, outlets and flow, some microfluidic devices can actually guide the assembling of small units into 1D, 2D and 3D structures.[256] Moreover, it has been shown that using the so-called multilayer-microfluidic devices, mosaic hydrogels with a well-defined spatial composition of materials, cells or pores can be prepared.[257]

Based on the oligonucleotide pairs complementarity principle, gel interfaces can be specifically assembled.[258, 259] Setting the spatial/surface presentation of the complementary sequences in the different units allows the formation of controlled assemblies. Although being very assemble-specific, this approach might be scale-up limitative. Other alternative methods, for both materials and cell controlled assembling, are based on bioprinting technologies. Bioprinting is a particular type of rapid prototyping technique that deposits small units of multiple materials and cells, instead of continuous filaments.[260] Highly complex organization with cellular vascular networks, multiple cells types and extracellular matrices were already shown to be achievable.[261]

Even though bottom-up approaches seem ideal to mimic a tissue organization, major developments and new concepts to improve the assembling and spatial organization of the assembling units still necessary. Limitations such as the weak control on the final 3D shape, the lack of scalability and the lack of understanding on the short and long-term interactions among the units and cell behavior, are yet to be further investigated.

I.6.3. Integrative approach

The combination of the top-down and bottom-up approaches constitutes a valuable strategy to increase the functionality of the devices for tissue engineering and achieve a multiscale control over the construct properties.

According to the integration between the bottom-up and top-down approaches, three sub-categories of integrative methods can be defined: i) sequential integration; ii) combination; and iii) technical integration – Figure I.5.

Employing an integrative approach could allow the increment of one or more feature/property in the construct without impairing the previous structure properties.[262] Thereby, fully customizable constructs with multiple scales of complexity could be designed. With such ideal control and the increment of measurable properties, *in silico* modulation could contribute greatly for the understanding of the relationship between multiscale properties and cell behavior. Those resulting models would allow the mathematical prediction of cell behavior, contributing to the constructs optimization and eventually to the reduction of *in vitro/in vivo* experimentation costs. [263]

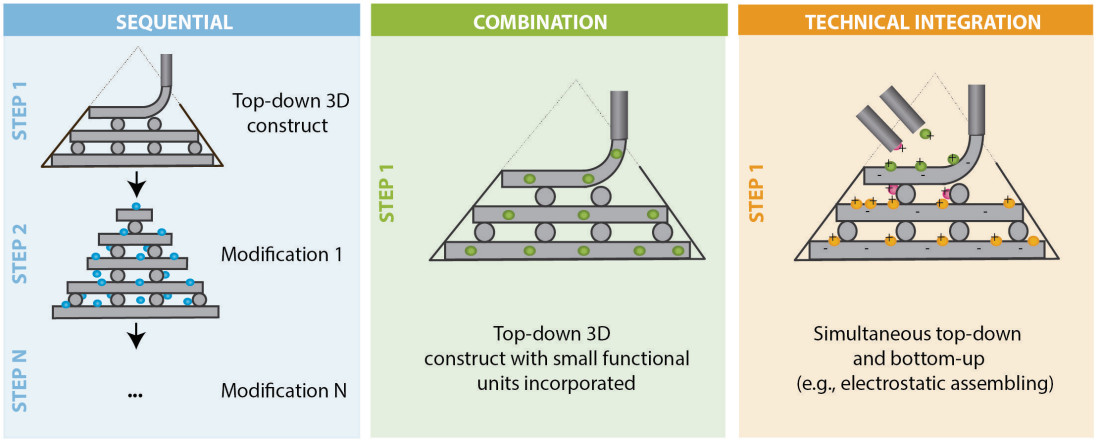

Figure I.5. Different integrative approaches for the preparation of 3D constructs: sequential, integration by combination and technical integration.

I.6.3.1. Sequential Integration

3D constructs may be prepared using different techniques in a step-wise manner; i.e., by sequential integration. In these cases, the constructs are step-by-step prepared using at least one top-down and one bottom-up method. This category is the most used to overcome the lack of bioactivity and cell instruction of the traditional 3D scaffolds prepared by top-down approaches. Modification techniques such as adsorption, layer-by-layer assembling, self-assembling and grafting can be used to modify 3D construct without impairing their initial features. Those methods have been used to include instructive cues such as adhesive proteins[264-267], GFs[268-271], modular peptides[272] and bioactive calcium phosphate particles[273]. Controlling the biochemistry and the incorporation of release system is manageable using sequential approaches; however, it is yet challenging to control the topographical cues on 3D top-down constructs. The use of microfabrication techniques for the preparation of micro-layers of the construct is an appealing solution. Several features might be controlled in each layer (biochemistry, topography, release system and cells), which are further assembled or stacked.[274, 275] However, assembling and stabilizing those layers is still challenging as in the case of the bottom-up approaches.

I.6.3.2. Combination

Contrary to the other categories, in the integration by combination, the building blocks are incorporated prior to the processing and the top-down method is performed as if in absence of such units. Thereby, this approach allows the incorporation of new features, such as release systems in the bulk structure of the constructs. For instance, supercritical CO_2 fluid foaming was used to prepare scaffolds of poly (L-lactic aci) with nanoparticles carrying platelet lysate.[276] The incorporation of those bioactive nanoparticles enhanced the osteogenic differentiation of human adipose derived stem cells on the foams. Polymeric microcarriers, which allow a controlled expansion and formation of cellular aggregates, were successfully combined with gelatin

methacrylamide-gellan gum bio-inks.[277] With this combination, 3D constructs with simultaneous high cell density, viability and improved mechanical performance could be achieved.

I.6.3.3. Technical Integration

The technical integration refers to the development of constructs recurring to specialized equipment for simultaneous top-down and bottom-up processing. With such type of equipment's, topography, release system, biochemistry, shape and cells could be ideally controlled.

A foreseen example employing this approach could be the combination of rapid prototyping and spraying of small-units containing instructive or topographical cues. Recurring to a software-assisted deposition of both, shape controlled constructs with spatially defined topography, release systems and biochemistry could be fabricated. Though very appealing, such sophisticated technologies have yet to be developed.

I.7. Conclusions and perspectives

Recent 3D instructive constructs have a controlled biochemistry that is rich in adhesive moieties, GFs, or other extracellular inspired epitopes, that activate cells and instruct their behavior.

The major nano/micro-environment properties and events occurring in the normal and regenerative tissue have been inspiring the selection or synthesis of instructive cues to include in the 3D constructs (e.g. platelets). However, there is still a need to understand which are the most effective spatial-temporal cues for each tissue. Besides the biochemistry, other construct features, e.g. topography, cells, cell anchorage and geometry, play major roles for the 3D construct success both *in vitro* and *in vivo*. High-content screening of 3D constructs properties and features promises a huge contribute in deciphering which cues, materials and methods will be more effective for the regeneration of each tissue. [278-281]

The control of all such features calls for processing approaches that allow a multiple scale control, i.e., integrative approaches. According to the combinations between the top-down and bottom-up techniques, different integrative approaches were defined: sequential, combination and technical integration. The assembling of building blocks in a single bottom-up approach is yet in its infancy, in regards to tissue engineering applications or the development of 3D tissue-models. However, their integration with top-down approaches, e.g. 3D printing, may accelerate their development and the preparation of a highly controlled multiscale 3D construct.

I.8. Acknowledgments

The research leading to these results has received funding from the European Research Council grant agreement ERC-2012-ADG-20120216-321266 for the project ComplexiTE. Portuguese Foundation for Science and Technology is gratefully acknowledged for fellowship of Sara M. Oliveira (SFRH/BD/70107/2010).

I.9. References

1. R. Lanza, R. Langer and J. P. Vacanti, Principles of tissue engineering, Academic press, 2011.
2. R. Langer and J. Vacanti, Tissue engineering, Science, 1993, 260, 920-926.
3. L. L. Hench and J. M. Polak, Third-generation biomedical materials, Science, 2002, 295, 1014-1017.
4. S. Franz, S. Rammelt, D. Scharnweber and J. C. Simon, Immune responses to implants–a review of the implications for the design of immunomodulatory biomaterials, Biomaterials, 2011, 32, 6692-6709.
5. G. C. Sephel and S. C. Woodward, Lippincott, Williams & Wilkins, Baltimore, 2001, pp. 84-117.
6. F. Groeber, M. Holeiter, M. Hampel, S. Hinderer and K. Schenke-Layland, Skin tissue engineering— In vivo and in vitro applications, Advanced drug delivery reviews, 2011, 63, 352-366.
7. N. S. Hwang, S. Varghese and J. Elisseeff, in Stem Cell Assays, Springer, 2007, pp. 351-373.
8. K. E. Healy and R. E. Guldberg, Bone tissue engineering, J Musculoskelet Neuronal Interact, 2007, 7, 328-330.
9. K. Hampson, N. Forsyth, A. El Haj and N. Maffulli, Tendon tissue engineering, Topics in tissue engineering, 2008, 4.
10. L. L. Chiu and M. Radisic, Cardiac tissue engineering, Current Opinion in Chemical Engineering, 2013, 2, 41-52.
11. C. A. Custodio, R. L. Reis and J. F. Mano, Engineering biomolecular microenvironments for cell instructive biomaterials, Adv Healthc Mater, 2014, 3, 797-810.
12. S. W. Lane, D. A. Williams and F. M. Watt, Modulating the stem cell niche for tissue regeneration, Nat Biotechnol, 2014, 32, 795-803.
13. R. Schofield, The relationship between the spleen colony-forming cell and the haemopoietic stem cell, Blood cells, 1977, 4, 7-25.
14. K. A. Moore and I. R. Lemischka, Stem cells and their niches, Science, 2006, 311, 1880-1885.
15. D. L. Jones and A. J. Wagers, No place like home: anatomy and function of the stem cell niche, Nature Reviews Molecular Cell Biology, 2008, 9, 11-21.
16. L. Li and T. Xie, Stem cell niche: structure and function, Annu. Rev. Cell Dev. Biol., 2005, 21, 605-631.
17. N. Nakatsuji, Mesoscopic science, where materials become life and life inspires materials. A great opportunity to push back the frontiers of life, materials, and biomaterials sciences, Biomaterials Science, 2013, 1, 9-10.
18. B. M. Gumbiner, Cell adhesion: the molecular basis of tissue architecture and morphogenesis, Cell, 1996, 84, 345-357.
19. R. O. Hynes, Integrins: bidirectional, allosteric signaling machines, Cell, 2002, 110, 673-687.
20. S.-H. Kim, J. Turnbull and S. Guimond, Extracellular matrix and cell signalling: the dynamic cooperation of integrin, proteoglycan and growth factor receptor, Journal of Endocrinology, 2011, 209, 139-151.
21. N. Borghi, M. Lowndes, V. Maruthamuthu, M. L. Gardel and W. J. Nelson, Regulation of cell motile behavior by crosstalk between cadherin-and integrin-mediated adhesions, Proceedings of the National Academy of Sciences, 2010, 107, 13324-13329.
22. M. Takeichi, Cadherin cell adhesion receptors as a morphogenetic regulator, Science, 1991, 251, 1451-1455.
23. M. A. Lemmon and J. Schlessinger, Cell signaling by receptor tyrosine kinases, Cell, 2010, 141, 1117-1134.
24. A. Ullrich and J. Schlessinger, Signal transduction by receptors with tyrosine kinase activity, Cell, 1990, 61, 203-212.
25. M. Bernfield, R. Kokenyesi, M. Kato, M. Hinkes, J. Spring, R. Gallo and E. Lose, Biology of the syndecans: a family of transmembrane heparan sulfate proteoglycans, Annual review of cell biology, 1992, 8, 365-393.
26. D. Carey, Syndecans: multifunctional cell-surface co-receptors, Biochem. J, 1997, 327, 1-16.
27. Y. Choi, H. Chung, H. Jung, J. R. Couchman and E.-S. Oh, Syndecans as cell surface receptors: unique structure equates with functional diversity, Matrix Biology, 2011, 30, 93-99.
28. J. D. Humphries, A. Byron and M. J. Humphries, Integrin ligands at a glance, Journal of cell science, 2006, 119, 3901-3903.
29. S. Guo and L. A. DiPietro, Factors affecting wound healing, Journal of dental research, 2010, 89, 219-229.

30. A. Gosain and L. A. DiPietro, Aging and wound healing, World journal of surgery, 2004, 28, 321-326.
31. S. Enoch and D. J. Leaper, Basic science of wound healing, Surgery (Oxford), 2008, 26, 31-37.
32. L. Claes, S. Recknagel and A. Ignatius, Fracture healing under healthy and inflammatory conditions, Nature Reviews Rheumatology, 2012, 8, 133-143.
33. R. J. d. Mendonça and J. Coutinho-Netto, Cellular aspects of wound healing, Anais brasileiros de dermatologia, 2009, 84, 257-262.
34. F. H. Epstein, A. J. Singer and R. A. Clark, Cutaneous wound healing, New England journal of medicine, 1999, 341, 738-746.
35. M. B. Witte and A. Barbul, General principles of wound healing, Surgical Clinics of North America, 1997, 77, 509-528.
36. S. J. Forbes and N. Rosenthal, Preparing the ground for tissue regeneration: from mechanism to therapy, Nat Med, 2014, 20, 857-869.
37. M. Mehta, K. Schmidt-Bleek, G. N. Duda and D. J. Mooney, Biomaterial delivery of morphogens to mimic the natural healing cascade in bone, Advanced drug delivery reviews, 2012, 64, 1257-1276.
38. E. R. Utz, E. A. Elster, D. K. Tadaki, F. Gage, P. W. Perdue, J. A. Forsberg, A. Stojadinovic, J. S. Hawksworth and T. S. Brown, Metalloproteinase expression is associated with traumatic wound failure, Journal of Surgical Research, 2010, 159, 633-639.
39. N. B. Menke, K. R. Ward, T. M. Witten, D. G. Bonchev and R. F. Diegelmann, Impaired wound healing, Clinics in dermatology, 2007, 25, 19-25.
40. M. Gawaz and S. Vogel, Platelets in tissue repair: control of apoptosis and interactions with regenerative cells, Blood, 2013, 122, 2550-2554.
41. K. Stellos, S. Kopf, A. Paul, J. U. Marquardt, M. Gawaz, J. Huard and H. F. Langer, Platelets in regeneration, 2010.
42. E. Anitua, I. Andia, B. Ardanza, P. Nurden and A. T. Nurden, Autologous platelets as a source of proteins for healing and tissue regeneration, THROMBOSIS AND HAEMOSTASIS-STUTTGART-, 2004, 91, 4-15.
43. A. Zarbock, R. K. Polanowska-Grabowska and K. Ley, Platelet-neutrophil-interactions: linking hemostasis and inflammation, Blood reviews, 2007, 21, 99-111.
44. J. W. Semple, J. E. Italiano and J. Freedman, Platelets and the immune continuum, Nature Reviews Immunology, 2011, 11, 264-274.
45. A. S. Weyrich and G. A. Zimmerman, Platelets: signaling cells in the immune continuum, Trends in immunology, 2004, 25, 489-495.
46. A. Vieira-de-Abreu, R. A. Campbell, A. S. Weyrich and G. A. Zimmerman, Platelets: versatile effector cells in hemostasis, inflammation, and the immune continuum, Semin Immunopathol, 2012, 34, 5-30.
47. V. E. Santo, M. E. Gomes, J. F. Mano and R. L. Reis, Chitosan-chondroitin sulphate nanoparticles for controlled delivery of platelet lysates in bone regenerative medicine, J Tissue Eng Regen Med, 2012, 6 Suppl 3, s47-59.
48. A. C. Lima, J. F. Mano, A. Concheiro and C. Alvarez-Lorenzo, Fast and mild strategy, using superhydrophobic surfaces, to produce collagen/platelet lysate gel beads for skin regeneration, Stem Cell Reviews and Reports, 2014, 1-19.
49. D. E. Discher, D. J. Mooney and P. W. Zandstra, Growth factors, matrices, and forces combine and control stem cells, Science, 2009, 324, 1673-1677.
50. G. S. Schultz and A. Wysocki, Interactions between extracellular matrix and growth factors in wound healing, Wound Repair and Regeneration, 2009, 17, 153-162.
51. J. Kreuger, D. Spillmann, J. P. Li and U. Lindahl, Interactions between heparan sulfate and proteins: the concept of specificity, Journal of Cell Biology, 2006, 174, 323-327.
52. S. K. Nigam and K. T. Bush, Growth factor–heparan sulfate “switches” regulating stages of branching morphogenesis, Pediatric Nephrology, 2014, 29, 727-735.
53. J. B. Sipe, J. Zhang, C. Waits, B. Skikne, R. Garimella and H. C. Anderson, Localization of bone morphogenetic proteins (BMPs)-2,-4, and-6 within megakaryocytes and platelets, Bone, 2004, 35, 1316-1322.
54. S. Kamath, A. Blann and G. Lip, Platelet activation: assessment and quantification, European heart journal, 2001, 22, 1561-1571.
55. Y.-H. Kim, H. Furuya and Y. Tabata, Enhancement of bone regeneration by dual release of a macrophage recruitment agent and platelet-rich plasma from gelatin hydrogels, Biomaterials, 2014, 35, 214-224.

56. G. Cinotti, A. Corsi, B. Sacchetti, M. Riminucci, P. Bianco and G. Giannicola, Bone ingrowth and vascular supply in experimental spinal fusion with platelet-rich plasma, Spine, 2013, 38, 385-391.
57. J. D. Kassolis, P. S. Rosen and M. A. Reynolds, Alveolar ridge and sinus augmentation utilizing platelet-rich plasma in combination with freeze-dried bone allograft: case series, Journal of Periodontology, 2000, 71, 1654-1661.
58. R. E. Marx, E. R. Carlson, R. M. Eichstaedt, S. R. Schimmele, J. E. Strauss and K. R. Georgeff, Platelet-rich plasma: growth factor enhancement for bone grafts, Oral Surgery, Oral Medicine, Oral Pathology, Oral Radiology, and Endodontology, 1998, 85, 638-646.
59. G. Weibrich, W. K. Kleis, G. Hafner and W. E. Hitzler, Growth factor levels in platelet-rich plasma and correlations with donor age, sex, and platelet count, Journal of Cranio-Maxillofacial Surgery, 2002, 30, 97-102.
60. I. Andia and N. Maffulli, Platelet-rich plasma for managing pain and inflammation in osteoarthritis, Nature Reviews Rheumatology, 2013, 9, 721-730.
61. J. W. Nichol and A. Khademhosseini, Modular tissue engineering: engineering biological tissues from the bottom up, Soft Matter, 2009, 5, 1312-1319.
62. M. Mizuno and Y. Kuboki, Osteoblast-related gene expression of bone marrow cells during the osteoblastic differentiation induced by type I collagen, Journal of biochemistry, 2001, 129, 133-138.
63. J. M. Anderson, M. Kushwaha, A. Tambralli, S. L. Bellis, R. P. Camata and H.-W. Jun, Osteogenic differentiation of human mesenchymal stem cells directed by extracellular matrix-mimicking ligands in a biomimetic self-assembled peptide amphiphile nanomatrix, Biomacromolecules, 2009, 10, 2935-2944.
64. H. Ceylan, S. Kocabey, H. Unal Gulsuner, O. S. Balcik, M. O. Guler and A. B. Tekinay, Bone-Like Mineral Nucleating Peptide Nanofibers Induce Differentiation of Human Mesenchymal Stem Cells into Mature Osteoblasts, Biomacromolecules, 2014, 15, 2407-2418.
65. K. G. Battiston, J. W. Cheung, D. Jain and J. P. Santerre, Biomaterials in co-culture systems: Towards optimizing tissue integration and cell signaling within scaffolds, Biomaterials, 2014, 35, 4465-4476.
66. P. R. Schneider, C. Buhrmann, A. Mobasheri, U. Matis and M. Shakibaei, Three-dimensional high-density co-culture with primary tenocytes induces tenogenic differentiation in mesenchymal stem cells, Journal of Orthopaedic Research, 2011, 29, 1351-1360.
67. J. Wang, Y. Ye, H. Tian, S. Yang, X. Jin, W. Tong and Y. Zhang, In vitro osteogenesis of human adipose-derived stem cells by coculture with human umbilical vein endothelial cells, Biochemical and biophysical research communications, 2011, 412, 143-149.
68. M. Cooke, A. Allon, T. Cheng, A. Kuo, H. Kim, T. Vail, R. Marcucio, R. Schneider, J. Lotz and T. Alliston, Structured three-dimensional co-culture of mesenchymal stem cells with chondrocytes promotes chondrogenic differentiation without hypertrophy, Osteoarthritis and Cartilage, 2011, 19, 1210-1218.
69. N. Mokarram and R. V. Bellamkonda, A Perspective on Immunomodulation and Tissue Repair, Annals of biomedical engineering, 2014, 42, 338-351.
70. J. A. Jones, D. T. Chang, H. Meyerson, E. Colton, I. K. Kwon, T. Matsuda and J. M. Anderson, Proteomic analysis and quantification of cytokines and chemokines from biomaterial surface-adherent macrophages and foreign body giant cells, Journal of biomedical materials research Part A, 2007, 83, 585-596.
71. L. Zhang, Z. Cao, T. Bai, L. Carr, J.-R. Ella-Menye, C. Irvin, B. D. Ratner and S. Jiang, Zwitterionic hydrogels implanted in mice resist the foreign-body reaction, Nature biotechnology, 2013, 31, 553-556.
72. E. K. Yim and K. W. Leong, Significance of synthetic nanostructures in dictating cellular response, Nanomedicine: Nanotechnology, Biology and Medicine, 2005, 1, 10-21.
73. J. Fink, R. Fuhrmann, T. Scharnweber and R. Franke, Stimulation of monocytes and macrophages: possible influence of surface roughness, Clinical hemorheology and microcirculation, 2008, 39, 205-212.
74. W. J. Kao and Y. Liu, Utilizing biomimetic oligopeptides to probe fibronectin-integrin binding and signaling in regulating macrophage function in vitro and in vivo, Frontiers in bioscience: a journal and virtual library, 2001, 6, D992-999.
75. W. J. Kao and D. Lee, In vivo modulation of host response and macrophage behavior by polymer networks grafted with fibronectin-derived biomimetic oligopeptides: the role of RGD and PHSRN domains, Biomaterials, 2001, 22, 2901-2909.

76. E. M. Hetrick, H. L. Prichard, B. Klitzman and M. H. Schoenfisch, Reduced foreign body response at nitric oxide-releasing subcutaneous implants, Biomaterials, 2007, 28, 4571-4580.
77. S. F. Makrydima, A. C. Pistiki, C. G. Chrelias, V. D. Sioulas, C. S. Siristatidis, E. J. Giamarellos-Bourboulis and D. P. Kassanos, The immunomodulatory and anti-apoptotic effect of dexamethasone in imminent preterm labor: An experimental study, European journal of pharmacology, 2014, 730, 31-35.
78. Y. K. Kim, R. Que, S. W. Wang and W. F. Liu, Modification of biomaterials with a self-protein inhibits the macrophage response, Adv Healthc Mater, 2014, 3, 989-994.
79. S. D. Patil, F. Papadmitrakopoulos and D. J. Burgess, Concurrent delivery of dexamethasone and VEGF for localized inflammation control and angiogenesis, Journal of Controlled Release, 2007, 117, 68-79.
80. J. H. Kehrl, A. B. Roberts, L. M. Wakefield, S. p. Jakowlew, M. Sporn and A. Fauci, Transforming growth factor beta is an important immunomodulatory protein for human B lymphocytes, The Journal of Immunology, 1986, 137, 3855-3860.
81. P.-M. Chen, K.-J. Liu, P.-J. Hsu, C.-F. Wei, C.-H. Bai, L.-J. Ho, H.-K. Sytwu and B. L. Yen, Induction of immunomodulatory monocytes by human mesenchymal stem cell-derived hepatocyte growth factor through ERK1/2, Journal of leukocyte biology, 2014, jlb. 3A0513-0242R.
82. N. G. Singer and A. I. Caplan, Mesenchymal stem cells: mechanisms of inflammation, Annual Review of Pathology: Mechanisms of Disease, 2011, 6, 457-478.
83. S. Hanson, R. N. D'Souza and P. Hematti, Biomaterial–Mesenchymal Stem Cell Constructs for Immunomodulation in Composite Tissue Engineering, Tissue Engineering Part A, 2014, 20, 2162-2168.
84. M. P. Lutolf, P. M. Gilbert and H. M. Blau, Designing materials to direct stem-cell fate, Nature, 2009, 462, 433-441.
85. R. A. Marklein and J. A. Burdick, Controlling stem cell fate with material design, Advanced Materials, 2010, 22, 175-189.
86. N. M. Alves, I. Pashkuleva, R. L. Reis and J. F. Mano, Controlling cell behavior through the design of polymer surfaces, Small, 2010, 6, 2208-2220.
87. V. L. Tsang, A. A. Chen, L. M. Cho, K. D. Jadin, R. L. Sah, S. DeLong, J. L. West and S. N. Bhatia, Fabrication of 3D hepatic tissues by additive photopatterning of cellular hydrogels, The FASEB Journal, 2007, 21, 790-801.
88. D. W. Hutmacher, M. Sittinger and M. V. Risbud, Scaffold-based tissue engineering: rationale for computer-aided design and solid free-form fabrication systems, Trends Biotechnol, 2004, 22, 354-362.
89. F. P. Melchels, M. A. Domingos, T. J. Klein, J. Malda, P. J. Bartolo and D. W. Hutmacher, Additive manufacturing of tissues and organs, Progress in Polymer Science, 2012, 37, 1079-1104.
90. H. Meng, J. Liao, Y. Zhou and Q. Zhang, Laser micro-processing of cardiovascular stent with fiber laser cutting system, Optics & Laser Technology, 2009, 41, 300-302.
91. C.-H. Chen, J. M.-J. Liu, C.-K. Chua, S.-M. Chou, V. B.-H. Shyu and J.-P. Chen, Cartilage tissue engineering with silk fibroin scaffolds fabricated by indirect additive manufacturing technology, Materials, 2014, 7, 2104-2119.
92. J. Zhang, H.-M. Yin, B. S. Hsiao, G.-J. Zhong and Z.-M. Li, Biodegradable poly (lactic acid)/hydroxyl apatite 3D porous scaffolds using high-pressure molding and salt leaching, Journal of Materials Science, 2014, 49, 1648-1658.
93. L. Wu, H. Zhang, J. Zhang and J. Ding, Fabrication of three-dimensional porous scaffolds of complicated shape for tissue engineering. I. Compression molding based on flexible-rigid combined mold, Tissue Eng, 2005, 11, 1105-1114.
94. J. D. Kretlow, L. Klouda and A. G. Mikos, Injectable matrices and scaffolds for drug delivery in tissue engineering, Adv Drug Deliv Rev, 2007, 59, 263-273.
95. S. T. Koshy, T. C. Ferrante, S. A. Lewin and D. J. Mooney, Injectable, porous, and cell-responsive gelatin cryogels, Biomaterials, 2014, 35, 2477-2487.
96. S. Larsson and G. Hannink, Injectable bone-graft substitutes: current products, their characteristics and indications, and new developments, Injury, 2011, 42, S30-S34.
97. D. W. Hutmacher, T. Schantz, I. Zein, K. W. Ng, S. H. Teoh and K. C. Tan, Mechanical properties and cell cultural response of polycaprolactone scaffolds designed and fabricated via fused deposition modeling, J Biomed Mater Res, 2001, 55, 203-216.
98. J. M. Sobral, S. G. Caridade, R. A. Sousa, J. F. Mano and R. L. Reis, Three-dimensional plotted scaffolds with controlled pore size gradients: Effect of scaffold geometry on mechanical performance and cell seeding efficiency, Acta Biomater, 2011, 7, 1009-1018.

99. C. Y. Lin, N. Kikuchi and S. J. Hollister, A novel method for biomaterial scaffold internal architecture design to match bone elastic properties with desired porosity, J Biomech, 2004, 37, 623-636.
100. D. Lacroix, A. Chateau, M. P. Ginebra and J. A. Planell, Micro-finite element models of bone tissue-engineering scaffolds, Biomaterials, 2006, 27, 5326-5334.
101. C. Sandino, J. A. Planell and D. Lacroix, A finite element study of mechanical stimuli in scaffolds for bone tissue engineering, J Biomech, 2008, 41, 1005-1014.
102. C. M. Bidan, K. P. Kommareddy, M. Rumpler, P. Kollmannsberger, P. Fratzl and J. W. Dunlop, Geometry as a factor for tissue growth: towards shape optimization of tissue engineering scaffolds, Advanced healthcare materials, 2013, 2, 186-194.
103. M. Rumpler, A. Woesz, J. W. Dunlop, J. T. van Dongen and P. Fratzl, The effect of geometry on three-dimensional tissue growth, J R Soc Interface, 2008, 5, 1173-1180.
104. S. H. Oh, I. K. Park, J. M. Kim and J. H. Lee, In vitro and in vivo characteristics of PCL scaffolds with pore size gradient fabricated by a centrifugation method, Biomaterials, 2007, 28, 1664-1671.
105. T. Woodfield, C. V. Blitterswijk, J. D. Wijn, T. Sims, A. Hollander and J. Riesle, Polymer scaffolds fabricated with pore-size gradients as a model for studying the zonal organization within tissue-engineered cartilage constructs, Tissue engineering, 2005, 11, 1297-1311.
106. J. Zeltinger, J. K. Sherwood, D. A. Graham, R. Mueller and L. G. Griffith, Effect of pore size and void fraction on cellular adhesion, proliferation, and matrix deposition, Tissue Eng, 2001, 7, 557-572.
107. V. Karageorgiou and D. Kaplan, Porosity of 3D biomaterial scaffolds and osteogenesis, Biomaterials, 2005, 26, 5474-5491.
108. P. Kasten, I. Beyen, P. Niemeyer, R. Luginbühl, M. Bohner and W. Richter, Porosity and pore size of β-tricalcium phosphate scaffold can influence protein production and osteogenic differentiation of human mesenchymal stem cells: an in vitro and in vivo study, Acta Biomaterialia, 2008, 4, 1904-1915.
109. J. M. Karp, F. Sarraf, M. S. Shoichet and J. E. Davies, Fibrin-filled scaffolds for bone-tissue engineering: An in vivo study, J Biomed Mater Res A, 2004, 71, 162-171.
110. C. Correia, W. Grayson, R. Eton, J. M. Gimble, R. A. Sousa, R. L. Reis and G. Vunjak-Novakovic, Human adipose-derived cells can serve as a single-cell source for the in vitro cultivation of vascularized bone grafts, Journal of tissue engineering and regenerative medicine, 2014 8, 629-39.
111. M. Prabaharan, M. A. Rodriguez-Perez, J. A. de Saja and J. F. Mano, Preparation and characterization of poly(L-lactic acid)-chitosan hybrid scaffolds with drug release capability, J Biomed Mater Res B Appl Biomater, 2007, 81, 427-434.
112. J. F. Mano, G. Hungerford and J. L. Gómez Ribelles, Bioactive poly (L-lactic acid)-chitosan hybrid scaffolds, Materials Science and Engineering: C, 2008, 28, 1356-1365.
113. G. Chen, T. Sato, T. Ushida, R. Hirochika, Y. Shirasaki, N. Ochiai and T. Tateishi, The use of a novel PLGA fiber/collagen composite web as a scaffold for engineering of articular cartilage tissue with adjustable thickness, Journal of Biomedical Materials Research Part A, 2003, 67, 1170-1180.
114. S. M. Oliveira, T. H. Silva, R. L. Reis and J. F. Mano, Hierarchical Fibrillar Scaffolds Obtained by Non-conventional Layer-By-Layer Electrostatic Self-Assembly, Advanced healthcare materials, 2013, 2, 422-427.
115. A. J. Engler, S. Sen, H. L. Sweeney and D. E. Discher, Matrix elasticity directs stem cell lineage specification, Cell, 2006, 126, 677-689.
116. F. Guilak, D. M. Cohen, B. T. Estes, J. M. Gimble, W. Liedtke and C. S. Chen, Control of stem cell fate by physical interactions with the extracellular matrix, Cell stem cell, 2009, 5, 17-26.
117. V. E. Santo, M. E. Gomes, J. F. Mano and R. L. Reis, From nano-to macro-scale: nanotechnology approaches for spatially controlled delivery of bioactive factors for bone and cartilage engineering, Nanomedicine, 2012, 7, 1045-1066.
118. V. E. Santo, M. E. Gomes, J. F. Mano and R. L. Reis, Controlled release strategies for bone, cartilage, and osteochondral engineering—part I: recapitulation of native tissue healing and variables for the design of delivery systems, Tissue Engineering Part B: Reviews, 2013, 19, 308-326.
119. S. Madduri and B. Gander, Growth factor delivery systems and repair strategies for damaged peripheral nerves, Journal of Controlled Release, 2012, 161, 274-282.
120. A. C. Lima, P. Sher and J. F. Mano, Production methodologies of polymeric and hydrogel particles for drug delivery applications, Expert Opin Drug Deliv, 2012, 9, 231-248.
121. M. B. Oliveira and J. F. Mano, Polymer-based microparticles in tissue engineering and regenerative medicine, Biotechnol Prog, 2011, 27, 897-912.

122. K. Kim, J. Lam, S. Lu, P. P. Spicer, A. Lueckgen, Y. Tabata, M. E. Wong, J. A. Jansen, A. G. Mikos and F. K. Kasper, Osteochondral tissue regeneration using a bilayered composite hydrogel with modulating dual growth factor release kinetics in a rabbit model, Journal of Controlled Release, 2013, 168, 166-178.
123. N. R. Johnson and Y. Wang, Controlled delivery of heparin-binding EGF-like growth factor yields fast and comprehensive wound healing, J Control Release, 2013, 166, 124-129.
124. Y. Tabata, Tissue regeneration based on growth factor release, Tissue Eng, 2003, 9 Suppl 1, S5-15.
125. T. P. Richardson, M. C. Peters, A. B. Ennett and D. J. Mooney, Polymeric system for dual growth factor delivery, Nat Biotechnol, 2001, 19, 1029-1034.
126. Q. Wang, J. Wang, Q. Lu, M. S. Detamore and C. Berkland, Injectable PLGA based colloidal gels for zero-order dexamethasone release in cranial defects, Biomaterials, 2010, 31, 4980-4986.
127. Y. Wang, B. Gu and D. J. Burgess, Microspheres prepared with PLGA blends for delivery of dexamethasone for implantable medical devices, Pharm Res, 2014, 31, 373-381.
128. A. R. C. Duarte, J. F. Mano and R. L. Reis, Preparation of chitosan scaffolds loaded with dexamethasone for tissue engineering applications using supercritical fluid technology, European Polymer Journal, 2009, 45, 141-148.
129. H. Li and J. Chang, Preparation, characterization and in vitro release of gentamicin from PHBV/wollastonite composite microspheres, J Control Release, 2005, 107, 463-473.
130. P. Gao, X. Nie, M. Zou, Y. Shi and G. Cheng, Recent advances in materials for extended-release antibiotic delivery system, J Antibiot (Tokyo), 2011, 64, 625-634.
131. M. Prabaharan and J. F. Mano, Hydroxypropyl chitosan bearing beta-cyclodextrin cavities: synthesis and slow release of its inclusion complex with a model hydrophobic drug, Macromol Biosci, 2005, 5, 965-973.
132. M. Prabaharan, R. L. Reis and J. F. Mano, Carboxymethyl chitosan-graft-phosphatidylethanolamine: Amphiphilic matrices for controlled drug delivery, Reactive and Functional Polymers, 2007, 67, 43-52.
133. V. E. Santo, A. R. Duarte, E. G. Popa, M. E. Gomes, J. F. Mano and R. L. Reis, Enhancement of osteogenic differentiation of human adipose derived stem cells by the controlled release of platelet lysates from hybrid scaffolds produced by supercritical fluid foaming, J Control Release, 2012, 162, 19-27.
134. J. A. Coppinger, G. Cagney, S. Toomey, T. Kislinger, O. Belton, J. P. McRedmond, D. J. Cahill, A. Emili, D. J. Fitzgerald and P. B. Maguire, Characterization of the proteins released from activated platelets leads to localization of novel platelet proteins in human atherosclerotic lesions, Blood, 2004, 103, 2096-2104.
135. T. Kawase, K. Okuda, L. F. Wolff and H. Yoshie, Platelet-rich plasma-derived fibrin clot formation stimulates collagen synthesis in periodontal ligament and osteoblastic cells in vitro, J Periodontol, 2003, 74, 858-864.
136. Y. H. Kim, H. Furuya and Y. Tabata, Enhancement of bone regeneration by dual release of a macrophage recruitment agent and platelet-rich plasma from gelatin hydrogels, Biomaterials, 2014, 35, 214-224.
137. A. Perets, Y. Baruch, F. Weisbuch, G. Shoshany, G. Neufeld and S. Cohen, Enhancing the vascularization of three-dimensional porous alginate scaffolds by incorporating controlled release basic fibroblast growth factor microspheres, J Biomed Mater Res A, 2003, 65, 489-497.
138. F. Gilde, O. Maniti, R. Guillot, J. F. Mano, D. Logeart-Avramoglou, F. Sailhan and C. Picart, Secondary structure of rhBMP-2 in a protective biopolymeric carrier material, Biomacromolecules, 2012, 13, 3620-3626.
139. L. I. Cabezas, I. Gracia, A. de Lucas and J. F. Rodríguez, Novel Model for the Description of the Controlled Release of 5-Fluorouracil from PLGA and PLA Foamed Scaffolds Impregnated in Supercritical CO2, Industrial & Engineering Chemistry Research, 2014.
140. M. Biondi, F. Ungaro, F. Quaglia and P. A. Netti, Controlled drug delivery in tissue engineering, Advanced Drug Delivery Reviews, 2008, 60, 229-242.
141. R. R. Costa, C. A. Custodio, A. M. Testera, F. J. Arias, J. C. Rodríguez-Cabello, N. M. Alves and J. F. Mano, Stimuli-Responsive Thin Coatings Using Elastin-Like Polymers for Biomedical Applications, Advanced Functional Materials, 2009, 19, 3210-3218.
142. J. Borges, L. C. Rodrigues, R. L. Reis and J. F. Mano, Layer-by-Layer Assembly of Light-Responsive Polymeric Multilayer Systems, Advanced Functional Materials, 2014, 24, 5624-48.

143. J. F. Mano, Stimuli-Responsive Polymeric Systems for Biomedical Applications, Advanced Engineering Materials, 2008, 10, 515-527.
144. M. A. Stuart, W. T. Huck, J. Genzer, M. Muller, C. Ober, M. Stamm, G. B. Sukhorukov, I. Szleifer, V. V. Tsukruk, M. Urban, F. Winnik, S. Zauscher, I. Luzinov and S. Minko, Emerging applications of stimuli-responsive polymer materials, Nat Mater, 2010, 9, 101-113.
145. R. M. da Silva, J. F. Mano and R. L. Reis, Smart thermoresponsive coatings and surfaces for tissue engineering: switching cell-material boundaries, Trends Biotechnol, 2007, 25, 577-583.
146. J. Shi, N. M. Alves and J. F. Mano, Thermally responsive biomineralization on biodegradable substrates, Advanced Functional Materials, 2007, 17, 3312-3318.
147. M. A. Cole, N. H. Voelcker, H. Thissen and H. J. Griesser, Stimuli-responsive interfaces and systems for the control of protein-surface and cell-surface interactions, Biomaterials, 2009, 30, 1827-1850.
148. S. Kern, H. Eichler, J. Stoeve, H. Kluter and K. Bieback, Comparative analysis of mesenchymal stem cells from bone marrow, umbilical cord blood, or adipose tissue, Stem Cells, 2006, 24, 1294-1301.
149. G. Chamberlain, J. Fox, B. Ashton and J. Middleton, Concise review: mesenchymal stem cells: their phenotype, differentiation capacity, immunological features, and potential for homing, Stem cells, 2007, 25, 2739-2749.
150. P. Bianco, M. Riminucci, S. Gronthos and P. G. Robey, Bone marrow stromal stem cells: nature, biology, and potential applications, Stem Cells, 2001, 19, 180-192.
151. J. S. Odorico, D. S. Kaufman and J. A. Thomson, Multilineage differentiation from human embryonic stem cell lines, Stem Cells, 2001, 19, 193-204.
152. E. Rodriguez, M. Perez, P. Casanova and L. Martinez, in Animal Cell Technology: From Target to Market, Springer, 2001, pp. 434-437.
153. Q. Wen-tao, Z. Ying, M. Juan, G. Xin, X. Yu-bing, W. Wei and M. Xiaojun, Optimization of the cell seeding density and modeling of cell growth and metabolism using the modified Gompertz model for microencapsulated animal cell culture, Biotechnology and bioengineering, 2006, 93, 887-895.
154. A. Dar, M. Shachar, J. Leor and S. Cohen, Optimization of cardiac cell seeding and distribution in 3D porous alginate scaffolds, Biotechnol Bioeng, 2002, 80, 305-312.
155. Y. Poumay and M. R. Pittelkow, Cell density and culture factors regulate keratinocyte commitment to differentiation and expression of suprabasal K1/K10 keratins, J Invest Dermatol, 1995, 104, 271-276.
156. S. Masur, H. Dewal, T. Dinh, I. Erenburg and S. Petridou, Myofibroblasts differentiate from fibroblasts when plated at low density, Proceedings of the National Academy of Sciences, 1996, 93, 4219-4223.
157. C. M. Lee and J. Hu, Cell density during differentiation can alter the phenotype of bone marrow-derived macrophages, Cell & bioscience, 2013, 3, 30-30.
158. M. Bitar, R. A. Brown, V. Salih, A. G. Kidane, J. C. Knowles and S. N. Nazhat, Effect of cell density on osteoblastic differentiation and matrix degradation of biomimetic dense collagen scaffolds, Biomacromolecules, 2008, 9, 129-135.
159. M. S. Lord, M. Foss and F. Besenbacher, Influence of nanoscale surface topography on protein adsorption and cellular response, Nano Today, 2010, 5, 66-78.
160. P. Roach, D. Farrar and C. C. Perry, Surface tailoring for controlled protein adsorption: effect of topography at the nanometer scale and chemistry, Journal of the American Chemical Society, 2006, 128, 3939-3945.
161. G. Raffaini and F. Ganazzoli, Surface topography effects in protein adsorption on nanostructured carbon allotropes, Langmuir, 2013, 29, 4883-4893.
162. W. Song and J. F. Mano, Interactions between cells or proteins and surfaces exhibiting extreme wettabilities, Soft Matter, 2013, 9, 2985-2999.
163. S. M. Oliveira, N. M. Alves and J. F. Mano, Cell interactions with superhydrophilic and superhydrophobic surfaces, Journal of Adhesion Science and Technology, 2014, 28, 843-863.
164. R. McBeath, D. M. Pirone, C. M. Nelson, K. Bhadriraju and C. S. Chen, Cell shape, cytoskeletal tension, and RhoA regulate stem cell lineage commitment, Dev Cell, 2004, 6, 483-495.
165. R. Singhvi, A. Kumar, G. P. Lopez, G. N. Stephanopoulos, D. I. Wang, G. M. Whitesides and D. E. Ingber, Engineering cell shape and function, Science, 1994, 264, 696-698.
166. L. Chou, J. D. Firth, V. J. Uitto and D. M. Brunette, Substratum surface topography alters cell shape and regulates fibronectin mRNA level, mRNA stability, secretion and assembly in human fibroblasts, J Cell Sci, 1995, 108 (Pt 4), 1563-1573.

167. P. B. Lucker, S. Javaherian, J. P. Soleas, D. Halverson, P. W. Zandstra and A. P. McGuigan, A microgroove patterned multiwell cell culture plate for high-throughput studies of cell alignment, Biotechnol Bioeng, 2014.
168. V. Hosseini, P. Kollmannsberger, S. Ahadian, S. Ostrovidov, H. Kaji, V. Vogel and A. Khademhosseini, Fiber-Assisted Molding (FAM) of Surfaces with Tunable Curvature to Guide Cell Alignment and Complex Tissue Architecture, Small, 2014.
169. K. E. McCloskey, in Emerging Trends in Cell and Gene Therapy, Springer, 2013, pp. 471-483.
170. Y. L. Han, S. Wang, X. Zhang, Y. Li, G. Huang, H. Qi, B. Pingguan-Murphy, Y. Li, T. J. Lu and F. Xu, Engineering physical microenvironment for stem cell based regenerative medicine, Drug discovery today, 2014.
171. M. Lutolf and J. Hubbell, Synthetic biomaterials as instructive extracellular microenvironments for morphogenesis in tissue engineering, Nature biotechnology, 2005, 23, 47-55.
172. T. Dvir, B. P. Timko, D. S. Kohane and R. Langer, Nanotechnological strategies for engineering complex tissues, Nature nanotechnology, 2011, 6, 13-22.
173. D. A. Brafman, Constructing stem cell microenvironments using bioengineering approaches, Physiological genomics, 2013, 45, 1123-1135.
174. H. Gitay-Goren, S. Soker, I. Vlodavsky and G. Neufeld, The binding of vascular endothelial growth factor to its receptors is dependent on cell surface-associated heparin-like molecules, Journal of Biological Chemistry, 1992, 267, 6093-6098.
175. W. J. King and P. H. Krebsbach, Growth factor delivery: How surface interactions modulate release in vitro and in vivo, Advanced drug delivery reviews, 2012, 64, 1239-1256.
176. J. E. Saik, D. J. Gould, E. M. Watkins, M. E. Dickinson and J. L. West, Covalently immobilized platelet-derived growth factor-BB promotes angiogenesis in biomimetic poly(ethylene glycol) hydrogels, Acta Biomater, 2011, 7, 133-143.
177. Y. Zhang, J. Venugopal, Z.-M. Huang, C. Lim and S. Ramakrishna, Characterization of the surface biocompatibility of the electrospun PCL-collagen nanofibers using fibroblasts, Biomacromolecules, 2005, 6, 2583-2589.
178. B. Sayyar, M. Dodd, L. Marquez-Curtis, A. Janowska-Wieczorek and G. Hortelano, Fibronectin-Alginate microcapsules improve cell viability and protein secretion of encapsulated Factor IX-engineered human mesenchymal stromal cells, Artif Cells Nanomed Biotechnol, 2014, 1-10.
179. J. van den Dolder, G. N. Bancroft, V. I. Sikavitsas, P. H. Spauwen, A. G. Mikos and J. A. Jansen, Effect of fibronectin-and collagen I-coated titanium fiber mesh on proliferation and differentiation of osteogenic cells, Tissue engineering, 2003, 9, 505-515.
180. D. S. da Costa, R. A. Pires, A. M. Frias, R. L. Reis and I. Pashkuleva, Sulfonic groups induce formation of filopodia in mesenchymal stem cells, Journal of Materials Chemistry, 2012, 22, 7172-7178.
181. S. Amorim, R. A. Pires, D. S. d. Costa, R. L. Reis and I. Pashkuleva, Interactions between exogenous FGF-2 and sulfonic groups: in situ characterization and impact on the morphology of human adipose-derived stem cells, Langmuir, 2013, 29, 7983-7992.
182. Y. Arima and H. Iwata, Effect of wettability and surface functional groups on protein adsorption and cell adhesion using well-defined mixed self-assembled monolayers, Biomaterials, 2007, 28, 3074-3082.
183. U. Hersel, C. Dahmen and H. Kessler, RGD modified polymers: biomaterials for stimulated cell adhesion and beyond, Biomaterials, 2003, 24, 4385-4415.
184. S. P. Massia and J. A. Hubbell, An RGD spacing of 440 nm is sufficient for integrin alpha V beta 3-mediated fibroblast spreading and 140 nm for focal contact and stress fiber formation, The Journal of cell biology, 1991, 114, 1089-1100.
185. S. P. Massia and J. A. Hubbell, Convalent surface immobilization of Arg-Gly-Asp-and Tyr-Ile-Gly-Ser-Arg-containing peptides to obtain well-defined cell-adhesive substrates, Analytical biochemistry, 1990, 187, 292-301.
186. C. S. Chen, J. Tan and J. Tien, Mechanotransduction at cell-matrix and cell-cell contacts, Annu. Rev. Biomed. Eng., 2004, 6, 275-302.
187. M. Lambert, F. Padilla and R. M. Mège, Immobilized dimers of N-cadherin-Fc chimera mimic cadherin-mediated cell contact formation: contribution of both outside-in and inside-out signals, Journal of cell science, 2000, 113, 2207-2219.
188. E. Jan and N. A. Kotov, Successful differentiation of mouse neural stem cells on layer-by-layer assembled single-walled carbon nanotube composite, Nano Lett, 2007, 7, 1123-1128.

189. M. L. Macdonald, R. E. Samuel, N. J. Shah, R. F. Padera, Y. M. Beben and P. T. Hammond, Tissue integration of growth factor-eluting layer-by-layer polyelectrolyte multilayer coated implants, Biomaterials, 2011, 32, 1446-1453.
190. S. M. Oliveira, T. H. Silva, R. L. Reis and J. F. Mano, Nanocoatings containing sulfated polysaccharides prepared by layer-by-layer assembly as models to study cell–material interactions, Journal of Materials Chemistry B, 2013, 1, 4406-4418.
191. A. I. Neto, A. C. Cibrao, C. R. Correia, R. R. Carvalho, G. M. Luz, G. G. Ferrer, G. Botelho, C. Picart, N. M. Alves and J. F. Mano, Nanostructured polymeric coatings based on chitosan and dopamine-modified hyaluronic acid for biomedical applications, Small, 2014, 10, 2459-2469.
192. G. V. Martins, E. G. Merino, J. F. Mano and N. M. Alves, Crosslink effect and albumin adsorption onto chitosan/alginate multilayered systems: an in situ QCM-D study, Macromol Biosci, 2010, 10, 1444-1455.
193. C. A. Custodio, V. San Miguel-Arranz, R. A. Gropeanu, M. Gropeanu, M. Wirkner, R. L. Reis, J. F. Mano and A. del Campo, Photopatterned antibodies for selective cell attachment, Langmuir, 2014, 30, 10066-10071.
194. C. Custódio, V. Santo, M. Oliveira, M. Gomes, R. Reis and J. Mano, Functionalized Microparticles Producing Scaffolds in Combination with Cells, Advanced Functional Materials, 2014, 24, 1391-1400.
195. A. I. Neto, C. A. Custódio, W. Song and J. F. Mano, High-throughput evaluation of interactions between biomaterials, proteins and cells using patterned superhydrophobic substrates, Soft Matter, 2011, 7, 4147-4151.
196. S. M. Oliveira, W. Song, N. M. Alves and J. F. Mano, Chemical modification of bioinspired superhydrophobic polystyrene surfaces to control cell attachment/proliferation, Soft Matter, 2011, 7, 8932-8941.
197. N. M. Alves, J. Shi, E. Oramas, J. L. Santos, H. Tomas and J. F. Mano, Bioinspired superhydrophobic poly(L-lactic acid) surfaces control bone marrow derived cells adhesion and proliferation, J Biomed Mater Res A, 2009, 91, 480-488.
198. W. Song, D. D. Veiga, C. A. Custódio and J. F. Mano, Bioinspired Degradable Substrates with Extreme Wettability Properties, Advanced Materials, 2009, 21, 1830-1834.
199. R. A. Gittens, L. Scheideler, F. Rupp, S. L. Hyzy, J. Geis-Gerstorfer, Z. Schwartz and B. D. Boyan, A review on the wettability of dental implant surfaces II: Biological and clinical aspects, Acta biomaterialia, 2014.
200. S. Haik, L. R. Gauthier, C. Granotier, J.-M. Peyrin, C. S. Lages, D. Dormont and F. D. Boussin, Fibroblast growth factor 2 up regulates telomerase activity in neural precursor cells, Oncogene, 2000, 19, 2957-2966.
201. P. Salehinejad, N. B. Alitheen, A. Mandegary, S. N. Nematollahi-mahani and E. Janzamin, Effect of EGF and FGF on the expansion properties of human umbilical cord mesenchymal cells, In Vitro Cellular & Developmental Biology-Animal, 2013, 49, 515-523.
202. J. Oh, Y. D. Lee and A. J. Wagers, Stem cell aging: mechanisms, regulators and therapeutic opportunities, Nature medicine, 2014, 20, 870-880.
203. C. Yang, M. W. Tibbitt, L. Basta and K. S. Anseth, Mechanical memory and dosing influence stem cell fate, Nature materials, 2014.
204. G.-S. Huang, P.-S. Hsieh, C.-S. Tseng and S.-h. Hsu, The substrate-dependent regeneration capacity of mesenchymal stem cell spheroids derived on various biomaterial surfaces, Biomaterials Science, 2014.
205. S.-h. Hsu and G.-s. Huang, Substrate-dependent Wnt signaling in MSC differentiation within biomaterial-derived 3D spheroids, Biomaterials, 2013, 34, 4725-4738.
206. Z. Li, C. Liu, Z. Xie, P. Song, R. C. Zhao, L. Guo, Z. Liu and Y. Wu, Epigenetic dysregulation in mesenchymal stem cell aging and spontaneous differentiation, PloS one, 2011, 6, e20526.
207. K. A. Kilian, B. Bugarija, B. T. Lahn and M. Mrksich, Geometric cues for directing the differentiation of mesenchymal stem cells, Proceedings of the National Academy of Sciences, 2010, 107, 4872-4877.
208. G. C. Reilly and A. J. Engler, Intrinsic extracellular matrix properties regulate stem cell differentiation, Journal of biomechanics, 2010, 43, 55-62.
209. X. Wu, Y. Liu, X. Li, P. Wen, Y. Zhang, Y. Long, X. Wang, Y. Guo, F. Xing and J. Gao, Preparation of aligned porous gelatin scaffolds by unidirectional freeze-drying method, Acta Biomater, 2010, 6, 1167-1177.
210. M.-H. Ho, P.-Y. Kuo, H.-J. Hsieh, T.-Y. Hsien, L.-T. Hou, J.-Y. Lai and D.-M. Wang, Preparation of porous scaffolds by using freeze-extraction and freeze-gelation methods, Biomaterials, 2004, 25, 129-138.

211. C. R. Correia, L. S. Moreira-Teixeira, L. Moroni, R. L. Reis, C. A. van Blitterswijk, M. Karperien and J. F. Mano, Chitosan scaffolds containing hyaluronic acid for cartilage tissue engineering, Tissue Eng Part C Methods, 2011, 17, 717-730.
212. N. Thadavirul, P. Pavasant and P. Supaphol, Development of polycaprolactone porous scaffolds by combining solvent casting, particulate leaching, and polymer leaching techniques for bone tissue engineering, J Biomed Mater Res A, 2014, 102, 3379-3392.
213. D. Sin, X. Miao, G. Liu, F. Wei, G. Chadwick, C. Yan and T. Friis, Polyurethane (PU) scaffolds prepared by solvent casting/particulate leaching (SCPL) combined with centrifugation, Materials Science and Engineering: C, 2010, 30, 78-85.
214. S. S. Silva, S. G. Caridade, J. F. Mano and R. L. Reis, Effect of crosslinking in chitosan/aloe vera-based membranes for biomedical applications, Carbohydr Polym, 2013, 98, 581-588.
215. J. Mota, N. Yu, S. G. Caridade, G. M. Luz, M. E. Gomes, R. L. Reis, J. A. Jansen, X. F. Walboomers and J. F. Mano, Chitosan/bioactive glass nanoparticle composite membranes for periodontal regeneration, Acta Biomater, 2012, 8, 4173-4180.
216. H. Yoshimoto, Y. M. Shin, H. Terai and J. P. Vacanti, A biodegradable nanofiber scaffold by electrospinning and its potential for bone tissue engineering, Biomaterials, 2003, 24, 2077-2082.
217. X. Zong, H. Bien, C. Y. Chung, L. Yin, D. Fang, B. S. Hsiao, B. Chu and E. Entcheva, Electrospun fine-textured scaffolds for heart tissue constructs, Biomaterials, 2005, 26, 5330-5338.
218. S. H. Park, T. G. Kim, H. C. Kim, D. Y. Yang and T. G. Park, Development of dual scale scaffolds via direct polymer melt deposition and electrospinning for applications in tissue regeneration, Acta Biomater, 2008, 4, 1198-1207.
219. S. Yang, K.-F. Leong, Z. Du and C.-K. Chua, The design of scaffolds for use in tissue engineering. Part II. Rapid prototyping techniques, Tissue engineering, 2002, 8, 1-11.
220. R. Landers, U. Hubner, R. Schmelzeisen and R. Mulhaupt, Rapid prototyping of scaffolds derived from thermoreversible hydrogels and tailored for applications in tissue engineering, Biomaterials, 2002, 23, 4437-4447.
221. N. A. Silva, A. J. Salgado, R. A. Sousa, J. T. Oliveira, A. J. Pedro, H. Leite-Almeida, R. Cerqueira, A. Almeida, F. Mastronardi, J. F. Mano, N. Sousa, N. M. Neves and R. L. Reis, Development and characterization of a Novel Hybrid Tissue Engineering–based scaffold for spinal cord injury repair, Tissue Engineering Part A, 2009, 16, 45-54.
222. A. R. C. Duarte, J. F. Mano and R. L. Reis, The role of organic solvent on the preparation of chitosan scaffolds by supercritical assisted phase inversion, The Journal of Supercritical Fluids, 2012, 72, 326-332.
223. M. Yeo and G. Kim, Cell-printed hierarchical scaffolds consisting of micro-sized polycaprolactone (PCL) and electrospun PCL nanofibers/cell-laden alginate struts for tissue regeneration, Journal of Materials Chemistry B, 2014, 2, 314-324.
224. W. Wang, D. Li, M.-c. Wang and Y.-l. Li, A hybrid scaffold of poly (lactide-co-glycolide) sponge filled with fibrin gel for cartilage tissue engineering, Chinese Journal of Polymer Science, 2011, 29, 233-240.
225. M. G. Yeo and G. H. Kim, Preparation and characterization of 3D composite scaffolds based on rapid-prototyped PCL/β-TCP struts and electrospun PCL coated with collagen and HA for bone regeneration, Chemistry of Materials, 2011, 24, 903-913.
226. K. Tuzlakoglu, N. Bolgen, A. J. Salgado, M. E. Gomes, E. Piskin and R. L. Reis, Nano- and micro-fiber combined scaffolds: a new architecture for bone tissue engineering, J Mater Sci Mater Med, 2005, 16, 1099-1104.
227. M. I. Santos, K. Tuzlakoglu, S. Fuchs, M. E. Gomes, K. Peters, R. E. Unger, E. Piskin, R. L. Reis and C. J. Kirkpatrick, Endothelial cell colonization and angiogenic potential of combined nano- and micro-fibrous scaffolds for bone tissue engineering, Biomaterials, 2008, 29, 4306-4313.
228. S. H. Park, U. H. Koh, M. Kim, D. Y. Yang, K. Y. Suh and J. H. Shin, Hierarchical multilayer assembly of an ordered nanofibrous scaffold via thermal fusion bonding, Biofabrication, 2014, 6, 024107.
229. Z. Tang, Y. Wang, P. Podsiadlo and N. A. Kotov, Biomedical Applications of Layer-by-Layer Assembly: From Biomimetics to Tissue Engineering, Advanced Materials, 2006, 18, 3203-3224.
230. J. Borges and J. F. Mano, Molecular Interactions Driving the Layer-by-Layer Assembly of Multilayers, Chem Rev, 2014, 114, 8883-8942.

231. E. S. Miranda, T. H. Silva, R. L. Reis and J. F. Mano, Nanostructured natural-based polyelectrolyte multilayers to agglomerate chitosan particles into scaffolds for tissue engineering, Tissue Engineering Part A, 2011, 17, 2663-2674.
232. P. Sher, C. A. Custódio and J. Mano, Layer-By-Layer Technique for Producing Porous Nanostructured 3D Constructs Using Moldable Freeform Assembly of Spherical Templates, Small, 2010, 6, 2644-2648.
233. J. M. Silva, N. Georgi, R. Costa, P. Sher, R. L. Reis, C. A. Van Blitterswijk, M. Karperien and J. F. Mano, Nanostructured 3D constructs based on chitosan and chondroitin sulphate multilayers for cartilage tissue engineering, PloS one, 2013, 8, e55451.
234. C. R. Correia, R. L. Reis and J. F. Mano, Multilayered hierarchical capsules providing cell adhesion sites, Biomacromolecules, 2013, 14, 743-751.
235. R. R. Costa, E. Castro, F. J. Arias, J. C. Rodriguez-Cabello and J. F. Mano, Multifunctional compartmentalized capsules with a hierarchical organization from the nano to the macro scales, Biomacromolecules, 2013, 14, 2403-2410.
236. R. R. Costa and J. F. Mano, Polyelectrolyte multilayered assemblies in biomedical technologies, Chem Soc Rev, 2014, 43, 3453-3479.
237. A. P. McGuigan and M. V. Sefton, Vascularized organoid engineered by modular assembly enables blood perfusion, Proceedings of the National Academy of Sciences, 2006, 103, 11461-11466.
238. M. B. Oliveira, W. Song, L. Martín, S. M. Oliveira, S. G. Caridade, M. Alonso, J. C. Rodríguez-Cabello and J. F. Mano, Development of an injectable system based on elastin-like recombinamer particles for tissue engineering applications, Soft Matter, 2011, 7, 6426-6434.
239. D. M. García Cruz, J. L. Escobar Ivirico, M. M. Gomes, J. L. Gómez Ribelles, M. S. Sánchez, R. L. Reis and J. F. Mano, Chitosan microparticles as injectable scaffolds for tissue engineering, Journal of tissue engineering and regenerative medicine, 2008, 2, 378-380.
240. J. Yang, M. Yamato, C. Kohno, A. Nishimoto, H. Sekine, F. Fukai and T. Okano, Cell sheet engineering: recreating tissues without biodegradable scaffolds, Biomaterials, 2005, 26, 6415-6422.
241. J. Yang, M. Yamato, T. Shimizu, H. Sekine, K. Ohashi, M. Kanzaki, T. Ohki, K. Nishida and T. Okano, Reconstruction of functional tissues with cell sheet engineering, Biomaterials, 2007, 28, 5033-5043.
242. P. Chetprayoon, K. Kadowaki, M. Matsusaki and M. Akashi, Survival and structural evaluations of three-dimensional tissues fabricated by the hierarchical cell manipulation technique, Acta biomaterialia, 2013, 9, 4698-4706.
243. M. Matsusaki, Development of three-dimensional tissue models based on hierarchical cell manipulation using nanofilms, Bulletin of the Chemical Society of Japan, 2012, 85, 401-414.
244. H. Abe, Y. Hara, S. Maeda and S. Hashimoto, Surface Modification Method for Adhesion of Gels, Chemistry Letters, 2014, 43, 243-245.
245. H. Abe, Y. Hara, S. Maeda and S. Hashimoto, Adhesion of Gels by Silica Particle, The Journal of Physical Chemistry B, 2014, 118, 2518-2522.
246. H. Tamagawa and Y. Takahashi, Adhesion force behavior between two gels attached with an electrolytic polymer liquid, Materials Chemistry and Physics, 2008, 107, 164-170.
247. S. Katayama, S. Maeda, Y. Hara and S. Hashimoto, A self-assembling method for polymer gel components, 2013, 79-84.
248. F. Xu, T. D. Finley, M. Turkaydin, Y. Sung, U. A. Gurkan, A. S. Yavuz, R. O. Guldiken and U. Demirci, The assembly of cell-encapsulating microscale hydrogels using acoustic waves, Biomaterials, 2011, 32, 7847-7855.
249. Y. L. Han, Y. Yang, S. Liu, J. Wu, Y. Chen, T. J. Lu and F. Xu, Directed self-assembly of microscale hydrogels by electrostatic interaction, Biofabrication, 2013, 5, 035004.
250. Y. Du, E. Lo, S. Ali and A. Khademhosseini, Directed assembly of cell-laden microgels for fabrication of 3D tissue constructs, Proceedings of the National Academy of Sciences, 2008, 105, 9522-9527.
251. G. R. Souza, J. R. Molina, R. M. Raphael, M. G. Ozawa, D. J. Stark, C. S. Levin, L. F. Bronk, J. S. Ananta, J. Mandelin and M.-M. Georgescu, Three-dimensional tissue culture based on magnetic cell levitation, Nature nanotechnology, 2010, 5, 291-296.
252. E. Castro and J. F. Mano, Magnetic force-based tissue engineering and regenerative medicine, J Biomed Nanotechnol, 2013, 9, 1129-1136.
253. F. Xu, C. a. M. Wu, V. Rengarajan, T. D. Finley, H. O. Keles, Y. Sung, B. Li, U. A. Gurkan and U. Demirci, Three-Dimensional Magnetic Assembly of Microscale Hydrogels, Advanced Materials, 2011, 23, 4254-4260.

254. W. Liu, Y. Li, S. Feng, J. Ning, J. Wang, M. Gou, H. Chen, F. Xu and Y. Du, Magnetically controllable 3D microtissues based on magnetic microcryogels, Lab on a Chip, 2014.
255. S. Gil and J. F. Mano, Magnetic composite biomaterials for tissue engineering, Biomaterials Science, 2014, 2, 812-818.
256. S. E. Chung, Y. Jung and S. Kwon, Three-Dimensional Fluidic Self-Assembly by Axis Translation of Two-Dimensionally Fabricated Microcomponents in Railed Microfluidics, small, 2011, 7, 796-803.
257. L. Leng, A. McAllister, B. Zhang, M. Radisic and A. Günther, Mosaic Hydrogels: One-Step Formation of Multiscale Soft Materials, Advanced materials, 2012, 24, 3650-3658.
258. H. Qi, M. Ghodousi, Y. Du, C. Grun, H. Bae, P. Yin and A. Khademhosseini, DNA-directed self-assembly of shape-controlled hydrogels, Nature communications, 2013, 4.
259. R. Deschner, H. Tang, P. Allen, C. Hall, R. Hlis, A. Ellington and C. G. Willson, Progress Report on the Generation of Polyfunctional Microscale Particles for Programmed Self-Assembly, Chemistry of Materials, 2014, 26, 1457-1462.
260. W. Schuurman, V. Khristov, M. Pot, P. Van Weeren, W. Dhert and J. Malda, Bioprinting of hybrid tissue constructs with tailorable mechanical properties, Biofabrication, 2011, 3, 021001.
261. D. B. Kolesky, R. L. Truby, A. Gladman, T. A. Busbee, K. A. Homan and J. A. Lewis, 3D Bioprinting of Vascularized, Heterogeneous Cell-Laden Tissue Constructs, Advanced Materials, 2014, 26, 3124-3130.
262. S. J. Hollister and W. L. Murphy, Scaffold translation: barriers between concept and clinic, Tissue Engineering Part B: Reviews, 2011, 17, 459-474.
263. J. Walpole, J. A. Papin and S. M. Peirce, Multiscale computational models of complex biological systems, Annual review of biomedical engineering, 2013, 15, 137.
264. S. K. Choi, J. K. Park, K. M. Lee, S. K. Lee and W. B. Jeon, Improved neural progenitor cell proliferation and differentiation on poly (lactide-co-glycolide) scaffolds coated with elastin-like polypeptide, Journal of Biomedical Materials Research Part B: Applied Biomaterials, 2013, 101, 1329-1339.
265. A. Assmann, C. Delfs, H. Munakata, F. Schiffer, K. Horstkötter, K. Huynh, M. Barth, V. R. Stoldt, H. Kamiya and U. Boeken, Acceleration of autologous *in vivo* recellularization of decellularized aortic conduits by fibronectin surface coating, Biomaterials, 2013, 34, 6015-6026.
266. Y. B. Truong, V. Glattauer, K. L. Briggs, S. Zappe and J. A. Ramshaw, Collagen-based layer-by-layer coating on electrospun polymer scaffolds, Biomaterials, 2012, 33, 9198-9204.
267. G. Ragetly, D. J. Griffon and Y. S. Chung, The effect of type II collagen coating of chitosan fibrous scaffolds on mesenchymal stem cell adhesion and chondrogenesis, Acta biomaterialia, 2010, 6, 3988-3997.
268. M. L. Macdonald, R. E. Samuel, N. J. Shah, R. F. Padera, Y. M. Beben and P. T. Hammond, Tissue integration of growth factor-eluting layer-by-layer polyelectrolyte multilayer coated implants, Biomaterials, 2011, 32, 1446-1453.
269. T. Crouzier, F. Sailhan, P. Becquart, R. Guillot, D. Logeart-Avramoglou and C. Picart, The performance of BMP-2 loaded TCP/HAP porous ceramics with a polyelectrolyte multilayer film coating, Biomaterials, 2011, 32, 7543-7554.
270. S. Tang, J. Zhu, Y. Xu, A. P. Xiang, M. H. Jiang and D. Quan, The effects of gradients of nerve growth factor immobilized PCLA scaffolds on neurite outgrowth *in vitro* and peripheral nerve regeneration in rats, Biomaterials, 2013, 34, 7086-7096.
271. N. J. Shah, M. N. Hyder, M. A. Quadir, N.-M. D. Courchesne, H. J. Seeherman, M. Nevins, M. Spector and P. T. Hammond, Adaptive growth factor delivery from a polyelectrolyte coating promotes synergistic bone tissue repair and reconstruction, Proceedings of the National Academy of Sciences, 2014, 201408035.
272. J. S. Lee, J. S. Lee, A. Wagoner-Johnson and W. L. Murphy, Modular Peptide Growth Factors for Substrate-Mediated Stem Cell Differentiation, Angewandte Chemie, 2009, 121, 6384-6387.
273. C. Zhou, X. Ye, Y. Fan, L. Ma, Y. Tan, F. Qing and X. Zhang, Biomimetic fabrication of a three-level hierarchical calcium phosphate/collagen/hydroxyapatite scaffold for bone tissue engineering, Biofabrication, 2014, 6, 035013.
274. M. Lima, R. Pirraco, R. Sousa, N. Neves, A. Marques, M. Bhattacharya, V. Correlo and R. Reis, Bottom-up approach to construct microfabricated multi-layer scaffolds for bone tissue engineering, Biomedical microdevices, 2014, 16, 69-78.
275. M. E. Kolewe, H. Park, C. Gray, X. Ye, R. Langer and L. E. Freed, 3D structural patterns in scalable, elastomeric scaffolds guide engineered tissue architecture, Advanced Materials, 2013, 25, 4459-4465.

276. V. E. Santo, A. R. C. Duarte, E. G. Popa, M. E. Gomes, J. F. Mano and R. L. Reis, Enhancement of osteogenic differentiation of human adipose derived stem cells by the controlled release of platelet lysates from hybrid scaffolds produced by supercritical fluid foaming, Journal of Controlled Release, 2012, 162, 19-27.
277. R. Levato, J. Visser, J. A. Planell, E. Engel, J. Malda and M. A. Mateos-Timoneda, Biofabrication of tissue constructs by 3D bioprinting of cell-laden microcarriers, Biofabrication, 2014, 6, 035020.
278. M. B. Oliveira, C. L. Salgado, W. Song and J. F. Mano, Combinatorial On-Chip Study of Miniaturized 3D Porous Scaffolds Using a Patterned Superhydrophobic Platform, Small, 2013, 9, 768-778.
279. M. B. Oliveira, M. P. Ribeiro, S. P. Miguel, A. I. Neto, P. Coutinho, I. J. Correia and J. F. Mano, *In Vivo* High-Content Evaluation of Three-Dimensional Scaffolds Biocompatibility, Tissue Eng Part C Methods, 2014.
280. A. L. Hook, D. G. Anderson, R. Langer, P. Williams, M. C. Davies and M. R. Alexander, High throughput methods applied in biomaterial development and discovery, Biomaterials, 2010, 31, 187-198.
281. C. G. Simon, Jr. and S. Lin-Gibson, Combinatorial and high-throughput screening of biomaterials, Adv Mater, 2011, 23, 369-387.

SECTION 2

EXPERIMENTAL SECTION

CHAPTER II

MATERIALS AND METHODS

CHAPTER II

Materials and Methods

This chapter details the materials, methods and techniques used during the course of the work developed in this thesis. This chapter intends to provide a more comprehensive and detailed description of the rationale of the developed methods

II.1. Materials

Several strategies in tissue engineering focus on recapitulating instructive characteristics of the extracellular matrix (ECM) into the 3D constructs. Natural origin materials have been among the materials of highest interest due to the high chemical similarity to ECM, biodegradation, and the presence of more cell recognition sites. Synthetic biomaterials are also widely used and may allow the preparation of systems with higher mechanical stability and lower batch-to-batch associated variability. In this thesis, a combination of synthetic with natural polymers was used as the source of mechanical stability, higher shape control and, as a source of instructive cues, respectively.

Five major classes of materials were used for the development of the 2D nanocoatings and the 3D multiscale scaffolds, specifically alginate, chitosan, carrageenan, heparin and polycaprolactone. Platelet Lysate was used as source of multiple instructive proteins to be incorporated within the multilayered 2D and 3D structures. Below has been provided some information about these classes of materials and the reasoning behind their selection.

II.1.1. Alginate

Alginate (Alg) is an anionic linear polysaccharides composed by homopolymeric blocks of (1-4)-linked β-D-mannuronate and its C-5 epimer α-L-guluronate (G) residues, covalently linked together in different sequences or blocks – Figure II.1. Alg is extracted from brown algae such as *Macrocystis pyrifera*, *Ascophyllum nodosum* and several types of *Laminaria*.[1, 2]

This polymer has been widely used, for example, for drug delivery, cell encapsulation and in the food industry, usually for gels preparation by ionotropic gelation with calcium ions. Alg's are known to lack mammalian cell-adhesive ligands, which are important to promote and regulate cellular interactions, and support low protein adsorption being frequently combined with other materials or modified. [3-5]

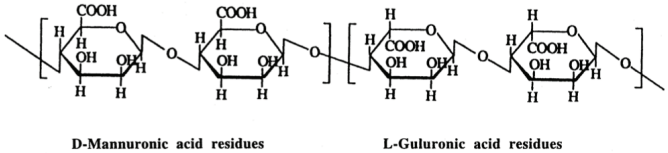

Figure II.1. Molecular structure of alginate.[1]

Alg was used as negative polyelectrolyte for layer-by-layer assembling, in combination with chitosan, in the work reported in chapter III to prove the concept of the multiscale approach.

II.1.2. Carrageenans

Carrageenans (Car's) are a family of anionic sulfated polysaccharides isolated from different species of red algae, which vary in the sulfation degree and on the molecular positioning of the -SO_3H groups. Figure II.2. shows the different molecular structures of several carrageenan, among them κ, ι and λ are commercial available. The backbone structure consists of a repeating disaccharide unit (1→4)-β-D-galactopyranosyl-(1→3)-α-D-galactopyranosyl also having 3,6-anydrogalactose residues.[6] These sulfated polymers can be found in several products in the food and pharmaceutical industry. In tissue engineering, kappa (κ; commonly extracted from *Kappaphycus alvarezii*) and iota (ι; from *Eucheuma denticullatum*) Car's have been proposed for the development of hydrogels for bone and cartilage tissue engineering[7-9]. The Car's with higher sulfation degree, such as lambda (λ; extracted from different species of *Gigartina* and *Chondrus genera*), haven't been as used due to the association with the osteoarthritis positive control model: a dose-dependent inflammatory response is triggered when 1-2% (w/v) of λ-Car gels are injected into the knee.[10] Nevertheless, such an inflammatory response was not observed with κ-Car hydrogels [11], which supports the idea that inflammatory response caused by Car's is highly dependent on parameters such as the sulfation degree and concentration. Despite the possible inflammatory response associated to Car's, the use of low amounts of Car combined with other materials may allow control of such response.

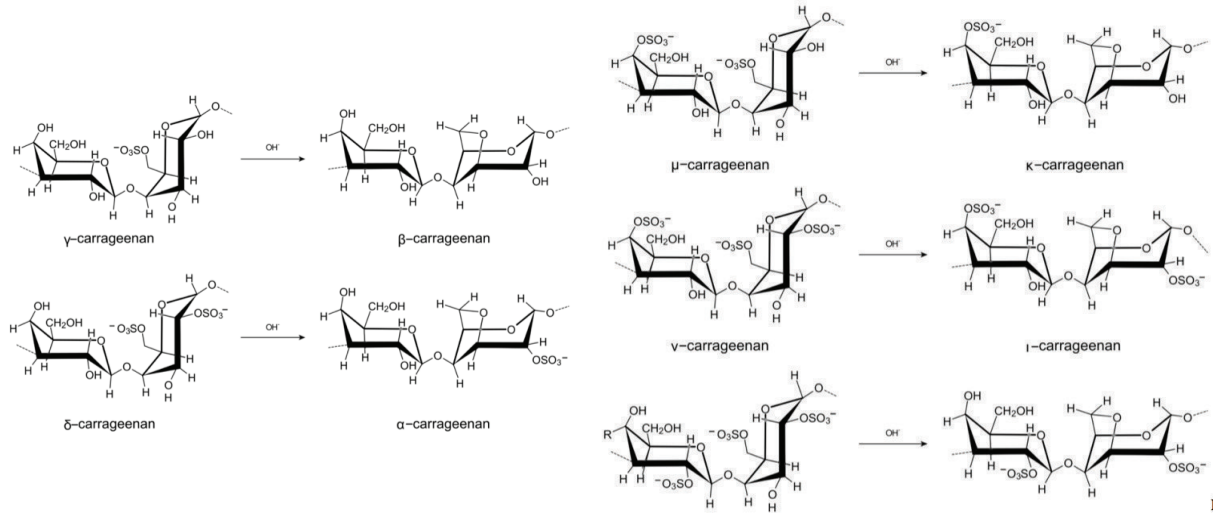

Figure II.2. Molecular structure of several carrageenans.[12]

Car's are very attractive due to their chemical similarity with glycosaminoglycans, whose sulfate groups also have high affinity for growth factors (GFs), capturing them and increasing the local concentration.[13] Car's may present different sulfation degrees and positioning of the sulfate groups which we believe may influence cell behavior and the incorporation of GFs. Thus, 3 types of Car's were selected: κ, ι and λ Car's which have a theoretical sulfation degree of 1, 2 and 3, respectively.

Car's were used as negative polyelectrolytes in the works reported in the chapters IV, V, VI and VII.

II.1.3. Chitosan

Chitosan (Chi) is a linear cationic polysaccharide comprised of glucosamine and β-(1-4)-linked D-glucosamine and N-acetyl-D-glucosamine with different proportions (predominance of the deacetylated monomer) and sequences[14] - Figure II.3. Chi is obtained by the deacetylation of chitin which can be extracted from the exoskeleton of crustaceans, fungi cellular wall, cephalopod endoskeletons or insects' cuticles.[15] It is soluble in acidic conditions, below its pKa~6, where its cationic nature makes it an atractive natural polymer to combine with negatively charged polymers by, e.g., complexation or layer-by-layer assembling, by electrostatic interactions.

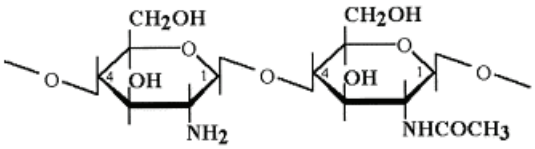

Figure II.3. Molecular structure of chitosan.[14]

Medium molecular weight Chi, with a degree of deacetylation of 80% (Sigma Aldrich, MKBB0566), was purified by a re-precipitation method. Briefly, Chi powder was first dissolved in 2% (v/v) acetic acid solution at a 1% (w/v) concentration. The mixture was maintained stirring overnight at room temperature. The impurities were then removed by four filtration cycles. Then, Chi was precipitated by the addition of 1 M NaOH while stirring. The final steps consisted of washing the Chi with distilled water until a neutral pH was reached and then dehydration by washing with ethanol–water mixtures with increasing ethanol content (20–100% v/v). Chi was freeze-dried for 3 days and ground.

Chitosan was used as a positive polyelectrolyte to perform layer-by-layer assembling in the works reported in chapters III, IV, V, VI and VII.

II.1.4. Heparin

Heparin (Hep) is a linear, unbranched, highly sulphated glycosaminoglycan and is a naturally occurring anticoagulant produced by basophils and mast cells. Hep consists of a variety of sulfated repeating disaccharide units such as 2-O-sulfated iduronic acid, 6-O-sulfated and N-sulfated glucosamine – Figure II.4. The commercially available heparins are usually obtained from beef lung or pork intestinal mucosa. Natural occurring Hep has a molecular weight ranging from 3 to 30 kDa while the medical grade, and unfractioned, one has a molecular weight in the range 12 to 16 kDa.

Hep has been used in tissue engineering as a stabilizer of GFs though[15, 16] it is widely used and known for its use in medicine as anticoagulant.

Thereby, Hep was used as a positive control for the incorporation of GFs from platelet lysate into the nanocoatings (Chapter V and VI).

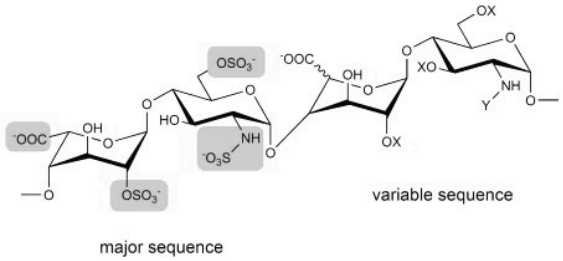

Figure II.4. Molecular structure of heparin.[17]

II.1.5. Poly (ε-caprolactone)

Poly (ε-caprolactone) (PCL) is a synthetic biodegradable polyester obtained by ring opening polymerization of ε-caprolactone – Figure II.5.[18] It is a hydrophobic and semicrystalline polymer whose crystallinity increases with increasing molecular weight. It has a glass transition temperature around -60 °C, melting point around 60°C and good solubility at room temperature in several organic solvents, which makes it suitable for both melt and solvent-based approaches in tissue engineering.[19] It has been approved by the Food and Drug Administration (FDA) for specific applications in the medical field, such as for drug delivery and sutures. *In vivo,* PCL degrades by hydrolysis of the ester linkages; however, the degradation is slow and its properties remain almost unchanged for at least 6 months and its shape may not change over a few years. Nonetheless, its degradation products do not accumulate in the body and are completely excreted and do not show adverse host tissue reactions but instead good biocompatibility.[20, 21] The slow hydrolytic degradation of PCL is dependent on its crystallinity, molecular weight, hydrophobicity, and on the scaffold porosity and surface-to-volume ratio.[22] Additionally, the degradation rate may also be tuned by preparing blends with materials with higher degradation ratios, such as some calcium phosphates and starch.[22, 23]

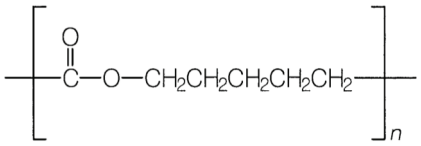

Figure II.5. Molecular structure of Poly (ε-caprolactone).[24]

PCL was selected for the preparation of the 2D and 3D templates by a melt-based approach, since it is a simple material to process (medical grade available), to modify and with a promising good compatibility.

PCL was used to prepare 3D prototyped scaffolds in the work reported in chapters III and VII, and to prepare 2D membranes in chapter IV.

II.2. Platelet Lysate

Human platelet lysate (PL) is a cost-effective source of multiple proteins comprising several biological capabilities – Table II.1. The complexity of the content of platelets makes PL preparations a source of instructive cues for several cell types and different tissues.

Table II.1. Several platelet 'constituents and respective functional categories adapted from [25] compiled with [26-29]. Underlined are the proteins with reported pro-angiogenic properties and with (*) are identified the anti-angiogenic ones, and also the ones with both abilities. Fn, fibronectin; Vn, vitronectin; TSP-1, Trombospondin-1; Fg, fibrinogen; gas6, Growth arrest-specific 6; PAI-1, Plasminogen activator inhibitor-1; μ-PA; TAFI, thrombin-activatable fibrinolysis inhibitor; PDGF, platelet derived growth factor; TGFβ, transforming growth factor β; EGF, epidermal growth factor; IGF-1, insulin-like growth factor-1; BMP, bone morphogenic protein; VEGF, vascular endothelial growth factor; bFGF, basic fibroblast growth factor; RANTES, Chemokine (C-C motif) ligand 5; IL, interleukin; MIP-1α, Macrophage Inflammatory Protein-1α; MCP-3, monocyte-specific chemokine 3; IGF BP3, Insulin-like growth factor-binding protein 3; SDF-1, stromal cell-derived factor 1; PF4, platelet factor 4; PECAM-1, Platelet endothelial cell adhesion molecule.

Category	Term	Biological activities
Adhesive proteins	vWF + pro-peptide, Fg, Fn*, Vn, TSP-1*, Laminin-8	Cell contact interactions, clotting, extracellular matrix composition
Clotting factors and associated proteins	Factor V/Va, Factor XI, mulimerin, gas6, protein S, high-molecular weight kininogen*, antithrombin*, tissue factor pathway inhibitor*	Thrombin production and its regulation, angiogenesis
Fibrinolytic factors and associated proteins	Plasminogen, PAI-I*, μ-PA, osteonectin*, α2-antiplasmin*, histidine-rich glycoprotein, TAFI, α2-macroglobulin	Plasmin production and vascular modeling
Proteases and anti-proteases	Tissue inhibitor of metalloprotease-4*, metalloprotease-4, platelet inhibitor of FIX, protease nexin-2*, C1 inhibitor, α1-antitrypsin*, heparanase	Angiogenesis, vascular modeling, regulation of coagulation, regulation of cellular behavior
Growth factors cytokines and chemokines	PDGF, TGF β (1* and 2), EGF*, IGF-1, BMP (2, 4, 6, 7, 9), VEGF (A and C), bFGF, hepatocyte growth factor*, RANTES, IL-8, MIP-1α, MCP-3, angiopoietin-1, IL-1β, IGF BP-3, neutrophil chemotactive protein, SDF-1	Chemotaxis, cell proliferation and differentiation, angiogenesis
Basic proteins and others	PF4*, β-thromboglobulin*, platelet basic protein, connective-tissue-activating peptide III, neutrophil-activating-peptide-2, endostatins*, Sphingosine 1-phosphate	Regulation of angiogenesis, vascular modeling, cellular interactions
Anti-microbial proteins	Thrombocidins	Bactericidal and fungicidal properties
Others	Chondroitin 4-sulfate, albumin, immunoglobulins	Diverse
Membrane glycoproteins	αIIbβ3, αvβ3, GPIb, PECAM-1, most plasma membrane constituents, receptors for primary agonists, CD40L, tissue factor, P-selectin	Platelet aggregation and adhesion, endocytosis of proteins, inflammation, thrombin generation, platelet-leukocyte interactions

Platelet concentrates were obtained from different platelet collections performed at the Instituto Português do Sangue (IPS, Porto, Portugal), under a previously established cooperation protocol. The components were obtained using the Trima Accel® Automated Blood Collection System. All the platelet products were biologically qualified according to the Portuguese legislation. The platelet count was performed at the IPS using the COULTER® LH 750 Hematology Analyzer and the sample volume adjusted to 1 million platelet.μL^{-1}. The collected samples were subjected to three repeated temperature cycles (frozen with liquid nitrogen at -196°C and heated at 37°C) and frozen at -20°C until further use. The remaining platelets were eliminated by centrifugation at 1400*g* for 10 min. Aliquots of Platelet lysate (PL) were stored at -20°C until final use.

PL was used as a source of instructive cues in chapters V, VI and VII to prepare several combinations of multilayers, in which the behavior of human adipose derived stem cells and human umbilical vein endothelial was assessed.

II.3. Cell sources

II.3.1. SaOs-2 cell line

Cell studies were performed using SaOs-2 cells, a human primary osteosarcoma cell line obtained from the European Collection of Cell Cultures (ECACC). These cells have been used as a model of osteoblastic activity since they exhibit the entire differentiation sequence of the osteoblastic cells: from proliferation to mineral nodule formation, matrix mineralization and differentiation into osteocytes.[30, 31] In tissue culture polystyrene and in basal media, SaOs-2 cells have basal ALP activity and basal extracellular matrix mineralization. In osteoconductive medium (includes ascorbic acid and β-glycerophosphate), the cell line shows a slightly increased production of mineralized collagenous matrix, as compared to base levels. For full differentiation and biomineralization, dexamethasone-mediated induction of SaOs-2 is necessary.[30, 31]

C[redacted]re grown in Dulbecco's Modified Eagle's medium low glucose (DMEM, Sigma -Aldrich) and supplemented with 10%, heat inactivated, fetal bovine serum (FBS, Alfagene) and 1% antibiotic-antimycotic solution (AT, Alfagene) in a humidified atmosphere with 5% CO_2 at 37°C. For expansion, confluent cell cultures were split in a ratio of 1/3 to 1/6 using 0.25% trypsin/EDTA. For cell seeding, samples were sterilized with ethylene oxide. SaOs-2 was used in passages between 20 and 24. Culture media was changed each 2-3 days.

II.3.2. Human adipose-derived stem cells

Human adipose derived stem cells (hASCs) are multipotent stem cells that can be easily obtained from adipose tissue harvested by liposuction surgeries, with low site associated morbidity. [32, 33] A considerably large amount of hASCs can be obtained, as opposed to other sources (e.g bone marrow aspirates).[34] From a clinical point of view this is an advantage. Additionally, decreasing the number of cellular doublings needed to obtain enough cells avoids the decrease of osteogenesis quality associated with *in vitro* induced cell aging and cell senescence.

Human subcutaneous adipose tissue samples were obtained from lipoaspiration procedures performed on women with ages between 35 and 50 years under a protocol previously established with the Department of Plastic Surgery of Hospital da Prelada in Oporto, Portugal. All the samples were processed within 24 h after the lipoaspiration procedure. hASCs were enzymatically isolated from subcutaneous adipose tissue, as previously described.[34] Briefly, the lipoaspirate samples were washed with a solution of PBS and 10% Antibiotic/Antimycotic. Liposuction tissue was digested with 0.2% Collagenase Type II solution for 90 min with intermittent shaking, at 37°C. The digested tissue was filtered using a 100μm filter mesh (Sigma-Aldrich,

Germany). The floating adipocytes were separated from the precipitation stromal fraction by centrifugation at 1250 rpm for 10 min. The cell pellet was re-suspended in lysis buffer for 10 min to disrupt the erythrocytes. After a centrifugation, at 800 rpm for 10 min, cells were again re-suspended and placed in culture flasks with Minimum Essential α Medium (Sigma-Aldrich) supplemented with sodium bicarbonate, antibiotic/antimycotic and 10% of Fetal Bovine Serum (Life Technologies). Cells were cultured until confluence at 37°C, 5% CO_2 incubator, changing the medium every 2 days.

II.3.3. Human umbilical vein endothelial cells

Human umbilical vein endothelial cells (HUVECs) are cells isolated from the endothelium of veins of the umbilical cords. HUVECs are widely used as cell model system to the study endothelial cell function and angiogenesis.[35]

HUVECs were used as a cell model in the work reported in chapter VI that comprises the assessment of the angiogenic potential of several combinations of polyelectrolytes and PL.

Human umbilical cords obtained by caesarean section, from healthy donors, were provided by Hospital de S. Marcos, Braga, Portugal. They were delivered in transport buffer, containing 0.14 M NaCl, 0.004 M KCl and 0.011 M glucose in 0.001M phosphate buffer at pH 7.4. HUVECs were isolated as described in the literature by Jaffe and others[36].

Biological samples were provided under a protocol approved by the Hospitals Ethical Committees and the 3B's Research Group. Cells were expanded using M199 supplemented with 50μg/ml endothelial cell growth supplement (ECGS, BDBiosciences), 50 μg/ml of heparin, 3.4 μl/ml Gibco® GlutaMAX™ (Life Tecnologies), 20% fetal bovine serum (FBS). Cells were cultured at 37ºC, 5%CO_2, 99% humidity and medium exchanged every 2-3 days.

II.4. Materials processing

II.4.1. Rapid Prototyping: Bioplotter™

Rapid prototyping comprises several types of techniques to automatically manufacture, layer by layer, 3D objects according to data drawn using computer aided design softwares, such as: fused deposition modeling, selective laser sintering, 3D printing and bioprinting. These techniques allow the preparation of complex and geometrically controlled 3D objects which can be patient customizable by recurring to 3D data acquisition (e.g., by micro-computerized tomography). It has been widely used to prepare constructs based on thermo-polymers, hydrogels and cells.[37, 38]

3D Bioplotter™ was the equipment used to produce PCL scaffold, with struts of consecutive layers aligned by 90 degrees - Figure II.6. This equipment has the capacity to build-up scaffolds using the widest range of materials of any singular rapid prototyping machine, from soft hydrogels to meltable polymers, to hard ceramics and metals. The deposition parameters used to produce the 3D structures were:

Needle diameter = fiber diameter: 0.5 mm
Layer thickness: 0.3 mm
Strand size: 0.5 mm
Scaffold size: 2×2 cm
Needle size: 2 mm
Compressed air pressure: 4-5 MPa
Temperature set: 90°C
Head velocity: 20%-35%
Number of layer build-up: 10

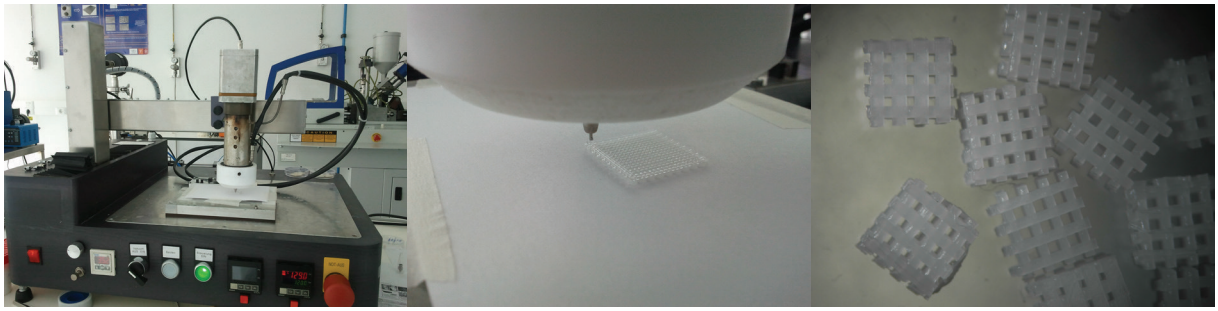

Figure II.6. Pictures regarding the preparation of prototyped 3D PCL scaffolds: left) BioplotterTM equipment used; center) PCL scaffold 2×2 cm during deposition; right) PCL scaffolds after deposition and cutting (dimensions ~ 0.5×0.5 cm, width×length).

II.4.2. Layer-by-Layer assembling

Layer-by-layer (LbL) is a simple and versatile bottom-up technology that has been widely used to produce nanostructured films for biomedical applications with controllable surface characteristics into both 2D and 3D structures using polymers, proteins and particles.[39, 40] LbL technology is often based on a simple alternated deposition of negative and positively charged polyelectrolytes – Figure II.7.

LbL was the technology used to confer instructive cues in both 2D and 3D substrates in the works reported in chapters III, IV, V, VI, and VII.

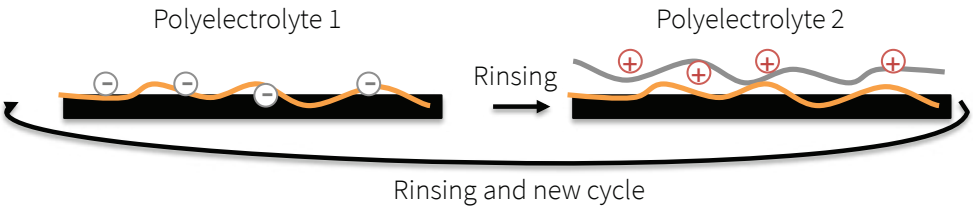

Figure II.7. Schematic representation of LbL assembling steps: i) deposition of polyelectrolyte 1; ii) rinsing to remove the weakly bound or unbound polyelectrolyte form the surface; iii) deposition of polyelectrolyte 2 which usually has the opposite charge of the polyelectrolyte 1; iv) rinsing and cycle repetition in order to assemble other layer.

II.4.2.1. 2D

II.4.2.1.1. PCL

In chapter IV, PCL surfaces were modified with several combinations of Car and Chi multilayers. A dipping LbL robot was used and the experimental apparatus can be observed in Figure II.8.

PCL surfaces prepared by melt-compression molding were pre-modified with a solution of 10% (v/v) of ethylenediamine in 2-propanol for 1 hour at 37ºC in order to introduce pH responsive amine groups and improve the binding of the first PE layer onto the surface. Then, the surfaces were extensively washed with ultrapure water. The immersion time in the PE solutions was 10 minutes followed by 2 rinsing steps of 5 minutes each. After the LbL modification finished, the samples were washed with the respective buffer/washing solutions and ultrapure water under mild agitation.

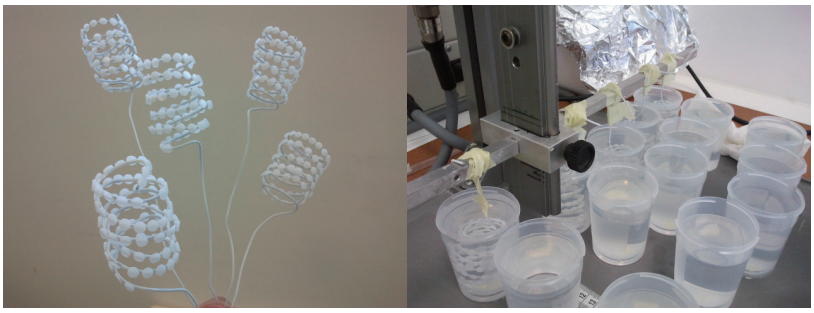

Figure II.8. Pictures regarding the modification of PCL membranes by LbL using the dipping robot: left) holders with PCL membranes fixed; right) robot with sample-holders, and polyelectrolytes and washing solutions for the modification of several samples.

II.4.2.1.2. 48-well Plates

In chapter V and VI, 48-well plates were modified with several combinations of polyelectrolytes and PL.

The 48-well plates were previously modified with 0.5 mL of 0.5% (w/v) PEI solution to confer a positive surface charge. Then, the solution was removed and the wells were extensively rinsed with distilled water in order to remove the unbound PEI. The LbL was started by the adsorption of the negative PE. In the case of Chi, an Alg layer was first adsorbed. The adsorption times and volumes used were: 4 minutes and 0.5 mL for the polysaccharides solutions; 0.5 mL and 10 minutes for the PL solution; intermediate rising steps x2 for 30 seconds using the respective buffers. The sequence was repeated 6 times.

II.4.2.2. 3D

3D PCL scaffolds were modified by LbL to create small complexes of polyelectrolytes which were further shaped into fibrillar structures by freeze-drying – Figure II.9.

This procedure was used in the work reported in chapter III (with Alg and Chi bilayers) and in chapter VII (with chitosan, ι carrageenan and PL tetralayers).

Previously the scaffolds, prepared using the Bioplotter™, were modified with ethylenediamine 10% (v/v) in 2-propanol for 1 hour at 37ºC to introduce positive charged amine groups on the surface and improve the binding between the first layer and the surface. This modification also increases the surface wettability, which facilitates the flow of the solution throughout the pores, diminishing the possibility of the pores to occlude, and the modification to not be homogeneous. Then, the scaffolds were extensively washed with ultrapure

water. 20-40 scaffolds per condition were fixed onto the dipping LbL robot arm using nylon fibers. The volume in each cup (60-120 mL of solution), the number of cups, and the number of cycles (5-30) were set accordingly to what is described in the respective chapter. The deposition time in each polyelectrolyte was 4-10 minutes for all conditions. After the LbL, the samples were washed with NaCl solution and ultrapure water under mild agitation. To allow ice crystal growth, scaffolds were frozen at -80ºC. To finish the modification, the water crystals were removed by freeze-drying over 2-3 days.

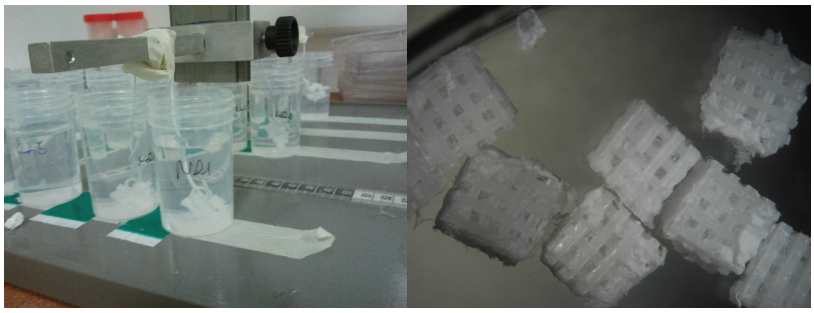

Figure II.9. Pictures regarding the modification of 3D PCL scaffolds by LbL (Alg and Chi) using the dipping robot, and freeze-drying: left) holders with scaffolds in the dipping robot; right) scaffolds after LbL and freeze-drying (dimensions ~ 0.5×0.5 cm, width×length).

II.5. Materials characterization methods

II.5.1. Quartz-crystal Microbalance with Dissipation

To monitor the LbL assembling of polyelectrolytes, a quartz-crystal microbalance with dissipation was used in the works reported in chapters IV, V and VII.

To consider the application of multilayers it is necessary to understand the way its construction and stability are affected by different experimental conditions, namely ionic strength and pH.

The QCM-D allows one to follow, in-situ, the construction of multilayers, through the change in resonance frequency of a quartz crystal when a certain amount of mass is deposited or removed from its surface. A quartz crystal vibrates at a certain frequency when an electric field is applied. With mass deposition on its surface, this vibration frequency is affected and one can relate the change in frequency with the deposited mass. For thin and rigid films and for measurements made in air, the relation between change in frequency and change in mass is given by Sauerbrey equation:

$$\Delta F = \frac{-2F_q^2}{A\sqrt{\rho_q \mu_q}}\Delta m,$$

where F_q is the fundamental resonance frequency of the crystal, A is the area, ρ_q is quartz density and μ_q is the quartz elastic modulus. However, for non-rigid films or for measurements in solution, it has been demonstrated that crystal vibration depends not only on quartz properties but also, on the properties of the deposited material and solution. Thus, the change in frequency may not be well described by Sauerbrey equation, making it necessary to consider a more complex methodology. The equipment used in the present

study allows one to explore that possibility, since it measures the dissipation of energy, related with the properties of the deposited material.

A Q-Sense E4 quartz crystal microbalance (Q-Sense AB, Sweden) with dissipation was used for in situ monitoring of the deposition of PE/PL bilayers at the surface of 100 nm gold-coated crystals. The crystals were first cleaned in an ultrasound bath at 30°C, and immersed successively in acetone, ethanol, and isopropanol.

Briefly, AT cut quartz crystals were excited at multiple overtones (1, 3, 5, 7, 11, and 13), which correspond to 5, 15, 25, 35, 45, 55 and 65 MHz, respectively. The PEs solutions (0.5 $mg.ml^{-1}$) were pumped with a constant flow rate of 50 μL.min-1, for 10 minutes at room temperature. As an intermediate step, the respective buffer solutions were pumped during 10 minutes to rinse the crystals.

II.5.2. Polyelectrolytes Staining

Alcian blue and eosin Y staining can be considered specific staining for Alg and Chi, respectively, since the structures are cell and extracellular matrix-free. Commercial solutions of Alcian blue and eosin Y were used to stain the scaffolds by adding 1 ml of the respective solutions and kept at room temperature for 1 hour. The excess of staining was then removed by washing with phosphate buffer saline solution (PBS). Scaffolds were further observed under stereomicroscope. The higher the intensiveness of the color, the higher the content of polyelectrolyte is.

Dried, modified and unmodified samples were also observed by reflected and transmitted microscope with a 480 nm light source to analyze the morphology. At this wavelength, the polyelectrolytes can be distinguished from the pure PCL since chitosan has high fluorescence intensity.

II.5.3. Platelet lysate adsorption

6-well plates were modified with PEI and the PEs, as described before. Two milliliters of PL 10% (v/v) or PL 100% (v/v), pH 6 and pH 7.4, were added to each well and let to adsorb for 30 minutes. The volume was removed and stored at -20°C for further quantification. Each well was rinsed with 2 ml of the respective buffer, which was then stored for further protein quantification.

The total protein was quantified in the following solutions: initial PL, PL before and after adsorption, and rinsing solutions. The measurements were performed using a NanoDrop 1000 Spectrophotometer (Thermo Scientific). The absorbance of 2 μl volume of solution was measured at the wavelength 280 nm (n=6). The amount of PDGF (PL10%), FGFb (PL100%) and VEGF (PL100%) was quantified using ELISA kits following the assay protocol provided with the kit. Optical density was read at 450 nm (n=6) on a multi-well microplate reader (Synergy HT, Bio-Tek Instruments).

II.5.4. Atomic Force Microscope

In order to assess surface roughness, AFM measurements were performed in a MultiMode STM microscope controlled by the NanoScope III from Digital Instruments system, operating in tapping mode at a frequency of 1 Hz. At least three measurements were performed in different specimens.

II.5.5. X-ray photoelectron spectroscopy

The chemical analysis of the surfaces was performed by XPS analysis in regards to the nitrogen, sulfur, carbon and oxygen content. XPS has a sampling depth of about 5 nm, and only detects the top layer(s) and not the complete multilayer, which, depending on the nature of the PE's, can have a fuzzy or more lamellar organization.[41,42]

XPS analysis was performed using a Thermo Scientific K-Alpha ESCA instrument with monochromatic Al-Ka radiation (h = 1486.92 eV) and a takeoff angle of 90° relative to the sample surface to record the C1s, O1s, S2p , N1s and survey spectra. The measurement was carried out in constant analyzer energy (CAE) mode with a 100 eV pass energy for survey spectra and a 20 eV pass energy for high-resolution spectra. The C1s peak was resolved into three peaks at 285.0 eV. Surface elemental composition was determined using the standard Scofield photoemission cross sections. The atomic concentrations were determined from the XPS peak areas using the Shirley background subtraction technique and the Scofield sensitivity factors. The ratios of sulfur/carbon, sulfur/oxygen, oxygen/carbon and nitrogen/carbon on modified surfaces were calculated by dividing the elemental percentages of each element. At least two measurements were performed in different specimens.

II.5.6. SEM-EDS

Scaffolds surface and structures morphology were observed using a Leica Cambridge S-360 scanning electron microscope (SEM, Leica Cambridge, UK). All surfaces were precoated with a conductive layer of sputtered gold. The SEM micrographs were taken at an accelerating voltage of 15 kV and at different magnifications.

II.5.7. Goniometrer

Wettability can be assessed by the contact angle that a droplet of water has with the materials surface. The static water contact angle (WCA) of the PCL samples in chapter IV was measured at room temperature using an OCA 15plus goinometer equipment (DataPhysics Instruments, Germany). The values were obtained by the sessile drop method. The liquid used was ultrapure water and the drop volume was 3 μL.

II.5.8. Water uptake

To assess the ability to uptake water, scaffolds of known weight (Wi) in chapter III were immersed in PBS solution (pH 7.4) and incubated at 37°C under static conditions for 30, 60, 90, 120 and 450 minutes. The water uptake percentage was calculated by the following formula:

%=Wf - WiWi×100, where, Wf is the final weight and Wi is the initial weight. To measure Wf, the swollen samples were weighted after the removal of excessive surface water with filter paper. Each experiment was repeated twice, and the average value was considered to be the water uptake value.

II.5.9. Micro computerized tomography

The morphology of the multiscale scaffolds (Chapter III) and the distribution of the new mineral formed within the scaffolds (Chapter VII) was analyzed by micro-computed tomography (μ-CT) using a desktop μ-CT scanner (1072; SkyScan, Kontich, Belgium) at a voltage of 40 kV and a current of 248 mA, with acquisitions carried out in high-resolution mode of 11μm x/y/z. Isotropic slice data were obtained by the system and reconstructed into 2D XY slice images. Around 600 slice images per sample were compiled and subsequently employed in the rendering of 3D XYZ images to obtain quantitative architectural parameters. A μ-CT analyzer and a μ-CT volume realistic 3D Visualization software (SkyScan) was used as an image processing tool for reconstruction and creation of 3D representation models for the observation of the distribution of the deposited apatite.

II.5.10. Mechanical Properties

In order to verify if our methodology alters the mechanical properties of the dried scaffolds (Chapter III), uniaxial compression tests were performed on the cubic scaffolds by using an Instron 4505 Universal Machine. A crosshead speed of 2 $mm.min^{-1}$ was used in the compression tests. The values reported are the average of at least five specimens per condition. The compressive modulus was determined in the linear region of the stress–strain graph and, in the cases that the yield stress was not clear, it was calculated as the stress at the intersection of a line drawn parallel to the linear region and intercepting the x-axis at 3 to 5% strain.

II.6. Cellular characterization methods

II.6.1. Morphology

Cell morphology of hASCs and HUVECs was assessed in the studies reported in chapters V and VI, respectively.

II.6.1.1. Fluoresce Microscope

After the culture periods, the samples were gently rinsed twice with sterile PBS and then fixed with formalin 2.5% (v/v) for 20 minutes. Cells were permeabilized with 0.5 mL of Triton 0.2% (v/v) in PBS for 2 minutes and

then rinsed with PBS. Samples were incubated in the dark with 100 μL of (1:100) Phalloidin-TRITC (Sigma-Aldrich) solution for 30 minutes and then washed with PBS. For cell nuclei staining, well plates were incubated in the dark for 5 min with 100 μL 4,6-diamino-2-phenyindole dilactate (DAPI, Sigma-Aldrich) diluted 1:1000 in PBS. Samples were observed using an inverted Axio Observer Fluorescence Inverted Microscope (Zeiss).

II.6.1.2. Image Analysis

II.6.1.2.1. Image J

Cell length, width and mean area were measured using the Image J software version 1.48 in Chapter V. Cell length was considered the longest distance between the tips of the filopodia. The width was measured on the cell nucleus position and usually in a, approximately, right angle to the cell length. Cell area was calculated dividing the total number of nucleus by the total area covered by the same cells. Cell aspect ratio was calculated by dividing cell length per cell width.

II.6.1.2.2. Angiogenesis Analyzer

Angiogenesis Analyzer is a toolset for Image J that allows the analysis of cellular networks images and it was used in the work reported in chapter VI to assess the angiogenic potential of the multilayers rich in PL.

Angiogenesis Analyzer is a simple tool to quantify endothelial tube formation assay images by extracting characteristic information of the network regarding segments, nodes, area and meshes – Figure II.10. The total length of the tube-like structures, number of nodes and master nodes, number of meshes and master meshes were quantified on cytoskeleton fluorescence images of HUVECs after 20 hours of incubation. A node is defined as pixels that have at least 3 neighbors, corresponding to a bifurcation. A junction is a node or fused nodes. The segments correspond to elements that are limited by two junctions/nodes while the branches are elements delimited by a junction and one extremity. The master segments are considered pieces of three, delimited by two junctions, but not exclusively implicated with one branch (master junctions). The master junctions link at least 3 master segments. The meshes are areas enclosed by the segments or master segments.

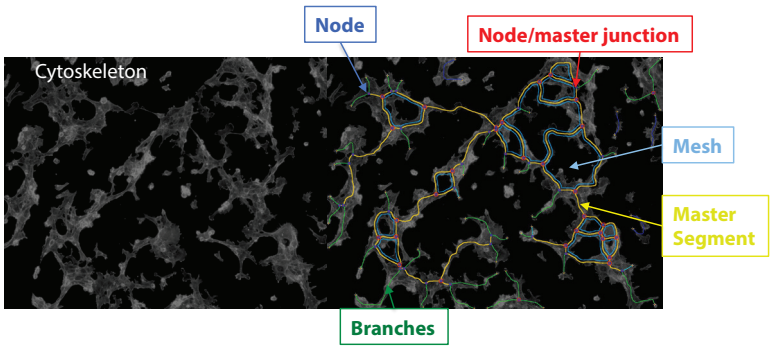

Figure II.10. Angiogenesis Analyzer features: Image of HUVECs cytoskeleton, before and after analysis, with the quantified features highlighted.

II.6.1.2.3. Cell Profiler

Cell Profiler allows the analysis of various biological features, including cell counting, size and also complex morphological assays such as cell/organelle shape and subcellular patterns of DNA.[43]

The morphological changes of HUVECs when cultured for 20 hours on the multilayers, in the presence or absence of inhibitors, was analyzed using the eccentricity, form factor and major and minor axis length features available with Cell Profiler. Eccentricity is defined as the ratio of the distance between the foci of the considered ellipse and its major axis length. The values vary between 0 and 1. Values equal to zero are actually circles while ellipses with eccentricity of 1 are lines. The form factor is calculate as 4π(Cell Area)/(Cell Perimeter)2, where 1 represent a perfect circular cell. The major and minor axis length (in pixels) correspond to the major and minor axis of the ellipse, respectively. The images used for Cell Profiler analyses were the same for Angiogenesis Analyzer.

Cell profiler pipeline

```
CellProfiler_Version,2014-07-23T17:39:57 6c2d896
ChannelType_Cyto,Color
ImageSet_Zip_Dictionary,"[ 60  63 120 ..., 111 112 109]"
Pipeline_Pipeline,"CellProfiler Pipeline: http://www.cellprofiler.org
Version:3
DateRevision:20140723173957
GitHash:6c2d896
ModuleCount:9
HasImagePlaneDetails:False
Images:[module_num:1|svn_version:\'Unknown\'|variable_revision_number:2|show_window:False|:
Filter images?:Images only
Select the rule criteria:and (extension does isimage) (directory doesnot containregexp
Metadata:[module_num:2|svn_version:\'Unknown\'|variable_revision_number:4|show_window:Fals
Extract metadata?:No
Metadata data type:Text
Metadata types:{}
Extraction method count:1
Metadata extraction method:Extract from file/folder names
Metadata source:File name
Regular expression:^(?P<Plate>.*)_(?P<Well>\x5BA-P\x5D\x5B0-9\x5D{2})_s(?P<Site>\x5B0-
Regular expression:(?P<Date>\x5B0-9\x5D{4}_\x5B0-9\x5D{2}_\x5B0-9\x5D{2})$
Extract metadata from:All images
Select the filtering criteria:and (file does contain """")
Metadata file location:
Match file and image metadata:\x5B\x5D
Use case insensitive matching?:No
NamesAndTypes:[module_num:3|svn_version:\'Unknown\'|variable_revision_number:5|show_window
Assign a name to:All images
Select the image type:Color image
Name to assign these images:Cyto
Match metadata:\x5B\x5D
Image set matching method:Order
Set intensity range from:Image metadata
Assignments count:1
Single images count:0
Select the rule criteria:and (file does contain """")
Name to assign these images:DNA
Name to assign these objects:Cell
Select the image type:Grayscale image
Set intensity range from:Image metadata
```

Retain outlines of loaded objects?:No
Name the outline image:LoadedOutlines
Groups:[module_num:4|svn_version:\'Unknown\'|variable_revision_number:2|show_window:False|
Do you want to group your images?:No
grouping metadata count:1
Metadata category:None
ColorToGray:[module_num:5|svn_version:\'Unknown\'|variable_revision_number:3|show_window:T
Select the input image:Cyto
Conversion method:Split
Image type:RGB
Name the output image:OrigGray
Relative weight of the red channel:1.0
Relative weight of the green channel:1.0
Relative weight of the blue channel:1.0
Convert red to gray?:Yes
Name the output image:OrigRed
Convert green to gray?:Yes
Name the output image:OrigGreen
Convert blue to gray?:Yes
Name the output image:OrigBlue
Convert hue to gray?:Yes
Name the output image:OrigHue
Convert saturation to gray?:Yes
Name the output image:OrigSaturation
Convert value to gray?:Yes
Name the output image:OrigValue
Channel count:1
Channel number:Red\x3A 1
Relative weight of the channel:1.0
Image name:Channel1
IdentifyPrimaryObjects:[module_num:6|svn_version:\'Unknown\'|variable_revision_number:10|s
Select the input image:OrigBlue
Name the primary objects to be identified:Nuclei
Typical diameter of objects, in pixel units (Min,Max):3,40
Discard objects outside the diameter range?:Yes
Try to merge too small objects with nearby larger objects?:No
Discard objects touching the border of the image?:Yes
Method to distinguish clumped objects:Intensity
Method to draw dividing lines between clumped objects:Intensity
Size of smoothing filter:10
Suppress local maxima that are closer than this minimum allowed distance:7.0
Speed up by using lower-resolution image to find local maxima?:Yes
Name the outline image:PrimaryOutlines
Fill holes in identified objects?:After both thresholding and declumping
Automatically calculate size of smoothing filter for declumping?:Yes
Automatically calculate minimum allowed distance between local maxima?:Yes
Retain outlines of the identified objects?:No
Automatically calculate the threshold using the Otsu method?:Yes
Enter Laplacian of Gaussian threshold:0.5
Automatically calculate the size of objects for the Laplacian of Gaussian filter?:Yes
Enter LoG filter diameter:5.0
Handling of objects if excessive number of objects identified:Continue
Maximum number of objects:500
Threshold setting version:1
Threshold strategy:Automatic
Thresholding method:Otsu
Select the smoothing method for thresholding:Automatic
Threshold smoothing scale:1.0
Threshold correction factor:1.0
Lower and upper bounds on threshold:0.0,1.0
Approximate fraction of image covered by objects?:0.01
Manual threshold:0.0
Select the measurement to threshold with:None
Select binary image:None

Masking objects:None
Two-class or three-class thresholding?:Two classes
Minimize the weighted variance or the entropy?:Weighted variance
Assign pixels in the middle intensity class to the foreground or the background?:Foreg
Method to calculate adaptive window size:Image size
Size of adaptive window:10
IdentifySecondaryObjects:[module_num:7|svn_version:\'Unknown\'|variable_revision_number:9|
Select the input objects:Nuclei
Name the objects to be identified:cytosk
Select the method to identify the secondary objects:Propagation
Select the input image:OrigRed
Number of pixels by which to expand the primary objects:10
Regularization factor:0.01
Name the outline image:SecondaryOutlines
Retain outlines of the identified secondary objects?:No
Discard secondary objects touching the border of the image?:Yes
Discard the associated primary objects?:No
Name the new primary objects:FilteredNuclei
Retain outlines of the new primary objects?:No
Name the new primary object outlines:FilteredNucleiOutlines
Fill holes in identified objects?:Yes
Threshold setting version:1
Threshold strategy:Adaptive
Thresholding method:RobustBackground
Select the smoothing method for thresholding:Manual
Threshold smoothing scale:1.0
Threshold correction factor:0.15
Lower and upper bounds on threshold:0.15,0.3
Approximate fraction of image covered by objects?:0.01
Manual threshold:0.0
Select the measurement to threshold with:None
Select binary image:OrigRed
Masking objects:Nuclei
Two-class or three-class thresholding?:Two classes
Minimize the weighted variance or the entropy?:Weighted variance
Assign pixels in the middle intensity class to the foreground or the background?:Foreg
Method to calculate adaptive window size:Image size
Size of adaptive window:10
MeasureObjectSizeShape:[module_num:8|svn_version:\'Unknown\'|variable_revision_number:1|sh
Select objects to measure:cytosk
Calculate the Zernike features?:No
ExportToSpreadsheet:[module_num:9|svn_version:\'Unknown\'|variable_revision_number:11|show
Select the column delimiter:Comma (",")
Add image metadata columns to your object data file?:No
Limit output to a size that is allowed in Excel?:No
Select the measurements to export:Yes
Calculate the per-image mean values for object measurements?:Yes
Calculate the per-image median values for object measurements?:No
Calculate the per-image standard deviation values for object measurements?:Yes
Output file location:Default Output Folder\x7C
Create a GenePattern GCT file?:No
Select source of sample row name:Metadata
Select the image to use as the identifier:None
Select the metadata to use as the identifier:None
Export all measurement types?:Yes
Press button to select measurements to export:cytosk\x7CLocation_Center_Y,cytosk\x7CLo
Representation of Nan/Inf:NaN
Add a prefix to file names?:No
Filename prefix\x3A:MyExpt_
Overwrite without warning?:Yes
Data to export:Do not use
Combine these object measurements with those of the previous object?:No
File name:DATA.csv
Use the object name for the file name?:Yes"

II.6.2. Proliferation and viability

II.6.2.1. Live/Dead Assay

Live/dead assay is used to measure cell viability. It is a two-color fluorescence assay that simultaneously highlights the living (green) and dead (red) cells. Briefly, the culture medium was removed and the samples washed twice with sterile PBS for 5 minutes, then 250 mL of calcein AM solution and propidium iodide/RNAse solution were added and samples left to incubate for 10 minutes in the incubator, protected from light. Then, the solutions were removed and samples washed twice with sterile PBS and observed under transmitted reflected microscope using the red and green fluorescence filters.

II.6.2.2. dsDNA quantification

In order to quantify cell attachment and proliferation, dsDNA was quantified using the Quant-iT™ PicoGreen® dsDNA assay kit (Molecular Probes/Invitrogen) that allows the measurement of the fluorescence produced when PicoGreen dye is excited by UV light while bound to dsDNA. After the incubation periods, the well plates were gently rinsed once with sterile PBS. Then, 1 mL of ultra-pure sterile water added and kept at -80°C until quantification. For the quantification, samples were defrosted at room temperature and the content was transferred to eppendorfs. 100 μL of Tris–EDTA buffer was transferred into a white opaque 96-well plate. Samples were vortexed and 28.8 μL of each, plus 71.2 μL of PicoGreen solution, were added to the wells. After 10 minutes of incubation in the dark, the plate was read in a microplate reader using an excitation wavelength of 485 nm and emission wavelength of 528 nm. A standard curve was created by varying the concentration of standard dsDNA standard from 0 to 2 $mg.mL^{-1}$, and triplicate dsDNA values of the samples were read off from the standard graph. At least six specimens were measured per sample.

II.6.2.3. ALP activity

ALP is a hydrolase enzyme responsible for removing phosphate groups from many types of molecules, including nucleotides, proteins, and alkaloids. In bone development, the enzyme participates in the regulation of biomineralization for instance by the regulation of inorganic pyrophosphates' levels. In vitro, alkaline phosphatase (ALP) is highly expressed in early osteogenesis, and is also considered a universal pluripotent marker for all types of pluripotent stem cells including embryonic stem cells, embryonic germ cells and induced pluripotent stem cells.[44, 45] In hASCs, a significant increase in ALP activity during normal medium conditions suggests a cell-commitment to the osteoblastic lineage or cell aging.[46]

ALP activity was quantified in the same samples used for dsDNA quantification. The activity of ALP is typically evaluated using the p-nitrophenol assay. Paranitrophenyl phosphate, which is colorless, is hydrolyzed by alkaline phosphatase enzyme at pH 9.8 and 37ºC to form free p-nitrophenol, which is yellowish. The reaction

was stopped by addition of NaOH and the absorbance read at 405 nm. Briefly, in each well 20 µl of each sample, previously vortexed, were mixed with 60 µl of the substrate solution which is 0.2% (w/v) p-nytrophenyl phosphate (Sigma-Aldrich) prepared in a substrate buffer of 1 M diethanolamine (Sigma-Aldrich) at pH 9.8. The plate was then incubated in the dark for 45 min at 37°C. After the incubation period, 80 µl stop solution, which is composed by 2 M NaOH (Panreac) plus 0.2 mM EDTA (Sigma-Aldrich), was added to each well. Standards were prepared with 10 µmol mL^{-1} p-nytrophenol (pNP, Sigma, USA) solution, to obtain a standard curve covering the 0–0.2 M range. Triplicates of each sample, and the standard, were made. Finally, absorbance was read at 405 nm in a microplate reader (Bio-Tek, Synergie HT) and sample concentrations in triplicate were read off from the standard curve.

II.6.3. Extracellular Matrix

II.6.3.1. Alizarin Red S Staining

Alizarin Red S, an anthraquinone derivative, can be used to identify calcium in tissue sections. Although the reaction is not strictly specific for calcium, also occurring with magnesium, manganese, barium, strontium, and iron, these elements usually do not occur in sufficient concentration to interfere with the staining. Calcium forms an Alizarin Red S-calcium complex in a chelation process. After culture, scaffolds were rinsed thrice with sterile PBS and cells fixed with 2.5% formalin for 30 minutes. The samples were then rinsed again with distilled water in order to remove any residual ions and 0.5 ml of Alizarin Red S solution (2g/100 ml, pH 4.1-4.3 adjusted with ammonium hydroxide) was added to each sample and left to react for around 5 minutes. The excess of dye was removed with distilled water, and samples were observed under stereomicroscopy. The content of calcium will be proportional to the red intensiveness. In order to elute the Alizarin Red S adsorbed to the scaffolds, 400 µL of 10% (v/v) acetic acid was added to each sample and incubated at room temperature for 30 min with shaking. Samples were vortexed for 30 seconds. After complete elution, the surfaces were discarded, and the liquid samples heated to 85°C for 10 min. The slurry was then centrifuged at 12,000g for 30 min and 400 µL of the supernatant was removed to a new microcentrifuge tube. Then 150 µL of 10% (v/v) ammonium hydroxide was added to neutralize the acid. The absorbance of triplicates of the samples was read at 405 nm in a microplate reader (Bio-Tek, Synergie HT). A calibration curve made of successive dilutions of an Alizarin Red S solution with known concentration was used in order to read off the alizarin content of the samples.

II.6.3.2. Oil Red O Staining

Oil red O staining is a lysochrome used for neutral triglycerides and lipids staining with the appearance of a red coloration. A stock solution was prepared by dissolving 300 mg of Oil Red O (Sigma, Aldrich) in 100 mL of 99% isopropanol. The work solution, which is stable for no longer than 2 hours, was prepared by mixing 3 parts (30 mL) of the stock solution with 2 parts (20 ml) of distilled water and allowed to sit at RT for 10 min. After the solution is filtered with filter paper, 1 mL (5 minutes) of it was added to each construct that had been fixed with

2.5% formalin (30 min), rinsed with distilled water, and with 60% isopropanol (2-5 minutes). Samples were rinsed with distilled water and then 0.5 mL of 100% isopropanol was added to each scaffold (10 minutes) with shaking in order to elute the staining.

The absorbance of triplicates of the samples was read at 500 nm in a microplate reader (Bio-Tek, Synergie HT).

II.6.3.3. SEM-EDS

The constructs were harvested after culture, rinsed with PBS, fixed with 2.5% glutaraldehyde and dehydrated through a graded series of ethanol (50, 70, 90, 100% v/v; each one for 10 minutes and twice) and dried at room temperature. Morphological analysis of the prepared constructs before and after cell culture was performed in an Ultra-high resolution Field Emission Gun Scanning Electron Microscopy (FEG-SEM; NOVA 200 Nano SEM, FEI Company). Secondary electron images were performed with an acceleration voltage of 5kV. Chemical analysis of samples was performed by Energy Dispersive Spectroscopy (EDS), using an EDAX Si(Li) detector with an acceleration voltage of 15 kV.

II.6.3.4. Immunocytochemistry

II.6.3.4.1. Immuno-localization of human Osteocalcin

After culture, samples were rinsed twice with sterile PBS and fixed with 2.5% formalin for 30 min at room temperature (RT). First the scaffolds were stained with Alizarin Red for detection of Calcium, as described before.

Afterwards cells were permeabilized with Triton X-100/PBS 0.2% (v/v) for 15 min at RT, proteins were blocked with 3% (w/v) Bovine Serum Albumin (BSA)/PBS for 45 minutes. Samples were incubated overnight at 4°C with the primary antibody anti-osteocalcin (mouse monoclonal anti-Osteocalcin, ab13418, Abcam) diluted 1:50 in 1% BSA/PBS. Afterwards, samples were rinsed with 0.025% Triton X-100/PBS, followed by 2 hours of incubation with the secondary antibody, anti-mouse Alexa Fluor 488 (Invitrogen), with a dilution of 1:100. After the incubation period, samples were rinsed in PBS and stained with 4,6-Diamidino-2-phenyindole dilactate (DAPI, 1:1000, D9564, Sigma-Aldrich). Scaffolds were observed under a microscope (Imager Z1m, Zeiss) and images acquired using a digital camera (AxioCam MRm5).

II.6.4. Flow cytometer

Flow cytometry was performed using anti-human CD90 APC (BD Pharmingen™), anti-human CD105 FITC (BioRad), anti-human CD73 PE (BD Pharmingen™), anti-human CD34 PE (BD Pharmingen™), anti-human CD31 APC (R&D Systems), anti-human CD45 FTIC (BD Pharmingen™).

Cells were trypsinized, counted and re-suspended in PBS with 2% (w/v) bovine serum albumin (BSA) (Sigma) with a concentration of $2x10^6$ cells/100ls and incubated with the antibodies at the concentration advised by the manufacturers. After incubation for 20 min at room temperature, protected from light, cells were washed

with PBS/BSA, re-suspended in PBS with 1% formaldehyde (Sigma) and analyzed in a BD FACSCaliburTM flow cytometer (BD Biosciences). Cells of interest were gated in a forward vs. side scatter dot plot with a linear scale. Isotype controls were made to discern non-specific from specific staining. A minimum of 10,000 gated events were acquired and labeled cells were quantified.

II.6.5. Gene expression

II.6.5.1. Real Time Polymerase Chain Reaction

The quantification of angiogenic gene expression of the HUVECs and the osteogenic, chondrogenic, adipogenic and angiogenic gene expression of hASCs, were performed using quantitative PCR by a two-step fluorogenic assay using the PerfeCtaTM SYBR® Green System (Quanta Biosciences) – see the target genes in Table II.2. and Table II.3.

The total RNA was extracted using the TRI® Reagent (Sigma-Aldrich), following the manufacture's instruction. Total RNA was quantified using Nanodrop® ND-100 spectrophotometer (Thermo Scientific) and first-strand complementary DNA (cDNA) was synthetized using 1 μg RNA of each sample and the qScript™ cDNA Synthesis Kit (Quanta Biosciences) for a 20μL reaction. The obtained cDNA was used as a template for the amplification of the target genes using a MasterCycler EP Gradient detection System (Eppendorf) termocycler and the PerfeCta™ SYBR® Green System kit following the manufactures' instructions. The Livak method, 2-ΔΔCt, was used to evaluate the relative expression of each target gene. ΔCt was calcuated by the difference between the Ct values of the target gene and the β-actin or GAPDH endogenous housekeeping gene. ΔΔCt was obtained by subtracting the ΔCt of the calibrator sample (TCPS) to the ΔCt of the sample. The results are represented as $2^{-\Delta\Delta Ct}$ and as gene expression relative to TCPS.

Table II.2. Sequences and melting temperature of the angiogenic genes analyzed.

Name	Primer sequence (Forward, Reverse 5'-3')	Tm (°C)
β-actin	ACTGGAACGGTGAAGGTGAC AGAGAAGTGGGGTGGCTTTT	59.5
GAPDH	ACAGTCAGCCGCATC GACAAGCTTCCCGTTCTCAG	58.4
Integrin β3	ACCAGTAACCTGCGGATTGG TCCGTGACACACTCTGCTTC	59.4
Integrin αv	CCGATTCCAAACTGGGAGCA GGCCACTGAAGATGGAGCAT	59.4
Integrin α5	TGGCCTTCGGTTTACAGTCC GGAGAGCCGAAAGGAAACCA	59.4
VEGFA	GACAGATCACAGGTACAGGG AGAAGCAGGTGAGAGTAAGC	58.4
FGFb	GAGCAAATCTGCCCTGCTCA TCCCGCATACTCTGGAGACA	59.4
Angiopoietin-1	GAAGGGAACCGAGCCTATTC GGGCACATTTGCACATACAG	58.4

Table II.3. Description of the target genes used in qPCR: name; lineage-related to the target gene; main functions; Forward and Reverse primers; melting temperature used.

Gene	Lineage	Function	Forward (5'-3')	Tm (°C)
Beta-actin	Housekeeping gene	Controls cell growth, migration, and the G-actin pool	ACTGGAACGGTGAAGGTGAC AGAGAAGTGGGGTGGCTTTT	59.5
Osteocalcin	Osteo -late	It is secreted solely by osteoblasts, it can be found in bone and dentin; participates in bone mineralization and calcium ion homeostasis.	GTGCAGAGTCCAGCAAAGG TCAGCCACTCGTCACAGC	59.4
Runx2	Osteo - early	Runt-related transcription factor 2 is a key transcription factor associated with osteoblast differentiation	TTCCAGACCAGCAGCACTC CAGCGTCAACACCATCATTC	58.1
PPARy2	Adipose - late	Peroxisome proliferator-activated receptor is expressed mainly in adipose tissue, in mature osteocytes	TGGGTGAAACTCTGGGAGAT GCGATCTCTGTGTCAACCAT	57.3
Leptin	Adipose - late	It is one of the most important adipose-derived hormones that play a key role in regulating energy intake and expenditure, including appetite and hunger, metabolism, and behavior.	CTCAGGGATCTTGCATTCCC CCATGCATTTGGCTGTTCAG	57.8
PECAM1/ CD31	Vascular	Cluster of differentiation 31 is a large portion of the endothelial cell intercellular junctions	AAGGCCAGATGCACATCC TTCTACCCAACATTAACTTAGCAGG	57.9
SOST	Osteo - late	Produced by mature osteocytes codes Sclerostin proteins that inhibit further mineralization	GTGCCAAGGTCACTTCCAGA CCAGGAGTTTGTCAGCCGTA	57.2
Col I	Osteo	Collagen I is a protein that strengthens and supports several tissue including bone	AAGAACCCCAAGGACAAGAG GTAGGTGATGTTCTGGGAGG	58.4
Col X	Cartilage/ Osteo -middle	Found in hypertrophic chondrocytes undergoing mineralization/osteoblastic differentiation	CAGGCATAAAAGGCCCACTA AGGACTTCCGTAGCCTGGTT	58.4
Adiponectin	Adipose - late	Adiponectin is exclusively secreted by adipose tissue or placenta and it is a hormone that modulates a number of metabolic processes, including glucose regulation and fatty acid oxidation	TGATCTCGGCTTACTGCAAC ACAAGGTCAGGAGTTCGAGA	57.3

II.7. References

1. W. R. Gombotz and S. F. Wee, Protein release from alginate matrices, Advanced Drug Delivery Reviews, 2012, 64, 194-205.
2. C. K. Kuo and P. X. Ma, Ionically crosslinked alginate hydrogels as scaffolds for tissue engineering: Part 1. Structure, gelation rate and mechanical properties, Biomaterials, 2001, 22, 511-521.
3. K. Y. Lee and D. J. Mooney, Alginate: properties and biomedical applications, Prog Polym Sci, 2011, 37, 106-26.
4. J. A. Rowley, G. Madlambayan and D. J. Mooney, Alginate hydrogels as synthetic extracellular matrix materials, Biomaterials, 1999, 20, 45-53.
5. J. Yu, K. T. Du, Q. Fang, Y. Gu, S. S. Mihardja, R. E. Sievers, J. C. Wu and R. J. Lee, The use of human mesenchymal stem cells encapsulated in RGD modified alginate microspheres in the repair of myocardial infarction in the rat, Biomaterials, 2010, 31, 7012-7020.
6. V. L. Campo, D. F. Kawano, D. B. da Silva and I. Carvalho, Carrageenans: Biological properties, chemical modifications and structural analysis - A review, Carbohyd Polym, 2009, 77, 167-180.
7. E. G. Popa, M. T. Rodrigues, D. F. Coutinho, M. B. Oliveira, J. F. Mano, R. L. Reis and M. E. Gomes, Cryopreservation of cell laden natural origin hydrogels for cartilage regeneration strategies, Soft Matter, 2013, 9, 875-885.
8. V. E. Santo, A. M. Frias, M. Carida, R. Cancedda, M. E. Gomes, J. F. Mano and R. L. Reis, Carrageenan-Based Hydrogels for the Controlled Delivery of PDGF-BB in Bone Tissue Engineering Applications, Biomacromolecules, 2009, 10, 1392-1401.
9. P. M. Rocha, V. E. Santo, M. E. Gomes, R. L. Reis and J. F. Mano, Encapsulation of adipose-derived stem cells and transforming growth factor-beta 1 in carrageenan-based hydrogels for cartilage tissue engineering, J Bioact Compat Pol, 2011, 26, 493-507.
10. C. J. Morris, in Inflammation Protocols, 2003, 225, 115-121.
11. E. G. Popa, P. Carvalho, A. Dias, V. E. Santo, A. Frias, A. Marques, I. R. Dias, C. A. Viegas, M. E. Gomes and R. Reis, *In vitro* and *in vivo* biocompatibility evaluation of k-carrageenan hydrogels aimed at applications in regenerative medicine, J Biomed Mater Res A, 2014, 101, 4087-97.
12. J. Necas and L. Bartosikova, Carrageenan: a review, Veterinarni Medicina, 2013, 58, 187-205.
13. R. Hoffman, Carrageenans inhibit growth-factor binding, Biochem J, 1993, 289 (Pt 2), 331-334.
14. J. K. Francis Suh and H. W. T. Matthew, Application of chitosan-based polysaccharide biomaterials in cartilage tissue engineering: a review, Biomaterials, 2000, 21, 2589-2598.
15. M. Klagsbrun, The affinity of fibroblast growth factors (FGFs) for heparin; FGF-heparan sulfate interactions in cells and extracellular matrix, Curr Opin Cell Biol, 1990, 2, 857-863.
16. D. B. Pike, S. Cai, K. R. Pomraning, M. A. Firpo, R. J. Fisher, X. Z. Shu, G. D. Prestwich and R. A. Peattie, Heparin-regulated release of growth factors in vitro and angiogenic response in vivo to implanted hyaluronan hydrogels containing VEGF and bFGF, Biomaterials, 2006, 27, 5242-5251.
17. C. Noti and P. H. Seeberger, Chemical approaches to define the structure-activity relationship of heparin-like glycosaminoglycans, Chem Biol, 2005, 12, 731-756.
18. M. Labet and W. Thielemans, Synthesis of polycaprolactone: a review, Chem Soc Rev, 2009, 38, 3484-3504.
19. M. A. Woodruff and D. W. Hutmacher, The return of a forgotten polymer—polycaprolactone in the 21st century, Progress in Polymer Science, 2010, 35, 1217-1256.
20. C. X. Lam, D. W. Hutmacher, J. T. Schantz, M. A. Woodruff and S. H. Teoh, Evaluation of polycaprolactone scaffold degradation for 6 months in vitro and in vivo, J Biomed Mater Res A, 2009, 90, 906-919.
21. H. Sun, L. Mei, C. Song, X. Cui and P. Wang, The in vivo degradation, absorption and excretion of PCL-based implant, Biomaterials, 2006, 27, 1735-1740.
22. C. X. Lam, S. H. Teoh and D. W. Hutmacher, Comparison of the degradation of polycaprolactone and polycaprolactone–(β-tricalcium phosphate) scaffolds in alkaline medium, Polymer international, 2007, 56, 718-728.
23. A. J. Salgado, O. P. Coutinho and R. L. Reis, Novel starch-based scaffolds for bone tissue engineering: cytotoxicity, cell culture, and protein expression, Tissue Eng, 2004, 10, 465-474.

24. K. Y. Lim, B. C. Kim and K. J. Yoon, The effect of molecular weight of polycaprolactone on the ester interchange reactions during melt blending with poly(ethylene terephthalate), Polymer Journal, 2002, 34, 313-319.
25. E. Anitua, I. Andia, B. Ardanza, P. Nurden and A. T. Nurden, Autologous platelets as a source of proteins for healing and tissue regeneration, THROMBOSIS AND HAEMOSTASIS-STUTTGART-, 2004, 91, 4-15.
26. K. Stellos, S. Kopf, A. Paul, J. U. Marquardt, M. Gawaz, J. Huard and H. F. Langer, Platelets in regeneration, 2010.
27. A. Kalén, O. Wahlström, C. H. Linder and P. Magnusson, The content of bone morphogenetic proteins in platelets varies greatly between different platelet donors, Biochemical and biophysical research communications, 2008, 375, 261-264.
28. M. Osada, O. Inoue, G. Ding, T. Shirai, H. Ichise, K. Hirayama, K. Takano, Y. Yatomi, M. Hirashima and H. Fujii, Platelet activation receptor CLEC-2 regulates blood/lymphatic vessel separation by inhibiting proliferation, migration, and tube formation of lymphatic endothelial cells, Journal of Biological Chemistry, 2012, 287, 22241-22252.
29. J. B. Sipe, J. Zhang, C. Waits, B. Skikne, R. Garimella and H. C. Anderson, Localization of bone morphogenetic proteins (BMPs)-2,-4, and-6 within megakaryocytes and platelets, Bone, 2004, 35, 1316-1322.
30. H. J. Hausser and R. E. Brenner, Phenotypic instability of Saos-2 cells in long-term culture, Biochem Bioph Res Co, 2005, 333, 216-222.
31. D. J. Mcquillan, M. D. Richardson and J. F. Bateman, Matrix Deposition by a Calcifying Human Osteogenic-Sarcoma Cell-Line (Saos-2), Bone, 1995, 16, 415-426.
32. P. A. Zuk, M. Zhu, P. Ashjian, D. A. De Ugarte, J. I. Huang, H. Mizuno, Z. C. Alfonso, J. K. Fraser, P. Benhaim and M. H. Hedrick, Human adipose tissue is a source of multipotent stem cells, Molecular biology of the cell, 2002, 13, 4279-4295.
33. J. M. Gimble, A. J. Katz and B. A. Bunnell, Adipose-derived stem cells for regenerative medicine, Circ Res, 2007, 100, 1249-1260.
34. M. Strioga, S. Viswanathan, A. Darinskas, O. Slaby and J. Michalek, Same or not the same? Comparison of adipose tissue-derived versus bone marrow-derived mesenchymal stem and stromal cells, Stem cells and development, 2012, 21, 2724-2752.
35. H.-J. Park, Y. Zhang, S. P. Georgescu, K. L. Johnson, D. Kong and J. B. Galper, Human umbilical vein endothelial cells and human dermal microvascular endothelial cells offer new insights into the relationship between lipid metabolism and angiogenesis, Stem cell reviews, 2006, 2, 93-101.
36. H. Obokata, M. Yamato, S. Tsuneda and T. Okano, Reproducible subcutaneous transplantation of cell sheets into recipient mice, Nature Protocols, 2011, 6, 1053-1059.
37. B. Derby, Bioprinting: inkjet printing proteins and hybrid cell-containing materials and structures, Journal of Materials Chemistry, 2008, 18, 5717-5721.
38. S. M. Peltola, F. P. Melchels, D. W. Grijpma and M. Kellomaki, A review of rapid prototyping techniques for tissue engineering purposes, Ann Med, 2008, 40, 268-280.
39. T. Boudou, T. Crouzier, K. F. Ren, G. Blin and C. Picart, Multiple Functionalities of Polyelectrolyte Multilayer Films: New Biomedical Applications, Adv Mater, 2010, 22, 441-467.
40. R. R. Costa and J. F. Mano, Polyelectrolyte multilayered assemblies in biomedical technologies, Chem Soc Rev, 2014, 43, 3453-3479.
41. H. Bubert, J. C. Rivière and W. S. M. Werner, in Surface and Thin Film Analysis, Wiley-VCH 2011, pp. 7-41.
42. C. Picart, J. Mutterer, L. Richert, Y. Luo, G. D. Prestwich, P. Schaaf, J. C. Voegel and P. Lavalle, Molecular basis for the explanation of the exponential growth of polyelectrolyte multilayers, P Natl Acad Sci USA, 2002, 99, 12531-12535.
43. A. E. Carpenter, T. R. Jones, M. R. Lamprecht, C. Clarke, I. H. Kang, O. Friman, D. A. Guertin, J. H. Chang, R. A. Lindquist, J. Moffat, P. Golland and D. M. Sabatini, CellProfiler: image analysis software for identifying and quantifying cell phenotypes, Genome Biol, 2006, 7, R100.
44. H. Hirai, N. Katoku-Kikyo, P. Karian, M. Firpo and N. Kikyo, Efficient iPS cell production with the MyoD transactivation domain in serum-free culture, PloS one, 2012, 7, e34149.
45. E. E. Golub and K. Boesze-Battaglia, The role of alkaline phosphatase in mineralization, Current Opinion in Orthopaedics, 2007, 18, 444-448.
46. Z. Li, C. Liu, Z. Xie, P. Song, R. C. Zhao, L. Guo, Z. Liu and Y. Wu, Epigenetic dysregulation in mesenchymal stem cell aging and spontaneous differentiation, PloS one, 2011, 6, e20526.

SECTION 3

NEW STRATEGY TO CREATE HIERARCHICAL AND HYBRID 3D SCAFFOLDS WITH TUNABLE SURFACE PROPERTIES

CHAPTER III

HIERARCHICAL FIBRILLAR SCAFFOLDS OBTAINED BY NON-CONVENTIONAL LAYER-BY-LAYER ELECTROSTATIC SELF-ASSEMBLY

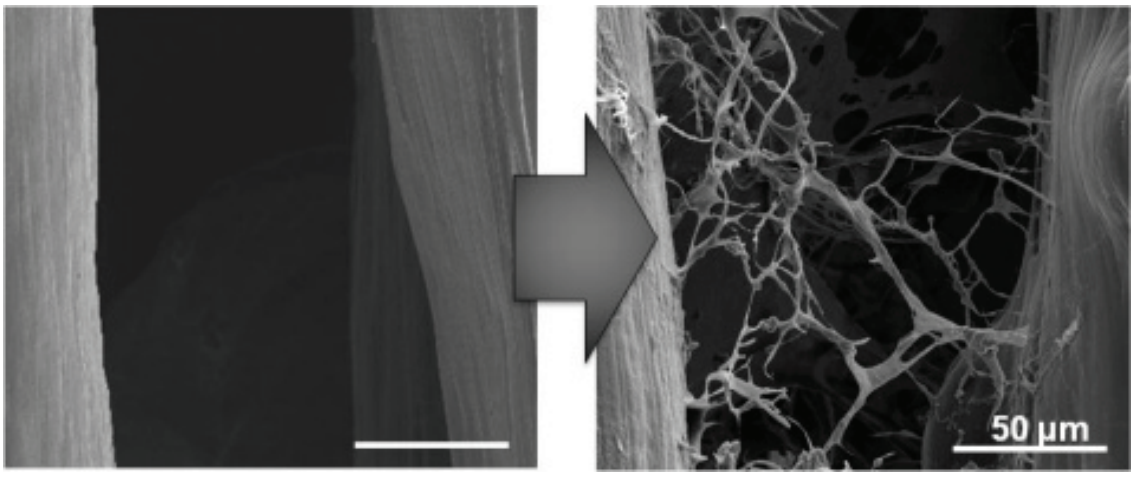

CHAPTER III*

Hierarchical fibrillar scaffolds obtained by non-conventional layer-by-layer electrostatic self-assembly

III.1. Abstract

A new approach for layer-by-layer assembling to create nano/micro fibrils or nanocoatings inside 3D scaffolds using non-fibrils polyelectrolytes for tissue engineering applications is disclosed. This approach shows to be promising for the development of advanced scaffolds, to improve biological performance, with controlled nano/micro environment, and nature and architecture similar to natural extracellular matrix.

Keywords: layer-by-layer, polyelectrolyte, multiscale, scaffolds, fibrillar, coatings, hierarchical, hybrid, alginate, chitosan.

*This chapter is based on the following publication:

Sara M. Oliveira, Tiago H. Silva, Rui L. Reis, João F. Mano. Hierarchical fibrillar scaffolds obtained by non-conventional layer-by-layer electrostatic self-assembly. Advanced Healthcare Materials. 2013

For the regeneration of hard tissues, the combination of synthetic and natural-origin materials arises as one of the best solutions to obtain 3D scaffolds with both adequate mechanical properties and similarly to extracellular matrix nature and architecture.[1] The ability to introduce nano/micro structures inside scaffolds is of great interest as a way to achieve those cells' environments and mimic the hierarchical organization of natural tissues. The external scaffolds may provide the necessary mechanical integrity and the macro/micro organization of the overall structure. The inner nano/micro environment presents anchorange points for cell attachment, with distinct biochemical properties for cell behavior control. With this purpose, micro/nano fibers produced by electrospinning have been combined with rapid prototyping and fiber-bonding techniques.[2] However, this processing method has been hampered by limited and heterogeneous distributions of micro/nano fibers throughout the scaffold's bare structure. In fact, only surface modification was achieved. In order to prepared scaffolds with internal nano/micro-structure, electrospinning has to be performed during the bare scaffold preparation, in a complex process that can lead to delamination of the final structure. Freeze-drying a polymeric structure inside a previously prepared scaffold is also an alternative to create a more native-like environment for cells; however, it is difficult to control the thickness and the morphology of those inner structures.[3,4]

Layer-by-layer (LbL) technique has been widely used to produce nanofilms for biomedical applications since its disclosure by Decher and co-workers.[5] LbL is based on a simple alternating deposition of polyanions and polycations, i.e. polyelectrolytes (PE's). The majority of the extracellular molecules and natural-origin polymers can be used as PE's, interacting with complementary PEs not only by electrostatic attraction, but also through hydrogen bonding or hydrophobic interactions. Studies regarding LbL assembly in 2D substractes have demonstrated control over surface chemistry, roughness, stiffness and cell behaviour, by playing with the type of PE's and the number of bilayers.[6–13] Modifidying 3D scaffolds with polyelectrolyte multilayers (PEMs) can improve cell-scaffold interactions [14] or those PEM's can provide growth factors reservoirs.[15] Using appropriate templates, highly porous scaffolds, entirely built by nanostructured multilayers, may also be prepared.[17]

To our knowledge, the LbL technology has not yet been utilized to develop inner structures inside previously fabricated scaffolds. In the conventional dipping LbL approaches, non-reacted or weakly bonded polyelectrolyte should be removed throughout the washing steps in order to obtain stable PEM films and coatings. Herein, by conjugating LbL assembly, based on incomplete washing steps to create small complexes, with ice crystal growth and water removal by freeze-drying, it was possible to modify synthetic 3D scaffolds with natural-origin polymers, creating hierarchical and fibrillar structures in the interior of the scaffolds.

With these structures, one can increase the available surface area for cell growth and create a biochemical and structural environment similar to that found in the natural fibrillar extracellular matrix, while maintaining the mechanical properties of the bare scaffold. Some works on the production of hybrid structures, combining hydrogels or collagen, scaffolds and freeze-drying are found in the literature.[18,19] However, those studies rely on the fibrous nature of collagen, not exhibited by most of the PE available, and such approaches produce mostly lamellar ones. Other advantages of our approach may be pointed out: i) no employment of toxic crosslinkers to sta- bilize the structures or improve the bonding with the scaffold; ii) virtually, the structures may be made

using any polycation/ polyanion; iii) ability to create highly controlled delivery systems on the coatings and fibrillar structures.

In our group, the LbL technology has been used in different tissue engineering approaches, in particular based on the electrostatic assembly of alginate (Alg) and chitosan (Chi) PEs.[20-22] Therefore, Chi and Alg were the pair of PEs selected to assess our approach for the modification of poly(ε-caprolactone) (PCL) scaffolds prepared by rapid prototyping - Figure III.1.a. PCL scaffolds were first fabricated using a rapid prototyping technique, using a Bioplotter, with strut diameters of approximately 0.5 mm and 10 consecutive layers, each oriented at 90 degrees with respect to the underlying layer.

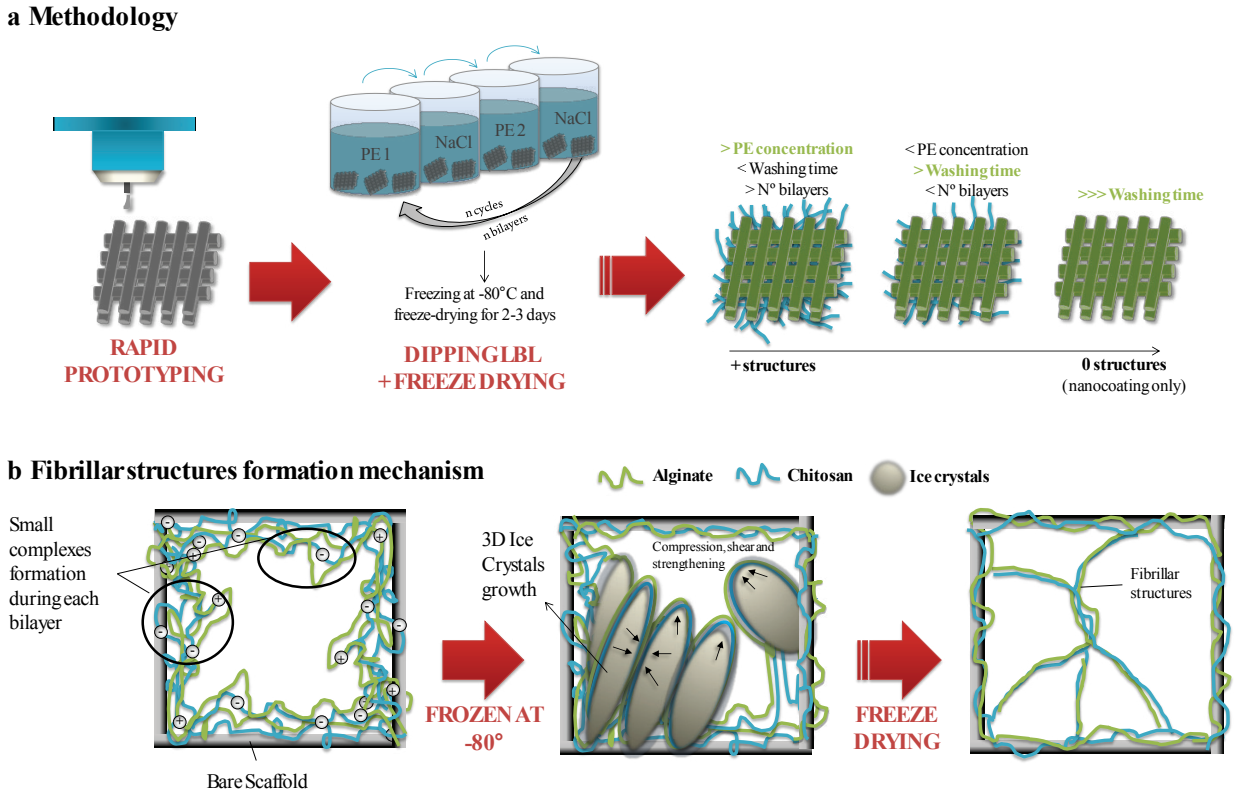

Figure III.1. (a) Steps for developing the hierarchical and hybrid 3D scaffolds. (b) Mechanism for the formation of the fibrillar structures.

Morphological properties of 2D PEM's, such as: roughness, topography and thickness, are influenced by several build parameters, such as PE type, charge density, ionic strength, pH, temperature, number of bilayers and washing time. When transposing the assmbling to 3D porous substrates, parameters exhibiting a higher impact on the final structure are expected to be those interfering with the flow of the solutions throughout the pores, such as: PE concentration, dipping velocity, number of bilayers and surface wettability. Thereby, in this study the influence of the number of bilayers, PE concentration, washing time and the outermost layer PE type were assessed. Briefly, a custom-made dipping robot was used to perform the LbL self-assembly by immersing diamine-modified PCL scaffolds: (1) in Alg solution during 10 minutes, (2) in a washing solution for 5 minutes, (3) in Chi solution for 10 minutes, and (4) in a washing solution for 5 minutes. This process was repeated until

the 15 PE double layers were attained, after which the scaffolds were washed several times with ultrapure water with agitation, and immediately frozen at −80 °C to let ice crystals to grow – Figure III.1.b. The final structure was obtained after freeze-drying, corresponding to the sample identified as 15 dL (15 double layers). By changing one of the experimental conditions, as summarized in Table III.1., other samples were produced: +Conc, by increasing the concentration of the PE's solutions; 30dL, by repeating the dipping cycle 30 times instead of only 15; +Alg, by depositing an additional Alg layer; and Coat, by increasing dramatically the duration of the washing steps.

Table III.1. Nomenclature of the samples and respective LbL building up parameters.

Sample	Nº bilayers	Outermost layer	Washing [min]	Conc. [mg ml^{-1}]
PCL	-	-	-	-
15dL	15	Chi	5	0.5
+Conc	15	Chi	5	5
30dL	30	Chi	5	0.5
+Alg	15	Alg	5	0.5
Coat	15	Chi	20+20	0.5

The morphology of the bare and modified scaffolds was observed by scanning electron microscopy (SEM)– Figure III.2. In addition, pores were observed in detail by stereomicroscopy, with respective images being depicted as shown in Figure III.S1. of the Supporting Information (SI). The scaffolds were also observed also by reflected microscopy with a 480 nm light source, since the high fluorescence intensity of Chi at this wavelength allows its detection on the structures. Chi was detected in all scaffolds except on the bare PCL. As it can be observed in the SEM micrographs in Figure III.2. (longitudinal section) and in the other images (top view), the fibrillar structures are not only present in one layer/section of the scaffold, but also on all the struts of the scaffold, vertical and horizontal.

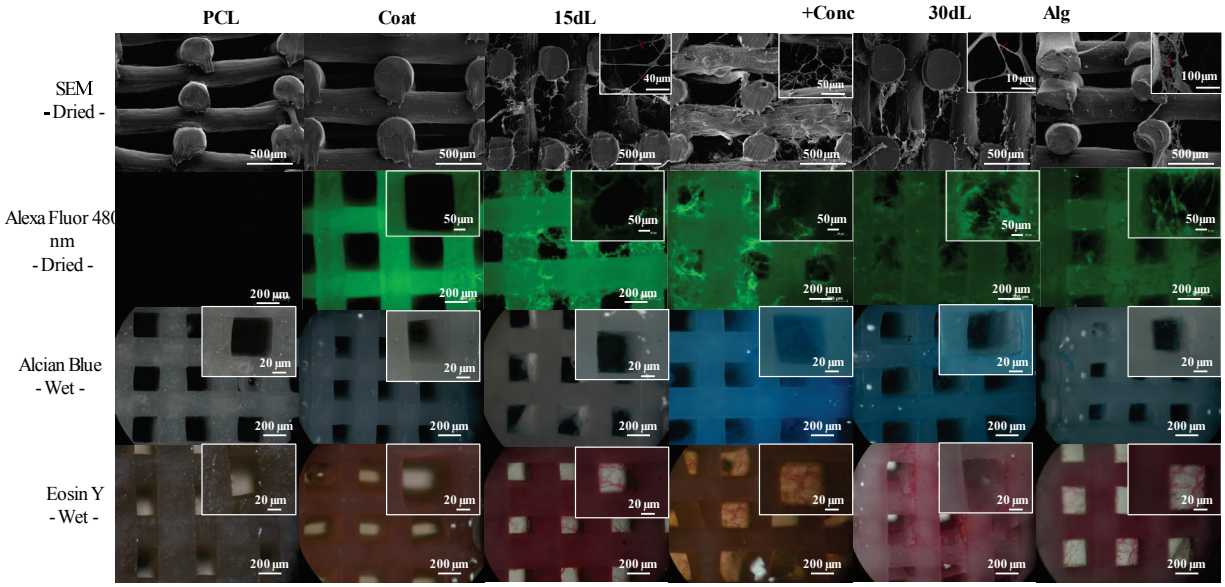

Figure III.2. Representative images of the structures of the scaffolds (from top to bottom): SEM micrographs; images of auto-fluorescence of chitosan under transmitted and reflected light microscope; stereomicroscope images of the Alcian blue staining; and stereomicroscope images of the eosin Y staining.

A distribution in xyz plans like this is not possible to obtain with hierarchical scaffolds employing electrospinning, where the fibers are deposited in just one xy plan. For the 15dL sample, used as reference, fibrillar structures ranging from nano to sub-micro scale were observed inside the dried scaffolds. The density could be increased in different directions: mostly closer to the struts by increasing number of bilayers (30dL) or uniformly inside the pores by increasing PEs concentration (+Conc). When using higher washing times, such fibrillar structures were not observed. In these cases, the PEM were assembled only over the surface of the PCL struts, corresponding to PE coatings (Coat). The formation of such fibrillar structures could then be attributed to the mechanism illustrated in Figure III.1.b. With shorter washing steps, excess quantities of PEs remained inside the pores, giving rise to small complexes next to the pores wall. Those complexes progressively grown with the multilayer build-up. Freezing the structures at −80 °C triggers the formation of ice crystals that compress, shear and stretch the LbL structures and small complexes, inducing the fibrillar-like morphology. In the case of higher concentration (+Conc), the viscosity of the PEs solutions was increased, limiting the efficiency of the washing step and enhancing the accumulation of remaining PEs inside the pores, which then promoted the development of more complexes in the whole volume of the scaffold.

On the other hand, when longer washing steps (Coat) were used, no PE remained free inside the pores and thus no PE complexes were promoted. The scaffolds were also observed by stereomicroscope, after specific staining for each PE: Alcian blue for Alg (blue color) and eosin Y for Chi (pink, red color); which color intensiveness increases with the polymer content–Figure III.2. Significant blue and pink colors were observed on all scaffolds (except in PCL), not only on the surface but also on the fibrillar structures, thus showing the presence of Alg and Chi on those scaffolds.

The morphology and 3D structure of the modified scaffolds were also observed by micro-computed tomography (μCT)–see Figure III.3. Within the limited resolution of μCT scanner it was possible to observe some of the PE structures distributed throughout the pores of the scaffold, namely in the sample +Conc–Figure III.3.a down, in opposition to bare scaffold–Figure III.3a. top, where no such structures were observed. The low definition of the fibrillar structures in the sample +Conc is attributed to their reduced dimensions: smaller than the resolution of the μCT scanner. In fact, SEM micrographs showed that some of those structures had thickness smaller than 1 μm.

The effect of the assembly over other relevant properties that can affect cell behavior was also assessed, namely: water uptake and mechanical properties. Introducing PEM coatings or fibrillar structures in PCL scaffolds is expected to give them the ability to uptake aqueous solutions due to the increase in surface charge density and thus hydrophilicity. The water uptake of modified scaffolds was determined as the change of the weight upon immersion in phosphate buffer saline (PBS) solution, at 37°C - Figure III.3.b. The presence of the LbL structures of the sample +Conc, has increased the water uptake by 40% relatively to PCL. The water uptake evidenced by PCL is attributed to be water retained inside the pores. The sample +Conc also showed a faster water uptake, indicating that with this condition a higher content of Alg/Chi structures was included in the PCL scaffolds. The analysis of the other samples has demonstrated that by controlling the concentration of the PEs

and the number of bilayers, one may adjust the swelling ratio of the hybrid scaffolds. This may be an important property for the preparation of ions/proteins reservoirs localized on the PEMs, to be explored in future works.

In order to verify whether the modification method impairs the mechanical properties of the scaffolds, the dried scaffolds were assessed by uniaxial compression tests. The compressive modulus was determined from the stress–strain data - see Figure III.3.c. The compressive moduli remained unchanged despite the assembly of PEs, being approximately 24 MPa. With 30 LbL cycles (30dL), the compression modulus has significantly increased to 30.8±5.4 MPa ($p<0.05$). This increase is attributed to a significant accumulation of PEs and structures mainly on the walls/structs of the PCL scaffolds, thus reinforcing the whole 3D structure. In fact, when the density of such structures inside the pores was higher and more uniformly distributed in whole pores volume, on +Conc sample, there was no significant increase in the compressive modulus. These observations indicate that playing with the assembly conditions, the density and localization of the LbL structures can be varied without compromising the original mechanical properties of the PCL scaffolds.

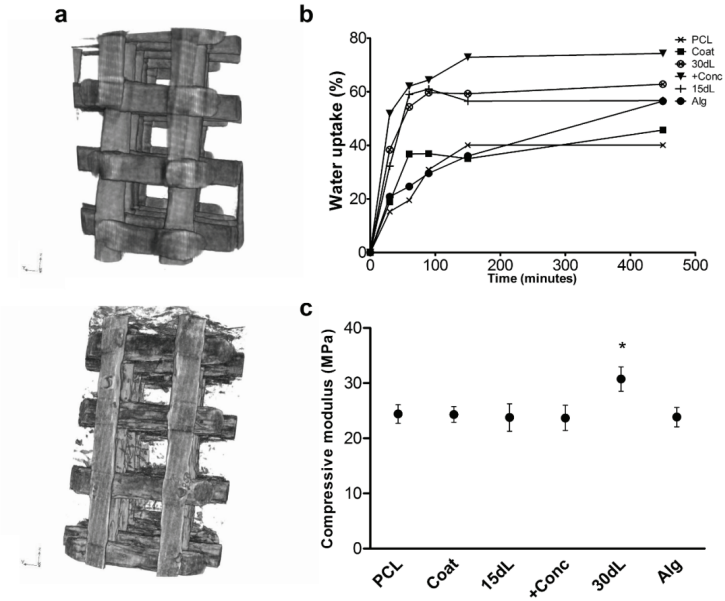

Figure III.3.(a) 3D scan of PCL (top) and +Conc (bottom) samples, obtained by µCT. (b) Water uptake behaviour as function of the immersion time in PBS at 37°C; (c) and compressive modulus of the studied scaffolds (* indicates all samples are statistically different from 30dL; samples with normal distribution were tested using t-test, $p<0.065$; $n>5$).

The ultimate goal of the purposed modification strategy is to improve cell seeding efficiency and cell behavior. In order to assess the biological behavior of the LbL modified scaffolds, their cytocompatibility was firstly evaluated, using SaOs-2 osteoblast-like cells, envisioning a bone tissue engineering application. Cells were cultured during 1 and 7 days for cell distribution analysis, by SEM and DAPI staining - Figure III.4., and proliferation and activity assessment, by dsDNA and ALP activity quantification - Figure III.5. To further characterize distribution of viable cells, live/dead assay was also performed, with results being available in the SI, Figure III.S2.

Cell attachment and adhesion occur within the first 24 hours in culture and are dictated by several surface properties including roughness, surface chemical groups, surface wettability, topography, protein adsorption,

medium conditions and cell type.[23] Rapid prototyped scaffolds have highly controlled and reproducible architectures, but those 3D structures are commonly characterized by big open pores and smooth surfaces that reduce cell seeding efficiency.

The introduction of Alg+Chi structures on the PCL prototyped scaffolds acted as cell entrapment networks where SaOs-2 cells were able to adhere, thus increasing cell attachment and cell seeding efficiency, particularly on sample +Conc, as can be seen by DAPI staining–Figure III.4.a 1day. Those findings are supported by SEM images, showing cell attachment in fibrillar structures (Figure III.4.b) and dsDNA quantification results (Figure III.5.a), showing higher dsDNA content on the scaffolds with fibrillar structures distributed in whole pore volume (+Conc) than on the ones where those fibrillar structures are more close to the walls (Coat, 15dL, 30dL, Alg samples).

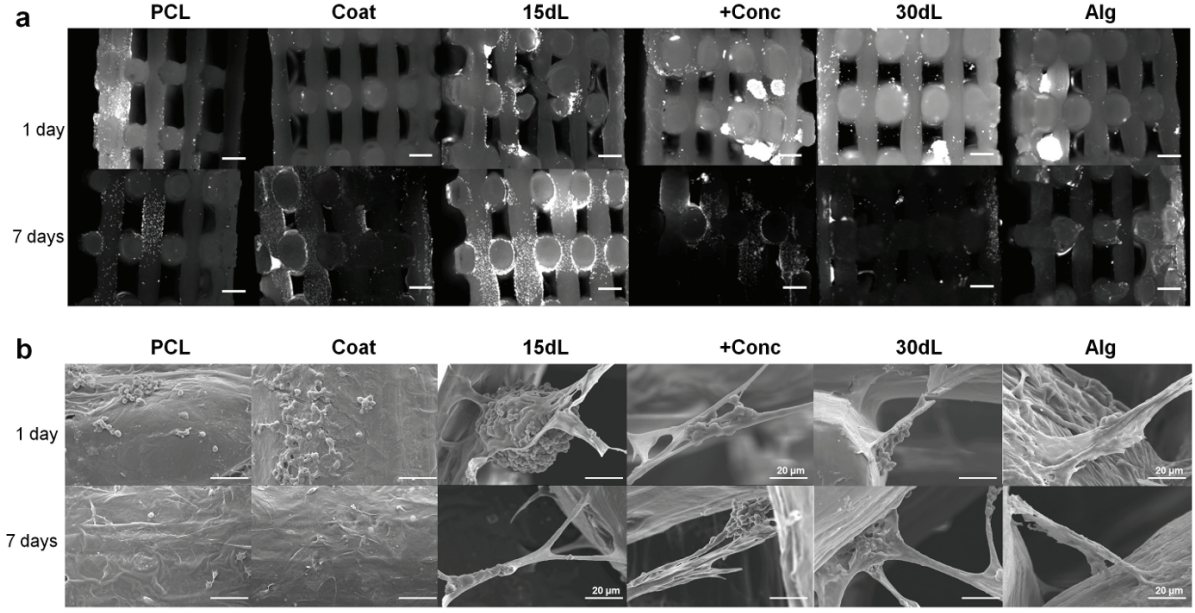

Figure III.4. (a) Scaffold longitudinal central section images of the cell nucleus stained with DAPI after 1 and 7 days in culture (Scale bar: 200 µm); (b) SEM micrographs showing SaOs-2 cell morphology and adhesion onto the surfaces or onto the fibrillar structures after 1 and 7 days in culture (Scale bar: 50 µm, where not indicated).

Alg lacks cell-adhesive ligands and support low protein adsorption which are important to promote and regulate cellular interactions [24, 25], which justifies the lowest dsDNA content observed for Alg sample (Alg as the outermost layer). The cationic nature of Chi allows electrostatic interactions with anionic glycosaminoglycans (GAGs) and proteoglycans. [26, 27] Moreover, Chi amine groups are known to increase the adsorption of proteins onto the PEM, creating more adhesive points for cells.[28] However, when assembled with Alg, cells have shown a tendency to form aggregates (Figure III.4.b 1 day) where the inner cells have lost viability (Figure III.S2. of the SI) and further come out of the scaffold after 7 days in culture (Figure III.4.b 7 days). The loss of cells upon formation of aggregates as a consequence of the low cell-adhesive groups on the Alg and Chi has made statistically undetectable cell proliferation on the fibrillar scaffolds (Figure III.5.a). In future, PE's able to enhance cell adhesion will be used to optimize the biological performance of the scaffolds. Nevertheless, in

the majority of the conditions, SaOs-2 cells were able to colonize whole longitudinal section, being present not only on the walls of the scaffolds but also in the fibrillar structures, as shown in Figure III.4.

Relatively to tissue culture polystyrene, in both modified and unmodified scaffolds, ALP activity was not altered after 1 day in culture, with expection of +Conc and Alg that showed oposite trends. With the culture time, ALP activity has increased in almost all the scaffolds with exception of Coat samples and reached values similar to +Conc (1 day).

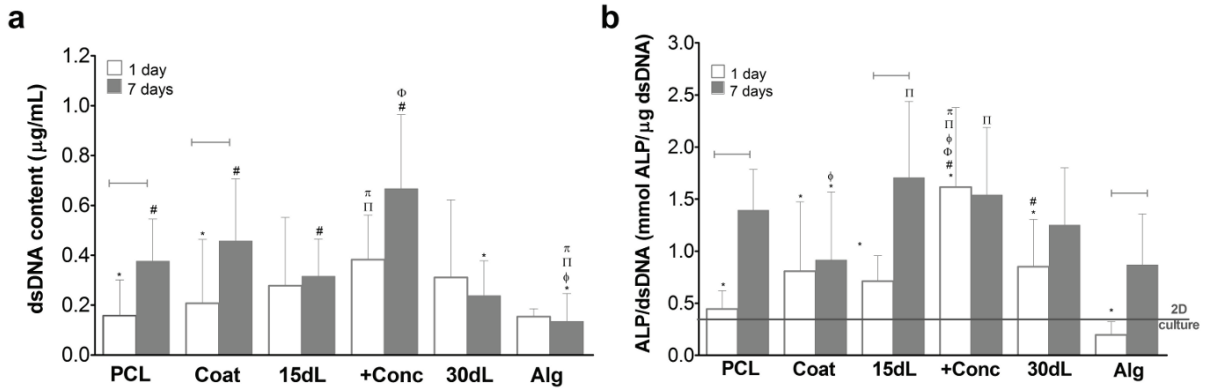

Figure III.5. (a) dsDNA content and (b) ALP activity of SaOs-2 per unit of dsDNA after 1 and 7 days in culture. All significant differences are indicated: ϕ - different from 15dL, Φ - different from 30dL, π - different from PCL, Π - different from Coat, * - different from +Conc, # - different from Alg (non-parametric Kruskal-Wallis and Dunn's post-hoc test were used, $p < 0.05$; $n > 6$).

The ability of some nanostructures to enhance ALP activity has been pointed out before, namely with carbon nanotubes[29] and PCL nanofiber meshes.[30]This suggests that the fibrillar structures can improve cell seeding and may also promote SaOs-2 activity and maturation as compared to 2D cultures.

In conclusion, the present work has revealed a new methodology to create nano/micro fibrillar structures composed of Alg and Chi inside 3D scaffolds, which may be extended to other types of PEs. By controlling the assembling parameters, namely washing time and PEs concentration, the density and distribution of these structures can be controlled. Although there is a lack of adhesive sites on Alg/Chi structures, which can be overcome with the selection of other PEs, SaOs-2 cells seeding efficiency has been improved in sample +Conc. Moreover, SaOs-2 were able to colonize the 3D scaffolds, including the introduced fibrillar structures, exhibiting also increased ALP activity in day 1. Thus, the introduction of such fibrillar features promises to play a role on the development of a new generation of hybrid scaffolds for tissue-engineering applications.

III.2. Experimental Section

Materials: PCL (Mw 70,000 to 90,000), Chi (medium Mw), ethylenediamine and sodium alginate (250 cP, 2%), 2-propanol, NaHO; DMEM, FBS, ATB, trypsin-EDTA and PBS were purchased from Sigma-Aldrich.

Fabrication of PCL scaffolds: PCL granules were inserted in the BioplotterTM cartridge and heated up to 90°C. Material was extruded by a 22G hypodermic needle with a strand size of 0.5 mm and layer thickness of 0.3 mm with struts aligned by 90° in 10 consecutive layers.

Introduction of fibrillar structures: Scaffolds were cut with 0.5×0.5 cm (width×length) and modified with 10% ethylenediamine in 2-propanol during 1 hour and 37°C. A custom-made robot was used to perform LbL assembly by immersing scaffolds first on alginate solution during 10 minutes, followed by the NaCl washing solution during 5 minutes, chitosan solution during 10 minutes and again washing solution during 5 minutes. This immersion sequence was repeated until completing 15 cycles – 15dL samples. Using different washing time, polyelectrolyte solution concentration and number of cycles, new groups of samples were obtained, according to Table 1. After the LbL, scaffolds were washed under mild agitation in NaCl solution and ultrapure water, and then, frozen at -80°C. Final step consisted on the water removal by freeze-drying.

Characterization: Scaffolds were characterized by the observation of the polyelectrolytes after staining, μCT, water uptake, and compression modulus. The water uptake percentage was calculated by the differences of weight between the dried and the wet scaffolds. Instron 4505 Universal Machine was used with a crosshead speed of 2 mm min-1 in the compression testing. The compressive modulus was determined in the most linear region of the stress–strain graph and in the cases that the yield stress was not clear it was calculated as the stress at the intersection of a line drawn parallel to the linear region and intercepting the x-axis at 3 to 5% strain. Scaffolds were observed under stereomicroscope after staining with Eosin Y (staining for chitosan) and Alcian Blue (staining for alginate) and under a light source of 480 nm under to observe the auto-fluorescent chitosan-based structures.

Cytocompatibility assessment: SaOs-2 were seeded on the developed scaffolds with a cellular density of 300,000 10 μL-1 during 2.70 hours and then 1mL of DMEM containing FBS. After 1 and 7 days in culture, cells were fixed using 2.5 % formalin. Then, a number of samples were stained with DAPI (1 mg/ml) and observed under the reflected transmitted microscope with a light source of 358 nm. Scaffolds with non-fixed cells were used to perform live/dead assay. dsDNA quantification was performed as indicated by the product provider (Quant-iT™ PicoGreen®; Invitrogen). The ALP was evaluated using p-nitrophenol assay. Paranitrophenyl phosphate, which is colourless, is hydrolysed by alkaline phosphatase at pH 9.8 and 37ºC to form free p-nitrophenol, which is coloured yellow. The reaction is stopped by addition of NaHO and the absorbance read at 405 nm. For SEM observation under Leica Cambridge microscope, cells were fixed with

III.3. Acknowledgements

This work was partially supported by the European Union/ EFDR through the POCTEP project 0330_IBEROMARE_1_P. Portuguese Foundation for Science and Technology is gratefully acknowledged for fellowships of S.M.O. (SFRH/BD/70107/2010) and T.H.S. (SFRH/BPD/34704/2007). The authors wish to acknowledge J. Miguel Oliveira for assistance with micro-CT measurements.

III.4. Supporting Information

III.4.1. Materials

Chitosan (Chi) bought from Sigma Aldrich was purified by a precipitation method. Briefly, Chi powder was dissolved in 2% (v/v) of acetic acid in a concentration of 1% (w/v). The solution was maintained under stirring overnight at room temperature. The impurities were removed by three/four filtration cycles. Then, Chi was precipitated using 1M NaOH while stirring. Final steps consisted on washing Chi with distilled water till reach a neutral pH and remove the excess of water washig with alcoholic solution. Chi was freeze-dried during 3 days and finally grinded. Poly(ε-caprolactone), Sodium alginate and ethylenediamine were obtained from Sigma Aldrich.

III.4.2. Methods

III.4.2.1. PCL scaffolds by Bioplotter

The equipment used to produce PCL scaffold was the 3D Bioplotter™. This equipment has the capacity of build-up scaffolds using the widest range of materials of any singular rapid prototyping machine, from soft hydrogels over polymer melts up to hard ceramics and metals. Poly(ε-caprolactone) was bought from Sigma (PCL; Ref: 440744) with an average molecular number between 70000 and 90000. After optimization, the best deposition parameters obtained which were used to produce the 3D structures for this work were:

- Needle diameter = fiber diameter: 0.5 mm
- Layer thickness: 0.3 mm
- Strand size: 0.5 mm
- Scaffold size: 2×2 cm
- Needle size: 2 mm
- Compressed air pressure: 4-5 MPa
- Temperature set at: 90°C
- Head velocity: 20%-35%
- Number of layer build-up: 10

III.4.2.2. Assembly of polyelectrolyte multilayers and constructs in PCL porous structure

Before starting the modification with polyelectrolytes, the scaffolds of Coat, +dL, +Conc, 15dL, +Alg and -Vel scaffolds were pre-modified with ethylenediamine 10% (v/v) in 2-propanol during 1 hour at 37ºC to introduce positive charged amine groups on the surface and improve the binding between the first layer and the surface. This modification also increases the surface wettability, which facilitates the flow of the solution throughout the pores, diminishing the possibility of the pores got occluded, therefore, making the modification more homogeneous. Then, the scaffolds were intensively washed several times with ultrapure water and 0.5 M NaCl pH 5.5. For the layer-by-layer (LbL) modification a homemade dipping robot was used. Approximately 20 scaffolds per condition were fixed onto the robot arm using nylon fibers. The time in each cup (40 ml of

solution), the number of cups, and the number of cycles were set according to what is described in Table 1. The deposition time in each polyelectrolyte was 10 minutes for all conditions. After the LbL, the samples were washed with NaCl solution and ultrapure water under mild agitation. To let ice crystals growth, scaffolds were frozen at -80ºC. To finish the modification, the water crystals were removed by freeze-drying during 2-3 days.

Samples were sterilized using ethylene oxide to preliminary cell culture tests.

III.4.3. Characterization

III.4.3.1. Polyelectrolyte staining

Alcian blue and eosin Y staining can be considered specific staining to alginate and chitosan, respectively once the structures are cell and extracellular matrix-free. Commercial solutions of alcian blue and eosin Y were used to stain the scaffolds by adding 1 ml of the respective solutions and kept at room temperature for 1 hour. The excess of staining was then removed by washing with phosphate buffer saline solution (PBS) and kept in PBS. Scaffolds were further observed under stereomicroscope. The higher the intensiveness of the color, the higher the content of polyelectrolyte is.

Dried, modified and unmodified samples were observed by reflected and transmitted microscope with a 480 nm light source to analyze the morphology. At this wavelength, the polyelectrolytes can be distinguished from the pure PCL once chitosan has high fluorescence intensity.

III.4.3.2. SEM

Scaffolds surface and structures morphology were observed using a Leica Cambridge S-360 scanning electron microscope (SEM, Leica Cambridge, UK). All surfaces were precoated with a conductive layer of sputtered gold. The SEM micrographs were taken at an accelerating voltage of 15 kV and at different magnifications

III.4.3.3. Water uptake

To assess the ability to uptake water, scaffolds of known weight (Wi) were immersed in PBS solution (pH 7.4) and incubated at 37°C under static conditions. The samples were left for 30, 60, 90, 120 and 450 minutes. The water uptake percentage was calculated by the following formula: %=Wf - WiWi×100, where, Wf is the final weight and Wi is the initial weight. To measure Wf, the swollen samples were weighted after the removal of excessive surface water with filter paper. Each experiment was repeated twice, and the average value was considered to be the water uptake value.

III.4.3.4. micro-CT

The architecture and porosity of the tubular scaffolds were analyzed by micro-computed tomography (μ-CT) using a desktop μ-CT scanner (1072; SkyScan, Kontich, Belgium) at voltage of 40 kV, current of 248 mA and in high resolution mode of 11 μm x/y/z. Isotropic slice data were obtained by the system and reconstructed into 2D XY slice images. Around 600 slice images per sample were compiled and subsequently employed in the rendering of 3D XYZ images. A μ-CT analyzer and a μ-CT volume realistic 3D Visualization software (SkyScan) was used as an image processing tool for reconstruction and creation=observation of 3D scaffold representations.

III.4.3.5. Mechanical Properties

In order to verify if our methodology alters the mechanical properties of the dried scaffolds, uniaxial compression testes where performed on the cubic scaffolds by Instron 4505 Universal Machine. A crosshead speed of 2 mm/min was used in the compression tests. The values reported are the average of at least five specimens per condition. The compressive modulus was determined in the most linear region of the stress–strain graph and in the cases that the yield stress was not clear it was calculated as the stress at the intersection of a line drawn parallel to the linear region and intercepting the x-axis at 3 to 5% strain.

III.4.4. Cell behavior characterization

III.4.4.1. Cell culture and seeding

The cytocompatibility of the developed scaffolds was evaluated using SaOs-2 cell lines, envisioning a bone tissue engineering application. SaOs-2 is a human primary osteoscarcoma cell line which was obtained from European Collection of Cell Cultures (ECACC) and is able to mimic the different stages of bone regeneration under specific stimulus. Cells were grown in Dulbecco's Modified Eagle's medium low glucose (DMEM, Sigma-Aldrich) with phenol red and supplemented with 10% heat inactivated fetal and 1% antibiotic-antimycotic solution (AT) in a humidified atmosphere with 5% CO_2 at 37°C. For expansion, confluent cells cultures were split 1:3 to 1:6 using 0.25% trypsin/EDTA. For cell seeding, samples were sterilized with ethylene oxide. Samples were immersed in DMEM containing FBS during 2 hours in order to allow the structures swelling and protein absorption. Cells were harvested by trypsinization and filter with cell strainer 100 μm to remove possible cell aggregates. The medium was removed and a drop of 10 μl of cell suspension containing 300,000 cells dripped onto the top of the scaffolds. The samples were incubated during 2.7 hours at 37°C with 5% of CO_2 to allow cell attachment. After this period 1 ml of DMEM containing FBS was added to each specimen. The samples were rinsed twice with sterile PBS and then fixed with formalin 2.5% (v/v) (for DAPI) or glutaraldehyde 2.5% (v/v) (for SEM), and washed extensively with PBS after these incubation. After 1 and 7 days in culture, the samples for SEM observation were dehydrated through a graded series of ethanol (50, 70, 90, 100 % v/v; each one during 10

minutes and twice) and dried at room temperature. The other part was stained with 4,6-diamidino-2-phenylindole (DAPI; 1 mg/ml) and incubated in the dark. DAPI is a fluorescent stain that binds strongly to dsDNA. Then, after 15 minutes, staining was removed and the samples were washed twice with PBS. A reflected/transmitted light microscope (wavelengths: excitation 358 nm and emission 460 nm) was used to visualize the nucleus of the cells.

III.4.4.2. dsDNA quantification

dsDNA content was quantified using the Quant-iT™ PicoGreen® dsDNA assay kit (Molecular Probes/Invitrogen) that allows the measurement of the fluorescence produced when PicoGreen dye is excited by UV light while bound to dsDNA. After incubation periods of 1 and 7 days, samples were rinsed twice with sterile PBS and transferred to small tubes, where 1 mL of ultra-pure sterile water was added. All samples were directly transferred to storage at -80°C and kept until quantification. For the quantification, samples were defrosted at room temperature and then sonicated during 30 minutes. 100 mL of Tris–EDTA buffer were transferred into a white opaque 96-well plate. Samples were vortexed and 28.8 mL of each plus 71.2 mL of PicoGreen solution were added to the wells. After 10 minutes of incubation in the dark, the plate was read on a microplate reader using an excitation wavelength of 485 nm and emission wavelength of 528 nm. A standard curve was created by varying the concentration of dsDNA standard from 0 to 2 mg/mL, and the DNA values of the samples were read off from the standard graph.

III.4.4.3. ALP activity quantification

Alkaline Phosphatae (ALP) is the most frequently used biochemical earlier marker of osteoblastic bone formation. ALP activity was quantified in the same samples used for dsDNA quantification. The activity of ALP is evaluated using p-nitrophenol assay. Paranitrophenyl phosphate, which is colorless, is hydrolysed by alkaline phosphatase at pH 9.8 and 37ºC to form free para-nitrophenol, which is colored yellow. The reaction is stopped by addition of NaOH and the absorbance read at 405 nm. Briefly, in each well of a 96-well plate, 20 µl of each sample previously vortexed, were mixed with 60 µl substrate solution and 0.2% wt/v p-nytrophenyl phosphate (Sigma-Aldrich), in a substrate buffer of 1 M diethanolamine (Sigma-Aldrich) at pH 9.8. The plate was then incubated in the dark for 45 min at 37°C. After the incubation period, 80 µl stop solution with is composed by 2 M NaOH (Panreac) plus 0.2 mM EDTA (Sigma-Aldrich), was added to each well. Standards were prepared with 10 µM/ml p-nytrophenol (pNP, Sigma, USA) solution, to obtain a standard curve covering the range 0–0.3 µM/ml. Triplicates of each sample and standard were made. Finally, absorbance was read at 405 nm in a microplate reader (Bio-Tek, Synergie HT) and sample concentrations were read off from the standard curve. The ALP concentrations were normalized against the dsDNA concentrations of the same samples to determine the ALP activity.

III.4.4.4. Live/dead assay

Live/dead assay is used to measure cell viability. It is a two-color fluorescence assay that simultaneously highlights the living (green) and dead (red) cells. Briefly, the culture medium was removed and the samples washed twice with PBS for 5 minutes, then 250 mL of calcein AM solution and propidium iodide/RNAse solution was added and incubated for 10 minutes in the cell incubator protected from light, after 1 and 7 days in culture. Then, the solutions were removed and samples washed twice with sterile PBS and observed under transmitted reflected microscope using the red and green fluorescence filters.

III.4.4.5. Scanning electron microscopy observation

The samples with cellular material, after being washed twice with sterile PBS, were fixed with 2.5% glutaraldehyde (Sigma, USA) for 1 h and at 4°C, to evaluate the cell morphology and distribution at the surface. Then, they were dehydrated through a graded series of ethanol (50, 70, 90 and 100%, v/v), each during 15 minutes and dried at room temperature. The surface morphology of the samples was observed using a Leica Cambridge S-360 scanning electron microscope (SEM, Leica Cambridge, UK). All surfaces were precoated with a conductive layer of sputtered gold. The SEM micrographs were taken at an accelerating voltage of 15 kV and at different magnifications

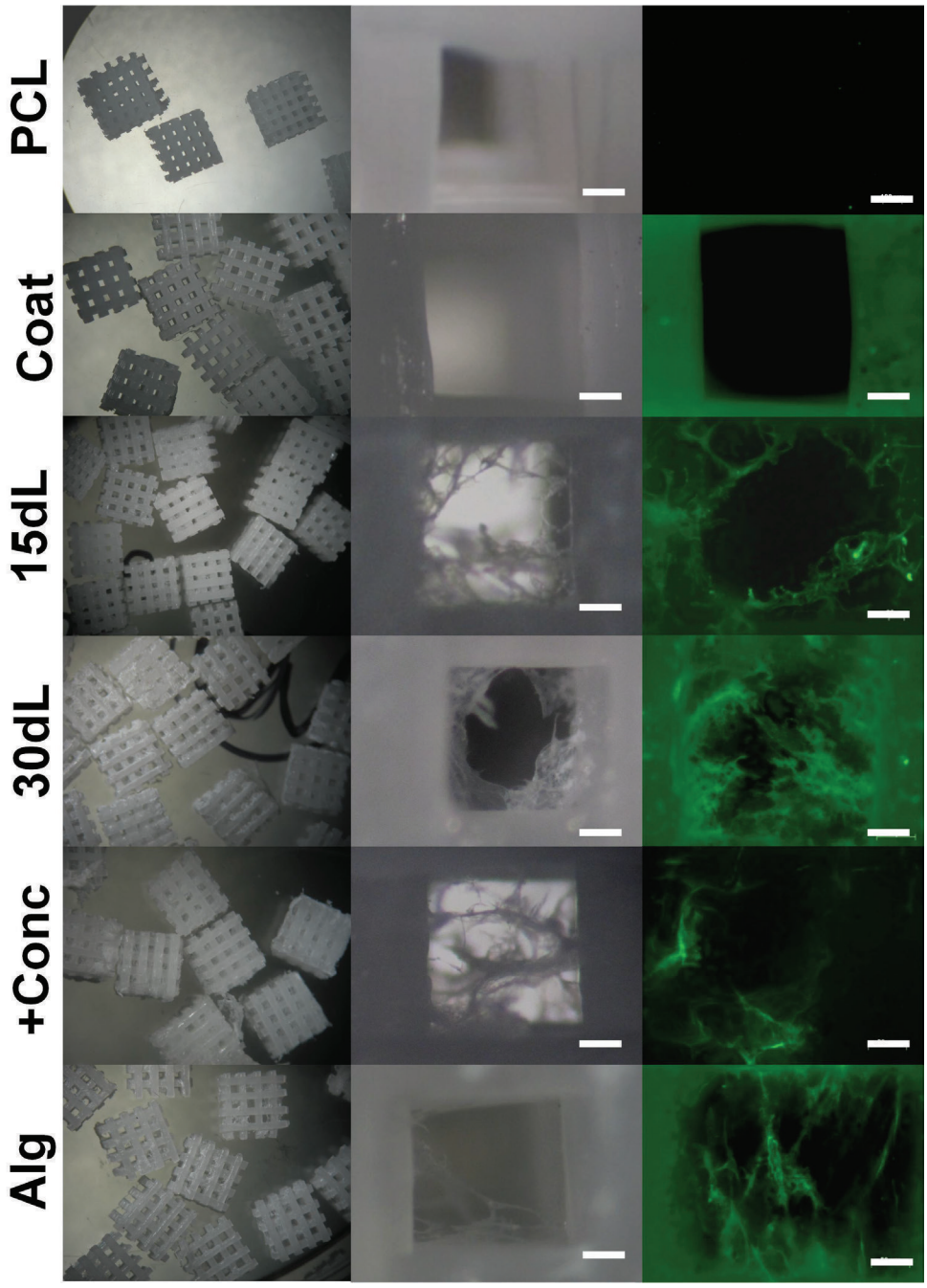

Figure III.S1. Photographs obtained by stereomicroscopy of the top view plan and pore magnification. Images obtained using green fluorescence microscope of the magnified pores. Scale bar: 50 µm.

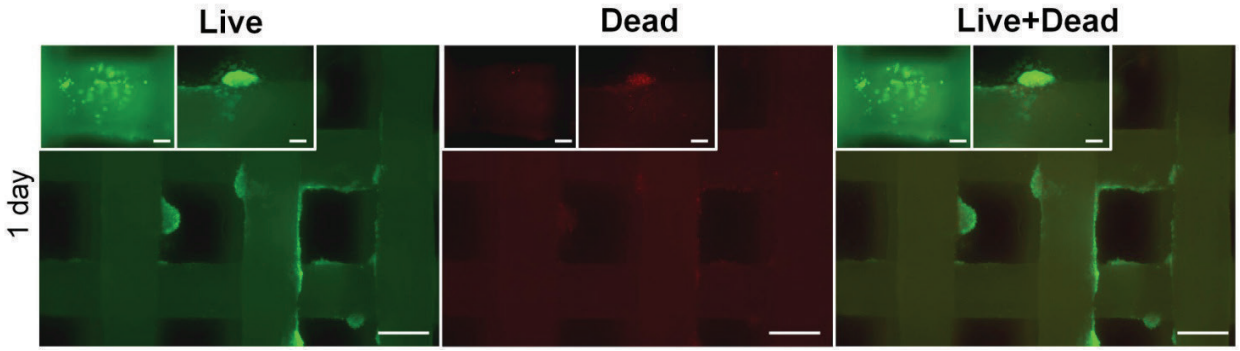

Figure III.S2. Live/dead assay images performed to +Conc sample after 1 and 7 days in culture. Scale bar: 200 µm. Inset bar scale: 50 µm

III.5. References

1. G. Chen, T. Sato, T. Ushida, N. Ochiai and T. Tateishi, Tissue engineering of cartilage using a hybrid scaffold of synthetic polymer and collagen, Tissue Engineering, 2004, 10, 323-330.

2. S. H. Park, T. G. Kim, H. C. Kim, D. Y. Yang and T. G. Park, Development of dual scale scaffolds via direct polymer melt deposition and electrospinning for applications in tissue regeneration, Acta Biomaterialia, 2008, 4, 1198-1207.
3. J. F. Mano, G. Hungerford and J. L. Gómez Ribelles, Bioactive poly (L-lactic acid)-chitosan hybrid scaffolds, Materials Science and Engineering: C, 2008, 28, 1356-1365.
4. J. Antunes, J. Oliveira, R. Reis, J. Soria, J. Gómez-Ribelles and J. Mano, Novel poly (L-lactic acid)/hyaluronic acid macroporous hybrid scaffolds: Characterization and assessment of cytotoxicity, Journal of Biomedical Materials Research Part A, 2010, 94, 856-869.
5. G. Decher, J. D. Hong and J. Schmitt, Buildup of ultrathin multilayer films by a self-assembly process .3. Consecutively alternating adsorption of anionic and cationic polyelectrolytes on charged surfaces, Thin Solid Films, 1992, 210, 831-835.
6. M. Zenobi-Wong, R. F. Mhanna and J. Voros, Layer-by-Layer Films Made from Extracellular Matrix Macromolecules on Silicone Substrates, Biomacromolecules, 2011, 12, 609-616.
7. P. R. Van Tassel, J. A. Phelps, S. Morisse, M. Hindie, M. C. Degat and E. Pauthe, Nanofilm Biomaterials: Localized Cross-Linking To Optimize Mechanical Rigidity and Bioactivity, Langmuir, 2011, 27, 1123-1130.
8. C. Picart, T. Boudou, T. Crouzier, C. Nicolas and K. Ren, Polyelectrolyte Multilayer Nanofilms Used as Thin Materials for Cell Mechano-Sensitivity Studies, Macromol Biosci, 2011, 11, 77-89.
9. T. Groth, M. S. Niepel and D. Peschel, Controlling fibroblast adhesion with pH modified polyelectrolyte multilayers, Int J Artif Organs, 2011, 34, 185-191.
10. B. H. Choi, Y. S. Choi and H. J. Cha, Osteoblast cell behavior on titanium surface coated with mussel adhesive protein and hyaluronic acid by layer-by-layer method, Abstr Pap Am Chem S, 2011, 241.
11. E. L. Chaikof', J. T. Wilson, W. X. Cui, V. Kozovskaya, E. Kharlampieva, D. Pan, Z. Qu, V. R. Krishnamurthy, J. Mets, V. Kumar, J. Wen, Y. H. Song and V. V. Tsukruk, Cell Surface Engineering with Polyelectrolyte Multilayer Thin Films, J Am Chem Soc, 2011, 133, 7054-7064.
12. J. H. Y. Ting, M. R. Haas, S. M. Valenzuela and D. K. Martin, Terminating polyelectrolyte in multilayer films influences growth and morphology of adhering cells, Iet Nanobiotechnol, 2010, 4, 77-90.
13. C. Picart, K. F. Ren, L. Fourel, C. G. Rouviere and C. Albiges-Rizo, Manipulation of the adhesive behaviour of skeletal muscle cells on soft and stiff polyelectrolyte multilayers, Acta Biomaterialia, 2010, 6, 4238-4248.
14. Y. H. Gong, Y. B. Zhu, Y. X. Liu, Z. W. Ma, C. Y. Gao and J. C. Shen, Layer-by-layer assembly of chondroitin sulfate and collagen on aminolyzed pOly(L-lactic acid) porous scaffolds to enhance their chondrogenesis, Acta Biomaterialia, 2007, 3, 677-685.
15. M. L. Macdonald, R. E. Samuel, N. J. Shah, R. F. Padera, Y. M. Beben and P. T. Hammond, Tissue integration of growth factor-eluting layer-by-layer polyelectrolyte multilayer coated implants, Biomaterials, 2011, 32, 1446-1453.
16. T. Crouzier, K. Ren, C. Nicolas, C. Roy and C. Picart, Layer-By-Layer Films as a Biomimetic Reservoir for rhBMP-2 Delivery: Controlled Differentiation of Myoblasts to Osteoblasts, Small, 2009, 5, 598-608.
17. P. Sher, C. A. Custódio and J. F. Mano, Layer-By-Layer Technique for Producing Porous Nanostructured 3D Constructs Using Moldable Freeform Assembly of Spherical Templates, Small, 2010, 6, 2644-2648.
18. G. P. Chen, T. Sato, T. Ushida, R. Hirochika, Y. Shirasaki, N. Ochiai, T. Tateishi, The use of a novel PLGA fiber/collagen composite web as a scaffold for engineering of articular cartilage tissue with adjustable thickness, J. Biomed. Mater. Res. A, 2003, 67, 1170-80.
19. W. D. Dai, N. Kawazoe, X. T. Lin, J. Dong, G. P. Chen, The influence of structural design of PLGA/collagen hybrid scaffolds in cartilage tissue engineering, Biomaterials, 2010, 31, 214152.
20. N. M. Alves, C. Picart and J. F. Mano, Self assembling and crosslinking of polyelectrolyte multilayer films of chitosan and alginate studied by QCM and IR spectroscopy, Macromol Biosci, 2009, 9, 776-785.
21. G. V. Martins, E. G. Merino, J. F. Mano and N. M. Alves, Crosslink Effect and Albumin Adsorption onto Chitosan/Alginate Multilayered Systems: An in situ QCM-D Study, Macromol Biosci, 2010, 10, 1444-1455.
22. E. S. Miranda, T. H. Silva, R. L. Reis and J. F. Mano, Nanostructured Natural-Based Polyelectrolyte Multilayers to Agglomerate Chitosan Particles into Scaffolds for Tissue Engineering, Tissue Eng Pt A, 2011, 17, 2663-2674.

23. N. M. Alves, I. Pashkuleva, R. L. Reis and J. F. Mano, Controlling Cell Behavior Through the Design of Polymer Surfaces, Small, 2010, 6, 2208-2220.
24. K. Y. Lee and D. J. Mooney, Alginate: properties and biomedical applications, Progress in Polymer Science, 2011.
25. J. A. Rowley, G. Madlambayan and D. J. Mooney, Alginate hydrogels as synthetic extracellular matrix materials, Biomaterials, 1999, 20, 45-53.
26. A. R. Costa-Pinto, R. L. Reis and N. M. Neves, Scaffolds based bone tissue engineering: the role of chitosan, Tissue Engineering Part B: Reviews, 2011.
27. T. W. Groeneveld, M. Oroszlan, R. T. Owens, M. C. Faber-Krol, A. C. Bakker, G. J. Arlaud, D. J. McQuillan, U. Kishore, M. R. Daha and A. Roos, Interactions of the extracellular matrix proteoglycans decorin and biglycan with C1q and collectins, J Immunol, 2005, 175, 4715-4723.
28. H. G. Xie, X. X. Li, G. J. Lv, W. Y. Xie, J. Zhu, T. Luxbacher, R. Ma and X. J. Ma, Effect of surface wettability and charge on protein adsorption onto implantable alginate-chitosan-alginate microcapsule surfaces, J Biomed Mater Res A, 2010, 92, 1357-1365.
29. X. M. Li, H. Gao, M. Uo, Y. Sato, T. Akasaka, S. Abe, Q. L. Feng, F. Z. Cui and F. Watari, Maturation of osteoblast-like SaoS2 induced by carbon nanotubes, Biomed Mater, 2009, 4, 015005.
30. P. Wutticharoenmongkol, N. Sanchavanakit, P. Pavasant and P. Supaphol, Novel bone scaffolds of electrospun polycaprolactone fibers filled with nanoparticles, J Nanosci Nanotechno, 2006, 6, 514-522.

SECTION 4

2D SULFATED LAYER-BY-LAYER ASSEMBLED NANOCOATINGS

CHAPTER IV

NANOCOATINGS CONTAINING SULFATED POLYSACCHARIDES PREPARED BY LAYER-BY-LAYER AS MODELS TO STUDY CELL-MATERIALS INTERACTIONS

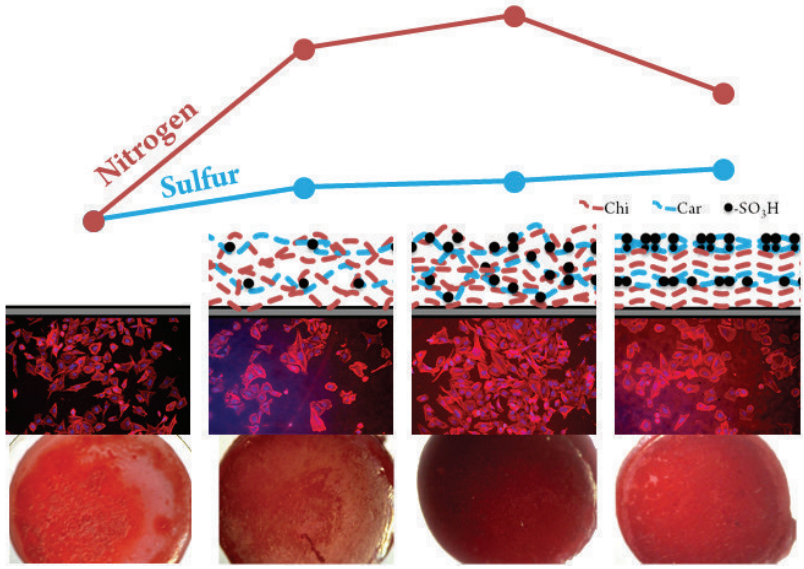

CHAPTER IV*

Nanocoatings containing sulfated polysaccharides prepared by Layer-by-Layer as models to study cell-materials interactions

IV.1. Abstract

The understanding of both cell-extracellular matrix (ECM) and cell-materials interactions is crucial for the success of implantable biomaterials including tissue engineering devices. ECM is rich in sulfated and aminated glycosaminoglycans and proteoglycans. In this way, the development of synthetic models containing those chemical groups is a major interest. Thin coatings of polysaccharides with controlled sulfur and nitrogen content were developed by Layer-by-Layer assembly. In particular, the multilayers were prepared by assembling chitosan with κ-, ι- and λ-carrageenan (increasing sulfur content). The nanostructured multilayers where characterized by quartz crystal microbalance with dissipation (QCM-D), atomic force microscopy (AFM), scanning electron microscopy (SEM), water contact angle, x-ray photoelectron spectroscopy (XPS) and used as models to study the effect of the sulfate groups over the behaviour of osteoblast-like cells. The biomimetic coatings increased ALP activity and proliferation comparing with unmodified polycaprolactone surfaces. Biomineralization on ι-carrageenan coatings was significantly higher than with other coatings, suggesting that the sulfate groups may interact positively with molecules involved in the osteoblastic activity, which depended on the sulfur and amine content of the surface. The developed nanocoatings can constitute an interesting model to understand the biological influence of the sulfate and amine groups existing on the surface of biomaterials.

Keywords: layer-by-layer, cell-materials interactions, cell behavior, sulfate, surface properties, bio-inspired surfaces, model study.

*This chapter is based on the following publication:

Sara M. Oliveira, Tiago H. Silva, Rui L. Reis, João F. Mano. Nanocoatings containing sulfated polysaccharides prepared by Layer-by-Layer as models to study cell-materials interactions, Journal of Materials Chemistry B, 2013.

IV.2. Introduction

Bone is a hierarchical composite material composed mainly by three types of cells - osteoblasts, osteoclasts and osteocytes, plus extracellular matrix (ECM) and vasculature.[1, 2] Normal ECM is composed by 50 to 70% of a mineral part of calcium phosphates ($[Ca_{10}(PO_4)_6(OH)_2]$), 20 to 40% of organic matrix, 5 to 10% of water, and < 3% of lipids.[1, 2] The organic and regulatory part is rich in glycosaminoglycans (GAG's), sialoproteins, bone "gla" proteins, and growth factors (GF's), being approximately 90% of the protein content collagen type I.[1, 2] GAG's are much more functional than just being cell supportive matrices: they form a functional network, participating for instance in the regulation of attachment, mineralization initiation or inhibition processes.[2-4] Most of polysaccharides in the human body are sulfated, with variable chain length and different number and position of sulfate groups per disaccharide.[5] Those are linked to core proteins in its majority, forming proteoglycans (PG's).[5] These ECM molecules are highly negative charged and rich in functional group such as -COOH, $-NH_2$, and $-SO_3H$. GAG's and PG's provide highly hydrated gels with varying pore size and charge density where cells are located, serving as selective sieves to regulate ions, molecules, and cell traffic and participation in crucial signalling pathways[5]. Sulfated GAG's such as chondroitin sulfate or dermatan sulfate have high binding affinity to GF's by the $-SO_3H$ groups (sulfate groups), capturing them and increasing their local concentration.[6, 7] Non-sulfated GAG's, namely hyaluronan, can bind to cell surface markers being also capable of modulating cell behaviour.[7, 8]

Many strategies in tissue engineering (TE) are based in recapitulating the general instructive characteristics of the ECM elements into biomaterials supports. Natural origin materials have been in the top interest materials in TE area for the development of cell supportive materials due to the high chemical ECM similarity, biodegradation, and the presence of more cell recognition sites.[9] Among those, marine-origin polymers represent both economic and environmental benefits, besides the opportunity to obtain natural materials with novel properties.[10] In particular, chitosan (Chi) and carrageenans (Car's) have been proposed for the preparation of different polymeric matrices to act as cell supportive materials, namely as TE scaffolds.[11-13] Chi is a linear cationic polysaccharide compose of glucosamine and β-(1-4)-linked D-glucosamine and N-acetyl-D-glucosamine with different proportions (but predominance of the deacetylated monomer) and sequence[14], obtained by the deacetylation of chitin extracted from the exoskeleton of crustaceans, fungi cellular wall, cephalopods endoskeletons or insects' cuticles (Figure IV.1a).[15] Car's are a family of anionic sulfated polysaccharides isolated from different species of red algae, which vary on the sulfation degree and on the molecular position of the $-SO_3H$ groups – Figure IV.1b,c,d show the molecular structure of some the commercially relevant Car's with the sulfate groups highlighted in blue. The backbone structure consists on repeating disaccharide unit (1→4)-β-D-galactopyranosyl-(1→3)-α-D-galactopyranosyl having also 3,6-anydrogalactose residues.[16] These sulfated polymers can be found in several products in food and pharmacy industry. In the field of TE, kappa (κ; commonly extracted from *Kappaphycus alvarezii*) and iota (ι; from *Eucheuma denticullatum*) Car's have been proposed for develop cytocompatible hydrogels for bone and cartilage [17-19]. The Car's with higher sulfation degree, as lambda (λ; extracted from different species of *Gigartina*

and *Chondrus genera*), have been not so much used due to the association with the osteoarthritis positive control model: a dose-dependent inflammatory response is triggered when 1-2% (w/v) of **λ**-Car gels are injected into the knee.[20] Nevertheless, such inflammatory response was not observed with **κ**-Car hydrogels [21], which supports the idea that inflammatory response caused by Car is highly dependent on parameters such as sulfation degree and total content.

Surface properties of 2D or 3D substrates are of major importance in the TE field.[22, 23] In particular, there has been some works where sulfonic/sulfate groups have been introduced in a controlled manner onto surfaces, which is relevant to study materials-cells interactions. Some of those studies have focused on: i) the improvement of surface bioactivity for apatite formation in simulated physiological environments[24] , ii) the effect of the chemical landscape on cell attachment[25, 26], and v) the interaction with GF's[7]. Surfaces have been functionalized with sulfonic/sulfate groups by covalent coupling[24], graft polymerization [25] or as self-assembled monolayer.[26] Layer-by-layer (LbL) is a simple and versatile technology that has been widely used to produce nanostructured films for biomedical applications with controllable surface characteristics.[27] It is often based on a simple alternated deposition of negative and positively charged polyelectrolytes (PE's). In our research group, LbL technology has been used to modify both 2D[28, 29] and 3D surfaces[30, 31] using natural-based PE's.

Herein, we propose well defined models to study the effect of sulfate groups on cell behaviour based on LbL assembling of marine-origin charged polysaccharides, namely Chi and distinct macromolecules of the Car's family - see Figure IV.1.

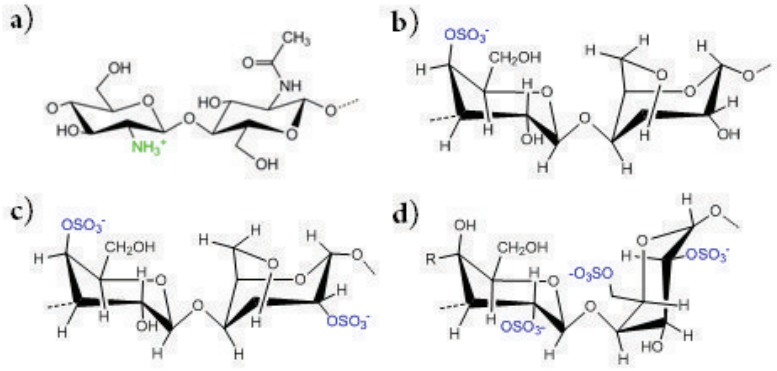

Figure IV.1. Molecular structures of the polysaccharides (ionized form) used in this work: (a) Chi, (b) **κ**-Car, (c) **ι**-Car, (d) **λ**-Car.

The polyanions used constitute a simple model where one can have different and controlled number of sulfate groups per disaccharide (1 to 3), acting as a valuable systems to study cell-ECM/biomaterials interactions *in vitro*. Despite the possible inflammatory response associated with Car, Chi and its derivatives are known to have anti-inflammatory properties[32]. In this way, there may be a balance between those intrinsic anti and inflammatory features, which together with the reduced polymer quantities used in LbL methodology, may turn these systems into interesting models for *in vitro/in vivo* inflammatory and tissue regeneration studies.

The first section of this work comprises the study of the LbL assembling of Chi with the three types of Car's. The second section evaluates the biological response of osteoblast-like cells on the multilayers containing Car's with different sulfation degree.

IV.3. Experimental Details

IV.3.1. Materials

Medium molecular weight chitosan (Chi) bought from Sigma Aldrich (MKBB0566) was purified by a precipitation method. Briefly, Chi powder was first dissolved in 2% (v/v) of acetic acid with a concentration of 1% (w/v). The solution was maintained under stirring overnight at room temperature. The impurities were removed by four filtration cycles. Then, Chi was precipitated using 1M NaOH while stirring. Final steps consisted on washing Chi with distilled water until reaching a neutral pH and on the removal of all the excess of water, washing with increasing concentrations of ethanol solutions (20-100% v/v). Chi was freeze-dried during 3 days and finally grinded. Poly(ε-caprolactone) (PCL, Sigma-Aldrich 440744), κ- (Sigma-Aldrich, 22048), ι- (Fluka, 22045), λ- Car (Sigma-Aldrich, 22049) and ethylenediamine were used as received.

IV.3.2. QCM-D assembling study

A Q-Sense E4 quartz crystal microbalance with dissipation monitoring system (QCM-D, Q-Sense AB, Sweden) was used for monitoring in situ the deposition of Chi/Car bilayers at the surface of gold-coated crystals. Very briefly, a AT cut quartz crystal is excited at its fundamental frequency (5 MHz) and at several overtones: 25, 35, and 45 MHz (fifth, seventh, and ninth overtones, respectively). When a thin film is deposited onto the sensor crystal the frequency decreases. If the film is thin and rigid the decrease in frequency (Δf) is proportional to the mass of the film. However, when using polymers, the adsorbed film is not rigid and this relation is not valid: the film begins dissipating energy and exhibiting the typical viscoelastic behaviour, which is evident by the change in the dissipation (ΔD).[33]

The crystals were first cleaned in an ultrasound bath at 30°C, and immersed successively in acetone, ethanol, and isopropanol. Adsorption took place at 25°C and at a constant flow rate of 50 ml/min. First the Chi solution was pumped for 10 minutes, and the weakly bound polyelectrolyte removed by pumping washing solution (i.e., the same buffer solutions of the PE). After this, the Car solution was pumped for 10 minutes, followed by the washing solution for more 10 minutes; this cycle repeated at least 5 times. The assembling of Chi/Car films was studied varying the concentrations of NaCl (from 0 to 1 M), the pH (4.5 and 5.5) and the type of Car's. Data was modelled using Voigt model and Q-Tools software (Q sense) in order to estimate the film growth type and the PEM thickness growth with the number of deposition steps.

IV.3.3. Samples preparation and modification with PEM's

PCL surfaces prepared by melt-compression moulding were pre-modified with a solution of 10% (v/v) of ethylenediamine in 2-propanol during 1 hour at 37ºC in order to introduce pH responsive amine groups and improve the binding of the first PE layer onto the surface. Then, the surfaces were intensively washed with ultrapure water. These films were coated with the LbL assembled nanocoatings - Table IV.1. depicts the

identification of the different multilayers prepared, according to the number of layers, the outermost layer and the type of Car. All PE solutions were prepared in 0.1 M acetate buffer solution with pH = 5.5 and 0.04 M NaCl. The immersion time in the PE solutions was 10 minutes followed by 2 rising steps of 5 minutes each.

After finished the LbL modification, the samples were washed with the respective buffer/washing solutions and ultrapure water under mild agitation. After drying the samples were sterilized using ethylene oxide composed by 88% CO_2 and 12% ethylene oxide at a temperature of 45 ºC ± 3ºC, pressure of 180 ± 3 kPa, and a humidity of 55 ± 10 % HR during 10 hours.

Table IV.1. Samples prepared using LbL

Sample	Car	Nº layers	Out. layer
PCL	-	-	-
$(\kappa\text{-Car/Chi})_{5.5}$	κ	11	Car
$(\kappa\text{-Car/Chi})_{10.5}$	κ	21	Car
$(\kappa\text{-Car/Chi})_{6}$	κ	12	Chi
$(\iota\text{-Car/Chi})_{5.5}$	ι	11	Car
$(\lambda\text{-Car/Chi})_{5.5}$	λ	11	Car

IV.3.4. Surfaces characterization

IV.3.4.1. Scanning electron microscopy (SEM)

The surface morphology of the samples was observed using a Leica Cambridge S-360 scanning electron microscope (SEM, Leica Cambridge, UK). All surfaces were precoated with a conductive layer of sputtered gold. The SEM micrographs were taken at an accelerating voltage of 15 kV and at different magnifications.

IV.3.4.2. Atomic Force Microscopy (AFM)

AFM measurements were performed in a MultiMode STM microscope controlled by the NanoScope III from Digital Instruments system, operating in tapping mode at a frequency of 1 Hz. At least three measurements were performed in different specimens.

IV.3.4.3. Contact Angle Measurement

The static water contact angle (WCA) of the samples was measured at room temperature using a OCA 15plus goinometer equipment (DataPhysics Instruments, Germany). The values were obtained by the sessile drop method. The used liquid was ultra pure water and the drop volume was 3 μL. At least five measurements were carried out for each sample.

IV.3.4.4. X-ray photoelectron microscopy (XPS)

XPS analysis was performed using a Thermo Scientific K-Alpha ESCA instrument with monochromatic Al-Ka radiation (*h* = 1486.92 eV) and a takeoff angle of 90° relative to the sample surface to record the C1s, O1s, S2p ,

N1s and survey spectra. The measurement was carried out in constant analyzer energy (CAE) mode with a 100 eV pass energy for survey spectra and a 20 eV pass energy for high-resolution spectra. The C1s peak was resolved into three peaks at 285.0 eV. Surface elemental composition was determined using the standard Scofield photoemission cross sections. The atomic concentrations were determined from the XPS peak areas using the Shirley background subtraction technique and the Scofield sensitivity factors. The ratios of sulfur/carbon, sulfur/oxygen, oxygen/carbon and nitrogen/carbon on modified surfaces were calculated by dividing the elemental percentages of each element. At least two measurements were performed in different specimens.

IV.3.5. Cell behavior study

IV.3.5.1. Cell culture and seeding

Cell studies were performed using SaOs-2 cells, a human primary osteosarcoma cell line obtained from the European Collection of Cell Cultures (ECACC). Cells were grown in Dulbecco's Modified Eagle's medium low glucose (DMEM, Sigma-Aldrich) with phenol red and supplemented with 10% heat inactivated fetal bovine serum (FBS, Alfagene) and 1% antibiotic-antimycotic solution (AT, Alfagene) in a humidified atmosphere with 5% CO_2 at 37°C. For expansion, confluent cell cultures were split in a ration of 1/3 to 1/6 using 0.25% trypsin/EDTA. For cell seeding, samples were sterilized with ethylene oxide. SaOs-2 was used in passages between 20 and 24.

To proceed with the cell seeding, cells were harvested by trypsinization and filtered with a cell strainer with 100 µm of pore size to remove possible cell aggregates. Two cellular suspensions with a cellular density of 0.4×10^6 cells/ml were prepared by cell trypsinization and couting: (i) in basal DMEM - containing 10% FBS and 1% AT; (ii) in osteogenic DMEM - containing 10% FBS, 1% AT and osteogenic supplements (50 µg/ml ascorbic acid, 10^{-8} M dexamethasone, 10 mM β-glycerophosphate). A volume of 10 µl of cell suspension containing 4,000 cells was dripped onto the surfaces and samples let to incubate during 2.7 hours at 37°C with 5% of CO_2 for cell attachment. After the incubation period, 1 ml of the respective culture media was added and samples incubated for 1 or 28 days. Culture media was changed each 2-3 days.

IV.3.5.2. Cell morphology observation.

After 1 day in culture, samples were rinsed thrice with sterile PBS and then fixed with formalin 2.5% (v/v) for cytoskeleton staining and nucleus, with phalloidin–tetramethylrhodamine B isothiocyanate (Phalloidin-TRITC, Sigma-Aldrich) and 4,6-diamino-2-phenyindole dilactate (DAPI, Sigma-Aldrich), respectively; or glutaraldehyde 2.5% (v/v), for scanning electron microscopy (SEM) observation, during 30 minutes, at room temperature and then extensive and carefully washed with PBS. Samples for SEM observation were dehydrated through a graded series of ethanol (50, 70, 90, 100 % v/v; each one during 10 minutes and twice) and dried at room temperature. Cell morphology was observed using a Leica Cambridge S-360 scanning electron microscope

(SEM, Leica Cambridge, UK). All surfaces were precoated with a conductive layer of sputtered gold. The SEM micrographs were taken at an accelerating voltage of 15 kV and at different magnifications.

For Phalloidin-TRITC/DAPI staining, cells were first permeabilized adding 1mL of Trinton 0.2% (v/v) in PBS during 2 minutes and then washed thrice with PBS. Samples were incubated in the dark with 120 µl of Phalloidin-TRITC solutions for 30 minutes and then washed with PBS. Samples were observed using a Imager Z1 fluorescence microscope (Zeiss) and photographed using an Axio Cam MRm (Zeiss).

IV.3.5.3. dsDNA quantification.

In order to quantify cell attachment after 1 day, and cell proliferation after 28 days in culture, dsDNA was quantified using the Quant-iT™ PicoGreen® dsDNA assay kit (Molecular Probes/Invitrogen) that allows the measurement of the fluorescence produced when PicoGreen dye is excited by UV light while bound to dsDNA. After incubation periods of 1 and 28 days, the samples were rinsed thrice with sterile PBS and transferred to small tubes, where 1 mL of ultra-pure sterile water was added. All samples were directly transferred to storage at -80°C and kept until quantification. For the quantification, samples were defrosted at room temperature and then sonicated during 10+10 minutes. 100 mL of Tris–EDTA buffer were transferred into a white opaque 96-well plate. Samples were vortexed and 28.8 mL of each plus 71.2 mL of PicoGreen solution were added to the wells. After 10 minutes of incubation in the dark, the plate was read on a microplate reader using an excitation wavelength of 485 nm and emission wavelength of 528 nm. A standard curve was created by varying the concentration of standard dsDNA standard from 0 to 2 mg mL^{-1}, and triplicates dsDNA values of the samples were read off from the standard graph. At least six specimens were measured per each sample. The experiment was repeated once.

IV.3.5.4. Alkaline phosphatase quantification.

Alkaline phosphatase (ALP) is the most frequently used biochemical earlier marker of osteoblastic bone formation. ALP is a hydrolase enzyme responsible for removing phosphate groups from many types of molecules, including nucleotides, proteins, and alkaloids. In bone development, the enzyme participates in the regulation of biomineralization for instance by the regulation of inorganic pyrophosphates' levels. ALP activity was quantified in the same samples used for dsDNA quantification. The activity of ALP is evaluated using p-nitrophenol assay. Paranitrophenyl phosphate, which is colourless, is hydrolysed by alkaline phosphatase enzyme at pH 9.8 and 37ºC to form free p-nitrophenol, which is coloured yellow. The reaction is stopped by addition of NaOH and the absorbance read at 405 nm. Briefly, in each well of a 96-well plate, 20 µl of each sample previously vortexed, were mixed with 60 µl of the substrate solution which is 0.2% wt/v p-nytrophenyl phosphate (Sigma-Aldrich) prepared in a substrate buffer of 1 M diethanolamine (Sigma-Aldrich) at pH 9.8. The plate was then incubated in the dark for 45 min at 37°C. After the incubation period, 80 µl stop solution, which is composed by 2 M NaOH (Panreac) plus 0.2 mM EDTA (Sigma-Aldrich), was added to each well. Standards were prepared with 10 µmol/ml p-nytrophenol (pNP, Sigma, USA) solution, to obtain a

standard curve covering the range 0–0.2 M. Triplicates of each sample and standard were made. Finally, absorbance was read at 405 nm in a microplate reader (Bio-Tek, Synergie HT) and sample concentrations in triplicate were read off from the standard curve. The ALP concentrations were normalized against the dsDNA concentrations of the same samples to determine the ALP activity.

IV.3.5.5. Alizarin Red S staining for indirect calcium quantification.

Alizarin Red S (ARS), an anthraquinone derivative, can be used to identify calcium in tissue sections. Although the reaction is not strictly specific for calcium, but also occurring with magnesium, manganese, barium, strontium, and iron, these elements usually do not occur in sufficient concentration to interfere with the staining. Calcium forms an ARS-calcium complex in a chelation process. After 28 days in culture, samples were washed thrice with sterile PBS and cells fixed with 2.5% formalin during 30 minutes. The samples were then washed with distilled water in order to remove any residual ions and 0.5 ml of alizarin red S solution (2g/100 ml, pH 4.1-4.3 adjusted with ammonium hydroxide) was added to each sample and let to react for around 5 minutes. The excess of dye was removed with distilled water, samples were observed under stereomicroscopy and pictures were taken.

The content of calcium will be proportional to the red intensiveness. In order to elute the ARS adsorbed to the surfaces, 400 µL of 10% (v/v) of acetic acid was added to each sample and incubated at room temperature for 30 min with shaking. Samples were vortexed for 30 seconds. After complete elution, the surfaces were discarded, and the liquid samples heated to 85 °C for 10 min. Then, the samples were transferred to ice for 5 min. The slurry was then centrifuged at 12,000g for 30 min and 400 µL of the supernatant was removed to a new microcentrifuge tube. Then 150 µL of 10% (v/v) ammonium hydroxide was added to neutralize the acid. The absorbance of triplicates of the samples was read at 405 nm in a microplate reader (Bio-Tek, Synergie HT). A calibration curve made of successive dilutions of Alizarin Red S solution with known concentration was used in order to read off the alizarin content of the samples.

IV.3.5.6. EDS-SEM analysis of calcium and phosphate deposits.

Morphological analysis was realized in an Ultra-high resolution Field Emission Gun Scanning Electron Microscopy (FEG-SEM), NOVA 200 Nano SEM, FEI Company. Secondary electron images were performed with an acceleration voltage of 5kV. Chemical analyses of samples were performed by Energy Dispersive Spectroscopy (EDS), using an EDAX Si(Li) detector with an acceleration voltage of 15 kV.

IV.3.6. Statistical Analysis

All dsDNA and ALP data were statistically analysed using non-parametric test once Shapiro–Wilk test indicated that data did not have a normal distribution. Kruskal-wallis test was performed considering $p<0.05$ and with the sample size n=6. The Dunn's test was used as a post-hoc test.

IV.4. Results and Discussion

IV.4.1. LbL assembling

In order to select the optimal LbL assembling conditions, Car's and Chi polyelectrolyte multilayers (PEM's) with at least 10 layers were monitored in-situ using QCM-D. The PE's assembling can be influenced by several physico-chemical conditions including: PE nature and concentration, ionic strength, pH, salt type and concentration, PE charge density, deposition time and rinsing step.[34] Those conditions influence the electrostatic interactions and solution *vs.* surface affinity that rules the assembly process, affecting the final properties of the assembled PEM's.

In this work, the parameters analysed in more detail were: salt concentration, PE charge density (by playing with pH and using Car's with different number of charged groups per repeating unit) and number of layers.

Figure IV.2. shows the monitored frequency and dissipation energy shifts during the injection of the PE's solutions in the system and subsequent deposition onto the quartz crystals.

The decrease in frequency is attributed to the deposition of material and the increase in dissipation to the formation of a viscoelastic film onto the surface of the quartz crystal. The effect of NaCl concentration on the build-up of ι-Car/Chi PEM's was tested within the range 0 to 1 M, at pH 5.5 (Figure IV.2.a). NaCl concentration strongly influenced the frequency shifts.

The both extreme salt concentrations tested led to both lower frequency decreases and lower dissipation increases, thus leading to less material being deposited and more rigid films (dissipation variations are smaller in those conditions). When the salt concentration is lower, the PE molecular chains tend to adopt a more extended conformation due to the electrostatic repulsion between charged groups in the chains. In that situation more rigid films are formed, with lower amounts of water, and thus involving less adsorbed mass. However, when the salt concentration is higher, the presence of small ions will have a charge shielding effect over the charged PE groups. In that case, the effective PE charge density is reduced and less quantity of materials is deposited. For intermediate concentration of salt one could observe a maximum in the total frequency variation. For the particular conditions used, the higher frequency variation is observed with 0.04 M NaCl. In order to infer the thickness of the PEM's from the frequency and dissipation values, a Voigt model was employed to fit the data (Figure IV.3.). For the ι-Car PEM's, an exponential film growth was observed in the presence of 0.04 M NaCl, while with all the other concentrations the film thickness tendency to growth with the number of layer is linear – Figure IV.3.c. The different NaCl concentrations lead to different PEM thickness upon 10 layers, being the film thickness higher when in presence of 0.04 M NaCl and approximately 80 nm, whereas varied between 40 and 65 nm in the others – Figure IV.3.a.

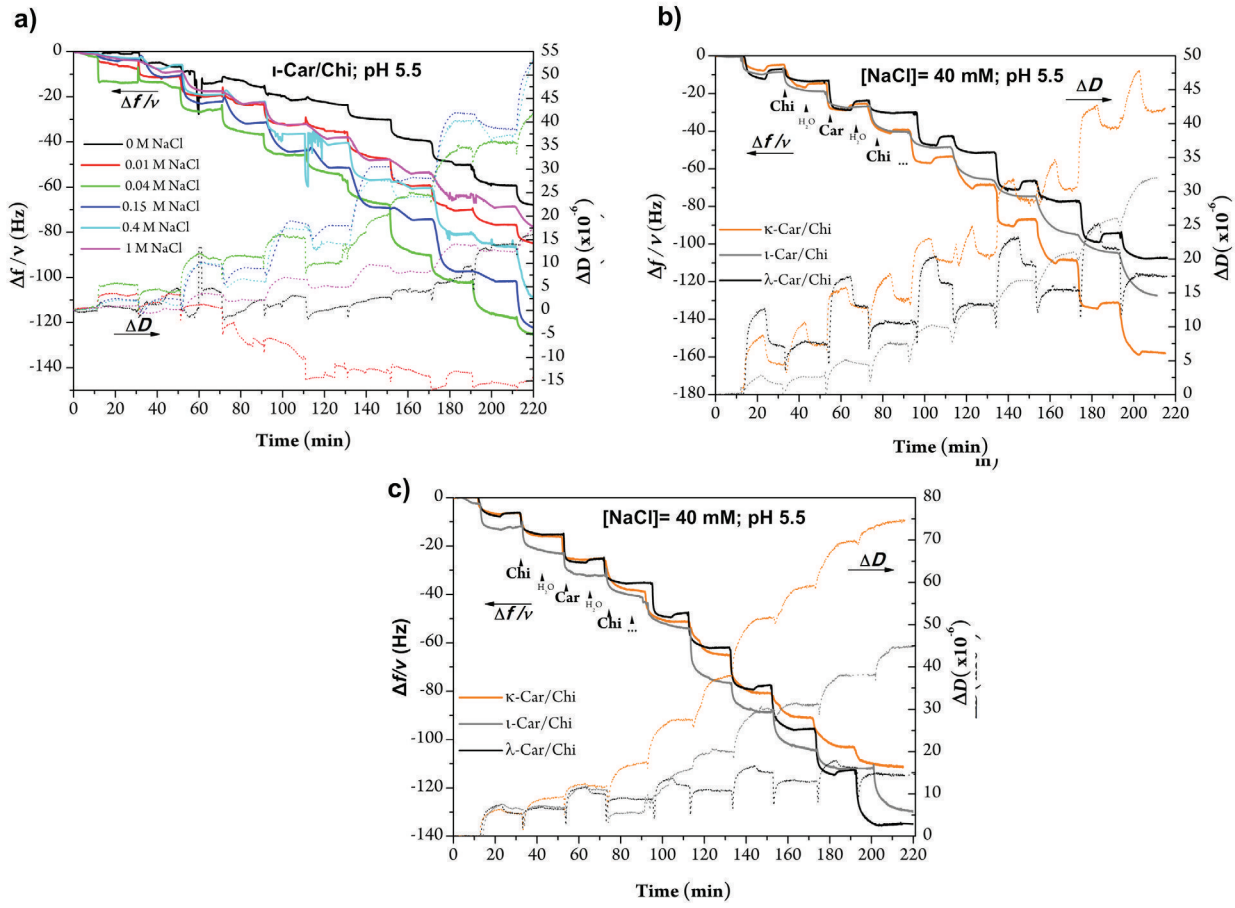

Figure IV.2. QCM-D results obtained during the construction of the Car's/Chi films in terms of normalized shifts in frequency ($\Delta f/\nu$) and dissipation ($\Delta D/\nu$) obtained at the third overtone of: (a) ι-Car/Chi films constructed at pH 5.5 with varied NaCl concentration (0 to 1 M); (b) κ, ι and λ-Car/Chi films build up at pH 4.5 in 0.04M NaCl; (c) κ-, ι- and λ-Car/Chin films build up at pH 5.5 in 0.04M NaCl .

κ-, ι- and λ-Car assembling with Chi was also assessed at different pHs (4.5, 5.5) in the presence of 0.04 M NaCl (Fig.ure IV.2.b,c). The variation of pH is expected to affect mainly the charge density of Chi, which amine group has a pKa of approximately 6.3 [35]: the sulfate groups in Car's, being formally derived from a strong acid such as sulfuric acid, are fully ionized under the studied conditions. Additionally, the variation of pH may affect also the polymer conformation, as reported before on chitosan and carrageenan complexes.[36, 37] The data of the assembling performed at pH 4.5 (Figure IV.2.b) suggested a stronger influence of the Car type on the multilayer construction than at pH 5.5. In fact, when comparing the values of film thickness upon 10 layers (Figure IV.3.b), the value of κ-Car PEM at pH 4.5 was much higher than in the other PEM's, being approximately 90 nm against ~55 nm for both ι- and λ-Car PEM's. Chi amine groups are almost completely (~99%) protonated at pH 4.5; thus, being the pH 5.5 more close to the pKa one can expect a lower protonation fraction (~90%) and then a different charge compensation during LbL. In fact, such influence is observed with ι- and λ-Car: higher thickness at pH 5.5 due to the higher quantity of chitosan needed to compensate its higher charge density (2 sulfate groups and 3 sulfate groups per repeating unit, respectively). However, with κ-Car such tendency was not observed, with thickness being slightly higher than with the other Car types at pH 4.5, and decreasing with the increase of the pH, though reaching similar value to the other PEM's. In this case, the intrinsic chemical

properties of the polymer, determined by the different interactions of the Car's with sodium ions and chitosan may be the leading effect: κ-Car showed the more viscous behaviour of the respective films with highest values of energy dissipation (ΔD). Such viscous behaviour will be promoted by the higher amount of water inside the film, causing a higher film thickness. At pH 5.5, the thickness is about 70 nm independently on the Car. Chi amines are slightly less protonated and there would be more interpenetration among polymer layers, vanishing the effect of the different charge densities of the Car types. Such effect is only predicted for multilayers with higher number of layers (Figure IV.3.d), where an increase in thickness with the increase of sulfate groups per Car repeating unit is foreseen, due to the increasing amount of chitosan needed for charge compensation.

For the following studies, multilayers prepared from PE's solutions with pH 5.5 and 0.04 M NaCl were selected since they were the ones exhibiting less effect on the thickness when varying the Car type and thus where the effect of the different number of sulphate groups on surface properties of multilayers can be better unravel.

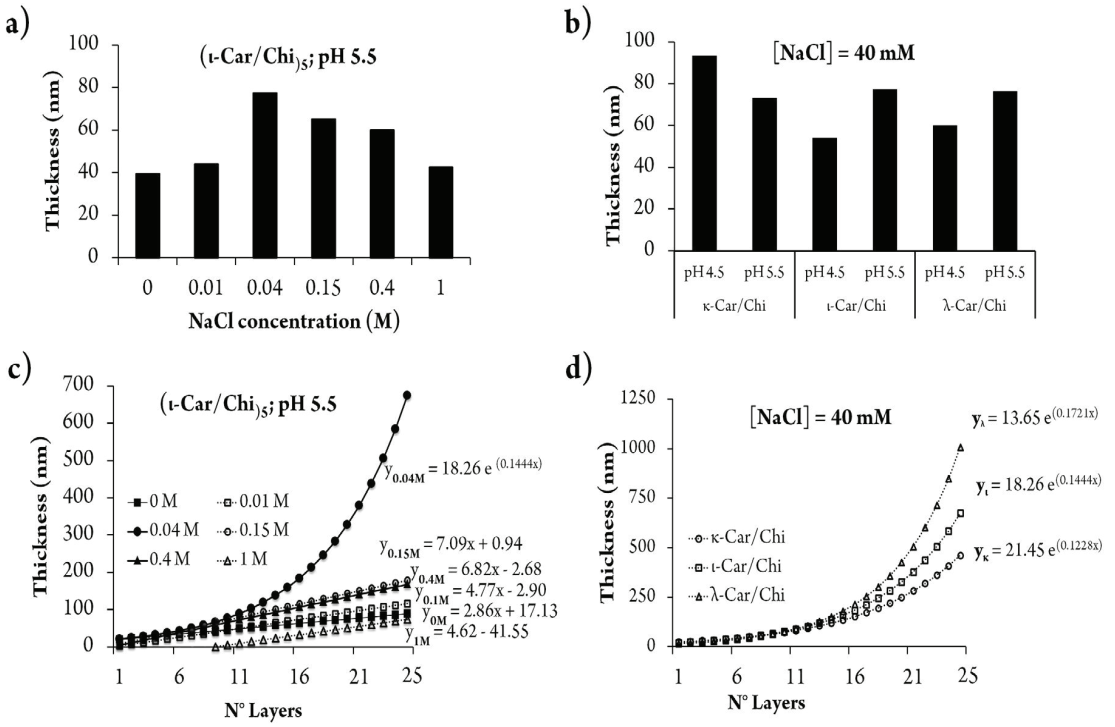

Figure IV.3. Estimation of the thickness of the PEM's using the Voigt model taking into account the results of Figure IV.2. Total thickness calculated for Car/Chi multilayers containing 10 layers, with Car as outermost layer: (a) variation of the film thickness varying the NaCl concentration of ι Car/Chi PEM's constructed at pH 5.5; (b) variation of film thickness when built in the presence of 40 mM NaCl according to the pH and the Car type. (c) Fitting of the data modelled using the Voigt model for ι-Car/Chi system at pH 5.5 when using different NaCl concentrations. (d) Fitting of the data modelled using the Voigt model for κ-, ι-, λ- Car/Chi systems at pH 5.5 in the presence of 40 mM NaCl.

IV.4.2. Surfaces characterization

Surface properties, such as surface chemistry, roughness and wettability can influence cell behaviour.[22] Thus, when using Chi and Car multilayers as models to study the influence of sulfate groups on cell behaviour, such surface properties were also analyzed. PCL membranes produced by melt-compression molding were

modified with distinct Chi/Car nanocoatings. The surface topography, roughness, wettability were first analysed - see Figure IV.4. and Table IV.2. The analysis of the images of the nanocoated surfaces obtained by SEM and AFM (Figure IV.4.a, b) indicates that the ones containing κ- and λ-Car with 11 layers had similar average roughness, in the range of 8.5-10 nm (Table IV.2.). With an additional chitosan layer the roughness increased by 2 nm. By doubling the number of layers, the roughness increased 4 times. ι-Car containing PEM's exhibit rougher surfaces than the corresponding PEM's with the other Car's. Such differences could be attributed to changes in polymer conformation. In fact, it is known that κ-, ι- and λ-Car in solution assume different interactions with ions, resulting in different conformations that leads to different gelling behaviour.[36, 38]

Table IV.2. Root mean square (Rq), average roughness (Ra) of the surfaces (n=3) and water contact angle (WCA, n=5, 3μL drop volume).

	PCL	**(κ car/chi)$_{5.5}$**	**(κ car/chi)$_{6}$**	**(κ car/chi)$_{10.5}$**	**(ι car/chi)$_{5.5}$**	**(λ car/chi)$_{5.5}$**
Rq (nm)	9.09 ± 0.86	11.43 ± 1.92	14.29 ± 2.51	68.16 ± 3.83	19.58 ± 2.08	13.58 ± 0.42
Ra (nm)	6.10 ± 0.74	8.56 ± 1.75	10.03 ± 1.51	46.50 ± 3.44	13.56 ± 1.42	9.90 ± 0.32
WCA (°)	77.77±4.33	22.10±1.46	17.98±3.02	19.02±1.602	19.98±2.15	20.53±1.84

The chemical analysis of the surfaces was performed by XPS analysis in regard to the nitrogen, sulfur, carbon and oxygen content - see Figure IV.5.

With increasing of the sulfate groups, the sulfur content increased, as it can be observed in the survey spectra and by the elements percentage (Figure IV.5.a,b). The same trend was not observed for nitrogen, i.e., the Chi absorption seemed to not increase with the increase of number of sulfate groups of the Car's, with λ-Car PEM exhibiting the lowest nitrogen percentage: ι > κ > λ. However, it must be taken into consideration that XPS has a sampling depth of about 5 nm.[39] Thus, it will only analyse the top layer(s) and not the complete multilayer which, dependently on the nature of the PE's can have a more fuzzy or lamellar organization.[40] In this case, the higher charge density of λ-Car leads to polymer chains with a more linear conformation and thus more lamellar nanostructures are obtained. Thus, XPS is sampling mostly the outermost λ-Car layer and a higher S/N ratio is observed (Figure IV.5.c) since relatively less N (less Chi) is detected. With κ- and ι-Car, with less charge density, more random coil polymers are allowed and more fuzzy films are obtained. Consequently, XPS is sampling both Car and Chi and equivalent S/N ratios (Figure IV.5.c) are observed. This fuzzy behaviour has been already discussed above to justify the equivalent thickness observed with all Car at pH 5.5 and these XPS results support such interpretation.

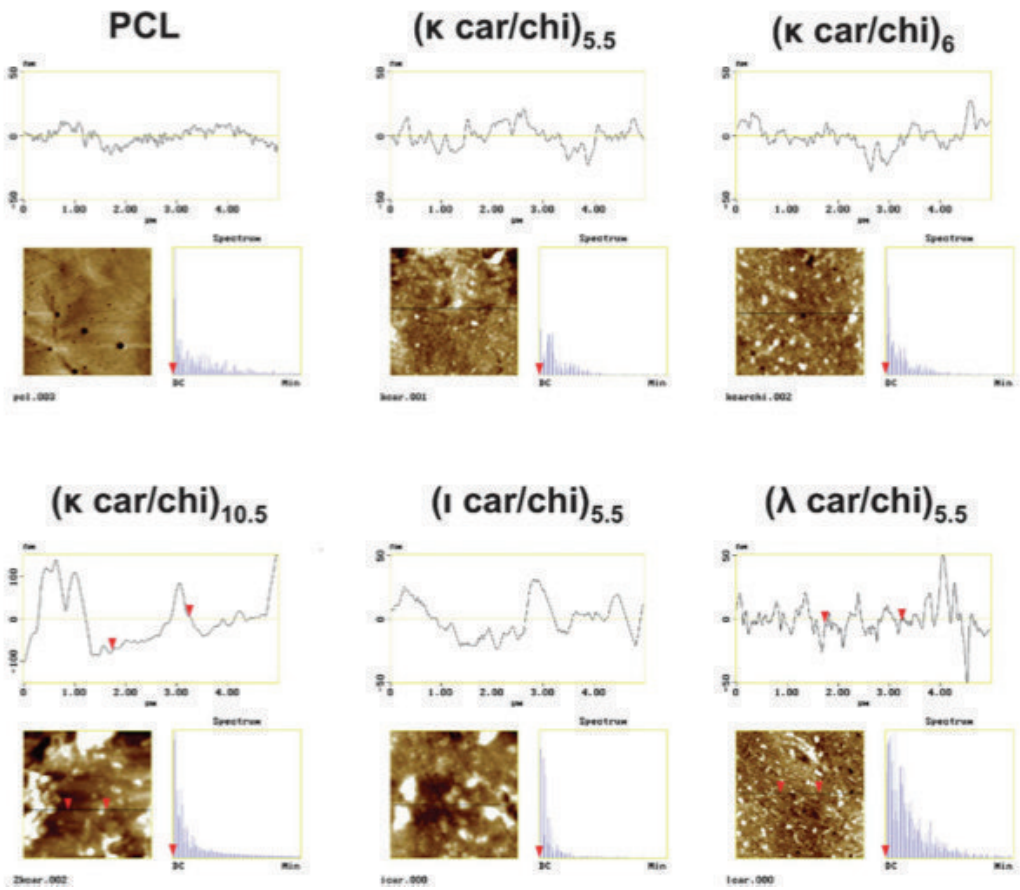

Figure IV.4. AFM images (5×5 μm² area) of the unmodified PCL and modified PCL surfaces with different Car/Chi PEM.

Considering all the physico-chemical characterization performed, Figure IV.5.d summarizes the main differences on the developed Car/Chi PEM's regarding surface amine and sulfur content, and PEM density/organization according to the Car type.

The wettability of the PEM's was determined by measuring the water contact angle (WCA) on the top of the PCL and PCL-PEM-modified surfaces - Table IV.2. PCL surfaces were moderately hydrophobic, with WCA of 77.8 ± 4.3°, but the subsequent assembly of PEM's result in hydrophilic surfaces with the PEM modification, reaching WCA ranging between 18.0 ± 3.0° and 22.1 ± 1.6°. The different assembled PEM's exhibited similar WCA. Therefore, among the PEM coated surfaces, WCA is not expected to affect significantly any difference observed in cell behaviour that will be discussed in the next section.

IV.4.3. Cell behavior

Sulfate groups are known to bind to calcium ions and to be effective for inducing apatite nucleation and growth in simulated body fluid media.[41, 42] Nakata Rio et al., has shown that λ-Car hydrogels have a higher ability to promote apatite formation that κ-Car, both prepared by ionic crosslinking with $CaCl_2$. Due to higher sulfur content in λ-Car hydrogels, the amount of Ca^{2+} ions was also higher, giving rise to a larger release of this ion into the SBF, contributing for a faster apatite formation. It would be interesting to verify if with more

sulfated materials one would obtain higher apatite formation by cellular mediated mineralization. One expects that LbL nanocoatings with higher sulfur content would induce higher cell biomineralization than the unmodified surfaces, under osteogenic conditions. The SaOs-2 osteoblast-like cell line was selected to perform this study.

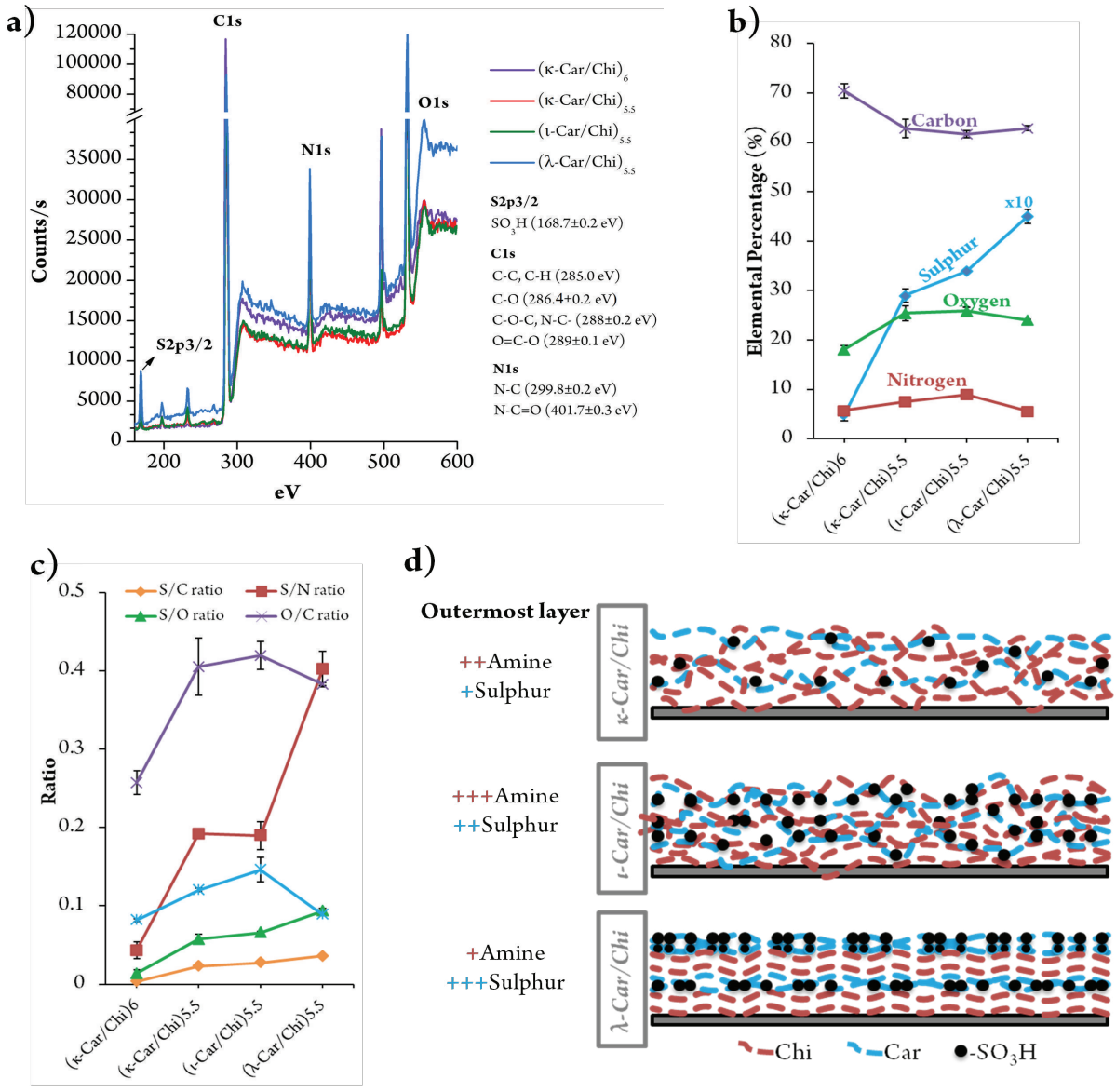

Figure IV.5. (a) Survey Spectra of S2p3/2, C1s, N1s and O1s obtained by XPS analysis. (b) Elemental percentage of Sulfur, nitrogen, oxygen and carbon of the same surfaces. (c) S/C, S/N, S/O and O/C surface ratios calculated using the elemental percentage measured by XPS. (d) Suggested model for the Car's/Chi PEM evidencing the influence of Car type on the amount of adsorbed Chi.

These cells have been used as model of osteoblastic activity once they exhibit the entire differentiation sequence of the osteoblastic cells: from proliferation to mineral nodules formation, matrix mineralization and differentiation into osteocytes.[43, 44] In tissue culture polystyrene and in basal media, SaOs-2 cells have basal ALP activity and basal extracellular matrix mineralization. In osteoconductive medium (including ascorbic acid and β-glycerophosphate) the cell line shows only a slightly increase on the production of mineralized

collagenous matrix. Since proliferative state does not stop, mineralization considerably increases in cellular passages higher that 50 due to instabilities in long-term cultures. For full differentiation and biomineralization, dexamethasone-mediated induction of SaOs-2 is necessary.[43,44]

Firstly it was studied how the PEM's could influence SaOs-2 morphology upon 24 hours of culture in both basal and osteogenic media in the presence of serum - see Figure IV.6.

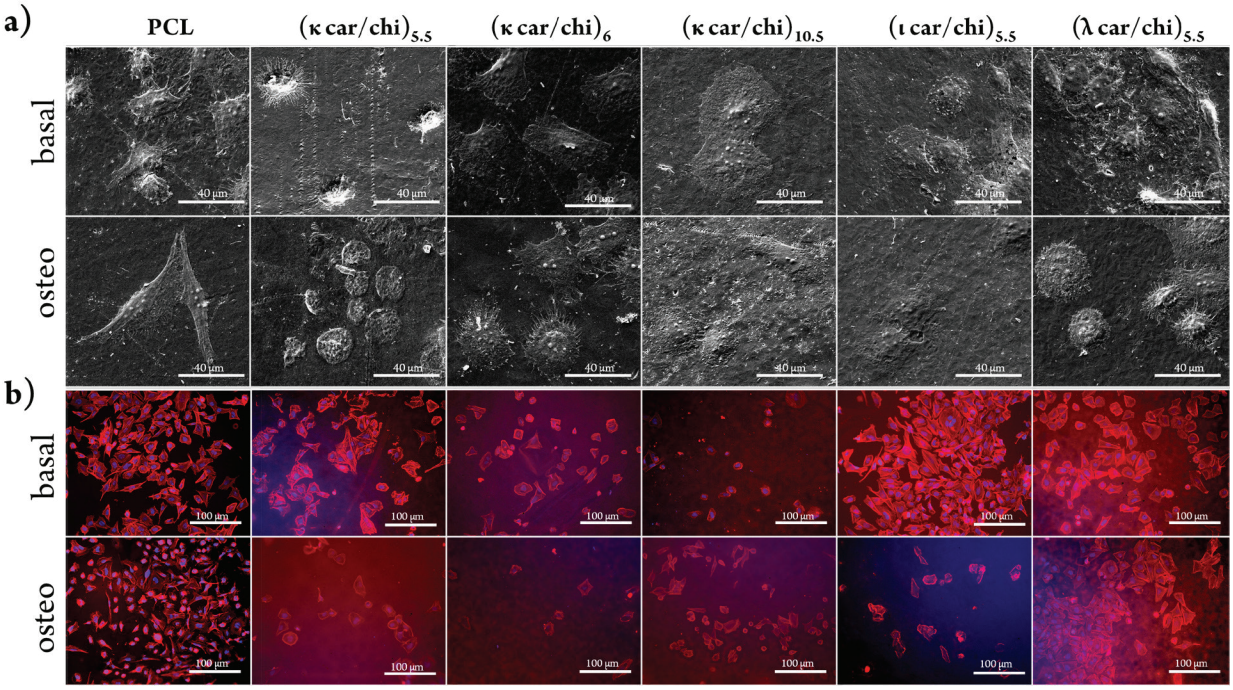

Figure IV.6. (a) SEM micrographs showing cell morphology after cultured on the samples during 24 hours in basal and ostegenic media. (b) Imagens of DAPI and phalloidin-rhodamine staining highlighting cell nucleus and cytoskeleton of SaOs-2 cells after 24 hours in culture in basal and osteogenic media.

In basal media, cells became more roundish and the cytoskeleton less spread in the PEM's containing κ-Car, being even more pronounced with Chi as outermost layer or increasing the number of layers from 11 to 21. In the case of ι-Car, where both the content of amine and sulfate groups was higher (comparing to κ-Car 11 layers sample) cell morphology presented trapezoidal-like shape. In λ-Car PEM's that present higher percentage of sulfur on the surface butlower nitrogen content (higher S/N ratio), cells were less elongated and trapezoidal-like.

SaOs-2 cell attachment and activity were quantified on the studied coatings and in PCL, after 1 and 28 days in culture, in both basal and osteogenic media - see Figure IV.7. Cell attachment and proliferation were assessed by dsDNA quantification. In basal media, dsDNA values were significantly higher on PCL and ι-Car, than in all other sample, for 1 day of culture (Figure IV.7.a). κ-Car with 11 layers which had similar S/N ratio to ι-Car PEM, even though had less sulfate and amine groups on the contacting face, possible had lead to a different protein adsorption in terms of conformation, concentration and type, affecting strongly cell adhesion.

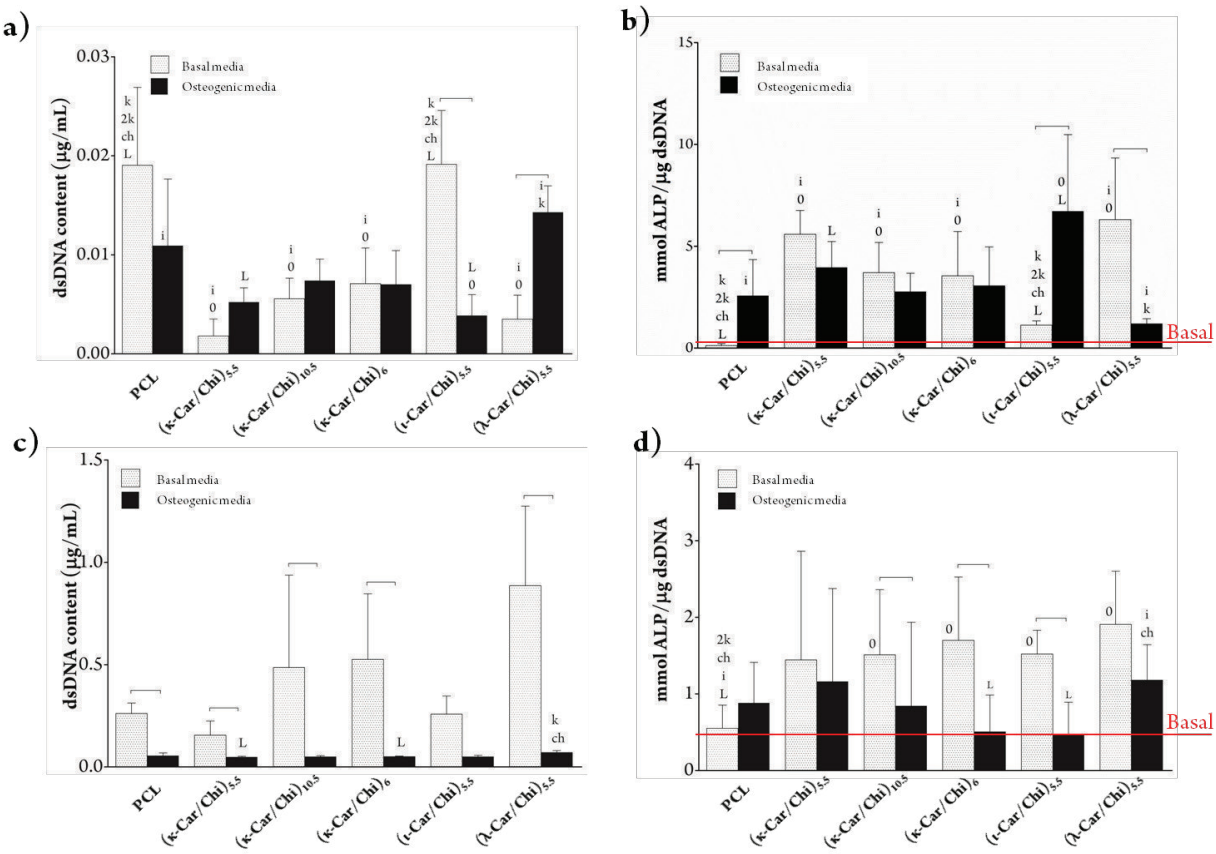

Figure IV.7. dsDNA quantification and ALP activity of SaOs-2 cells after 1 - (a) and (b), and 28 days - (c) and (d), in culture in basal and osteogenic media, respectively. All data was analysed using the non-parametric Kruskal-wallis test and Dunn's post-hoc test and all the significances are identified: bars (the samples are different), 0 (different from PCL), k (different from κ-Car/$Chi_{5.5}$), 2k (different from κ-Car/$Chi_{10.5}$), chi (different from κ-Car/Chi_{6}), i (different from ι-Car/$Chi_{5.5}$), L (different from λ-Car/$Chi_{5.5}$) (ρ<0.05; n= 6).

In the presence of the osteogenic factors, cells became more stretched on PCL, slightly more in λ-Car, much less cells in ι-Car and with the same morphology in the others, as compared with the respective ones in basal medium (Figure IV.6.). In general the amount of cells attached was not statistically influenced by the addition of osteogenic factors with exception of the PEM containing ι- and λ-Car (Figure IV.7.a). Therefore, the surface chemistries have led to different surface interaction with the serum protein and the osteogenic factors, interfering with the cell attachment process. Moreover, in some cases the osteogenic factors could actually improved cell attachment. In the case of ι-Car PEM, the effect was negative and cell attachment was significantly lower in the osteogenic medium, but an opposite effect was observed in the λ-Car PEM.

Figure IV.7.b shows the ALP activity quantification. Contrarily to dsDNA content, ALP activity decreased significantly with the addition of osteogenic factors in λ-Car containing PEM's; the opposite effect took place in the ι-Car PEM. Cell number and activity are different properties: SaOs-2 cells have revealed to be more active on the PEM's where cell attachment was significantly lower, though with increased ALP activity in basal media, comparing with normal basal SaOs-2 activity on tissue culture polystyrene (usually lower that 1 mmol ALP/µg dsDNA[43]).

Cell attachment and proliferation are two different phenomena, and 28 days was the selected time point to both assess proliferation and biomineralization. More tests were performed for 28 days of culture to assess information about cell proliferation (Figure IV.7.c), activity (Figure IV.7.d). Considering dsDNA content at 1 day (Figure IV.7.a) and 28 days (Figure IV.7.c), the increase of cell number was: 13-fold in PCL surfaces, 86-fold in $(\kappa\text{-Car/Chi})_{5.5}$, 87-fold in $(\kappa\text{-Car/Chi})_{10.5}$, 74-fold in $(\kappa\text{-Car/Chi})_{6}$, 13-fold $(\iota\text{-Car/Chi})_{5.5}$ and 254-fold in $(\lambda\text{-Car/Chi})_{5.5}$. This suggested that higher S/N, S/C or S/O ratios may promote cell proliferation. In osteogenic media, cell proliferation is not so evident once intracellular processes are focusing biomineralization: for the same sequence the dsDNA fold increase was: 4, 9, 6, 6, 13 and 4. Figure IV.7.d shows that after 28 days in culture, ALP activity of the cells in osteogenic media reached the basal value (around 0.4 mmol ALP/μg dsDNA). In most of the PEM's in basal medium, ALP content was significantly higher and significantly different from PCL whose values remained basal. These results revealed the ability of those PEM's to up-regulate ALP activity of SaOs-2 cells.

The amount of calcium and phosphorous on the surfaces may be indication of the mineralization rate or even mineralization quality. After 28 days in culture, it was evaluated regarding the content of calcium mineral on the surfaces by Alizarin Red S staining (ARS) - see Figure IV.8. ARS binds to calcium deposited on the surface resulted from mineralization being its concentration in solution upon dissolution of the inorganic layer proportional to the concentration of calcium. Photographs were taken to the surfaces after staining with ARS, and different colour intensiveness could be seen. The presence of mineralization crystals was also confirmed by SEM – Figure IV.8.a. ARS quantification, resultant from dye elution, is shown in Figure IV.8.a, b for the different surfaces culture without and with cells, respectively, for 28 days in basal and osteogenic media.

Elemental surface analysis was performed by EDS analysis onto the surfaces cultured during 28 days in order to quantify calcium and phosphorous - see Figure IV.8.b,c (left Y) and Figure IV.9. Ca and P were scarse or undetected in the samples cultured in basal media. Therefore, only the spectra for osteogenic media in presence and absence of cells are included herein – Figure IV.9.a,b. To verify the possibility of acellular calcification be caused by the materials on the surface, e.g., nucleation of calcium mediated by the sulfate groups, ARS content was quantified and the surfaces were characterized by EDS in the absence of SaOs-2 cells - see Figure IV.8.c, Figure IV.9.b.

From the comparison with the results on uncoated PCL, calcium deposition on the acellular surfaces increased slightly by the presence of the PEM's in a non significant range. When cells are cultured onto the surfaces in basal medium, the content of calcium remained very low, independently on the Car type. On the other hand, in osteogenic media, phosphorous and calcium content on the surfaces was much higher than in basal media, being visible the tendency for the amount of calcium be higher than in unmodified PCL. Among those, $(\iota\text{-Car/Chi})_{5.5}$ coatings induced a significantly higher biomineralization with the presence of cells, that can be confirm by the ARS intensiveness, content and EDS spectra. The inset of Figure IV.8.c shows that the acellular mineralization in the same PEM is much less pronounced.

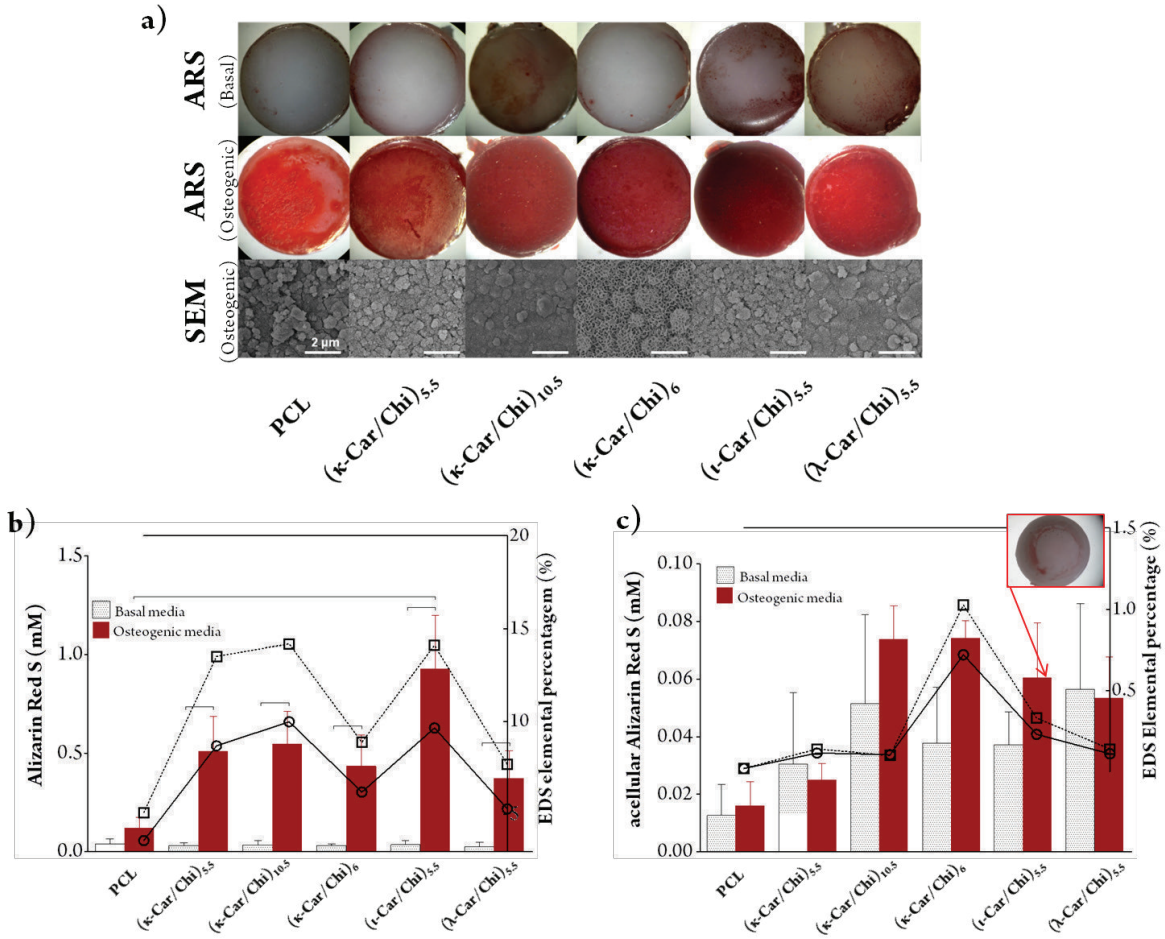

Figure IV.8. (a) Top and middle - photographs of the cellular samples in basal and osteogenic media, respectively, after 28 day in culture. Bottom - SEM micrographs showing the calcium phosphate crystals with the typical cauliflower morphology resultant from the biomineralization in osteogenic medium after 28 days in culture. (b) left Y - ARS staining concentration after 28 days in culture of SaOs-2 cells in absence and presence of osteogenic inducers (total ARS of the cellular samples subtracted with the total ARS of the acellular ones); Right Y - calcium atomic percentage detected by EDS (squares), phosphorous surface percentage detected by EDS (circles). (c) left Y - ARS staining concentration after 28 days in culture without cells in absence and presence of osteogenic inducers (total ARS of the cellular samples subtracted with the total ARS of the acellular ones); Right Y - calcium atomic percentage detected by EDS (squares), phosphorous surface percentage detected by EDS (circles). Inset: photograph of a (ι-Car/Chi)$_{5.5}$ stained surface with ARS which were cultured during 28 days in osteogenic media in absence of cells.

EDS results permitted to estimate the Ca/P of the precipitates - see Figure IV.9.c. The apatite crystals had a Ca/P ratio between 1.4 and 1.6 with those deposited onto PCL surfaces among the ones with the smallest values. The crystals presented the typical cauliflower morphology with Ca/P ratios close to the expected stoichiometric value of 1.67 for hydroxyapatite. The observed differences could be due to sulfate groups of Car that may have attracted and bound more

Several GF's of interest in TE and regenerative medicine present a heparin binding affinity. Sulfation is a common characteristic between heparins and Car's whose sulfate groups have high affinity to GF's turning these materials very good candidates in this field. Car's have high and different affinities for different GF's.[45] Sulfate groups are known to interfere with GF's that participate in the regulation of osteoblastic lineage, such as bFGF, TGF β1, BMP-2 (Bone morphogenic protein-2) and 3, IGF-II, for example.[46] When Car's are in the cell media mixed with the GF's, they antagonise and inhibit the activity of those GF's over the cells, probably by

capturing and reducing the interaction with cells.[45, 47] Hausser and Brenner have reported that the treatment of SaOs-2 cultures with different concentrations of heparin have a non-monotomic effect on the matrix production and biomineralization, being stimulatory at low concentration (5-500 ng/ml) and inhibitory at high concentration (≥5μg/ml) 46. Literature results indicated that the inhibitory/stimulatory effect is concentration-depend, which means that both extreme concentration represent different scenarios of availability and conformation of the GFs when presented to the cells.

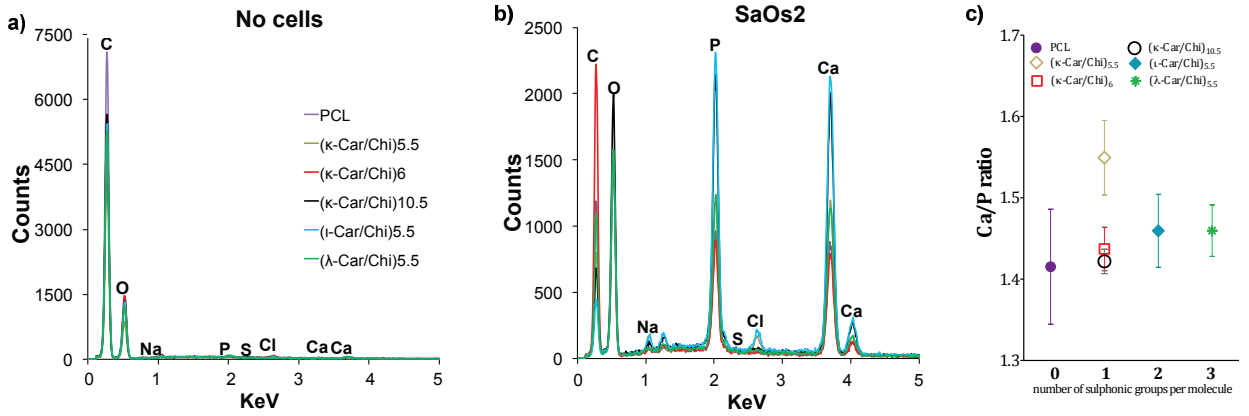

Figure IV.9. (a) EDS spectra of the surfaces of PCL unmodified and modified with the Car PEM's which were in culture with SaOs-2 in osteogenic media during 28 days. (b) Same surfaces of (a) which were in osteogenic media, changed with the same frequency but in the absence of cells. (c) Ca/P ratio of the samples, calculated from the elemental percentages of (a).

Basing on the evidences from the literature, one believes that in the present work, the PCL surfaces modified with PE's may have the ability interact with GF's that cell may be producing or that are present in the medium serum. In fact, SaOs-2 cells secrete several proteins and GF's such as collagen type I, osteocalcin, decorin, BMP-2 and BMP-4, bFGF, TGF-β_1, among others, even in basal medium [43, 46]. Therefore, all those observation made to expect that the Car's PEM's could work as bioactive capturing system, creating a favourable environment for improving the biomineralization process. In general, some PEM's studied in this work induced higher ALP activity after 1 day in culture, and higher mineral deposition by dexamethasone stimulus and higher proliferation after 28 days in culture, than the unmodified PCL surfaces. After 28 days, even in basal media some PEM (e.g., ι-Car PEM's) showed up-regulated ALP activity.

In osteogenic media, ι-Car PEM's allowed a significantly higher biomineralization than all the other tested conditions. Cells played an important role in the biomineralization process as compared with the acellular mineralization on the ι-Car PEM's after 28 days in culture. Even not being the PEM with higher surface sulfur content, ι-Car PEM had the highest content of amine and oxygen together with a high density of the sulfate groups, which may lead to different interaction with proteins/GFs, besides Ca and P, improving the biomineralization even more than in the cases of κ- and λ-Car PEM's.

These results underline how important the density/conformation of amine and sulfate groups can be regarding cell behaviour.

IV.5. Conclusions

Herein nanostructured filmes composed of sulfate and aminated polysaccharides, namely, Car's and Chi with bioactive potential were reported. These coatings are interesting in a point of view of studying cell-materials interactions once they have high and controlled content of chemical groups (amine and sulfate) that are present in the cell extracellular matrix.

Layer-by-Layer assembling of κ-, ι- and λ-Car with Chi was monitored using QCM-D which has proven that films with distinct sulfation content can be constructed and that the final properties depend on parameters such as salt content, pH and Car type.

The nature of the obtained PEM's affects cell morphology and attachment, and may improve proliferation, ALP activity and mineralization when compared with the non-modified PCL surfaces. Biomineralization is significantly higher on ι-Car PEM's which is the nanocoating more rich in oxygen and amine together with high content of sulfur. This PEM may have higher affinity to bioactive molecules from the culture media and not just by capture of β-glycerophosphate and calcium ions, improving even more the calcium and phosphate content on the mineralized surfaces.

This works highlights the importance of the density/conformation of the sulfate and amine groups regarding cell behaviour and demonstrates that LbL may be used to fabricate model coatings valuable for several *in vitro* studies regarding cell-materials interactions.

IV.6. Acknowledgments

This work was partially supported by the European Union/ EFDR through the POCTEP project 0330_IBEROMARE_1_P. Portuguese Foundation for Science and Technology is gratefully acknowledged for fellowships of S.M.O. (SFRH/BD/70107/2010) and T.H.S. (SFRH/BPD/34704/2007).

IV.7. References

1. J. R. Porter, T. T. Ruckh and K. C. Popat, Bone Tissue Engineering: A Review in Bone Biomimetics and Drug Delivery Strategies, Biotechnol Progr, 2009, 25, 1539-1560.
2. B. Clarke, Normal Bone Anatomy and Physiology, Clin J Am Soc Nephro, 2008, 3, S131-S139.
3. J. E. Aubin, Regulation of osteoblast formation and function, Reviews in endocrine & metabolic disorders, 2001, 2, 81-94.
4. J. B. Lian and G. S. Stein, Concepts of osteoblast growth and differentiation: basis for modulation of bone cell development and tissue formation, Crit Rev Oral Biol M, 1992, 3, 269-305.
5. J. L. Arias, A. Neira-Carrillo, J. I. Arias, C. Escobar, M. Bodero, M. David and M. S. Fernandez, Sulfated polymers in biological mineralization: a plausible source for bio-inspired engineering, J Mater Chem, 2004, 14, 2154-2160.
6. R. O. Hynes, The extracellular matrix: not just pretty fibrils, Science, 2009, 326, 1216-1219.
7. T. Miyazaki, S. Miyauchi, A. Tawada, T. Anada, S. Matsuzaka and O. Suzuki, Oversulfated chondroitin sulfate-E binds to BMP-4 and enhances osteoblast differentiation, J Cell Physiol, 2008, 217, 769-777.
8. S. Mathews, S. A. Mathew, P. K. Gupta, R. Bhonde and S. Totey, Glycosaminoglycans enhance osteoblast differentiation of bone marrow derived human mesenchymal stem cells, J Tissue Eng Regen M, 2012, 1-10.
9. J. Mano, G. Silva, H. Azevedo, P. Malafaya, R. Sousa, S. Silva, L. Boesel, J. Oliveira, T. Santos and A. Marques, Natural origin biodegradable systems in tissue engineering and regenerative medicine: present status and some moving trends, J R Soc Interface, 2007, 4, 999-1030.
10. T. H. Silva, A. Alves, B. M. Ferreira, J. M. Oliveira, L. L. Reys, R. J. F. Ferreira, R. A. Sousa, S. S. Silva, J. F. Mano and R. L. Reis, Materials of marine origin: a review on polymers and ceramics of biomedical interest, Int Mater Rev, 2012, 57, 276-307.
11. A. Di Martino, M. Sittinger and M. V. Risbud, Chitosan: A versatile biopolymer for orthopaedic tissue-engineering, Biomaterials, 2005, 26, 5983-5990.
12. J. M. Oliveira, M. T. Rodrigues, S. S. Silva, P. B. Malafaya, M. E. Gomes, C. A. Viegas, I. R. Dias, J. T. Azevedo, J. F. Mano and R. L. Reis, Novel hydroxyapatite/chitosan bilayered scaffold for osteochondral tissue-engineering applications: Scaffold design and its performance when seeded with goat bone marrow stromal cells, Biomaterials, 2006, 27, 6123-6137.
13. N. M. Alves and J. F. Mano, Chitosan derivatives obtained by chemical modifications for biomedical and environmental applications, Int J Biol Macromol, 2008, 43, 401-414.
14. K. Kurita, Chemistry and application of chitin and chitosan, Polym Degrad Stabil, 1998, 59, 117-120.
15. M. N. V. R. Kumar, A review of chitin and chitosan applications, React Funct Polym, 2000, 46, 1-27.
16. V. L. Campo, D. F. Kawano, D. B. da Silva and I. Carvalho, Carrageenans: Biological properties, chemical modifications and structural analysis - A review, Carbohyd Polym, 2009, 77, 167-180.
17. E. G. Popa, M. T. Rodrigues, D. F. Coutinho, M. B. Oliveira, J. F. Mano, R. L. Reis and M. E. Gomes, Cryopreservation of cell laden natural origin hydrogels for cartilage regeneration strategies, Soft Matter, 2013, 9, 875-885.
18. V. E. Santo, A. M. Frias, M. Carida, R. Cancedda, M. E. Gomes, J. F. Mano and R. L. Reis, Carrageenan-Based Hydrogels for the Controlled Delivery of PDGF-BB in Bone Tissue Engineering Applications, Biomacromolecules, 2009, 10, 1392-1401.
19. P. M. Rocha, V. E. Santo, M. E. Gomes, R. L. Reis and J. F. Mano, Encapsulation of adipose-derived stem cells and transforming growth factor-beta 1 in carrageenan-based hydrogels for cartilage tissue engineering, J Bioact Compat Pol, 2011, 26, 493-507.
20. C. J. Morris, in Inflammation Protocols, 2003, vol. 225, pp. 115-121.
21. E. G. Popa, P. Carvalho, A. Dias, V. E. Santo, A. Frias, A. Marques, I. R. Dias, C. A. Viegas, M. E. Gomes and R. Reis, In vitro and in vivo biocompatibility evaluation of k-carrageenan hydrogels aimed at applications in regenerative medicine, 2011.
22. N. M. Alves, I. H. Pashkuleva, R. L. Reis and J. F. Mano, Controlling Cell Behavior Through the Design of Polymer Surfaces, Small, 2010, 6, 2208-2220.
23. S. M. Oliveira, N. M. Alves and J. F. Mano, Cell interactions with superhydrophilic and superhydrophobic surfaces, J Adhes Sci Technol, 2012, 1-21.

24. I. B. Leonor, H. M. Kim, F. Balas, M. Kawashita, R. L. Reis, T. Kokubo and T. Nakamura, Surface potential change in bioactive polymer during the process of biomimetic apatite formation in a simulated body fluid, J Mater Chem, 2007, 17, 4057-4063.
25. P. M. Lopez-Perez, A. P. Marques, R. M. P. da Silva, I. Pashkuleva and R. L. Reis, Effect of chitosan membrane surface modification via plasma induced polymerization on the adhesion of osteoblast-like cells, J Mater Chem, 2007, 17, 4064-4071.
26. D. S. da Costa, R. A. Pires, A. M. Frias, R. L. Reis and I. Pashkuleva, Sulfonic groups induce formation of filopodia in mesenchymal stem cells, J Mater Chem, 2012, 22, 7172-7178.
27. T. Boudou, T. Crouzier, K. F. Ren, G. Blin and C. Picart, Multiple Functionalities of Polyelectrolyte Multilayer Films: New Biomedical Applications, Adv Mater, 2010, 22, 441-467.
28. N. M. Alves, C. Picart and J. F. Mano, Self Assembling and Crosslinking of Polyelectrolyte Multilayer Films of Chitosan and Alginate Studied by QCM and IR Spectroscopy, Macromol Biosci, 2009, 9, 776-785.
29. R. R. Costa, C. A. Custodio, F. J. Arias, J. C. Rodriguez-Cabello and J. F. Mano, Layer-by-Layer Assembly of Chitosan and Recombinant Biopolymers into Biomimetic Coatings with Multiple Stimuli-Responsive Properties, Small, 2011, 7, 2640-2649.
30. P. Sher, C. A. Custodio and J. F. Mano, Layer-By-Layer Technique for Producing Porous Nanostructured 3D Constructs Using Moldable Freeform Assembly of Spherical Templates, Small, 2010, 6, 2644-2648.
31. S. M. Oliveira, T. H. Silva, R. L. Reis and J. F. Mano, Hierarchical Fibrillar Scaffolds Obtained by Non-conventional Layer-By-Layer Electrostatic Self-Assembly, Advanced Healthcare Materials, 2013, 2, 422-27.
32. K. Moon-Moo and K. Se-Kwon, in Chitin, Chitosan, Oligosaccharides and Their Derivatives, CRC Press, 2010, pp. 215-221.
33. G. Sauerbrey, Verwendung von Schwingquarzen zur Wägung dünner Schichten und zur Mikrowägung, Z. Physik, 1959, 155, 206-222.
34. L. Richert, P. Lavalle, E. Payan, X. Z. Shu, G. D. Prestwich, J. F. Stoltz, P. Schaaf, J. C. Voegel and C. Picart, Layer by layer buildup of polysaccharide films: Physical chemistry and cellular adhesion aspects, Langmuir, 2004, 20, 448-458.
35. M. Kumar, R. Muzzarelli, C. Muzzarelli, H. Sashiwa and A. Domb, Chitosan chemistry and pharmaceutical perspectives, Chem Rev, 2004, 104, 6017-6084.
36. A. Hugerth, N. Caram-Lelham and L. O. Sundelof, The effect of charge density and conformation on the polyelectrolyte complex formation between carrageenan and chitosan, Carbohyd Polym, 1997, 34, 149-156.
37. A. Bartkowiak and D. Hunkeler, Carrageenan–oligochitosan microcapsules: optimization of the formation process, Colloids and Surfaces B: Biointerfaces, 2001, 21, 285-298.
38. T. H. Silva, A. Alves, E. G. Popa, L. L. Reys, M. E. Gomes, R. A. Sousa, S. S. Silva, J. F. Mano and R. L. Reis, Marine algae sulfated polysaccharides for tissue engineering and drug delivery approaches, Biomatter, 2012, 2, 278-289.
39. H. Bubert, J. C. Rivière and W. S. M. Werner, in Surface and Thin Film Analysis, Wiley-VCH 2011, pp. 7-41.
40. C. Picart, J. Mutterer, L. Richert, Y. Luo, G. D. Prestwich, P. Schaaf, J. C. Voegel and P. Lavalle, Molecular basis for the explanation of the exponential growth of polyelectrolyte multilayers, P Natl Acad Sci USA, 2002, 99, 12531-12535.
41. I. B. Leonor, H. M. Kim, F. Balas, M. Kawashita, R. L. Reis, T. Kokubo and T. Nakamura, Functionalization of different polymers with sulfonic groups as a way to coat them with a biomimetic apatite layer, J Mater Sci-Mater M, 2007, 18, 1923-1930.
42. I. Y. Kim, R. Iwatsuki, K. Kikuta, Y. Morita, T. Miyazaki and C. Ohtsuki, Thermoreversible behavior of κ-carrageenan and its apatite-forming ability in simulated body fluid, Materials Science and Engineering: C, 2011, 31, 1472-1476.
43. H. J. Hausser and R. E. Brenner, Phenotypic instability of Saos-2 cells in long-term culture, Biochem Bioph Res Co, 2005, 333, 216-222.
44. D. J. Mcquillan, M. D. Richardson and J. F. Bateman, Matrix Deposition by a Calcifying Human Osteogenic-Sarcoma Cell-Line (Saos-2), Bone, 1995, 16, 415-426.
45. R. Hoffman, Carrageenans Inhibit Growth-Factor Binding, Biochem J, 1993, 289, 331-334.
46. H. J. Hausser and R. E. Brenner, Low doses and high doses of heparin have different effects on osteoblast-like Saos-2 cells in vitro, J Cell Biochem, 2004, 91, 1062-1073.

47. R. Hoffman, W. W. Burns and D. H. Paper, Selective-Inhibition of Cell-Proliferation and DNA-Synthesis by the Polysulfated Carbohydrate Iota-Carrageenan, Cancer Chemoth Pharm, 1995, 36, 325-334.

SECTION 5

2D PLATELET LYSATE LAYER-BY-LAYER ASSEMBLED NANOCOATINGS

CHAPTER V

LAYER-BY-LAYER ASSEMBLED CELL INSTRUCTIVE NANOCOATINGS CONTAINING PLATELET LYSATE

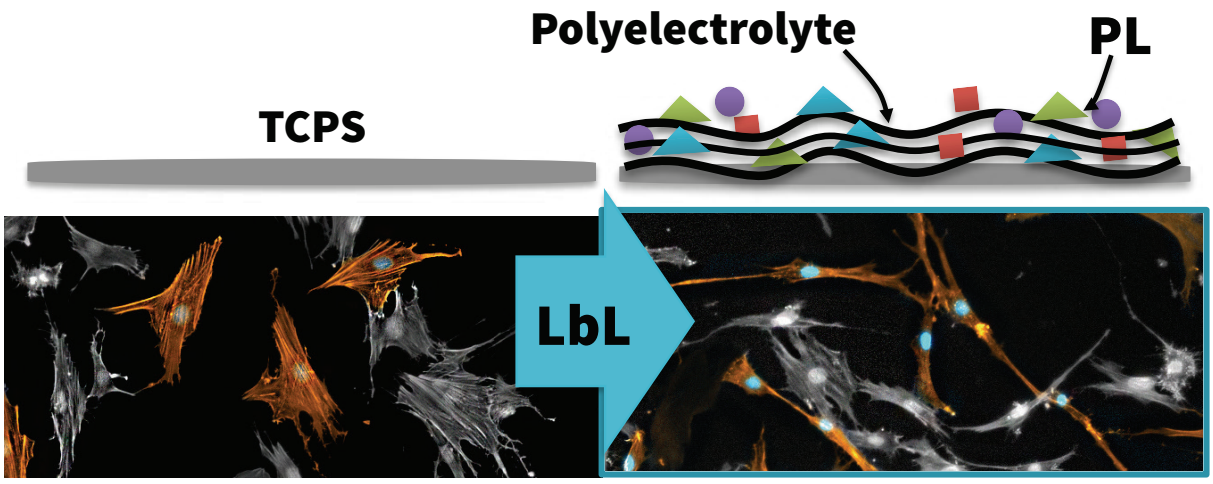

CHAPTER V*

Layer-by-Layer Assembled Cell Instructive Nanocoatings containing Platelet Lysate

V.1. Abstract

Great efforts have been made to introduce growth factors (GFs) onto 2D/3D constructs in order to control cell behavior. Platelet Lysate (PL) presents itself as a cost-effective source of multiple GFs and other proteins. The instruction given by a construct-PL combination will depend on how its instructive cues are presented to the cells. The content, stability and conformation of the GFs affect their instruction. Strategies for a controlled incorporation of PL are needed. Herein, PL was incorporated into nanocoatings by layer-by-layer assembling with polysaccharides presenting different sulfation degrees (SD) and charges. Heparin and several marine polysaccharides were tested to evaluate their PL and GF incorporation capability. The consequent effects of those multilayers on human adipose derived stem cells (hASCs) were assessed in short-term cultures. Both nature of the polysaccharide and SD were important properties that influenced the adsorption of PL, vascular endothelial growth factor (VEGF), fibroblast growth factor b (FGFb) and platelet derived growth factor (PDGF). The sulfated polysaccharides-PL multilayers showed to be efficient in the promotion of morphological changes, serum-free adhesion and proliferation of high passage hASCs (P>5). These biomimetic multilayers promise to be versatile platforms to fabricate instructive devices allowing a tunable incorporation of PL.

Keywords: layer-by-layer assembling, instructive surfaces, platelet lysate, growth factors, cell behavior; platelet derivative, VEGF, FGF, PDGF.

*This chapter is based on the following publication:

Sara M. Oliveira, Vítor E. Santo, Manuela E. Gomes, Reis R.L. and João F. Mano, Layer-by-Layer Assembled Cell Instructive Nanocoatings containing Platelet Lysate, submitted, 2014.

V.2. Introduction

The design of cell instructive surfaces is of major interest in the field of tissue engineering and regenerative medicine. Cell behavior is dictated by the interactions occurring between cell surface macromolecules, e.g. transmembrane proteins, glycolipids, glycoproteins and carbohydrates with the extracellular environment.[1-4] Cells are embedded in extracellular matrix (ECM), which is rich in glycosaminoglycans, proteoglycans, water and growth factors (GFs), and confers mechanical support and anchorage points. GFs are cytokines present either in soluble form or non-covalently bound to ECM polysaccharides presenting various sulfation degrees. GFs bind to cell tyrosine kinase receptors triggering intracellular events, making them very attractive molecules for cell behavior manipulation.[5] Cell behavior is affected by the concentration of GFs, as well as, by the presence or absence of their conjugations with sulfated polysaccharides.[6] GFs have a short half-life and so, strategies for their stabilization and exposure to cells at adequate doses, to trigger the adequate cell responses, are very important for many therapeutic applications.[7, 8] Several methodologies for the introduction of one or two different recombinant GFs (rGFs) have been used: covalent binding[9, 10,] absorption[10], biotinylated heparin-avidin bonding[11], layer-by-layer (LbL) assembling[12], GF absorption onto pre-built LbL multilayers[13], 14, and electrostatic binding with heparin.[15, 16] However, more translational developments in this area have been hindered by the high cost of rGFs, and difficulties to introduce simultaneously several GFs.

Platelets arise as a cost-effective autologous source of multiple GFs and other bioactive proteins – Figure V.1.a. Among them, some have a proven ability to improve, for instance, adhesion, mitogenesis and cell differentiation.[17-19] The instructive potential of platelet derivatives as a media supplement has been shown to vary with the GF content and also displays variability associated with the donor.[20-22] Platelet's derived GFs have been successfully included onto surfaces employing adsorption[23, 24] and antigen specific GF recruitment from Platelet Lysate (PL).[25] Sole absorption of GFs only allows for a short-term control over cells since, typically, they are quickly released. Covalent binding of a GF allows a more stable presentation to the cells. However, its activity may be compromised by changes in the GFs conformation, masking the active sites, or by GF-receptor complexes cell internalization inhibition.[26]

LbL is a simple and versatile technology that has been employed in the development of a large variety of biomedical devices.[27, 28] It is often based on a simple alternated deposition of negatively and positively charged polyelectrolytes (PEs). LbL can be performed in protein-mild conditions on virtually any substrate, ranging from nanoparticles to 3D scaffolds and hydrogels.[27, 28] There are reports on the beneficial use of one or two rGFs in LbL approaches.[12, 29, 30]

We believe that it would be advantageous to include multiple GFs from human sources as structural components of the multilayers, increasing both the complexity of the structures and the similarity with the ECM. We propose the use of LbL assembling for the development of multilayers nanocoatings containing PL in their structural composition, in which cell instructive cues can be preserved. PL was combined with several polyelectrolytes (PEs) presenting different SD (from 0 to 3 sulfate groups per sugar unit), different charges, functional groups conformation, and compared to the gold standard for protein stabilization - heparin.

Heparin is a highly sulfated polysaccharide that has been widely used to stabilize and attract rGFs[15, 16, 31, 32] and has been inspiring the synthesis of new polymeric matrices with heparin-analogue ending groups.[33] PEs were assessed for their capability to adsorb PL, including the following specific GFs: VEGF, PDGF and FGFb. The role of the PE used and the bioactivity of those multilayers were evaluated by assessing its mitogenic, morphological and phenotypic effects on human adipose derived stem cells (hASCs).

V.3. Materials and Methods

V.3.1. Materials

Medium molecular weight chitosan (Chi), with a degree of deacetylation of 80% (Sigma Aldrich, MKBB0566), was purified by a re-precipitation method. Briefly, Chi powder was first dissolved in 2% (v/v) acetic acid solution at a 1% (w/v) concentration. The mixture was maintained under stirring overnight at room temperature. The impurities were removed by four filtration cycles. Then, Chi was precipitated by addition of 1 M NaOH while stirring. Final steps consisted of washing Chi with distilled water until reaching a neutral pH and of dehydration by washing with ethanol–water mixtures with increasing ethanol content (20–100% v/v). Chi was freeze-dried for 3 days and grinded. κ- (Sigma-Aldrich, 22048), ι- (Fluka, 22045), λ-carrageenan (Car; Sigma-Aldrich, 22049), sodium heparin (Hep; Sigma-Aldrich, H3149), sodium alginate (Alg; Sigma Aldrich, 250 cP), and poly(ethyleneimine) solution (PEI; Sigma-Aldrich, P3143) were used as received.

V.3.2. Materials preparation

V.3.2.1. Preparation of Platelet Lysate

Platelet concentrates were obtained from different platelet collections performed at Instituto Português do Sangue (IPS, Porto, Portugal), under a previously established cooperation protocol. The components were obtained using either the Trima Accel® Automated Blood Collection System. All the platelet products were biologically qualified according to the Portuguese legislation. The platelet count was performed at the IPS using the COULTER® LH 750 Hematology Analyzer and the sample volume adjusted to 1 million platelet.μL^{-1}. The collected samples were subject to three repeated temperature cycles (frozen with liquid nitrogen at -196°C and heated at 37°C) and frozen at -20°C until further use. The remaining platelets were eliminated by centrifugation at 1400*g* for 10 min. Aliquots of Platelet lysate (PL) were stored at -20°C until final use.

V.3.2.2. Polyelectrolytes solutions

κ-,ι-, λ-Car, Hep and Alg were prepared in 1M Tris HCL 40 nM NaCl pH 7.4 with a concentration of 0.5 $mg.mL^{-1}$. Chi was dissolved in sodium acetate buffer with a concentration of 0.5 $mg\ mL^{-1}$. All the solutions were gently

stirred overnight. PL was 10-fold diluted with Tris HCL buffer or in 1M sodium acetate 40 mM NaCl pH 6 when to be combined with Chi.

V.3.2.3. QCM-D monitoring

A Q-Sense E4 quartz crystal microbalance (QCM-D, Q-Sense AB, Sweden) with dissipation was used for *in situ* monitoring the deposition of PE/PL bilayers at the surface of 100 nm gold-coated crystals. The crystals were first cleaned in an ultrasound bath at 30°C, and immersed successively in acetone, ethanol, and isopropanol. All crystals were initially modified with PEI to confer a initial positive charge. A 0.5% w/v PEI solution (Mw 750,000, Sigma Aldrich) was pumped for approximately 30 min following by extensive rinsing. The initial layer in the case of the combination Chi/PL was Alg.

The different polysaccharides were assembled with PL at pH 7.4, or 6 in the case of Chi, in the respective buffer solutions above mentioned. Briefly, AT cut quartz crystals were excited at multiple overtones (1, 3, 5, 7, 11, and 13), which correspond to 5, 15, 25, 35, 45, 55 and 65 MHz, respectively. The PEs solutions (0.5 $mg.ml^{-1}$) were pumped with a constant flow rate of 50 $\mu L.min^{-1}$, for 10 minutes at room temperature. As intermediate step, the respective buffer solutions were pumped during 10 minutes to rinse the crystals.

V.3.2.4. Coatings preparation in 48-well plates

48-well plates were modified with 0.5 mL of 0.5% (w/v) PEI solution to confer a positive surface charge. Then, the solution was removed and the wells were extensively rinsed with distilled water in order to remove the unbound PEI. The LbL was started by the adsorption of the negative PE. In the case of Chi, an Alg layer was first adsorbed. The adsorption times and volumes used were: 4 minutes and 0.5 mL for the polysaccharides solutions; 0.5 mL and 10 minutes for the PL solution; intermediate rising steps x2 for 30 seconds using the respective buffers. The sequence was repeated 6 times. The well plates were let to air-dry overnight and then sterilized using a UV light for 40 minutes.

V.3.2.5. Protein adsorption

6-well plates were modified with PEI and the PEs, as described before. Two milliliters of PL 10% (v/v) or PL 100% (v/v), pH 6 and pH 7.4, were added to each well and let to adsorb for 30 minutes. The volume was removed and stored at -20°C for further quantification. Each well was rinsed with 2 ml of the respective buffer, which was then stored for further protein quantification.

The total protein was quantified in the following solutions: initial PL, PL before and after adsorption, and rising solutions. The measurements were performed using a NanoDrop 1000 Spectrophotometer (Thermo Scientific). The absorbance of 2 µl volume of solution was measured at the wavelength 280 nm (n=6). The amount of PDGF (PL10%), FGFb (PL100%) and VEGF (PL100%) was quantified using ELISA kits following the assay protocol provided with the kit. Optical density was read at 450 nm (n=6) on a multi-well microplate reader (Synergy HT, Bio-Tek Instruments).

V.3.3. Cell behavior assessment

V.3.3.1. hASCs isolation

Human subcutaneous adipose tissue samples were obtained from lipoaspiration procedures performed on women with ages between 35 and 50 years under a protocol previously established with the Department of Plastic Surgery of Hospital da Prelada in Porto, Portugal. All the samples were processed within 24 h after the lipoaspiration procedure. hASCs were enzymatically isolated from subcutaneous adipose tissue as previously described.[34] Briefly, the lipoaspirate samples were firstly washed with a solution of PBS and 10% Antibiotic/Antimycotic. Liposuction tissue was digested with 0.2% Collagenase Type II solution for 90 min with intermittent shaking, at 37 °C. The digested tissue was filtered using a 100 μm filter mesh (Sigma-Aldrich, Germany). The floating adipocytes were separated from the precipitation stromal fraction by centrifugation at 1250 rpm for 10 min. The cell pellet was re-suspended in lysis buffer for 10 min to disrupt the erythrocytes. After a centrifugation at 800 rpm for 10 min, cells were again re-suspended and placed in culture flasks with Minimum Essential α Medium (Sigma-Aldrich) supplemented with sodium bicarbonate, antibiotic/antimycotic and 10% of Fetal Bovine Serum (Life Technologies). Cells were cultured until confluence at 37°C, 5% CO_2 incubator, changing the medium every 2 days.

V.3.3.2. Cell seeding

To proceed with the cell seeding, expanded cells were harvested by trypsinization and filtered with a 100 μm cell strainer to remove possible cell aggregates. Two cellular suspensions with a density of 1×10^4 cells.mL^{-1} were prepared in minimum essential α medium supplemented with 0% or 10% FBS. A volume of 500 μl of cell suspension was dripped into each well. Well-plates were incubated for 20 hours or 4 days for the assessment of cell adhesion, morphology, proliferation, ALP activity/cell and phenotype, without changing the medium. hASCs from two different donors and between passage 5 and 6 were used.

V.3.3.3. Cell morphology

After 20 hours in culture, samples were gently rinsed twice with sterile PBS and then fixed with formalin 2.5% (v/v) during 20 minutes. Cells were permeabilized with 0.5 mL of Triton 0.2% (v/v) in PBS during 2 minutes and then rinsed with PBS. Samples were incubated in the dark with 100 μL of (1:100) Phalloidin-TRITC (Sigma-Aldrich) solution for 30 minutes and then washed with PBS. For cell nuclei staining, well plates were incubated in the dark for 5 min with 100 μL 4,6-diamino-2-phenyindole dilactate (DAPI, Sigma-Aldrich) diluted 1:1000 in PBS. Samples were observed using an inverted Axio Observer Fluorescence Inverted Microscope (Zeiss).

V.3.3.4. Cell morphology analysis

Cell length, width and mean area were measured using the Image J software version 1.48. Cell length was considered the longest distance between the tips of the filopodias (200<n<300 cells from 8 images). The width

was measured on the cell nucleus position and usually in an angle approximately right to the cell length (200<n<400 cells from 8 images). Cell area was calculated dividing the total number of nucleus by the total area covered by the same cells (n=8). Cell aspect ratio was calculated by diving cell length per cell width.

V.3.3.5. dsDNA quantification

In order to quantify cell attachment and proliferation after 20 hours and 4 days in culture, dsDNA was quantified using the Quant-iT™ PicoGreen® dsDNA assay kit (Molecular Probes/Invitrogen) that allows the measurement of the fluorescence produced when PicoGreen dye is excited by UV light while bound to dsDNA. After incubation periods, the well plates were gently rinsed once with sterile PBS. Then, 1 mL of ultra-pure sterile water added and kept at -80°C until quantification. For the quantification, samples were defrosted at room temperature and the content was transferred to eppendorfs. 100 μL of Tris–EDTA buffer were transferred into a white opaque 96-well plate. Samples were vortexed and 28.8 μL of each plus 71.2 μL of PicoGreen solution were added to the wells. After 10 minutes of incubation in the dark, the plate was read in a microplate reader using an excitation wavelength of 485 nm and emission wavelength of 528 nm. A standard curve was created by varying the concentration of standard dsDNA standard from 0 to 2 $mg.mL^{-1}$, and triplicates dsDNA values of the samples were read off from the standard graph. At least six specimens were measured per each sample. The experiment was repeated once more.

Cell proliferation was calculated by assuming as 1-fold the difference between the dsDNA content at 20 hours and 4 days in TCPS.

V.3.3.6. ALP quantification

ALP activity was quantified in the same samples used for dsDNA quantification. The activity of ALP is typically evaluated using the p-nitrophenol assay. Paranitrophenyl phosphate, which is colourless, is hydrolysed by alkaline phosphatase enzyme at pH 9.8 and 37ºC to form free p-nitrophenol, which is yellowish. The reaction was stopped by addition of NaOH and the absorbance read at 405 nm. Briefly, in each well 20 µl of each sample, previously vortexed, were mixed with 60 µl of the substrate solution which is 0.2% (w/v) p-nytrophenyl phosphate (Sigma-Aldrich) prepared in a substrate buffer of 1 M diethanolamine (Sigma-Aldrich) at pH 9.8. The plate was then incubated in the dark for 45 min at 37°C. After the incubation period, 80 µl stop solution, which is composed by 2 M NaOH (Panreac) plus 0.2 mM EDTA (Sigma-Aldrich), was added to each well. Standards were prepared with 10 µmol mL^{-1} p-nytrophenol (pNP, Sigma, USA) solution, to obtain a standard curve covering the range 0–0.2 M. Triplicates of each sample and the standard were made. Finally, absorbance was read at 405 nm in a microplate reader (Bio-Tek, Synergie HT) and sample concentrations in triplicate were read off from the standard curve. The ALP concentrations were normalized against the dsDNA concentrations of the same samples to determine the cellular ALP activity.

V.3.3.7. Flow cytometry

Flow cytometry was performed using anti-human CD90 APC (BD Pharmingen™), anti-human CD105 FITC (BioRad), anti-human CD73 PE (BD Pharmingen™), anti-human CD34 PE (BD Pharmingen™), anti-human CD31 APC (R&D Systems), anti-human CD45 FTIC (BD Pharmingen™). Experiments were performed using hASCs in passages between 5-6, before the seeding and after 4 days in culture on the unmodified and modified surfaces.

Cells were trypsinized, counted and re-suspended in PBS with 2% (w/v) bovine serum albumin (BSA) (Sigma) with a concentration of $2x10^6$ cells/100ls and incubated with the antibodies at the concentration advised by the manufacturers. After incubation for 20 min at room temperature, protected from light, cells were washed with PBS/BSA, re-suspended in PBS with 1% formaldehyde (Sigma) and analyzed in a BD FACSCalibur™ flow cytometer (BD Biosciences). Cells of interest were gated in a forward vs. side scatter dot plot with a linear scale. Isotype controls were made to discern non-specific from specific staining. A minimum of 10,000 gated events were acquired and labeled cells were quantified.

CD's variations were calculated relatively to their initial content in the hASCs before seeding, for each sample. The calculation consisted in the difference between the percentages of each CD before and after 4 days in culture, for both donors.

V.3.4. Statistical Analysis

First, it was verified with Shapiro–Wilk test that most of the data did not passed the normality test. All data was statistically analyzed by using non-parametric tests. The unpaired one-tailed t-test with Welch's correction for non-parametric data was used ($p \leq 0.05$).

Spearman's Correlation was computed to assess the relationship between several variable pairs to verify the existence of any positive or negative monotonic correlation, using Graphpad Prism.

V.4. Results and Discussion

V.4.1. Nanocoatings assembling

LbL assembling is a versatile and simple technique in the context of cell-surface interactions design. This work has focused on the development of cell instructive multilayers prepared by combining distinct polysaccharides with proteins derived from human PL – Figure V.1.a, b. Nature offers a wide range of PEs with several molecular properties that may affect the PL adsorption regarding several aspects, including: the total adsorbed PL, the amount of each GF, the net charge of the proteins, as well as, their stability. Sulfated polysaccharides are good candidates for GFs stabilization by preserving both their conformation and bioactivity through the favorable interactions with sulfate or sulfonic groups.[35-37] Herein, PEs with varying charge and number of functional groups were selected: alginate (Alg; -1) and chitosan (Chi; +1), as unsulfated ones; and κ-, ι-, and λ-carrageenan (κ, ι, λ-Car; -1, -2, -3 respectively), as sulfated ones; along with heparin (Hep;

-3), as a sulfonic one and control – Figure V.1.c. We hypothesize that the chemical diversity of such PEs will allow tuning of the incorporation of bioactive factors from PL and, consequently, cellular response.

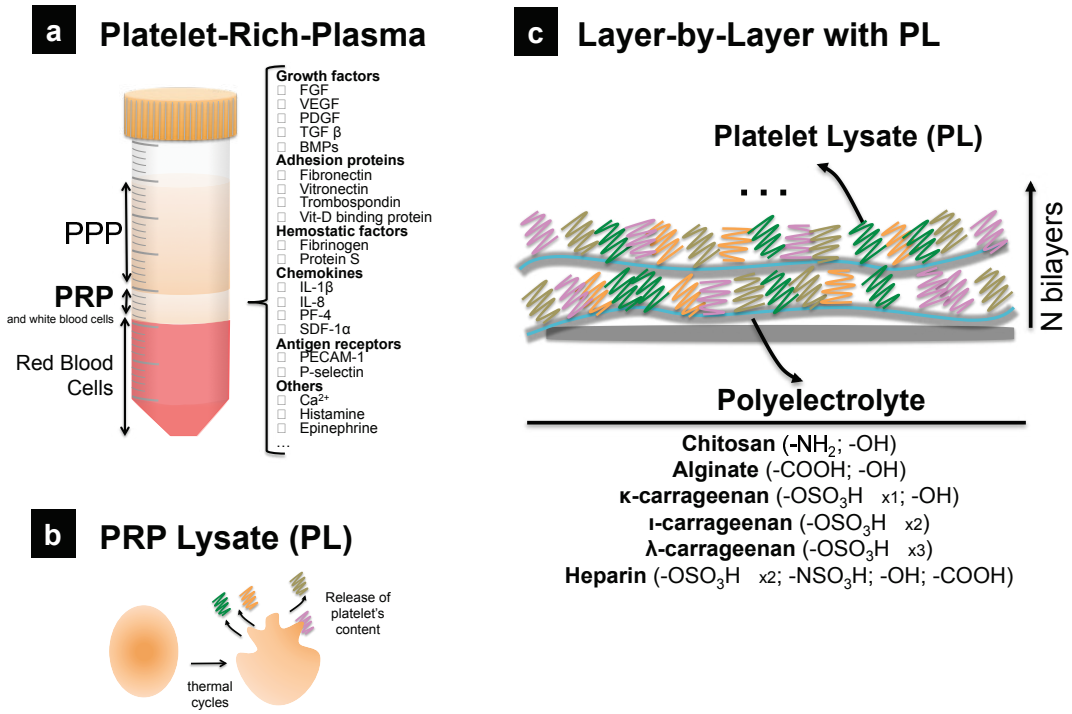

Figure V.1. Main steps for the preparation of PL/Polysaccharides Layer-by-Layer assembled nanocoatings. a) Platelet isolation from human blood as Platelet-Rich-Plasma (PRP) and examples of bioactive proteins than can be found in the enriched protein cocktail. b) PL preparation: PRP activation by platelet disruption induced by thermal cycles for the release of the inner content. c) Layer-by-Layer deposition combining PL with several PEs which respective functional groups and content are indicated.

The assembling of the PE/PL combinations was monitored using QCM-D – Figure V.2.a. It was observed that proteins from PL (10% v/v) adsorbed independently of the PE charge or SD. Alg/PL, Chi/PL, κPL, ι/PL, λPL and Hep/PL nanocoatings, with 6 bilayers, were assembled on silicon wafers. The mean thicknesses were measured by ellipsometry on dried samples - Figure V.2.b. These varied between 30 and 50 nm, being similar among most of the conditions. The nanocoatings produced with the positively charged PE, Chi, were shown to be the thickest ($p<0.05$) though similar to the one containing ι/PL. A large fraction of the PL proteins are negatively charged in a pH range of 5.5-6 (as opposed to several GFs), which may explain the higher thickness of Chi/PL nanocoatings. The multilayers were amenable to being produced using negatively charged PEs as well. Electrostatic interactions should contribute significantly to the stabilization of the multilayers, although other kinds of interactions could participate in the LbL construction, such as, hydrophobic or hydrogen bonds.[38]

Total protein quantification indicated that the profile of protein adsorption may be affected by PL concentration – Figure V.3.a, b. With PL 10% (v/v), Chi and κ could adsorb a higher content, as compared to all other PEs ($p<0.05$). Increasing the PL concentration, from 10% to 100%, highly increased the content of protein ($p<0.005$; 3 to 5 fold) on the unsulfated and on the more sulfated PEs (SD=3).

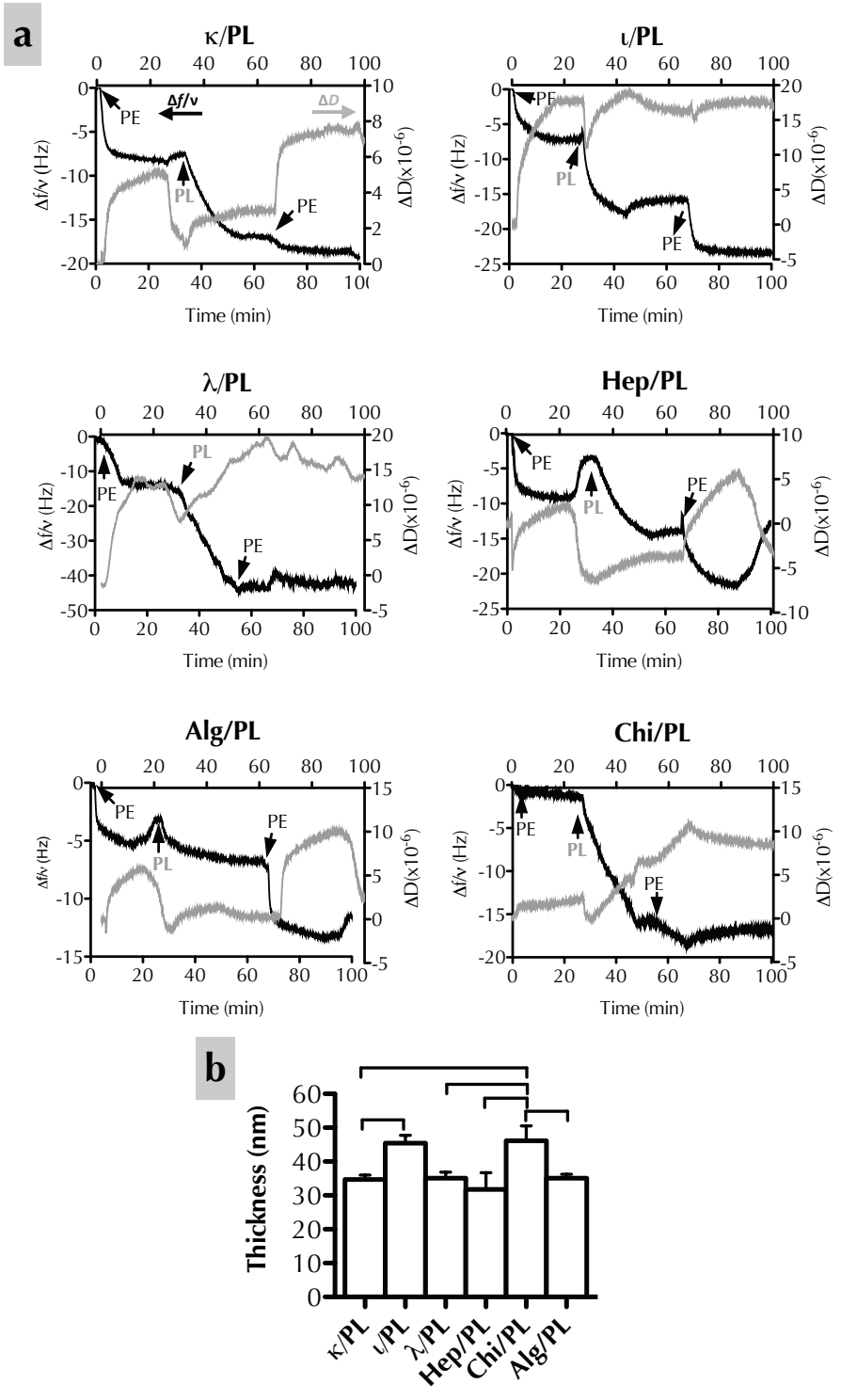

Figure V.2. Nanocoatings characterization: a) QCM-D monitoring of the normalized frequency ($\Delta f/\nu$) and dissipation (ΔD), obtained for the seventh overtone for the LbL deposition of PE-PL-PE and intermediate rinsing steps; b) Thickness of the nanocoatings with 6 bilayers measured by ellipsometry (n=6; mean±SEM). All combinations of pairs of samples were compared and bars indicate the statistical different ones ($p<0.05$; n=6; data represented as mean±SEM).

The binding of specific GFs, namely PDGF, FGFb and VEGF, was investigated – see Figure V.3.c, d and e, respectively. The type of PE revealed to have a huge impact in the total content of PL, as well as, in the incorporation of the GFs. Even though sulfate groups are appropriated to bind GF through electrostatic

interaction, higher SD may not imply higher adsorption. Actually, the densities of VEGF and FGFb did not correlate with the SD, nor with the total protein adsorbed – Table V.S2. Moreover, the adsorption of PDGF tended to decrease with the increase of the SD. Consequently the VEGF/PDGF and FGFb/PDGF ratios were increased with the increase of the SD – Table V.S2. Nevertheless, when comparing with the unsulfated, the sulfated ones and Hep could achieve high levels of GFs adsorption. But, interestingly, they have shown different adsorption abilities. Hep could adsorb a high content of VEGF, while κ was more prompt for a high PDGF and intermediate VEGF adsorption. On the other hand, ιCar achieved the highest levels of VEGF, FGFb and PDGF adsorption. Contrarily, λ Car has not shown the ability to highly adsorb any of the quantified GFs.

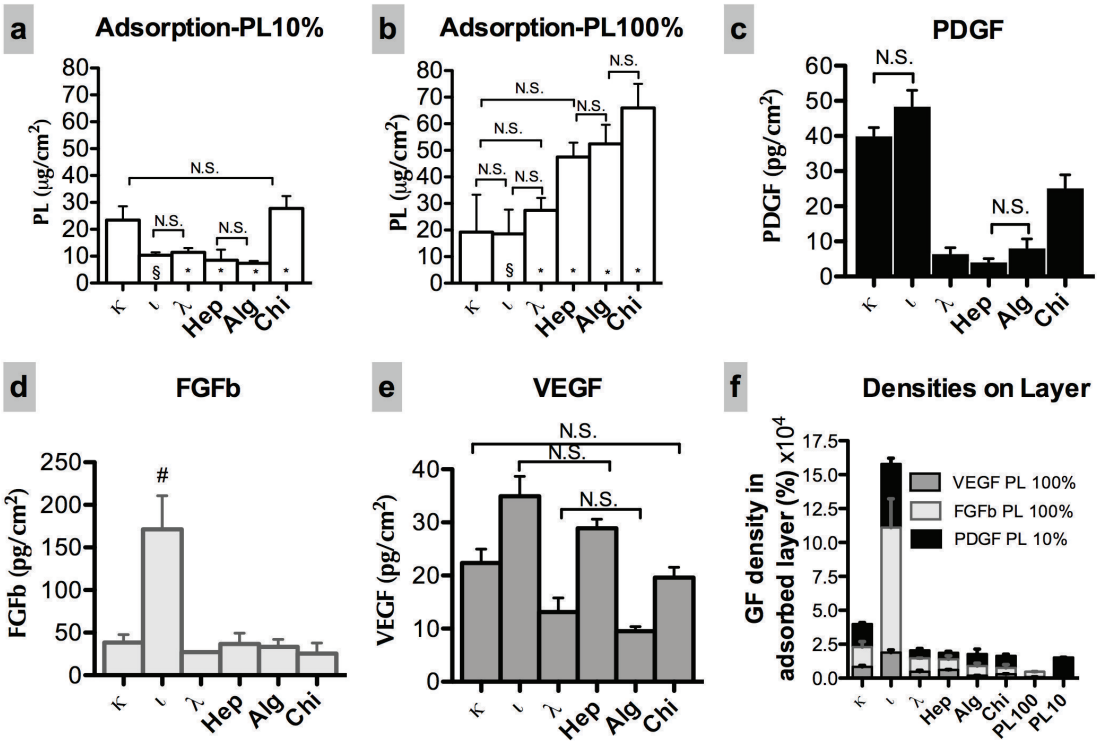

Figure V.3. Quantification of PL, VEGF, bFGF and PDGF adsorption onto different PEs layers. Total protein adsorbed according to the initial PL concentration: a) PL 10%(v/v), b) PL 100% (v/v). Content of GF adsorbed: c) PDGF, d) bFGF, e) VEGF. d) Density of GFs in the formed protein-layer. All combinations of pairs of samples were compared and only the pairs not statistically similar (with $p>0.05$) are indicated with exception of d) where # represents the only significant differences ($p<0.05$): ι is significantly different to all the other samples. In a) and b), § and * mean significant difference between the total protein adsorption with PL 10% and PL 100% with $p(<0.05)$ or $p(<0.005)$, respectively. Statistical analysis of f) can be consulted in Table V.S1. Data represented as mean±SEM; n=6.

In general, the total content of protein adsorbed did not allow predicting of the respective content of GFs incorporated. In fact, several significant differences were detected in the PL layer relatively to its local density of VEGF, FGF and PDGF – see Figure V.3.f and Table V.S1. The PEs showed different patterns for the incorporation of GFs. This highlights the importance of the initial surface chemistry regarding the interaction of platelets derivatives with biomaterials.

Overall, the ratios of GFs can be varied with the PE, as well with the SD. This may represent a simple way of adjusting or improving the cell instructive cues of 2D/3D biomaterials, according with the target applications.

V.4.2. Cell morphology

Stem cell cytoskeleton organization has been correlated with cell fate commitment, besides being informative about cell senescence.[39-42] The proliferation rate of stem cells decays with increasing number of passages, and ultimately cells reach a senescent state. In the case of mesenchymal stem cells, senescence is defined by an enlarged morphology (larger width), reduced expression of surface markers and decreased differentiation potential.[43]

The potential of the developed nanocoatings to induce any significant changes on the morphology was assessed by characterization of the width and length – Figure V.S1., cell aspect ratio (length/width) and mean area –Figure V.5., after 20 hours of culture. In our study, hASCs (P6-7) cultured on TCPS were approximately 50 μm wide - Figure V.S1.a, b. The presence of SO_3H end groups reduced cell width in comparison with TCPS. Introducing PL on the nanocoatings further decreased the cell width for almost half of what was measured in TCPS. Correlation's analysis suggested that there was a moderate correlation between FGF/VEGF and FGF/PDGF ratios with cell width – Table V.S2. Among the sulfated/sulfonic-PL nanocoatings, cell width tended to reduce when the ratio of FGF/VEGF was increased, when FGF/PDGF was decreased and VEGF density was lowered – Table V.S2.

On the other hand, hASCs length tended to increase with the presence of SO_3H – Figure V.S1.c, d. Comparing these with the respective surfaces with PL, its presence did not significantly alter cell length, with exception of λ/PL and Hep/PL nanocoatings where it was a slightly decreased ($p<0.05$). The increased cohesion between cells with the incorporation of PL may have masked the tips of the filopodia and/or actually reduced cell length on those two samples. Nevertheless, Spearman's correlation pointed out that cell length tended very strongly to increase with increase of PDGF and PL, which simultaneously, represented a decrease in VEGF/PDGF and FGF/PDGF ratios.

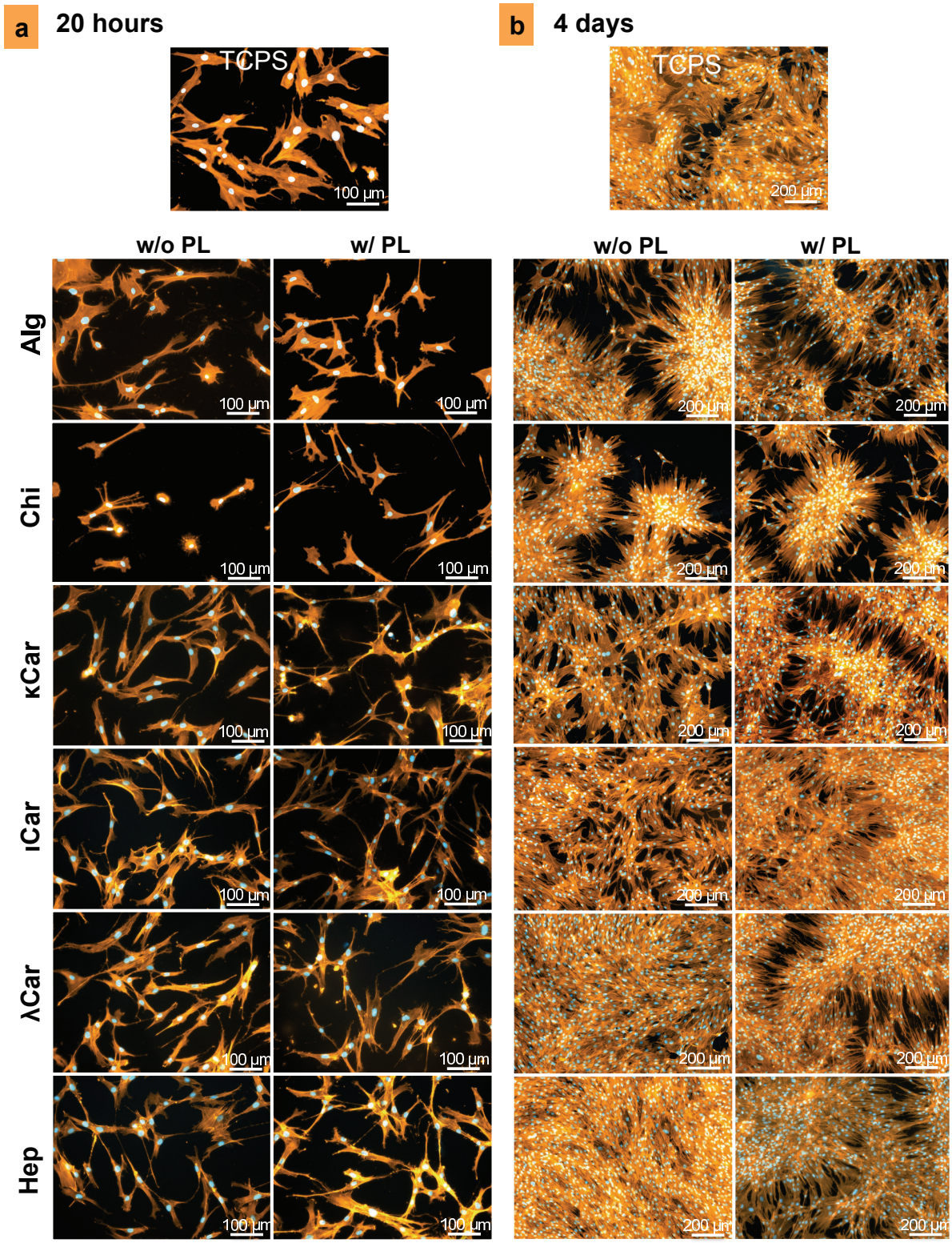

Figure V.4. a) hASCs morphology after 20 hours and b) 4 days in culture, in presence of 10% of serum. (Blue – nuclei; orange – cytoskeleton).

All the width and length variations induced by the presence of the multilayers led to a huge reduction on cell mean area by 1/4 to 1/2 from the initial 4000 μm^2 on TCPS. However, the cytoskeleton was elongated, representing an increased aspect ratio (length/width) – Figure V.5.a, b.

Overall, the presence of SO_3H on the surface made the cells achieve a slightly higher length and smaller width that further diminished when PL was incorporated. Consequently, cell aspect ratio was increased to 6-8 on the multilayers containing PL– Figure V.5.c. The developed nanocoatings reverted the enlarged morphology observed on TCPS.

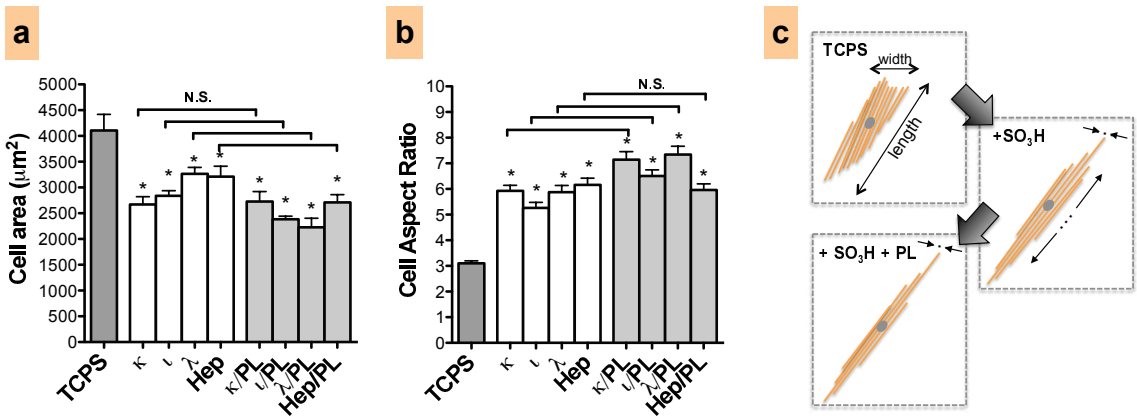

Figure V.5. hASCs morphological analysis after 20 hours in culture. a) Mean cell area. b) Cell aspect ratio (Length/width). c) Scheme evidencing cell length and width behavior observed with the presence of SO3H groups and PL. All the significances are identified: bars (the samples are different), * (samples are statistically significantly different comparing to TCPS); ($p<0.05$; n=8 cell area; 200<n<300 cell aspect ratio).

V.4.3. Cell adhesion, proliferation and ALP activity

In order to verify the bioactive ability of the developed multilayers, their effect over hASCs adhesion and proliferation was assessed in short-term cultures – Figure V.6.

48-well culture plates were modified with PE, and PE/PL multilayers with 6 bilayers. Cells were seeded at an initial density of 5000 cells.cm^{-2} in the presence and absence of serum proteins.

In the absence of both PL and medium serum, cell adhesion was very limited and almost no differences were detected between TCPS and the PEs coatings – Figure V.6.a. The presence of PL significantly increased cell adhesion in the cases of κ/PL and ι/PL, by 5 and 8-fold, respectively, as compared to TCPS ($p<0.05$). This suggested that those might be the nanocoatings which are richer in cell-adhesive moieties, or that cell adhesion could have been mediated by interactions between surface PDGF and cell PDGF receptors. When serum was included in the culture media, cell attachment was not as affected by the presence or absence of PL – Figure V.6.b. However, the surfaces containing PL, namely ι/PL and Hep/PL, allowed for a higher cell attachment than TCPS ($p<0.05$).

The proliferation rate of hASCs usually decreases with increasing passage number. PL media supplementation has been reported to enhance cell proliferation and even refresh high passage cells.44, 45 We believe that the expansion of high passage hASCs onto the PL-multilayers might be a way to increase the proliferation ratio and avoid/delay senescence. hASCs (passage 5-6) were, therefore, cultured on the developed nanocoatings. dsDNA quantification and proliferation ratios upon 4 days of culture are shown in Figure V.6.c and Figure V.7.a, respectively. Overall, hASCs were able to proliferate on all the surfaces, and to reach over-confluence on the

coatings with more SO_3H groups and PL – Figure V.4.b. Those also allowed a higher hASCs proliferation as compared with TCPS. Regarding the multilayers, ι/PL and Hep/PL have shown the highest ability to improve cells proliferation (~2 fold relatively to TCPS) – Figure V.7.a. Chi/PL nanocoatings were the only samples whose proliferation was impaired ($p<0.05$). This suggests that solely Chi, or a positively charged PE, may not be adequate to attract bioactive proteins suitable to promote cell proliferation. Moreover, since Chi is uncharged during the culture, it may not ensure sufficient stabilization, or an adequate conformation of the adsorbed bioactive proteins.

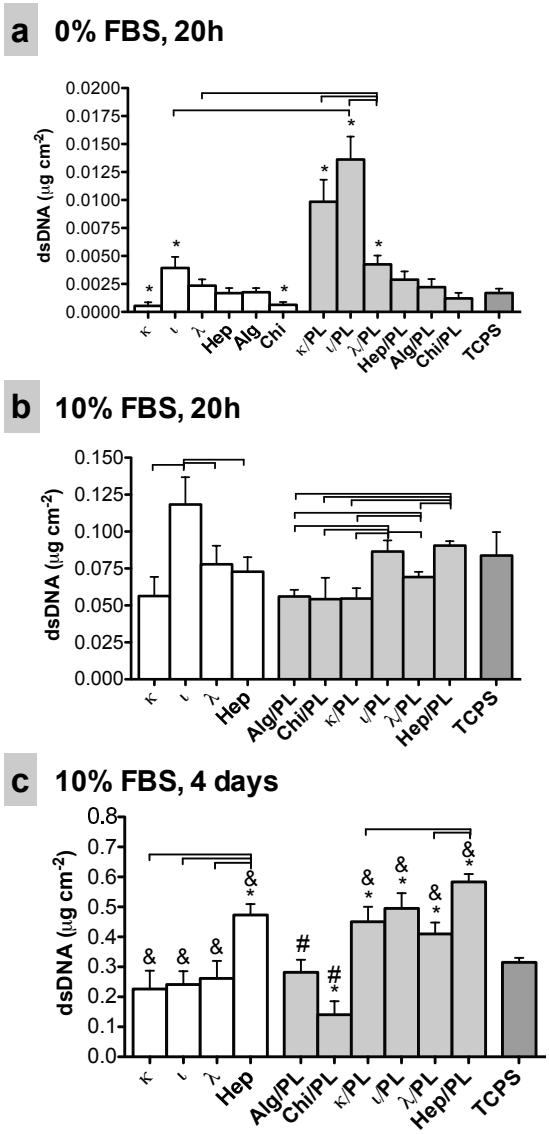

Figure V.6. hASCs adhesion and proliferation after 20 hours and 4 days of culture. a) hASCs adhesion in serum free conditions after 20 hours in culture. b) hASCs adhesion in presence of 10% FBS. c) dsDNA content after 4 days in culture. All the significances are identified: bars (the samples are different), * (different from TPCS), # (different to all other samples with PL), & (sample PE1/PL is different to PE1); ($p\leq0.05$; n=10; 2 donors). Data represented as mean±SEM.

The mitogenic induction can be accomplished by supplementing culture medium with GFs, such as VEGF[46], FGF[47], PDGF[48-50] and EGF[47], in a dose-dependent manner. Those mitogenic GFs can be found in PL, which is already established as medium supplement, to improve cell proliferation. Its mitogenic potential has been correlated with the concentration of PDGF.[48] As shown in the previous section, depending on the PE, the

percentage of the mitogenic GFs cannot be assumed as equivalent to the total content of proteins adsorbed. Moreover, the sole ability of the PE to attract a specific GF may not be a good proliferation predictor factor if the PE itself improves cell proliferation. For example, proliferation on Hep surfaces was higher when compared with the other coatings without PL. The ability of Hep to improve cell proliferation has also been reported elsewhere.[51, 52] By verifying the existence of correlations between GF surface density and cell proliferation, it was possible to detect a moderately positive correlation with VEGF and FGF. A higher ability of the PE to adsorb VEGF or FGF may be a moderate indication of a higher cell proliferation – Table V.S2. In addition, the morphological features showed to be correlated with proliferation. Cell proliferation tended to be higher on cells with higher cell aspect ratios and with decreased widths. In general, the culture of hASCs on these PL-multilayers has reverted the enlarged morphology, which is a senescence-associated feature, and has increased cell proliferation.

In vitro, alkaline phosphatase (ALP) is highly expressed in early osteogenesis, and is also considered a universal pluripotent marker for all types of pluripotent stem cells including embryonic stem cells, embryonic germ cells and induced pluripotent stem cells.[53, 54] In hASCs, a significant increase in ALP activity during normal medium conditions suggests a cell-commitment to the osteoblastic lineage or cell aging.[55] Therefore, when solely expanding multipotent stem cells, a highly significant ALP increase might be unwelcome since it may compromise stemness. The ALP activity per lysed cell was quantified after 20 hours and 4 days in culture – see Figure V.7.b. ALP significantly increased ($p<0.05$) with increasing culture time although, at different extents depending on the coating. On κ, λ, ι/PL, λ/PL and the Hep/PL nanocoatings, ALP activity increase was much lower than TCPS ($p<0.05$). The variations in ALP activity, upon 4 days in culture, were not correlated with cell content, proliferation, GFs and PL content, nor with the assessed morphological features – see Table V.S2. Nevertheless, there was a moderate positive correlation between the samples with and without PL, which also denotes the importance of the surface chemistry. One cannot exclude that the PE coatings may have adsorb similar proteins from media serum, although in lower concentration. The overall variations in ALP may be related with the presence of other proteins, or proteins ratios not contemplated in the analysis. ALP activity has been shown to vary with the ratio of the GFs used as medium supplement. For instance, FGFb has been reported to decrease ALP activity when used as media supplement, as opposed to VEGF.[56] When FGFb was combined with VEGF, the ALP activity reached values within the range of VEGF and FGFb alone but, lower than the increased value when cultured only with VEGF.[56] Herein, as mentioned above, there was no correlation between FGF/VEGF ratio and the ALP variations. This suggests that other important factors, not contemplated in the analysis, may have been decisive for hASCs behavior.

Different combinations of PE and PL could be used to tune the ALP activity and proliferation and translate different osteogenic potentials in longer-term cultures.

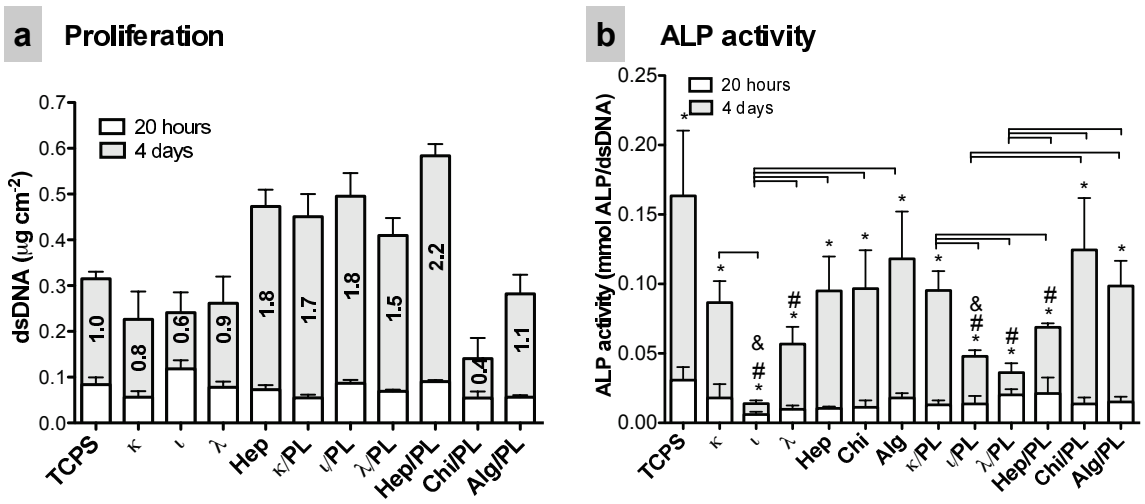

Figure V.7. hASCs proliferation ratios and ALP activity after 20 hours and after 4 days of culture on the nanocoatings. a) Each set of superimposed bars show the dsDNA content at 20 hours and 4 days with the proliferation ratios (relative to TCPS) indicated in the bars inset; b) Each set of superimposed bars corresponds to the ALP/cell after 20 hours and 4 days in culture. All the statistical significances are identified: bars refer to the data of 4 days in culture, * (ALP varied from 20 hours to 4 days), # (ALP at 4 days is different from ALP on TCPS 4 days), & (ALP on sample PE1/PL is different to PE1, after 4 days in culture); ($p \leq 0.05$; n=10; 2 donors). Data presented as mean±SEM.

V.4.4. hASCs phenotype

Cultured population of hASCs are strongly characterized by being positive to CD105, CD90 and CD73 regardless of their passage or time in culture and weak or negative for CD34 and CD31.[57, 58] Within lower passages the multipotency and the proliferation capability is not altered. However, the cell phenotype changes: both CD34 and CD31 expression declines, being accompanied by an increase of CD90 and CD105.[57, 58] Suga *et al.*[59] reported that the expression of CD34 in hASCs can be reversed. hASCs lost CD34 expression upon culturing with DMEM but regained expression after being cultured with endothelial basal medium.[59] The same authors also suggested that the loss of CD34 may be related with the physiological process of commitment and/or differentiation from immature status into specific lineages such as adipose, bone and smooth muscle.[59] The hASCs phenotype was characterized before seeding (P5-P6) and after 4 days in culture, on some of the multilayers that showed improved cell proliferation: ι/PL and κ/PL using TPCS and ι as controls. Results in Table V.1 are shown as the variation on the percentage of each CD with the culture on each respective surface, in relation to the original phenotype before seeding.

TCPS showed the common trend of decreasing CD34, CD31 and CD45 positive cells while increasing CD105 and CD73 positive cells. On the other hand, SO_3H and PL interfered with the percentage of CD31 and CD34 positive cell. A plausible reason for such variation would be the binding of CD31/CD34 positive cells (positive cells for VEGF receptor) mediated by VEGF or other specific GFs that had been incorporated.

The results suggest less sulfated nanocoatings as more beneficial for cell proliferation applications. Whereas higher sulfated coatings might be more suitable for differentiation purposes or, more specifically, for bone and vascular engineering, since they present higher FGF/PDGF and VEGF/PDGF ratios.

Table V.1. Flow cytometry assessment of the phenotype changes between P5-6 to P6-7 when cultured on the nanocoatings or TCPS for 4 days. Table shows the CD (Cluster of Differentiation) variation comparing with the phenotype before seeding (mean±SD; 2 donors).

	TCPS	ι	ι/PL	κ/PL
CD105	0.0±0.1	-1.6±0.5	-1.3±0.9	-1.2±0.0
CD73	0.2±0.1	-0.3±0.4	-0.4±0.8	-1.0±0.4
CD90	0.0±0.1	0.2±0.2	0.2±0.2	-0.8±0.2
CD45	-0.4±0.2	0.2±0.7	-0.6±0.9	-2.2±0.6
CD34	-0.3±0.1	1.0±2.4	0.5±1.7	-1.3±0.2
CD31	-0.2±0.9	1.9±2.4	1.4±2.9	0.2±0.4

V.5. Conclusions

hASCs are anchorage-dependent cells and the interactions with the biomaterial surface dictate their behavior and fate. PL is a cost-effective source of several autologous bioactive proteins, e.g. GFs. Herein, we show the preparation of cell instructive multilayers by assembling PL with several PEs using LbL.

The PE nature and the SD, are important features that have influenced the adsorption of PL, VEGF, FGFb and PDGF. Intermediate sulfated polysaccharides were more prompt for high FGFb, VEGF and PDGF incorporation. The low sulfated polysaccharides could adsorb high PDGF and intermediate VEGF, while Hep showed only high VEGF adsorption. Consequently, by increasing the SD, the VEGF/PDGF and FGF/PDGF ratios tended to increase. Overall, the biomimetic sulfated PL-multilayers were shown to be efficient in the promotion of morphological changes, serum-free cell adhesion and cell proliferation. The results highlight the importance of the initial surface chemistry regarding the incorporation of platelets derivatives into biomaterials. For instance, the more sulfated PL nanocoatings might be more adequate for vascular or differentiation purposes since they permit a lower FGFb and PDGF incorporation than the less sulfated ones. The specific interactions of the PL containing coatings with endothelial cells will be investigated in future work.

V.6. Acknowledgements

Portuguese Foundation for Science and Technology is gratefully acknowledged for fellowships of Sara M. Oliveira. (SFRH/BD/70107/2010).

The research leading to these results has received funding from the European Union's Seventh Framework Programme (FP7/ 2007-2013) under grant agreement no REGPOT-CT2012-316331- POLARIS and FP7-KBBE-2010-4-266033 – SPECIAL. This work was also supported by the European Research Council grant agreement ERC-2012-ADG 20120216-321266 for the project ComplexiTE.

The authors acknowledge Rogério P. Pirraco for the Flow cytometry analysis.

V.7. Supporting Information

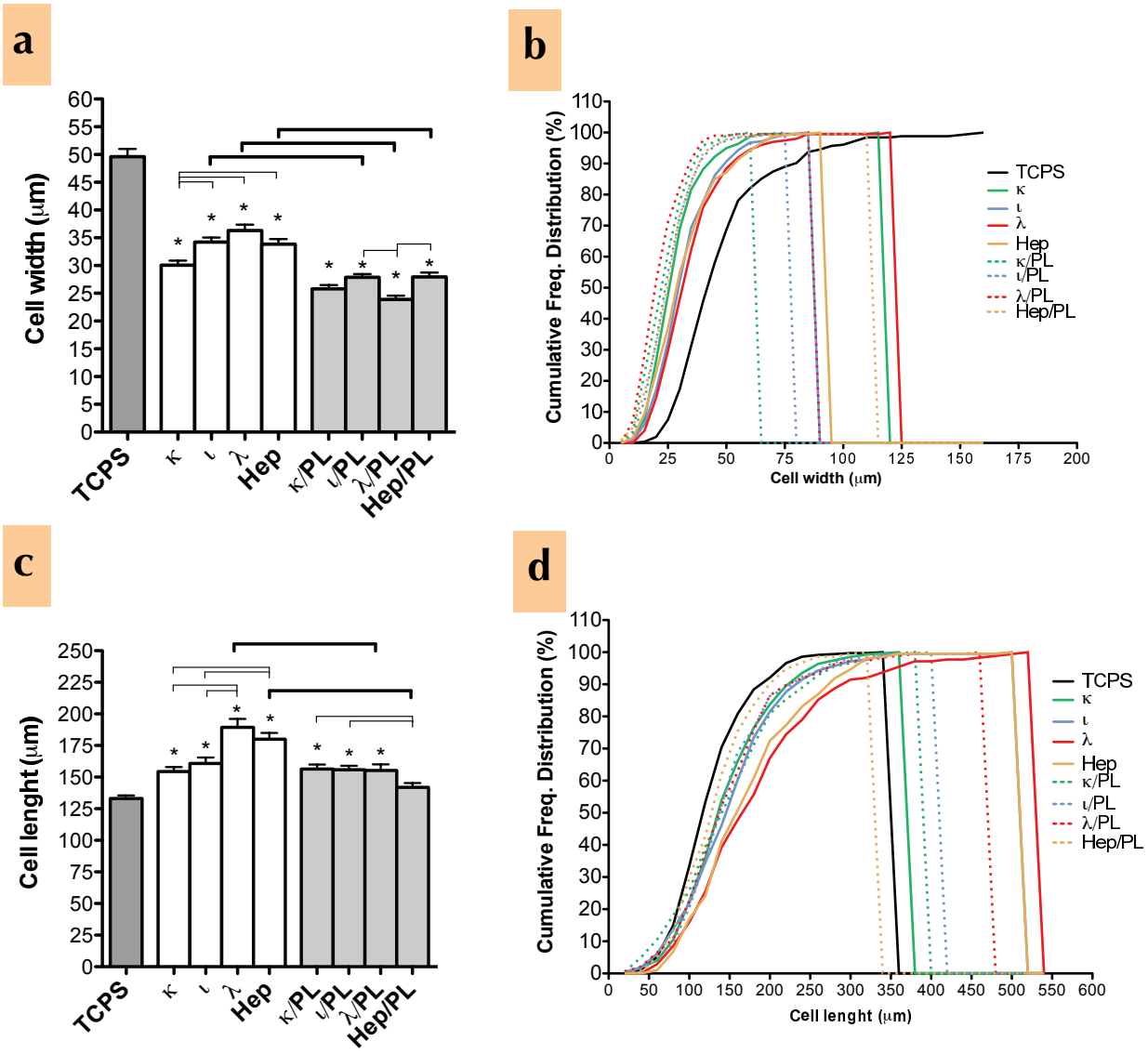

Figure V.S1. hASCs morphological analysis after 20 hours in culture. a) Cell mean width. b) Cumulative frequency distribution of cell width among all the individual measured cells. c) Cell mean length. d) Cumulative frequency distribution of cell length among all the individual measured cells. All the significances are identified: bars (the samples are statistical significantly different), * (samples are statistical significantly different comparing to TCPS); ($p<0.05$; $200<n<300$). Data represented as mean±SEM.

Table V.S1. Multi-comparisons of the density of VEGF, FGF and PDGF on the PL adsorbed layer according to the polyelectrolyte used (percentage of GF in the total amount of proteins adsorbed). All significant differences are indicated with * ($p<0.05$) and non significant with x ($p>0.05$).

VEGF density in adsorbed layer (100%PL)								
	κ	ι	λ	Hep	Alg	Chi	PL10%	PL100%
κ	-	*	*	*	*	*	-	*
ι	*	-	*	*	*	*	-	*
λ	*	*	-	x	*	x	-	*
Hep	*	*	x	-	*	*	-	*
Alg	*	*	*	*	-	*	-	*
Chi	*	*	x	*	*	-	-	*
PL10%	-	-	-	-	-	-	-	-
PL100%	*	*	*	*	*	*	-	-

FGFb density in adsorbed layer (100%PL)								
	κ	ι	λ	Hep	Alg	Chi	PL10%	PL100%
κ	-	*	x	x	x	*	-	*
ι	*	-	*	*	*	*	-	*
λ	x	*	-	x	x	x	-	*
Hep	x	*	x	-	x	x	-	x
Alg	x	*	x	x	-	x	-	x
Chi	*	*	x	x	x	-	-	x
PL10%	-	-	-	-	-	-	-	-
PL100%	*	*	*	x	x	x	-	-

PDGF density in adsorbed layer (10%PL)								
	κ	ι	λ	Hep	Alg	Chi	PL10%	PL100%
κ	-	*	*	*	*	*	x	-
ι	*	-	*	*	*	*	*	-
λ	*	*	-	x	x	x	*	-
Hep	*	*	x	-	x	*	*	-
Alg	*	*	x	x	-	x	x	-
Chi	*	*	x	*	x	-	*	-
PL10%	x	*	*	*	x	*	-	-
PL100%	-	-	-	-	-	-	-	-

Table V.S2. Spearman's Correlation was computed to assess the relationship between the indicated pairs of variables in order to verify the existence of any positive or negative monotonic correlation. The respective Spearman's r coefficients and significances are indicated.

x	y	Spearman r; number of XY pairs	p-value	Sig.
SD	VEGF100	-0.05; 11	0.44	No correlation
SD	FGF100	-0.33; 11	0.16	No correlation
SD	PDGF10	-0.76; 12	*0.003	Strong -
SD	PL10	-0.62; 29	*0.0002	Strong -
SD	FGF/VEGF	-0.21; 11	0.26	No correlation
SD	FGF/PDGF	0.82; 11	*0.0016	Very Strong +
SD	VEGF/PDGF	0.85; 11	*0.0009	Very Strong +
SD	PL100	0.51; 12	*0.05	Moderate +
PL100	VEGF100	-0.24; 17	0.18	No correlation
PL100	FGF100	-0.36; 15	0.1	No correlation
PL10	PDGF10	0.51; 18	*0.016	Moderate +
FGF100	VEGF100	0.37; 15	0.09	No correlation
FGF100	PDGF10	0.55; 15	*0.02	Moderate +
VEGF100	PDGF10	-0.38; 18	0.06	No correlation
nDNA	ALP4D	0.12; 22	0.20	No correlation
DNAvar	ALPvar	0.15; 22	0.25	No correlation
ALP20h	ALP4D	0.38; 22	*0.04	Weak +
DNAvar	ALP4D	0.18; 22	0.21	No correlation
DNA20h	ALP4d	-0.04; 22	0.44	No correlation
DNA4d	ALP4d	0.06; 22	0.40	No correlation
DNA20h	ALPvar	-0.02; 22	0.46	No correlation
ALPvar no PL	ALPvar with PL	0.59; 12	*0.02	Moderate +
DNA4d	ALPvar	0.04; 22	0.43	No correlation
Cell Aspect Ratio	nDNA	0.63; 18	*0.002	Strong +
Cell Aspect Ratio	DNAvar	0.65; 18	*0.002	Strong +
Cell Aspect Ratio	ALP20h	0.11; 18	0.33	No correlation
Cell Aspect Ratio	DNA20h	-0.24; 18	0.17	No correlation
Cell Aspect Ratio	ALPvar	-0.12; 18	0.32	No correlation
Cell Aspect Ratio	VEGF100	-0.64; 11	*0.02	Strong -
Cell Aspect Ratio	FGF100	-0.33; 11	0.16	No correlation
Cell Aspect Ratio	PDGF10	0.04; 12	0.45	No correlation
Cell Aspect Ratio	PL100	-0.39; 12	0.10	No correlation
Cell Aspect Ratio	PL10	0.52; 12	*0.04	Moderate +
Cell Aspect Ratio	ALP4d	-0.08; 18	0.38	No correlation
Cell Aspect Ratio	VEGF/PDGF	-0.43; 11	0.09	No correlation
Cell Aspect Ratio	FGF/PDGF	-0.60; 11	*0.03	Strong -
Cell Aspect Ratio	VEGF/FGF	0.014; 12	0.49	No correlation
Cell length	ALPvar	-0.23; 18	0.18	No correlation
Cell length	DNAvar	-0.11; 18	0.33	No correlation
Cell length	VEGF/PDGF	-0.88; 11	*0.0003	Very Strong -
Cell length	FGF/PDGF	-0.88;11	*0.0003	Very Strong -
Cell length	FGF/VEGF	0.25; 11	0.22	No correlation
Cell length	VEGF100	-0.09; 11	0.39	No correlation
Cell length	FGF100	0.25; 11	0.23	No correlation
Cell length	PL10	0.73; 12	*0.004	Strong +
Cell length	PDGF	0.76; 12	*0.003	Strong +
Cell width	ALPvar	0.17; 18	0.24	No correlation
Cell width	DNAvar	-0.58; 18	*0.006	Moderate -
Cell width	VEGF/PDGF	0.43; 11	0.09	No correlation
Cell width	FGF/PDGF	0.60; 11	*0.03	Strong +
Cell width	FGF/VEGF	-0.60; 11	*0.03	Strong -
Cell width	VEGF100	0.64; 11	*0.02	Strong +
Cell width	PDGF	-0.06; 12	0.45	No correlation
Cell width	FGF100	0.33; 11	0.15	No correlation
Cell width	PL10	-0.06; 12	0.45	No correlation
PDGF10	ALPvar	0.16, 12	0.32	No correlation

ALPvar	VEGF/PDGF	-0.30; 12	0.17	No correlation
ALPvar	FGF/PDGF	-0.45; 12	0.07	No correlation
ALPvar	VEGF100	-0.13; 12	0.35	No correlation
ALPvar	FGF/VEGF	0.05; 11	0.44	No correlation
PL10	ALPvar	0.23; 12	0.24	No correlation
PDGF10	DNAvar	-0.06; 12	0.43	No correlation
VEGF100	DNAvar	0.54; 12	*0.04	Moderate +
FGF100	DNAvar	0.54; 12	*0.04	Moderate +
PL10	DNAvar	-0.28; 12	0.18	No correlation

Abbreviations used in Table S1:
* Significantly different ($p<0.05$)
N.S. = Non Significant
+ = Positive monotonic correlation
- = Negative monotonic correlation
ALP20h = ALP activity per cell after 20h in culture
ALP4D = ALP activity per cell after 4 days in culture
DNAvar = DNA4D - DNA 20h
ALPvar = ALP4D - DNA20h
nDNA = proliferation ratio relatively to TCPS
VEGF100, FGF100 – density of GF adsorbed in one layer measured using PL 100%
PDGF100 – density of GF adsorbed in one layer measured using PL 10%

Correlation classification criteria (for both $-1< r <1$):
- .00-.19 “very weak”
- .20-.39 “weak”
- .40-.59 “moderate”
- .60-.79 “strong”
- .80-1.0 “very strong”

V.8. References

1. F. Guilak, D. M. Cohen, B. T. Estes, J. M. Gimble, W. Liedtke and C. S. Chen, Control of Stem Cell Fate by Physical Interactions with the Extracellular Matrix, Cell Stem Cell, 2009, 5, 17-26.
2. N. M. Alves, I. Pashkuleva, R. L. Reis and J. F. Mano, Controlling Cell Behavior Through the Design of Polymer Surfaces, Small, 2010, 6, 2208-2220.
3. C. A. Custódio, R. L. Reis and J. F. Mano, Engineering Biomolecular Microenvironments for Cell Instructive Biomaterials, Advanced Healthcare Materials, 2014, 3, 797-810.
4. C. A. Buck and A. F. Horwitz, Cell surface receptors for extracellular matrix molecules, Annual review of cell biology, 1987, 3, 179-205.
5. K. Lee, E. A. Silva and D. J. Mooney, Growth factor delivery-based tissue engineering: general approaches and a review of recent developments, Journal of the Royal Society Interface, 2011, 8, 153-170.
6. J. R. Bishop, M. Schuksz and J. D. Esko, Heparan sulphate proteoglycans fine-tune mammalian physiology, Nature, 2007, 446, 1030-1037.
7. T. D. Henry, B. H. Annex, G. R. McKendall, M. A. Azrin, J. J. Lopez, F. J. Giordano, P. Shah, J. T. Willerson, R. L. Benza and D. S. Berman, The VIVA Trial Vascular endothelial growth factor in ischemia for vascular angiogenesis, Circulation, 2003, 107, 1359-1365.
8. S. M. Eppler, D. L. Combs, T. D. Henry, J. J. Lopez, S. G. Ellis, J. H. Yi, B. H. Annex, E. R. McCluskey and T. F. Zioncheck, A target-mediated model to describe the pharmacokinetics and hemodynamic effects of recombinant human vascular endothelial growth factor in humans, Clinical Pharmacology & Therapeutics, 2002, 72, 20-32.
9. T. L. Pohl, E. H. Schwab and E. A. Cavalcanti-Adam, Covalent Binding of BMP-2 on Surfaces Using a Self-assembled Monolayer Approach, JoVE (Journal of Visualized Experiments), 2013, e50842-e50842.
10. F. Thorey, H. Menzel, C. Lorenz, G. Gross, A. Hoffmann and H. Windhagen, Osseointegration by bone morphogenetic protein-2 and transforming growth factor beta2 coated titanium implants in femora of New Zealand white rabbits, Indian journal of orthopaedics, 2011, 45, 57.
11. S. Liu, T. Liu, J. Chen, M. Maitz, C. Chen and N. Huang, Influence of a layer-by-layer-assembled multilayer of anti-CD34 antibody, vascular endothelial growth factor, and heparin on the endothelialization and anticoagulation of titanium surface, Journal of Biomedical Materials Research Part A, 2012, 101, 1144-57.
12. N. J. Shah, J. Hong, M. N. Hyder and P. T. Hammond, Osteophilic Multilayer Coatings for Accelerated Bone Tissue Growth, Advanced Materials, 2012, 24, 1445-1450.
13. T. Crouzier, K. Ren, C. Nicolas, C. Roy and C. Picart, Layer-By-Layer Films as a Biomimetic Reservoir for rhBMP-2 Delivery: Controlled Differentiation of Myoblasts to Osteoblasts, Small, 2009, 5, 598-608.
14. J. Almodóvar, R. Guillot, C. Monge, J. Vollaire, Š. Selimović, J.-L. Coll, A. Khademhosseini and C. Picart, Spatial patterning of BMP-2 and BMP-7 on biopolymeric films and the guidance of muscle cell fate, Biomaterials, 2014, 35, 3975-3985.
15. H. Wang, T. Yin, S. Ge, Q. Zhang, Q. Dong, D. Lei, D. Sun and G. Wang, Biofunctionalization of titanium surface with multilayer films modified by heparin-VEGF-fibronectin complex to improve endothelial cell proliferation and blood compatibility, Journal of Biomedical Materials Research Part A, 2013, 101, 413-420.
16. L. J. De Cock, S. De Koker, F. De Vos, C. Vervaet, J.-P. Remon and B. G. De Geest, Layer-by-layer incorporation of growth factors in decellularized aortic heart valve leaflets, Biomacromolecules, 2010, 11, 1002-1008.
17. R. E. Marx, E. R. Carlson, R. M. Eichstaedt, S. R. Schimmele, J. E. Strauss and K. R. Georgeff, Platelet-rich plasma: growth factor enhancement for bone grafts, Oral Surgery, Oral Medicine, Oral Pathology, Oral Radiology, and Endodontology, 1998, 85, 638-646.
18. G. Weibrich, W. K. Kleis, G. Hafner and W. E. Hitzler, Growth factor levels in platelet-rich plasma and correlations with donor age, sex, and platelet count, Journal of Cranio-Maxillofacial Surgery, 2002, 30, 97-102.
19. I. Andia and N. Maffulli, Platelet-rich plasma for managing pain and inflammation in osteoarthritis, Nature Reviews Rheumatology, 2013, 9, 721-730.
20. L. Chen, X. Yang, G. Huang, D. Song, X.-S. Ye, H. Xu and W. Li, Platelet-rich plasma promotes healing of osteoporotic fractures, Orthopedics, 2013, 36, e687-e694.

21. M. Kawasumi, H. Kitoh, K. Siwicka and N. Ishiguro, The effect of the platelet concentration in platelet-rich plasma gel on the regeneration of bone, Journal of Bone & Joint Surgery, British Volume, 2008, 90, 966-972.
22. Y. Man, P. Wang, Y. Guo, L. Xiang, Y. Yang, Y. Qu, P. Gong and L. Deng, Angiogenic and osteogenic potential of platelet-rich plasma and adipose-derived stem cell laden alginate microspheres, Biomaterials, 2012, 33, 8802-8811.
23. V. E. Santo, A. R. C. Duarte, E. G. Popa, M. E. Gomes, J. F. Mano and R. L. Reis, Enhancement of osteogenic differentiation of human adipose derived stem cells by the controlled release of platelet lysates from hybrid scaffolds produced by supercritical fluid foaming, Journal of Controlled Release, 2012, 162, 19-27.
24. J. Leotot, L. Coquelin, G. Bodivit, P. Bierling, P. Hernigou, H. Rouard and N. Chevallier, Platelet lysate coating on scaffolds directly and indirectly enhances cell migration, improving bone and blood vessel formation, Acta biomaterialia, 2013, 9, 6630-6640.
25. C. Custódio, V. Santo, M. Oliveira, M. Gomes, R. Reis and J. Mano, Functionalized Microparticles Producing Scaffolds in Combination with Cells, Advanced Functional Materials, 2014, 24, 1391-1400.
26. G. A. Hudalla and W. L. Murphy, Biomaterials that regulate growth factor activity via bioinspired interactions, Advanced functional materials, 2011, 21, 1754-1768.
27. T. Boudou, T. Crouzier, K. Ren, G. Blin and C. Picart, Multiple functionalities of polyelectrolyte multilayer films: new biomedical applications, Advanced Materials, 2010, 22, 441-467.
28. R. R. Costa and J. F. Mano, Polyelectrolyte multilayered assemblies in biomedical technologies, Chemical Society Reviews, 2014, 43, 3453-3479.
29. N. J. Shah, M. L. Macdonald, Y. M. Beben, R. F. Padera, R. E. Samuel and P. T. Hammond, Tunable dual growth factor delivery from polyelectrolyte multilayer films, Biomaterials, 2011, 32, 6183-6193.
30. T. Crouzier, F. Sailhan, P. Becquart, R. Guillot, D. Logeart-Avramoglou and C. Picart, The performance of BMP-2 loaded TCP/HAP porous ceramics with a polyelectrolyte multilayer film coating, Biomaterials, 2011, 32, 7543-7554.
31. S. E. Sakiyama-Elbert and J. A. Hubbell, Controlled release of nerve growth factor from a heparin-containing fibrin-based cell ingrowth matrix, Journal of Controlled Release, 2000, 69, 149-158.
32. X. F. Ye, H. Z. Wang, J. X. Zhou, H. Q. Li, J. Liu, Z. Wang, A. Q. Chen and Q. Zhao, The Effect of Heparin-VEGF Multilayer on the Biocompatibility of Decellularized Aortic Valve with Platelet and Endothelial Progenitor Cells, Plos One, 2013, 8.
33. S. Cai, Y. Liu, X. Zheng Shu and G. D. Prestwich, Injectable glycosaminoglycan hydrogels for controlled release of human basic fibroblast growth factor, Biomaterials, 2005, 26, 6054-6067.
34. T. Rada, R. L. Reis and A. E. Gomes, Novel method for the isolation of adipose stem cells (ASCs), Journal of Tissue Engineering and Regenerative Medicine, 2009, 3, 158-159.
35. I. Vlodavsky, H.-Q. Miao, B. Medalion, P. Danagher and D. Ron, Involvement of heparan sulfate and related molecules in sequestration and growth promoting activity of fibroblast growth factor, Cancer and Metastasis Reviews, 1996, 15, 177-186.
36. D. B. Volkin, P. Tsai, J. M. Dabora, J. O. Gress, C. J. Burke, R. J. Linhardt and C. R. Middaugh, Physical stabilization of acidic fibroblast growth factor by polyanions, Archives of biochemistry and biophysics, 1993, 300, 30-41.
37. J. Folkman and Y. Shing, in Heparin and related polysaccharides, Springer, 1992, pp. 355-364.
38. João Borges and J.F. Mano, Molecular Interactions Driving the Layer-by-Layer Assembling of Multilayers: A Review, Chem. Rev., 2014, 114, 8883-8942.
39. X. Yao, R. Peng and J. Ding, Effects of aspect ratios of stem cells on lineage commitments with and without induction media, Biomaterials, 2013, 34, 930-939.
40. J. T. Connelly, J. E. Gautrot, B. Trappmann, D. W.-M. Tan, G. Donati, W. T. Huck and F. M. Watt, Actin and serum response factor transduce physical cues from the microenvironment to regulate epidermal stem cell fate decisions, nature cell biology, 2010, 12, 711-718.
41. M. D. Treiser, E. H. Yang, S. Gordonov, D. M. Cohen, I. P. Androulakis, J. Kohn, C. S. Chen and P. V. Moghe, Cytoskeleton-based forecasting of stem cell lineage fates, Proceedings of the National Academy of Sciences, 2010, 107, 610-615.
42. G. Kumar, C. K. Tison, K. Chatterjee, P. S. Pine, J. H. McDaniel, M. L. Salit, M. F. Young and C. G. Simon Jr, The determination of stem cell fate by 3D scaffold structures through the control of cell shape, Biomaterials, 2011, 32, 9188-9196.

43. A. Banfi, A. Muraglia, B. Dozin, M. Mastrogiacomo, R. Cancedda and R. Quarto, Proliferation kinetics and differentiation potential of ex vivo expanded human bone marrow stromal cells: implications for their use in cell therapy, Experimental hematology, 2000, 28, 707-715.
44. D. Cholewa, T. Stiehl, A. Schellenberg, G. Bokermann, S. Joussen, C. Koch, T. Walenda, N. Pallua, A. Marciniak-Czochra and C. V. Suschek, Expansion of adipose mesenchymal stromal cells is affected by human platelet lysate and plating density, Cell transplantation, 2011, 20, 1409-1422.
45. S. Griffiths, P. R. Baraniak, I. B. Copland, R. M. Nerem and T. C. McDevitt, Human platelet lysate stimulates high-passage and senescent human multipotent mesenchymal stromal cell growth and rejuvenation< i> in vitro</i>, Cytotherapy, 2013, 15, 1469-1483.
46. G. Chen, X. Shi, C. Sun, M. Li, Q. Zhou, C. Zhang, J. Huang, Y. Qiu, X. Wen and Y. Zhang, VEGF-Mediated Proliferation of Human Adipose Tissue-Derived Stem Cells, PloS one, 2013, 8, e73673.
47. T. L. Hebert, X. Wu, G. Yu, B. C. Goh, Y. D. C. Halvorsen, Z. Wang, C. Moro and J. M. Gimble, Culture effects of epidermal growth factor (EGF) and basic fibroblast growth factor (bFGF) on cryopreserved human adipose-derived stromal/stem cell proliferation and adipogenesis, Journal of tissue engineering and regenerative medicine, 2009, 3, 553-561.
48. P. Horn, G. Bokermann, D. Cholewa, S. Bork, T. Walenda, C. Koch, W. Drescher, G. Hutschenreuther, M. Zenke and A. D. Ho, Impact of individual platelet lysates on isolation and growth of human mesenchymal stromal cells, Cytotherapy, 2010, 12, 888-898.
49. P. Qiu, W. Song, Z. Niu, Y. Bai, W. Li, S. Pan, S. Peng and J. Hua, Platelet-derived growth factor promotes the proliferation of human umbilical cord-derived mesenchymal stem cells, Cell biochemistry and function, 2013, 31, 159-165.
50. C.-H. Heldin, Å. Wasteson and B. Westermark, Platelet-derived growth factor, Molecular and cellular endocrinology, 1985, 39, 169-187.
51. M. Kim, Y. H. Kim and G. Tae, Human mesenchymal stem cell culture on heparin-based hydrogels and the modulation of interactions by gel elasticity and heparin amount, Acta biomaterialia, 2013, 9, 7833-7844.
52. M. K. Furue, J. Na, J. P. Jackson, T. Okamoto, M. Jones, D. Baker, R.-I. Hata, H. D. Moore, J. D. Sato and P. W. Andrews, Heparin promotes the growth of human embryonic stem cells in a defined serum-free medium, Proceedings of the National Academy of Sciences, 2008, 105, 13409-13414.
53. H. Hirai, N. Katoku-Kikyo, P. Karian, M. Firpo and N. Kikyo, Efficient iPS cell production with the MyoD transactivation domain in serum-free culture, PloS one, 2012, 7, e34149.
54. E. E. Golub and K. Boesze-Battaglia, The role of alkaline phosphatase in mineralization, Current Opinion in Orthopaedics, 2007, 18, 444-448.
55. Z. Li, C. Liu, Z. Xie, P. Song, R. C. Zhao, L. Guo, Z. Liu and Y. Wu, Epigenetic dysregulation in mesenchymal stem cell aging and spontaneous differentiation, PloS one, 2011, 6, e20526.
56. J.-H. Lee, S. Um, J.-H. Jang and B. M. Seo, Effects of VEGF and FGF-2 on proliferation and differentiation of human periodontal ligament stem cells, Cell and tissue research, 2012, 348, 475-484.
57. J. B. Mitchell, K. McIntosh, S. Zvonic, S. Garrett, Z. E. Floyd, A. Kloster, Y. Di Halvorsen, R. W. Storms, B. Goh and G. Kilroy, Immunophenotype of Human Adipose-Derived Cells: Temporal Changes in Stromal-Associated and Stem Cell–Associated Markers, Stem cells, 2006, 24, 376-385.
58. K. Yoshimura, T. Shigeura, D. Matsumoto, T. Sato, Y. Takaki, E. Aiba-Kojima, K. Sato, K. Inoue, T. Nagase and I. Koshima, Characterization of freshly isolated and cultured cells derived from the fatty and fluid portions of liposuction aspirates, Journal of cellular physiology, 2006, 208, 64-76.
59. H. Suga, D. Matsumoto, H. Eto, K. Inoue, N. Aoi, H. Kato, J. Araki and K. Yoshimura, Functional implications of CD34 expression in human adipose-derived stem/progenitor cells, Stem cells and development, 2009, 18, 1201-1210.

CHAPTER VI

PRO-ANGIOGENIC NANOCOATINGS CONTAINING PLATELET LYSATE

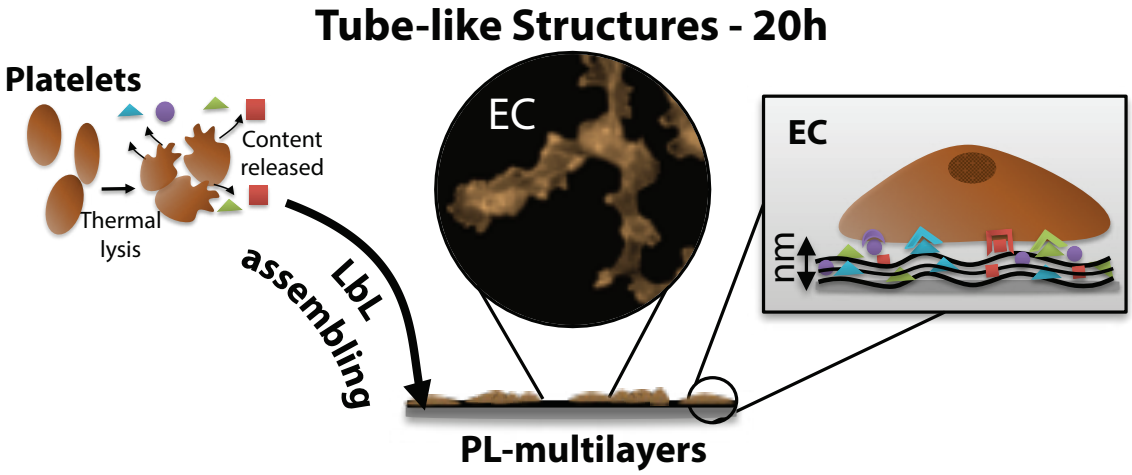

CHAPTER VI*

Pro-Angiogenic Nanocoatings Containing Platelet Lysate

VI.1. Abstract

Human platelet lysate (PL) is a cost-effective and human source of multiple and potent pro-angiogenic proteins. Nanocoatings prepared by layer-by-layer assembling incorporating PL are shown to activate endothelial cells inducing the formation of tube-like structures and angiogenic gene expression.

Keywords: platelet lysate, growth factors, VEGF, FGF, PDGF, angiogenesis, tube-like, nanocoatings, basement membranes, instruction.

*This chapter is based on the following publication:

Sara M. Oliveira, Rogério P. Pirraco, Alexandra P. Marques, Vítor E. Santo, Manuela E. Gomes, Rui L. Reis, João F. Mano, Pro-Angiogenic Nanocoatings Containing Platelet Lysate, submitted, 2014.

The development of tissue engineering constructs containing functional and mature pre-vasculature is still a major challenge.[1-3] In the absence of such a network, the viability and regeneration potential of thick constructs will be compromised due to the limitation of nutrients and cell debris diffusion. In order to overcome this issue, researchers have been recurring either to material-based and cell-based approaches aiming to create an adequate vasculature inside engineered constructs. Material approaches focus on the development of cellular or acellular 3D organized vessel-like structures through microfabrication and cell seeding methodologies.[4, 5] On the other hand, cell-based approaches aim at the instruction and activation of the involved angiogenic cells (e.g., endothelial and pericytes) leading to their cellular assembling into stable cellular tubular networks (i.e., tubulogenesis). The specific instruction of endothelial cells (EC) towards the formation of stable tube-like structures has been extensively investigated.[6, 7] Incorporation of extracellular cues, natural or synthetic, such as collagen, fibrin, growth factors (GFs) or similar epitopes, can activate specific integrins and/or tyrosine kinase receptors and efficiently promote angiogenic cells activation and assembling. However, most of those instructive cues/constructs are frequently obtained from animal and costly sources, or need complicated procedures.

The formation of neo-vessels involves a complex crosstalk between several cell types, platelets releasates, extracellular matrix and their secreted bioactive proteins (pro and anti-angiogenic). Vascular endothelial growth factor (VEGF) and fibroblast growth factor b (FGFb) are considered the most potent angiogenic GF being frequently used in angiogenic biomaterials. The angiogenesis is initiated and regulated by several cells types, GFs and other bioactive proteins and environmental cues such as hypoxia.[8] The ECs are activated, proliferate, migrate and, in the final stage, their tubular structures are stabilized by pericytes, smooth vascular cells and synthetized ECM.[8]

Recent works have been highlighting the importance of the provision of multiple GFs in order to achieve better networks regarding both size features and stability.[1, 9-12] This has been explored by the combination of multiple recombinant GFs or other cell types able to provide such bioactive moieties to EC. Platelets, natural players during the healing process, are very attractive sources of multiple GFs and metalloproteinases involved in angiogenesis.[13]

Recently, it has been reported that platelets derivatives can stimulate ECs proliferation, migration and enhance *in vitro* and *in vivo* angiogenesis. [9, 14-20] For angiogenic purposes, platelets has been mainly used as: platelet-rich-plasma (PRP) in combination with other biomaterials [9, 18, 19]; platelet lysate adsorbed onto scaffolds [20]; as PRP-gel[17]; or PRP [14-16]. Some reports have shown that PRP, used as extract in GFs-reduced Matrigel, can promote the formation of tube-like structures (TLS) of ECs within less than 24 hours.[14-16] However, Matrigel or other similar rich basement membranes are from animal sarcoma origin, thus are not considered a suitable option for human application.[21]

Herein, we propose the reconstruction of angiogenic basement membranes-like constructs by using platelet lysate (PL) – as a source of multiple GFs -, marine-origin polysaccharides - as stabilizers -, and layer-by-layer assembling (LbL) – for a controlled assembling – Figure VI.1.a. PL is obtained by lysing human platelet concentrates by freezing-thawing cycles – Figure VI.1.b. LbL is a simple and versatile technique comprising the

alternated deposition of polyelectrolytes (PEs) interacting by electrostatic, or other types of interactions, and can be performed in mild conditions.[22, 23] In order to achieve an efficient EC activation mediated by GFs, their stability, conformation and density presented to the cells must be adequate. Moreover, the type of binding between the GF and their stabilizer will affect the intracellular signal transduction – Figure VI.1.c. Also, a complete signal transduction may require the endocytosis of the GF-cell tyrosine kinase receptor complexes, such as in the case of VEGF/VEGFR2. [24]

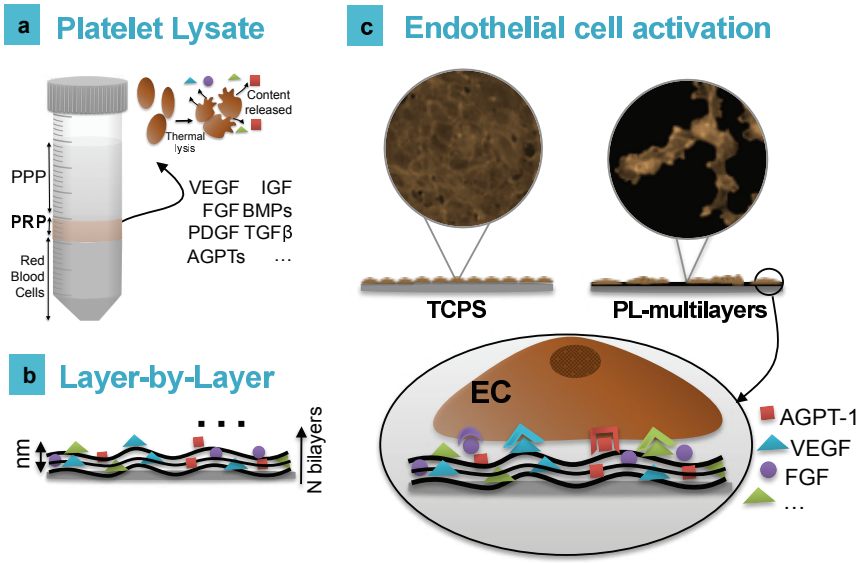

Figure VI.1. Schematic representation of the approach: (a) PL preparation; (b) Layer-by-Layer assembling. (c) Culture of ECs during 20 hours inducing the formation of tube-like structures mediated by their interactions with multiple proteins on the nanocoatings.

In the natural ECM, glycosaminoglycans present various molecular arrangements and different sulfation degrees (SD), binding and stabilizing GFs mainly by electrostatic interactions.[25-27] Heparin, or synthetic heparin-analogue ending sulfate/sulfonic groups, are widely used to stabilize and attract GFs.[28, 29] Since they present high affinity and the interactions are primarily electrostatic, the conformation and bioactivity of the GFs is usually preserved. Marine resources offer a wide range of PEs with several molecular properties and SD that may affect the incorporation of GFs from PL onto the coatings.[30-32] Therefore, marine-origin polysaccharides can be considered convenient and cost-effective sources of PEs to attract, stabilize, buildup and tune PL nanocoatings prepared by LbL assembling. PEs with different charge and functional groups were combined with PL, namely: alginate (Alg; -1) and chitosan (Chi; +1), as non-sulfated PEs; and κ-, ι-, and λ-carrageenan (κ, ι λ; -1, -2, -3 respectively), as sulfated PEs; along with heparin (Hep; -3), as a sulfonic PE and control. Their capability to adsorb fibroblast growth factor b (FGFb), vascular endothelial growth factor (VEGF) and platelet derived growth factor (PDGF) was previously analyzed (Chapter V). It has been observed that the content of those GFs is highly influenced by the nature of the PE. Briefly, the sulfated PEs and Hep adsorbed higher levels of GFs; however, higher SD did not imply higher incorporation. Namely, PDGF adsorption decreased with the increase of SD, and while VEGF reached the highest contents on Hep and ιCar; only ιCar adsorbed a high content of all the measured GFs. Consequently, higher SD represented increased VEGF/PDGF and FGFb/PDGF ratios suggesting them to be more adequate for the morphogenic activation of EC.

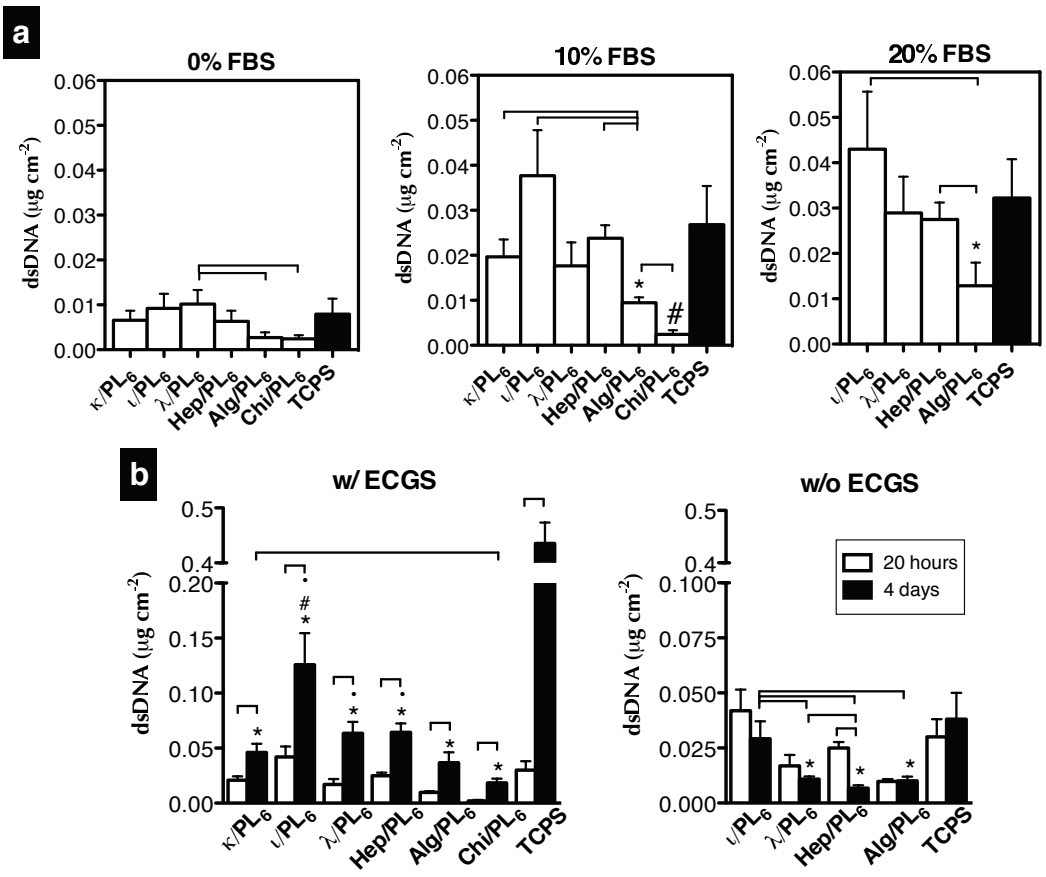

Figure VI.2. HUVECs adhesion after 20 hours in culture in absence of ECGS and: a) 0% FBS, b) 10% FBS, c) 20% FBS. All significances are indicate with: * (different to TCPS), # (different to all, after 4 days), •(different to Chi/PL and Alg/PL), ($p<0.05$, n=6; mean±sem).

In order to preliminarily assess the pro-angiogenic potential of the nanocoatings, human umbilical vein ECs (HUVECs) behavior was analyzed regarding their adhesion, proliferation, morphology and gene expression. Coatings with 6 bilayers of Alg/PL, Chi/PL, κCar/PL, ιCar/PL, λCar/PL and Hep/PL (abbreviated as PE/PL_n; n, number bilayers) were seeded with 10,000 cells/cm^2 in the absence of both EC growth supplement (ECGS) and heparin (common EC medium supplements), with varied concentrations of fetal bovine serum (FBS, 0%, 10% and 20%) during 20 hours.

In absence of serum, the adhesion of HUVECs was limited and all samples were similar to tissue culture polystyrene (TCPS) - Figure VI.2.a. With 10% FBS, cell adhesion was not significantly affected by the presence of the multilayers with exception of Alg and Chi ($p<0.05$). Increasing the content of FBS to 20% has also not altered much the adhesion of HUVECS relatively to TCPS. Nonetheless, in presence of serum, HUVECS tended to adhere more on $\iota Car/PL_6$ ($p<0.05$). On the other hand, the non-sulfated nanocoatings showed a tendency to impair cell adhesion.

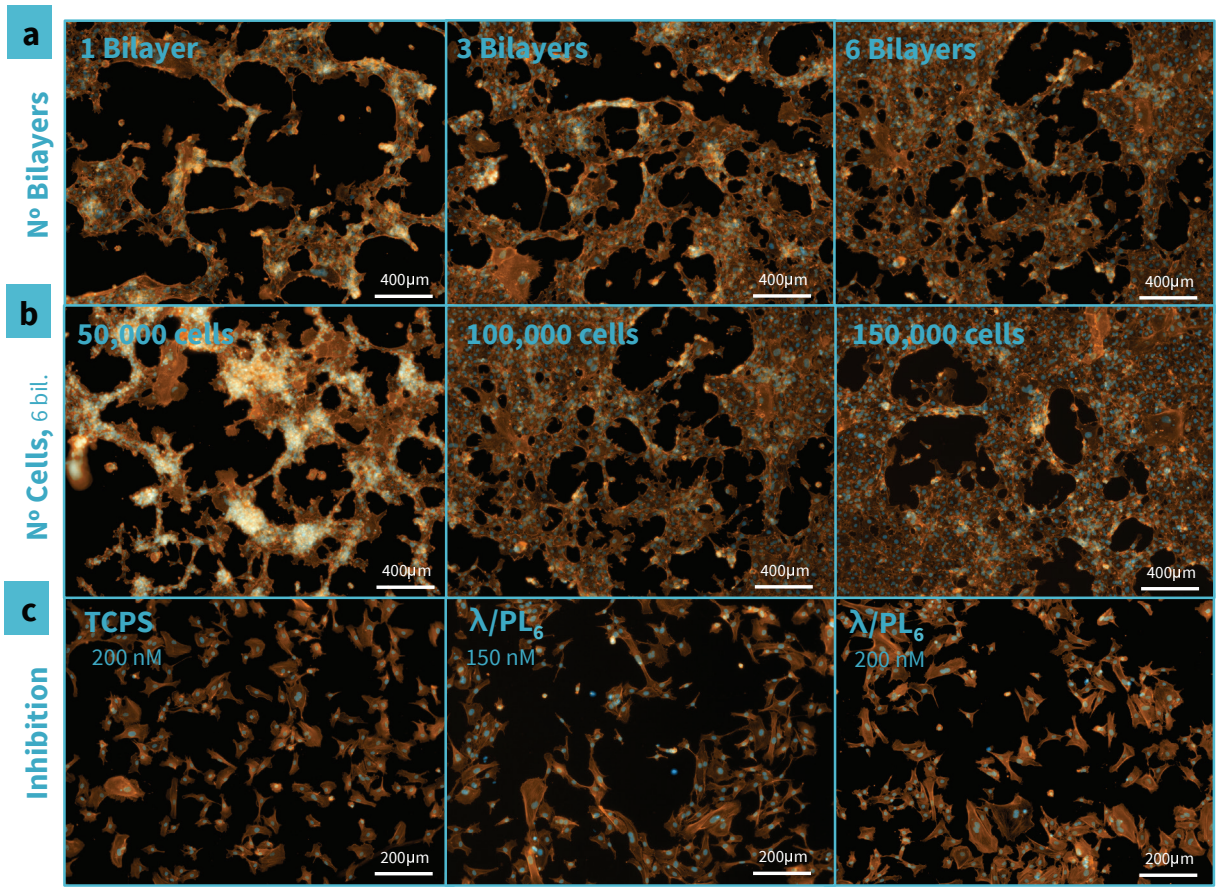

Figure VI.3. EC morphology onto several λ/PL multilayers, after 20 hours of culture, in presence of 10% FBS and absence of ECGS and Hep. (a) Morphology on multilayers with different number of bilayers: λ/PL_1, λ/PL_3 and λ/PL_6. (b) Effect of seeding density on the morphology of HUVECs on λ/PL_6 multilayers. (c) Morphology of HUVECs seeded on λ/PL_6 with a density of 50,000 cells/cm^2, and TCPS, in presence of VEGF/FGF tyrosine kinase receptor inhibitor and DMSO. (nuclei: blue, cytoskeleton: orange).

The ability of those multilayers to activate ECs towards the formation of tube-like structures (TLS) was also assessed. HUVECs were seeded with a density of 100,000 cells/cm^2 in presence of 10% FBS and their morphology was observed after 20 hours of incubation. Figure VI.3 and Figure VI.S1. show the HUVECs morphology on all the assessed conditions. λ/PL_6 and Hep/PL_6 induced considerably higher cell cohesion, forming branching anastomosing tubes-like with multicentric junctions giving rise to a network of TLS – Figure VI.4. No clear TLS were observed in Alg/PL_6, Chi/PL_6 nor ι/PL_6. Although Chi and Alg polyelectrolytes significantly adsorb PL (Chapter V), the nature or stability of their pro-angiogenic cues were not enough to induce the cellular assembling. In the case of ι/PL, TLS structures were observed under other cell density conditions (53,000 cells/cm^2) – Figure VI.S2. The ECs highly adhered onto ι/PL_6, which is believed to consequently inhibit TLS formation. This could be caused by VE cadherin complexation with VEGF receptor, which inhibits its phosphorylation by VEGF and consequently the formation of TLS.[33]

The number of bilayers forming the nanocoatings could also affect the density of instructive proteins presented to the cells. Thereby, the cell seeding density of HUVECs and the number of bilayers of the λ/PL pair were also varied. Respectively, 50000, 100000 and 150000 cells/cm^2 were seeded on λ/PL_6, and 100000 cells/cm^2 seeded on nanocoatings prepared with 1, 3 and 6 bilayers (λ/PL_1, λ/PL_3 and λ/PL_6) – Figure VI.3. Total

tube-length, number of meshes, number of nodes and master junctions formed were quantified on fluorescence images (5x) using Angiogenesis Analyzer for Image J – Figure VI.5. A single bilayer of λ/PL was sufficient to promote the formation of a network with 100000 cells, which total tube length could be increased with increasing number of layers. With 6 bilayers, a lower cell density has shown to be more adequate in obtaining a better network formation than with fewer layers. This indicates that cell adhesion and TLS are dependent on the number of bilayers and increasing the number of layers allows a decrease of the required cell density.

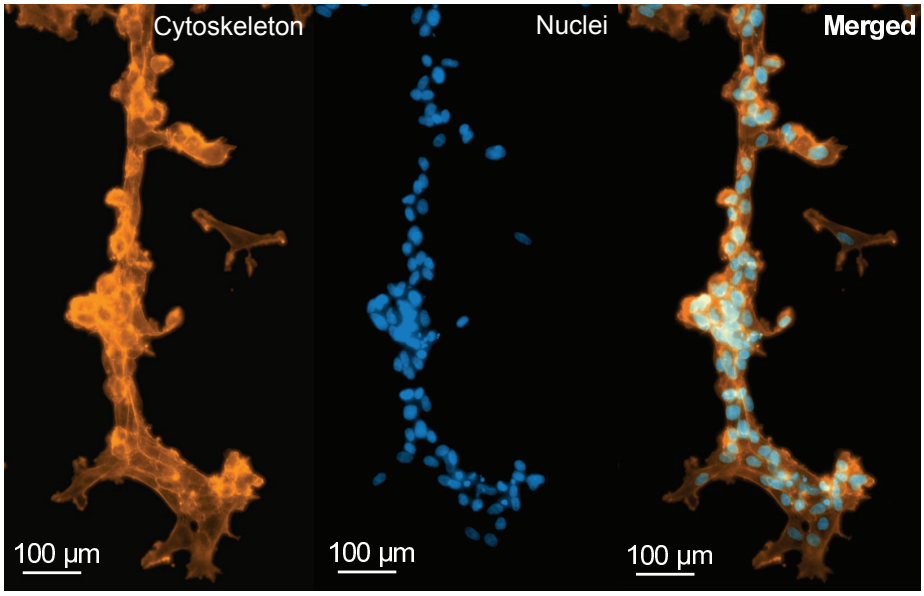

Figure VI.4. Magnification of HUVECs assembled into a tube-like structure after 20 hours in culture on Hep/PL_6 (nuclei: blue, cytoskeleton: orange).

Besides the total tube length, the number of nodes and meshes were also influenced by the number of layers. A tendency was observed in that all these features to increase with an increasing number of layers. In general, Hep/PL_6 (100,000 cells) and λ/PL_6 (50,000 cells) have shown similar results, though on λ-type a higher number of total nodes could be counted.

Cell Profiler was used to analyze cell form factor (i.e., roundness), eccentricity (i.e., elongation), major axis (i.e., cell length) and minor axis (i.e., cell width) – Figure VI.S3. This analysis revealed that under the tested conditions, the EC morphology was significantly changed when seeded on the multilayers in comparison to TCPS. While on TCPS cells show the normal cobblestone-like morphology, they become rounder on the instructive multilayers (form factor closer to 1). However, on the multilayers that successfully induced TLS, the cells elongation factor was similar to TCPS. Both width and length decreased on the multilayers, thus not altering significantly the elongation relatively to TCPS.

Frequently, on hydrogel-like basement membranes, cells tend to be more elongated after 20-24 hours of incubation. [34] Herein, the surface properties (non-gel), the time of incubation and the cell number may have caused the reduction of the size and the lack of cytoskeleton elongation.

In order to assess cell proliferation capability, the medium was replaced with fresh medium with or without ECGS-Hep and cells were incubated for more 3 days – Figure VI.2.b. Morphology was observed after 4 days in culture – Figure VI.S4. Even though the initial media was changed, removing possible released GFs, HUVECs kept some cell alignment after 4 days in culture on λPL_6 5^4. On the other hand, in presence of ECGS cells have lost the TLS and reached confluence.

Independently of the surface, in absence of growth supplement, cells were unable to proliferate. In particular, Hep/PL_6 has not supported cell viability, and cell number was slightly reduced ($p<0.05$) which suggests a lower pro-survival stimulation.

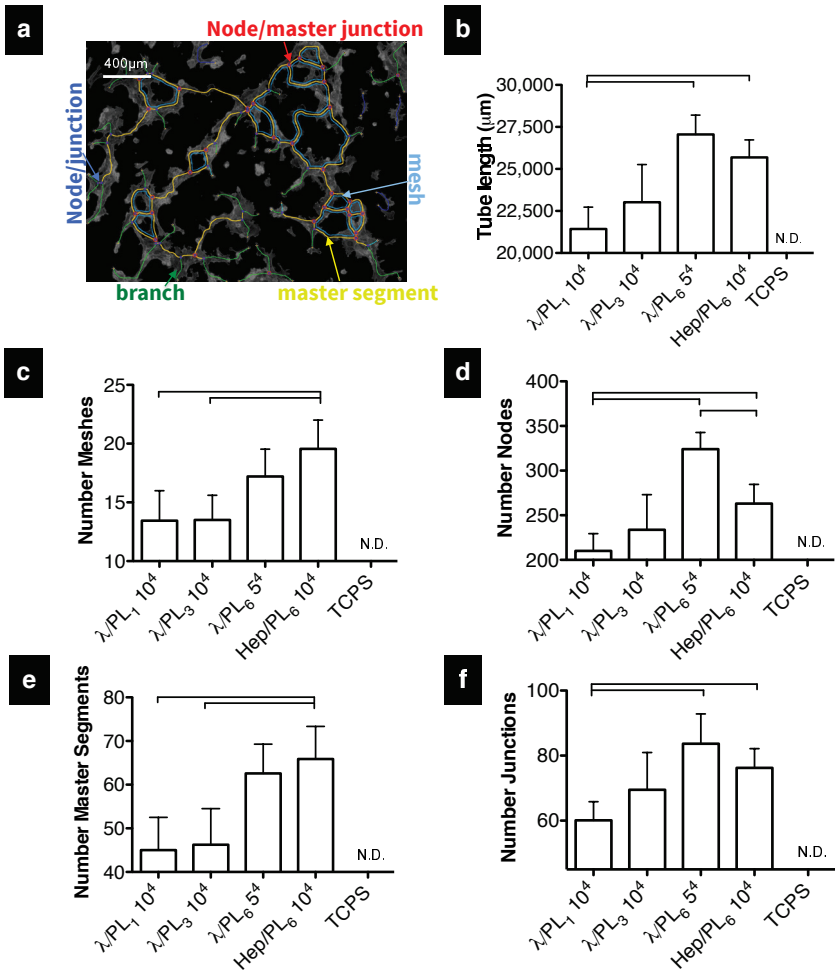

Figure VI.5. a) Angiogenic parameters quantified with Angiogenesis Analyzer on cytoskeleton-stained images; b) total tube length; c) number of meshes; d) number of nodes; e) number of master segments; f) number of junctions. All pairs of samples were compared and significances are indicated ($p<0.05$, n=6, mean±sem).

Medium supplementation with ECGS allowed a minimal proliferation of the ECs, being this effect more pronounced on TCPS ($p<0.05$). Among the multilayers, ι/PL_6 showed the highest HUVECs proliferation. This improvement might be related with the higher capability of ι to incorporate FGFb, which growth factor is reported to be able of stimulating EC proliferation.[35] Nonetheless, the overall behavior suggested that these multilayers do not promote ECs proliferation, and TLS formation in some cases. This corroborates the reported tendency of matrixes that lead to extensive tubule formation (e.g., collagen IV, V and Matrigel) of allowing only

a minimal EC proliferation.[6, 36] This proliferation inhibition effect could be promoted by specific GFs that are simultaneously capable of eliciting the formation of TLS and inhibit EC proliferation. For instance, transforming growth factor beta 1 (TGF-β1) induces angiogenesis through VEGF-mediated apoptosis.[37] TGF-β1 is one of the multiple GF that can be found in PL. The simultaneous presence of TGF-β1 and other GFs, rather than only promoting angiogenesis or mitogenesis (e.g., by FGFb and VEGF, PDGF), could both elicit angiogenesis and impair proliferation or cell apoptosis.

During the angiogenesis stages (activation, proliferation, migration and stabilization) the gene expression of the ECs is regulated by several pro and anti-angiogenic factors. GFs such as VEGF and FGFb activate ECs and promote their proliferation. Integrin such as α5, αν, β3 play important roles during EC migration while angiopoientin-1, PDGF and TGF-β regulate maturation and vessels stabilization. [8, 38, 39] Herein, gene expression of VEGFA, FGFb, integrins (α5, αν and β3) and angiopoietin-1 were quantified after 20 hours of culture – Figure VI.S5.

In accordance with the literature, the angiogenic-gene expression alterations during TLS formation are expected to be of small magnitude (<2-fold) or even negative, as related to TCPS. [38, 40] Indeed, for the majority of conditions, gene expression was similar or significantly lower than TCPS with the exception of the expression of VEGFA and angiopoietin-1. Regarding the expression of integrins, λ/PL_6 (50,000 cells), λ/PL_3 (100,000 cells), ι/PL_6 (100,000 cells) and Hep/PL_6 (100,000 cells) have, in general, shown lower or similar expression to TCPS ($p<0.05$). Exogenous FGFb is known to be able to promote angiogenesis, both *in vivo* and *in vitro*, by up-regulating the expression of VEGFA and the endogenous VEGFA in ECs.[41] However, the expression of FGFb was decreased on ι/PL_6 (100,000 cells), λ/PL_3 (100,000 cells), λ/PL_6 (50,000 cells), λ/PL_6 (100,000 cells), with exception of Hep/PL_6.

Both VEGFA and angiopoietin-1 are strong pro-angiogenic factors with distinct functions and bidirectional dependent: one up-regulates the other. While VEGFA causes vascular permeability, angiopoieitin-1 stabilizes the blood vessels and avoids plasma leakage induced by VEGFA.[42, 43] Although being frequently related with different angiogenesis stages, the simultaneously stimulation of ECs with VEGFA and angiopoietin-1 has previously shown a synergistic improvement of angiogenesis.[44]

Recently, it has been reported that PRP contains high amounts of angiopoietin-1 (~300fold more than VEGFA).[16] The same study has shown that angiopoietin-1 and its respective cell receptor (Tie2) are crucial in promoting angiogenesis when using a preparation of 250-fold diluted PRP.

Both the expression of VEGF-A and angiopoietin-1 were simultaneously increased with exception of TCPS, Alg/PL_6 and ι/PL_6. Angiopoietin-1 was increased even on the multilayers not promoting TLS which suggests that surface VEGFA or FGFb (which primarily up-regulates VEGFA[41]) might have up-regulated angiopoietin-1.[45] Whether a significant amount of angiopoietin-1 had been incorporated in the coatings, it could have up-regulate VEGFA expression and VEGFA endogenous content, and consequently, indirectly stimulating the formation of TLS.[44, 46, 47]

HUVECs were cultured in presence of a FGF/VEGF tyrosine kinase receptor inhibitor to understand whether the morphogenic changes were driven by those pro-angiogenic GFs. This compound would block the interaction

of FGF and VEGF from the nanocoating, or the soluble form, with their respective cell receptors (e.g., FGFR2 and VEGFR2). A condition that was shown to induce TLS was selected: 50,000 cells/cm^2 onto λ/PL$_6$. Cells were seeded with a manufacture's recommended range of concentrations of inhibitor dissolved with DMSO (150nM and 200nM, containing 0.0075% v/v and 0.01% v/v DMSO, respectively) or only with DMSO (0.0075% v/v and 0.01% v/v of DMSO – named DMSO 150 and DMSO 200) during 20 hours. The use of DMSO as a solvent has diminished the observed cellular density and made cells more elongated – Figure VI.3.c. However, the ability of HUVECS to be more cohesive and to align was further reduced with the presence of the inhibitor and with its increased concentration. Cell Profiler analysis has not revealed significant differences between λ/PL$_6$ (50,000 cells) with inhibitor and only with DMSO, both for 150 nM and for 200 nM – Figure VI.S3. DMSO is reported as being able to decrease cell adhesion even at low concentrations (1.55% v/v).[48] Concentrations higher than 1% v/v have also been reported to impair the formation of TLS on Matrigel.[49] Thereby, one cannot exclude the inhibition of TLS and changes in cell morphology to be in part caused by DMSO. Nonetheless, there are indications that at least at some extent, FGF/VEGF has mediated the formation of TLS.

Overall, the results suggest that by tuning the layer-by-layer constructed basement membranes-like it is possible to promote a pro-angiogenic phenotype and gene expression in HUVECs. This may be a cost-effective approach to modify 2D/3D constructs and guide ECs towards the formation of tube-like structures driven by multiple and synergistic stimulations through e.g. VEGF, FGF, TGF-β and angiopoietin-1.

VI.2. Conclusions

There is still a current need to develop cost effective cell-interfaces able to promote angiogenesis and the formation of stable vasculature.

PL is a source of several pro-angiogenic and other proteins involved in the angiogenesis from the earliest to the maturation phases. Herein, PL was incorporated in layer-by-layer assembled nanocoatings with varied polysaccharides and number of layers. The nanocoatings prepared with the more sulfated polysaccharides elicited the formation of tube-like structures in ECs within 20 hours of incubation. These morphogenic changes were accompanied by differences in gene expressions, mainly higher VEGFA and higher angiopoietin-1.

Layer-by-Layer assembling including PL might be a simple methodology to introduce and tune cost-effective pro-angiogenic interfaces in 2D/3D biomaterials.

VI.3. Acknowledgments

The research leading to these results has received funding from European Union's Seventh Framework Program (FP7/2007-2013) under grant agreement nª REGPOT-CT2012-316331 – POLARIS and FP7-KBBE-2010-4-266033 – SPECIAL. This work was also supported by the European Research Council grant agreement ERC-2012-ADG-20120216-321266 for the project ComplexiTE. Portuguese Foundation for Science and Technology is gratefully acknowledged for fellowship of Sara M. Oliveira (SFRH/BD/70107/2010). The researcher contract of

R.P. Pirraco through RL3-TECT-NORTE-01-0124-FEDER-000020, co-financed by North Portugal Regional Operational Program (ON.2-O Novo Norte), under the National Strategic Reference Framework, through the European Regional Development Fund is also acknowledged.

VI.4. Support Information

VI.4.1. Figures

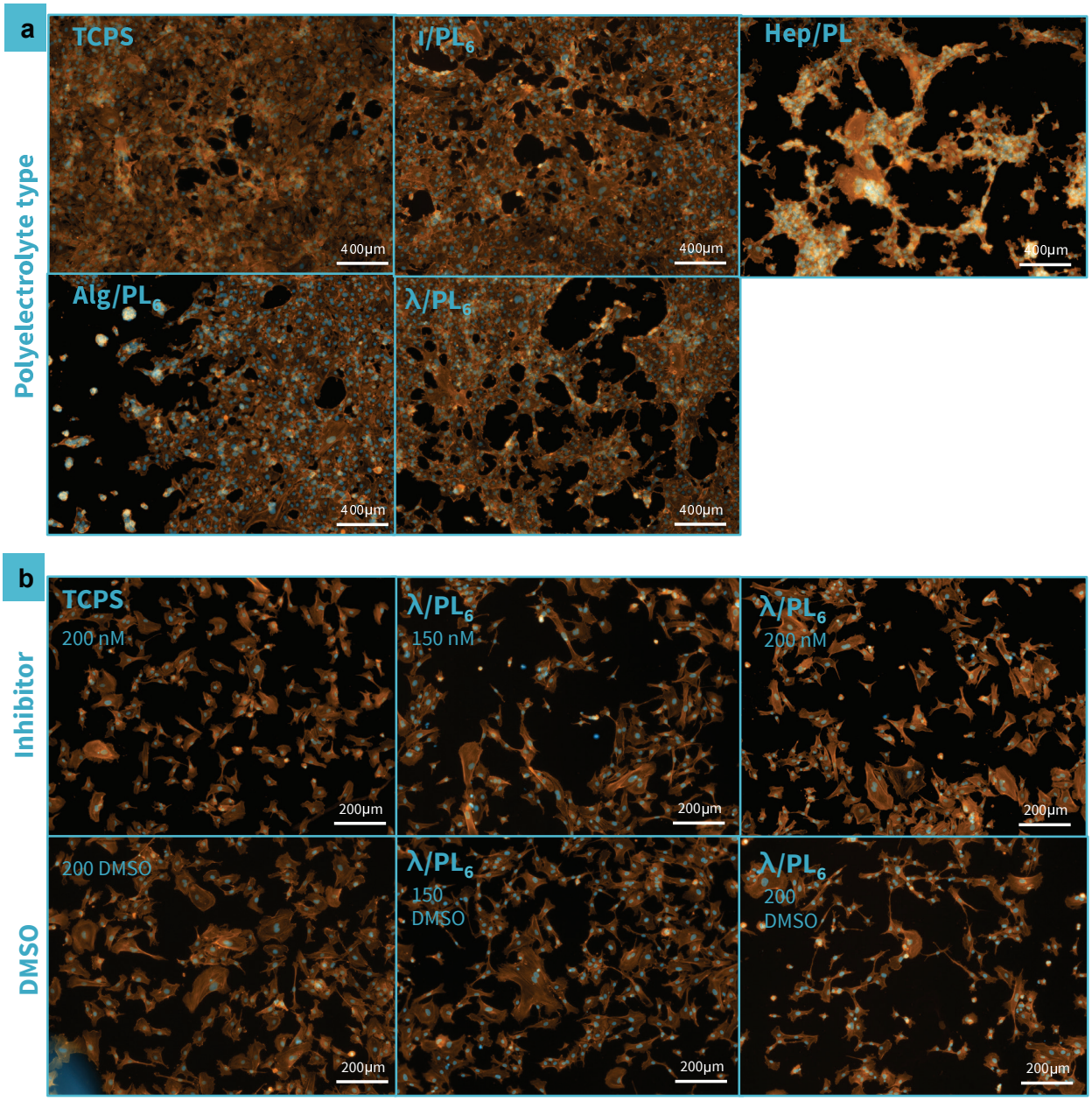

Figure VI.S1. a) HUVECs morphology after 20 hours in culture showing the formation of tube-like structures (TLS) on some of the polyelectrolyte/PL nanocoatings (100,000 cells/cm^2). b) Cell morphology of HUVECs seeded on λ/PL$_6$ and TPCs in presence of VEGF/FGF receptor kinase inhibitor (or DMSO) inhibiting the formation of TLS (50,000 cells/cm^2). (cytoskleton: orange; nuclei: blue).

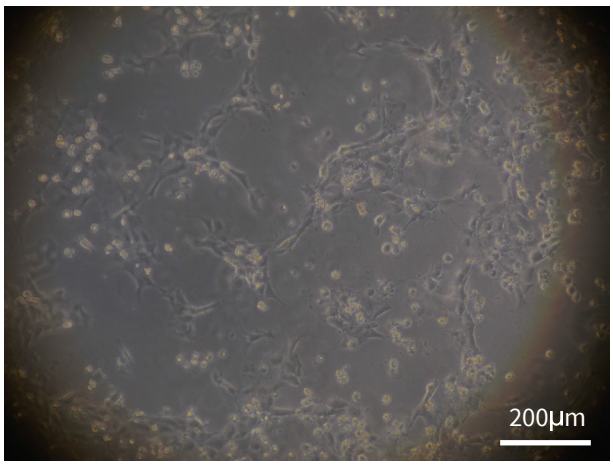

Figure VI.S2. HUVECs morphology after 20 hours in culture showing the formation of tube-like structures (TLS) on ι/PL$_6$ (53,000 cells/cm^2).

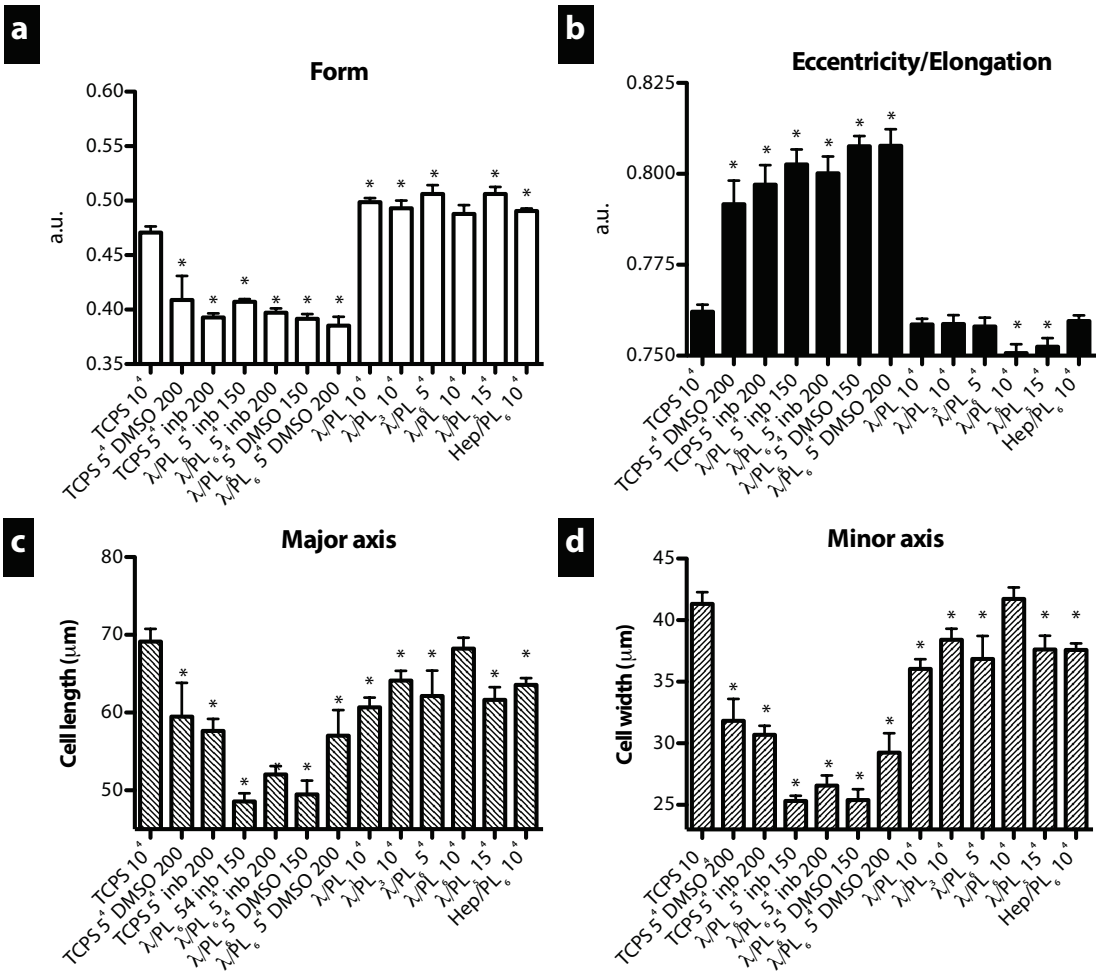

Figure VI.S3. Cell morphological analysis using Cell Profiler: (a) Form factor, (b) minor axis, (c) major axis and (d) eccentricity of HUVECs after 20 hours of incubation. Data is presented as mean±SEM, 13≥n≥5. 5^4= 50,000 cells/cm^2; 10^4=100,000 cells/cm^2; 15^4=150,000 cells/cm^2.

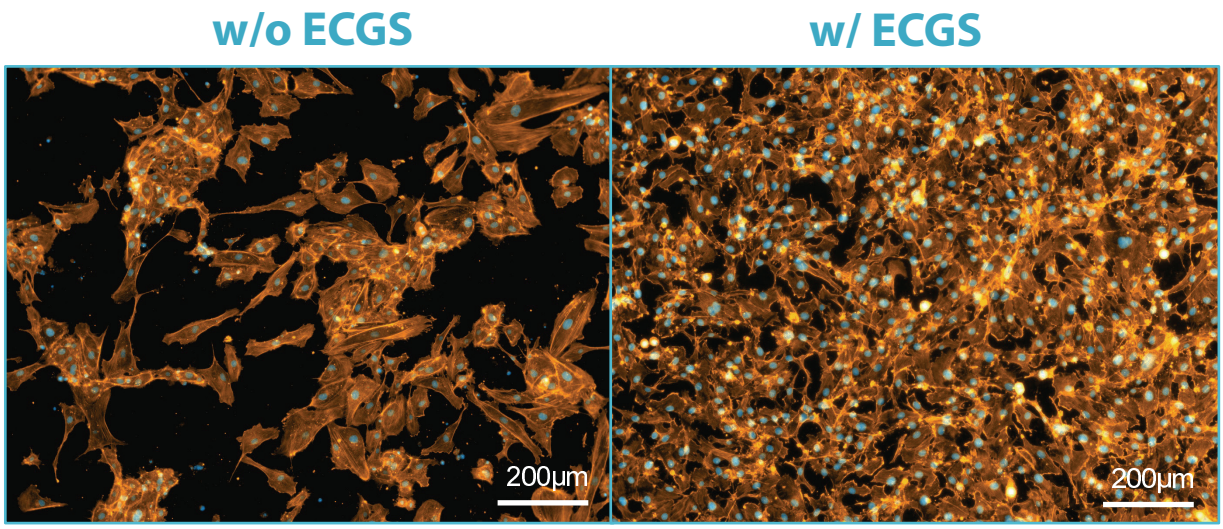

Figure VI.S4. HUVECs (λ/PL$_6$ 50,000 cells/cm^2) morphology after 4 days in culture showing some remaining TLS when cultured in absence of ECGS-hep (10%FBS), while in presence of ECGS-hep (10%FBS) cells had disassembled, proliferated and reached confluence.

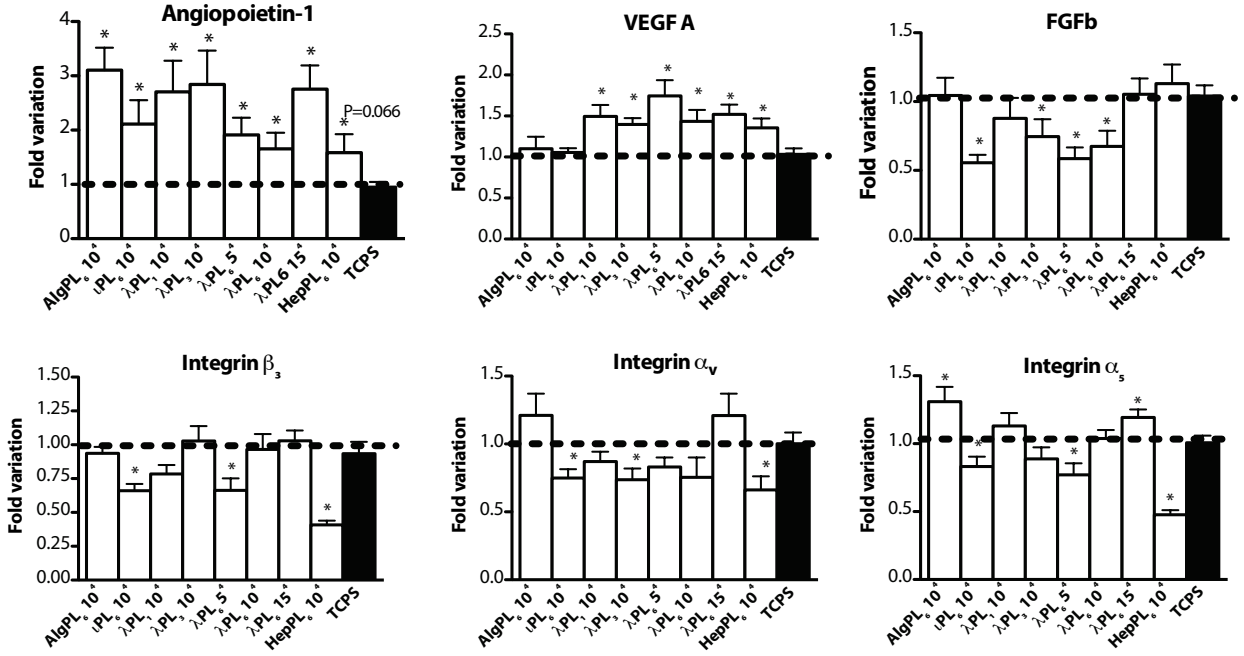

Figure VI.S5. Gene expression fold variation of Angiopoietin-1, VEGF-A, FGFb and integrins α_v, α_5, β_3 relatively to TCPS. The expression of theses genes was normalized against the housekeeping β-actin gene or GAPHD (in case of VEGFA) and calculated by the Livak method ($2^{-\Delta\Delta Ct}$). Samples were compared with the control (TPCS) and differences are identified with * ($p<0.05$, n=8, mean±sem). 5^4= 50,000 cells/cm^2; 10^4=100,000 cells/cm^2; 15^4=150,000 cells/cm^2.

VI.4.2. Materials and Methods

VI.4.2.1. Materials

Medium molecular weight chitosan (Chi), with a degree of deacetylation of 80% (Sigma Aldrich, MKBB0566), was purified by a re-precipitation method. Briefly, Chi powder was dissolved in 2% (v/v) acetic acid solution with 1% (w/v) concentration. The mixture was stirred overnight at room temperature. The impurities were removed by four filtration cycles. Then, Chi was precipitated by addition of 1 M NaOH while stirring. Final steps consisted on washing Chi with distilled water until reaching a neutral pH and on Chi dehydration rising with ethanol–water mixtures with increasing ethanol content (20–100% v/v). Chi was freeze-dried for 3 days and ground. κ- (Sigma-Aldrich, 22048), ι- (Fluka, 22045), λ-carrageenan (Car; Sigma-Aldrich, 22049), sodium heparin (Hep; Sigma-Aldrich, H3149), sodium alginate (Alg; Sigma Aldrich, 250 cP), and poly(ethyleneimine) solution (PEI; Sigma-Aldrich, P3143) were used as received.

VI.4.2.2. Materials preparation

VI.4.2.2.1. Preparation of Platelet Lysate

Platelet concentrates were obtained from different platelet collections performed at Instituto Português do Sangue (IPS, Porto, Portugal), under a previously established cooperation protocol. The components were obtained using the Trima Accel® Automated Blood Collection System. All the platelet products were biologically qualified according to the Portuguese legislation. The platelet count was performed at the IPS using the COULTER® LH 750 Hematology Analyzer and the sample volume adjusted to 1 million platelet.μL^{-1}. The collected samples were subject to three repeated temperature cycles (frozen with liquid nitrogen at -196°C and heated at 37°C) and frozen at -20°C until further use. The remaining platelets were eliminated by centrifugation at 1400*g* for 10 min. Aliquots of Platelet lysate (PL) were stored at -20°C until final use.

VI.4.2.2.2. Polyelectrolytes solutions

κ-, ι-, λ-Car, Hep and Alg were prepared in 1M Tris HCL 40 nM NaCl pH 7.4 with a concentration of 0.5 $mg.mL^{-1}$. Chi was dissolved in sodium acetate buffer with a concentration of 0.5 $mg\ mL^{-1}$. PL was 10-fold diluted with Tris HCL buffer or in 1M sodium acetate 40 mM NaCl pH 6 when to be combined with Chi.

VI.4.2.2.3. Coatings preparation in 48-well plates

48-well plates were modified with 0.5 mL of 0.5% (w/v) PEI solution to confer a positive surface charge. Then, the solution was removed and the wells were extensively rinsed with distilled water in order to remove the unbound PEI. LbL assembling was started by the adsorption of the negative PE. In the case of Chi, an Alg layer was first adsorbed. The adsorption times and volumes used were: 4 minutes and 0.5 mL for the polysaccharides solutions; 0.5 mL and 10 minutes for the PL solution; intermediate rising steps x2 for 30

seconds using the respective buffers. The sequence was repeated 6 times. The well plates were let to air-dry overnight and then sterilized using a UV light for 40 minutes.

VI.4.2.3. Cell behavior assessment

VI.4.2.3.1. HUVECs Isolation

Human umbilical cords obtained after caesarean sections from healthy donors were provided by Hospital de S. Marcos, Braga, Portugal. They were delivered in transport buffer, containing 0.14 M NaCl, 0.004 MKCI and 0.011 M glucose in 0.001M phosphate buffer at pH 7.4. Human umbilical cord vein endothelial cells (ECs) (HUVECS) were isolated as described in literature by Jaffe and others[1].

Biological samples were provided under a protocol approved by the Hospitals Ethical Committees and the 3B's Research Group. Cells were expanded using M199 supplemented with 50μg/ml endothelial cell growth supplement (ECGS, BDBiosciences), 50 μg/ml of heparin, 3.4 μl/ml Gibco® GlutaMAX™ (Life Tecnologies), 20% fetal bovine serum (FBS). Cells were cultured at 37ºC, 5%CO_2, 99% humidity and medium exchanged every 2-3 days.

VI.4.2.3.2. Cell seeding

To proceed with the cell seeding, expanded cells were harvested by trypsinization and filtered with a 100μm cell strainer to remove possible cell aggregates. Different cell densities were prepared: 20000 cells/ml with 0% FBS, 20000 cells/ml with 10% FBS, 20000 cells/ml with 20% FBS for cell adhesion and proliferation quantification; 100000 cells/ml, 200000 cell/ml, 300,000 cells/ml with 10% FBS for cell morphology studies. A volume of 500 μl of cell suspension was dispensed into each well. Well-plates were incubated for 20 hours. After 20h, medium was replaced with fresh one with 10% FBS. Half of the samples were supplemented with ECGS and heparin for proliferation quantification. HUVECs from two different donors and between passage 4 and 7 were used. Cells were incubated at 37ºC, 5%CO_2, 99% humidity.

For FGF/VEGF blockage test, M199 medium was supplemented with 10% FBS and DMSO or FGF/VEGF Receptor Tyrosine Kinase Inhibitor (PD173074). The inhibitor was first dissolved with DMSO. HUVECs (50,000 cells/500ul) were seeded onto 1cm^2-coated well plates and supplemented with 150nM (0.0075% DMSO) or 200 nM (0.01%) of inhibitor or only DMSO (0.0075% and 0.01%). Cells were incubated for 20 hours and used between passage 4-7.

VI.4.2.3.3. Cell morphology

After 20 ho[redacted]

formalin 10% (v/v) during 20 minutes. Cells were permeabilized with 0.5 mL of Triton 0.2% (v/v) in PBS during 2 minutes and then rinsed with PBS. Samples were incubated in the dark with 100 μL of (1:100) Phalloidin-TRITC (Sigma-Aldrich) solution for 30 minutes and then washed with PBS. For cell nuclei staining, well plates were

incubated in the dark for 5 min with 100 μL 4,6-diamino-2-phenyindole dilactate (DAPI, Sigma-Aldrich) diluted 1:1000 in PBS. Samples were observed using an inverted Axio Observer Fluorescence Inverted Microscope (Zeiss) and random images recorded.

VI.4.2.3.4. Cell morphology analysis

Angiogenesis Analyzer

Angiogenesis Analyzer is a toolset for Image J that allows the analysis of cellular networks images and it was used in the work reported in chapter VI to assess the angiogenic potential of the multilayers rich in PL.

Angiogenesis Analyzer is a simple tool to quantify endothelial tube formation assay images by extracting characteristic information of the network regarding segments, nodes, area and meshes. The total length of the tube-like structures, number of nodes and master nodes, number of meshes and master meshes were quantified on cytoskeleton fluorescence images of HUVECs after 20 hours of incubation. A node is defined as pixels that have at least 3 neighbors, corresponding to a bifurcation. A junction is a node or fused nodes. The segments correspond to elements that are limited by two junctions/nodes while the branches are elements delimited by a junction and one extremity. The master segments are considered pieces of three, delimited by two junctions, but not exclusively implicated with one branch (master junctions). The master junctions link at least 3 master segments. The meshes are areas enclosed by the segments or master segments.

Cell profiler

Cell Profiler allows the analysis of various biological features, including cell counting, size and also complex morphological assays such as cell/organelle shape and subcellular patterns of DNA.[43]

The morphological changes of HUVECs when cultured for 20 hours on the multilayers, in the presence or absence of inhibitors, was analyzed using the eccentricity, form factor and major and minor axis length features available with Cell Profiler. Eccentricity is defined as the ratio of the distance between the foci of the considered ellipse and its major axis length. The values vary between 0 and 1. Values equal to zero are actually circles while ellipses with eccentricity of 1 are lines. The form factor is calculate as 4π(Cell Area)/(Cell Perimeter)2, where 1 represent a perfect circular cell. The major and minor axis length (in pixels) correspond to the major and minor axis of the ellipse, respectively. The images used for Cell Profiler analyses were the same for Angiogenesis Analyzer.

VI.4.2.3.5. dsDNA quantification

In order to quantify cell attachment and proliferation after 20 hours and 4 days in culture, dsDNA was quantified using the Quant-iT™ PicoGreen® dsDNA assay kit (Molecular Probes/Invitrogen) that allows the [illegible] DNA.

After incubation periods, the well plates were gently rinsed once with sterile PBS. Then, 1 mL of ultra-pure

sterile water was added, the samples homogenized by vigorous pipetting and kept at -80°C until quantification. For the quantification, samples were defrosted at room temperature and the content was transferred to eppendorfs. 100 μL of Tris–EDTA buffer were transferred into a white opaque 96-well plate. Samples were vortexed and 28.8 μL of each plus 71.2 μL of PicoGreen solution were added to the wells. After 10 minutes of incubation in the dark, the plate was read in a microplate reader using an excitation wavelength of 485 nm and emission wavelength of 528 nm. A standard curve was created by varying the concentration of standard dsDNA standard from 0 to 2 $mg.mL^{-1}$, and triplicates dsDNA values of the samples were read off from the standard graph. At least five specimens were measured per each sample. The experiment was repeated once more.

VI.4.2.3.6. RT-PCR

The quantification of angiogenic gene expression of the HUVECS which were cultured on the multilayers and TPCS during 20 hours, was performed using quantitative PCR by a two-step fluorogenic assay using the PerfeCta™ SYBR® Green System (Quanta Biosciences) – see the target genes in Table VI.S1.

Table VI.S1. Sequences and melting temperature of the angiogenic genes analyzed.

Name	Primer sequence (Forward, Reverse 5'-3')	Tm (°C)
β-actin	ACTGGAACGGTGAAGGTGAC AGAGAAGTGGGGTGGCTTTT	59.5
GAPDH	ACAGTCAGCCGCATC GACAAGCTTCCCGTTCTCAG	58.4
Integrin β3	ACCAGTAACCTGCGGATTGG TCCGTGACACACTCTGCTTC	59.4
Integrin αv	CCGATTCCAAACTGGGAGCA GGCCACTGAAGATGGAGCAT	59.4
Integrin α5	TGGCCTTCGGTTTACAGTCC GGAGAGCCGAAAGGAAACCA	59.4
VEGFA	GACAGATCACAGGTACAGGG AGAAGCAGGTGAGAGTAAGC	58.4
FGFb	GAGCAAATCTGCCCTGCTCA TCCCGCATACTCTGGAGACA	59.4
Angiopoietin-1	GAAGGGAACCGAGCCTATTC GGGCACATTTGCACATACAG	58.4

The total RNA was extracted using the TRI® Reagent (Sigma-Aldrich), following the manufacturer's instruction. Total RNA was quantified using Nanodrop® ND-100 spectrophotometer (thermo Scientific) and first-strand complementary DNA (cDNA) was synthetized using 1 μg RNA of each sample and the qScriptTM cDNA Synthesis Kit (Quanta Biosciences) for a 20μL reaction. The obtained cDNA was used as a template for the amplification of the target genes using a MasterCycler EP Gradient detection System (Eppendorf) thermocycler and the PerfeCtaTM SYBR® Green System kit following the manufacturers' instructions. The Livak method, $2^{-\Delta\Delta Ct}$, was used to evaluate the relative expression of each target gene. ΔCt was calculated by the difference between the Ct values of the target gene and the β-actin or GAPDH endogenous housekeeping gene. ΔΔCt was

obtained by subtracting the ΔCt of the calibrator sample (TCPS) to the ΔCt of the sample. The results are represented as $2^{-\Delta\Delta Ct}$ and as gene expression relative to TCPS.

VI.4.3. Statistical Analysis

First, it was verified with Shapiro–Wilk test that most of the data did not passed the normality test. All data was statistically analyzed by using non-parametric tests. The unpaired one-tailed t-test with Welch's correction for non-parametric data was used ($p \leq 0.05$).

VI.5. References

1. F. A. Auger, L. Gibot and D. Lacroix, The pivotal role of vascularization in tissue engineering, Annu Rev Biomed Eng, 2013, 15, 177-200.
2. E. C. Novosel, C. Kleinhans and P. J. Kluger, Vascularization is the key challenge in tissue engineering, Adv Drug Deliv Rev, 2011, 63, 300-311.
3. M. I. Santos and R. L. Reis, Vascularization in bone tissue engineering: physiology, current strategies, major hurdles and future challenges, Macromol Biosci, 2010, 10, 12-27.
4. Y. Blinder, D. Mooney and S. Levenberg, Engineering approaches for inducing blood vessel formation, Current Opinion in Chemical Engineering, 2014, 3, 56-61.
5. L. E. Bertassoni, M. Cecconi, V. Manoharan, M. Nikkhah, J. Hjortnaes, A. L. Cristino, G. Barabaschi, D. Demarchi, M. R. Dokmeci, Y. Yang and A. Khademhosseini, Hydrogel bioprinted microchannel networks for vascularization of tissue engineering constructs, Lab Chip, 2014, 14, 2202-2211.
6. C. A. Staton, M. W. Reed and N. J. Brown, A critical analysis of current in vitro and in vivo angiogenesis assays, Int J Exp Pathol, 2009, 90, 195-221.
7. M. W. Irvin, A. Zijlstra, J. P. Wikswo and A. Pozzi, Techniques and assays for the study of angiogenesis, Exp Biol Med (Maywood), 2014, 1535370214529386.
8. X. M. van Wijk and T. H. van Kuppevelt, Heparan sulfate in angiogenesis: a target for therapy, Angiogenesis, 2014, 17, 443-462.
9. M. Matsui and Y. Tabata, Enhanced angiogenesis by multiple release of platelet-rich plasma contents and basic fibroblast growth factor from gelatin hydrogels, Acta Biomater, 2012, 8, 1792-1801.
10. G. Sufen, Y. Xianghong, C. Yongxia and P. Qian, bFGF and PDGF-BB have a synergistic effect on the proliferation, migration and VEGF release of endothelial progenitor cells, Cell biology international, 2011, 35, 545-551.
11. G. Sun, Y. I. Shen, S. Kusuma, K. Fox-Talbot, C. J. Steenbergen and S. Gerecht, Functional neovascularization of biodegradable dextran hydrogels with multiple angiogenic growth factors, Biomaterials, 2011, 32, 95-106.
12. Q. Sun, E. A. Silva, A. Wang, J. C. Fritton, D. J. Mooney, M. B. Schaffler, P. M. Grossman and S. Rajagopalan, Sustained release of multiple growth factors from injectable polymeric system as a novel therapeutic approach towards angiogenesis, Pharm Res, 2010, 27, 264-271.
13. K. Stellos, S. Kopf, A. Paul, J. U. Marquardt, M. Gawaz, J. Huard and H. F. Langer, Platelets in regeneration, 2010.
14. S. C. Bir, J. Esaki, A. Marui, K. Yamahara, H. Tsubota, T. Ikeda and R. Sakata, Angiogenic properties of sustained release platelet-rich plasma: characterization in-vitro and in the ischemic hind limb of the mouse, J Vasc Surg, 2009, 50, 870-879 e872.
15. N. Kakudo, N. Morimoto, S. Kushida, T. Ogawa and K. Kusumoto, Platelet-rich plasma releasate promotes angiogenesis in vitro and in vivo, Med Mol Morphol, 2014, 47, 83-89.
16. T. Mammoto, A. Jiang, E. Jiang and A. Mammoto, Platelet rich plasma extract promotes angiogenesis through the angiopoietin1-Tie2 pathway, Microvascular Research, 2013, 89, 15-24.
17. B. Zhou, J. Ren, C. Ding, Y. Wu, D. Hu, G. Gu and J. Li, Rapidly in situ forming platelet-rich plasma gel enhances angiogenic responses and augments early wound healing after open abdomen, Gastroenterol Res Pract, 2013, 2013, 926764.
18. Y. Man, P. Wang, Y. Guo, L. Xiang, Y. Yang, Y. Qu, P. Gong and L. Deng, Angiogenic and osteogenic potential of platelet-rich plasma and adipose-derived stem cell laden alginate microspheres, Biomaterials, 2012, 33, 8802-8811.
19. F. Findikcioglu, K. Findikcioglu, R. Yavuzer, N. Lortlar and K. Atabay, Effect of preoperative subcutaneous platelet-rich plasma and fibrin glue application on skin flap survival, Aesthetic Plast Surg, 2012, 36, 1246-1253.
20. J. Leotot, L. Coquelin, G. Bodivit, P. Bierling, P. Hernigou, H. Rouard and N. Chevallier, Platelet lysate coating on scaffolds directly and indirectly enhances cell migration, improving bone and blood vessel formation, Acta Biomater, 2013, 9, 6630-6640.
21. E. Polykandriotis, A. Arkudas, R. E. Horch, U. Kneser and G. Mitchell, To matrigel or not to matrigel, The American journal of pathology, 2008, 172, 1441-1442.
22. J. Borges and J. F. Mano, Molecular Interactions Driving the Layer-by-Layer Assembly of Multilayers, Chemical reviews, 2014, 114, 8883-8942.

23. R. R. Costa and J. F. Mano, Polyelectrolyte multilayered assemblies in biomedical technologies, Chemical Society reviews, 2014, 43, 3453-3479.
24. K. Gaengel and C. Betsholtz, Endocytosis regulates VEGF signalling during angiogenesis, Nat Cell Biol, 2013, 15, 233-235.
25. J. Kreuger, D. Spillmann, J. P. Li and U. Lindahl, Interactions between heparan sulfate and proteins: the concept of specificity, J Cell Biol, 2006, 174, 323-327.
26. G. S. Schultz and A. Wysocki, Interactions between extracellular matrix and growth factors in wound healing, Wound Repair Regen, 2009, 17, 153-162.
27. S. K. Nigam and K. T. Bush, Growth factor-heparan sulfate "switches" regulating stages of branching morphogenesis, Pediatr Nephrol, 2014, 29, 727-735.
28. T. H. Nguyen, S. H. Kim, C. G. Decker, D. Y. Wong, J. A. Loo and H. D. Maynard, A heparin-mimicking polymer conjugate stabilizes basic fibroblast growth factor, Nat Chem, 2013, 5, 221-227.
29. T. N. Vo, F. K. Kasper and A. G. Mikos, Strategies for controlled delivery of growth factors and cells for bone regeneration, Advanced drug delivery reviews, 2012, 64, 1292-1309.
30. T. H. Silva, A. Alves, B. M. Ferreira, J. M. Oliveira, L. L. Reys, R. J. F. Ferreira, R. A. Sousa, S. S. Silva, J. F. Mano and R. L. Reis, Materials of marine origin: a review on polymers and ceramics of biomedical interest, International Materials Reviews, 2012, 57, 276-307.
31. K. Senni, J. Pereira, F. Gueniche, C. Delbarre-Ladrat, C. Sinquin, J. Ratiskol, G. Godeau, A. M. Fischer, D. Helley and S. Colliec-Jouault, Marine polysaccharides: a source of bioactive molecules for cell therapy and tissue engineering, Mar Drugs, 2011, 9, 1664-1681.
32. T. H. Silva, A. Alves, E. G. Popa, L. L. Reys, M. E. Gomes, R. A. Sousa, S. S. Silva, J. F. Mano and R. L. Reis, Marine algae sulfated polysaccharides for tissue engineering and drug delivery approaches, Biomatter, 2012, 2, 278-289.
33. M. G. Lampugnani, F. Orsenigo, M. C. Gagliani, C. Tacchetti and E. Dejana, Vascular endothelial cadherin controls VEGFR-2 internalization and signaling from intracellular compartments, J Cell Biol, 2006, 174, 593-604.
34. P. J. Stahl, T. R. Chan, Y. I. Shen, G. Sun, S. Gerecht and S. Yu, Capillary Network-Like Organization of Endothelial Cells in PEGDA Scaffolds Encoded with Angiogenic Signals via Triple Helical Hybridization, Advanced Functional Materials, 2014.
35. A. Sahni and C. W. Francis, Stimulation of endothelial cell proliferation by FGF-2 in the presence of fibrinogen requires $\alpha v\beta 3$, 2004.
36. J. A. Madri and S. K. Williams, Capillary endothelial cell cultures: phenotypic modulation by matrix components, J Cell Biol, 1983, 97, 153-165.
37. G. Ferrari, B. D. Cook, V. Terushkin, G. Pintucci and P. Mignatti, Transforming growth factor-beta 1 (TGF-$\beta 1$) induces angiogenesis through vascular endothelial growth factor (VEGF)-mediated apoptosis, Journal of cellular physiology, 2009, 219, 449-458.
38. R. Mammadov, B. Mammadov, S. Toksoz, B. Aydin, R. Yagci, A. B. Tekinay and M. O. Guler, Heparin mimetic peptide nanofibers promote angiogenesis, Biomacromolecules, 2011, 12, 3508-3519.
39. K. P. Claffey, Molecular profiling of angiogenic markers: a step towards interpretive analysis of a complex biological function, Am J Pathol, 2002, 161, 7-11.
40. A. D. Grove, V. V. Prabhu, B. L. Young, F. C. Lee, V. Kulpa, P. J. Munson and E. C. Kohn, Both protein activation and gene expression are involved in early vascular tube formation in vitro, Clinical Cancer Research, 2002, 8, 3019-3026.
41. G. Seghezzi, S. Patel, C. J. Ren, A. Gualandris, G. Pintucci, E. S. Robbins, R. L. Shapiro, A. C. Galloway, D. B. Rifkin and P. Mignatti, Fibroblast growth factor-2 (FGF-2) induces vascular endothelial growth factor (VEGF) expression in the endothelial cells of forming capillaries: an autocrine mechanism contributing to angiogenesis, J Cell Biol, 1998, 141, 1659-1673.
42. J. Gavard, V. Patel and J. S. Gutkind, Angiopoietin-1 prevents VEGF-induced endothelial permeability by sequestering src through mDia, Developmental Cell, 2008, 14, 25-36.
43. S. P. Ngok, R. Geyer, M. Liu, A. Kourtidis, S. Agrawal, C. Wu, H. R. Seerapu, L. J. Lewis-Tuffin, K. L. Moodie, D. Huveldt, R. Marx, J. M. Baraban, P. Storz, A. Horowitz and P. Z. Anastasiadis, VEGF and Angiopoietin-1 exert opposing effects on cell junctions by regulating the Rho GEF Syx, J Cell Biol, 2012, 199, 1103-1115.
44. T. I. Koblizek, C. Weiss, G. D. Yancopoulos, U. Deutsch and W. Risau, Angiopoietin-1 induces sprouting angiogenesis *in vitro*, Current biology, 1998, 8, 529-532.

45. M. Hangai, T. Murata, N. Miyawaki, C. Spee, J. I. Lim, S. He, D. R. Hinton and S. J. Ryan, Angiopoietin-1 upregulation by vascular endothelial growth factor in human retinal pigment epithelial cells, Invest Ophthalmol Vis Sci, 2001, 42, 1617-1625.
46. W. H. Zhu, A. MacIntyre and R. F. Nicosia, Regulation of angiogenesis by vascular endothelial growth factor and angiopoietin-1 in the rat aorta model: distinct temporal patterns of intracellular signaling correlate with induction of angiogenic sprouting, Am J Pathol, 2002, 161, 823-830.
47. S. Kanda, H. Kanetake and Y. Miyata, Role of Src in angiopoietin 1-induced capillary morphogenesis of endothelial cells: Effect of chronic hypoxia on Src inhibition by PP2, Cell Signal, 2007, 19, 472-480.
48. N. Eter and M. Spitznas, DMSO mimics inhibitory effect of thalidomide on choriocapillary endothelial cell proliferation in culture, Br J Ophthalmol, 2002, 86, 1303-1305.
49. K. Koizumi, Y. Tsutsumi, Y. Yoshioka, M. Watanabe, T. Okamoto, Y. Mukai, S. Nakagawa and T. Mayumi, Anti-angiogenic effects of dimethyl sulfoxide on endothelial cells, Biol Pharm Bull, 2003, 26, 1295-1298.

SECTION 6

3D LAYER-BY-LAYER ASSEMBLED PLATELET LYSATE

CHAPTER VII

ASSEMBLING HUMAN PLATELET LYSATE INTO MULTISCALE 3D SCAFFOLDS FOR BONE TISSUE ENGINEERING

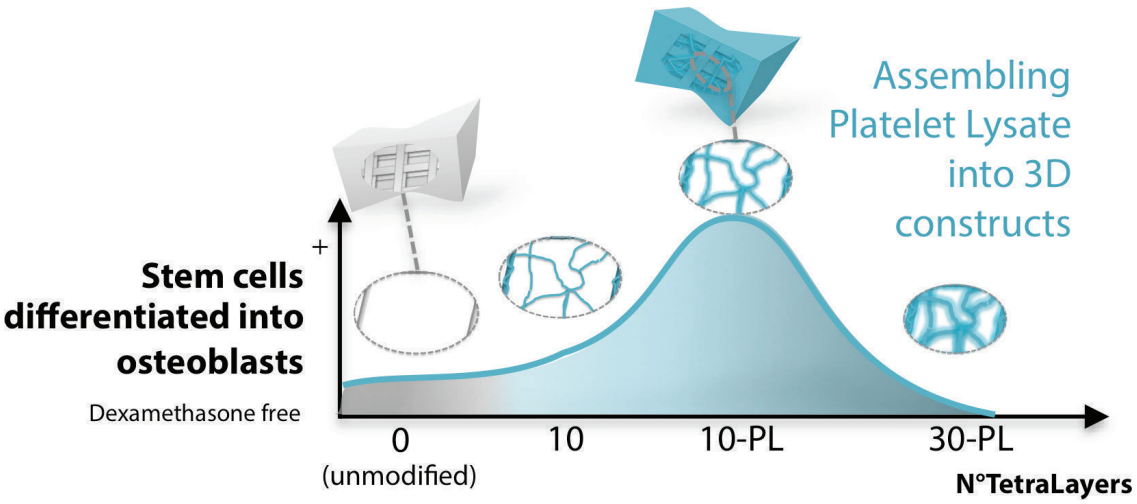

CHAPTER VII*

Assembling human Platelet Lysate into Multiscale 3D Scaffolds for Bone Tissue Engineering

VII.1. Abstract

Scaffolds for bone tissue engineering lack often control of cellular instructions. We propose a triple sequential approach for customizing scaffold features from the macro to the nanoscale. The nano/meso-scale is composed by human platelet lysate and marine-origin polysaccharides assembled by layer-by-layer and shaped into fibrils by freeze-drying. We show that osteogenic induction of stem cells is tunable within a low range of layers. This approach has the potential to develop new scaffolds with enhanced cell-instructive capabilities using affordable autologous sources of bioactive molecules.

Keywords: layer-by-layer, cell-materials interactions, cell behavior, sulfonic, surface properties, bio-inspired surfaces, model study.

*This chapter is based on the following publication:

Sara M. Oliveira, Rui L. Reis, João F. Mano, Assembling human Platelet Lysate into Multiscale 3D Scaffolds for Bone Tissue Engineering, submitted, 2014.

Nowadays, the challenge to develop bioinstructive, cost-effective and patient customizable bone tissue engineered constructs, still remains. The development of hierarchical and sequential scaffolds, whose properties can be controlled from nano to macro scale, has been considered the best approach for developing translational bone engineering products.[1] Also, the release or incorporation of growth factors (GFs) is a powerful strategy for cell fate control.[2-3] Presently, the clinically available recombinant GFs are costly and may raise immunogenic concerns.[4] Platelets present themselves as a cost-effective autologous source of multiple bioactive proteins (e.g., GFs and adhesive proteins) with proven ability to enhance several cell functions.[5-6] Their huge potential is however, compromised by the GFs stability, release, concentration and donor variability.[7-9]

Several attempts have been made to combine platelets derivatives with apatite and polymeric biomaterials for osteogenic ends, but some reports are inconclusive in regards to their efficacy.[10-13] New design concepts to improve their osteogenic efficacy on scaffolds are needed.[14] LbL has been used to incorporate recombinant GFs within sets of multilayers[15-16] or for their adsorption onto previously assembled multilayers.[17-18] We believe that the incorporation of multi-GFs from a human source, with biopolymers, may represent important economic and biological advantages. The aminated and sulfated nature of the chosen polysaccharides increases the similarity to native extracellular matrix (ECM). Moreover, the sulfated polysaccharides are good candidates for both GFs conformation and bioactivity preservation through the favorable interactions with sulfate groups.[19-22]

In this work, we disclose the preparation of sequential scaffolds with tunable osteogenic ability: macro-microscale control by rapid prototyping (I); nano/meso scale control by layer-by-layer (LbL) assembling containing platelet lysate (II) and freeze-drying (III) – Figure 1a.

First, scaffolds were prepared by rapid prototyping to buildup a macro/micro scale controlled porous structure. Then, the scaffolds were modified with human Platelet Lysate (PL) and marine-origin polysaccharides using LbL – an adequate technique to process nanostructured multilayered films through spontaneous sequential adsorption of distinct materials.[23-26] This step being performed at mild conditions does not impair the macroscopic mechanical properties of the scaffolds. Instead, it adds a new bio-instructive length-scale and new cell-anchorage points without compromising porosity and the large-scale geometrical features. Simple adjustments, such as number of layers and polysaccharide type for PL adsorption, are expected to have an impact on cell fate.

The third step comprises scaffold freeze-drying to shape the LbL structures, created in module II, into sub/micro-nano fibrils and nanocoatings. Those fibrillar structures, contain PL and increase cell-anchorage points which allow a better 3D cell arrangement than the bare 3D scaffolds.[27]

We hypothesize that this approach, for the PL incorporation, may provide, and control, the capability for osteogenesis. Moreover, the incorporation of PL with sulfated polysaccharides may represent a synergistic effect: reducing the number of layers needed for a favorable osteogenic instruction.

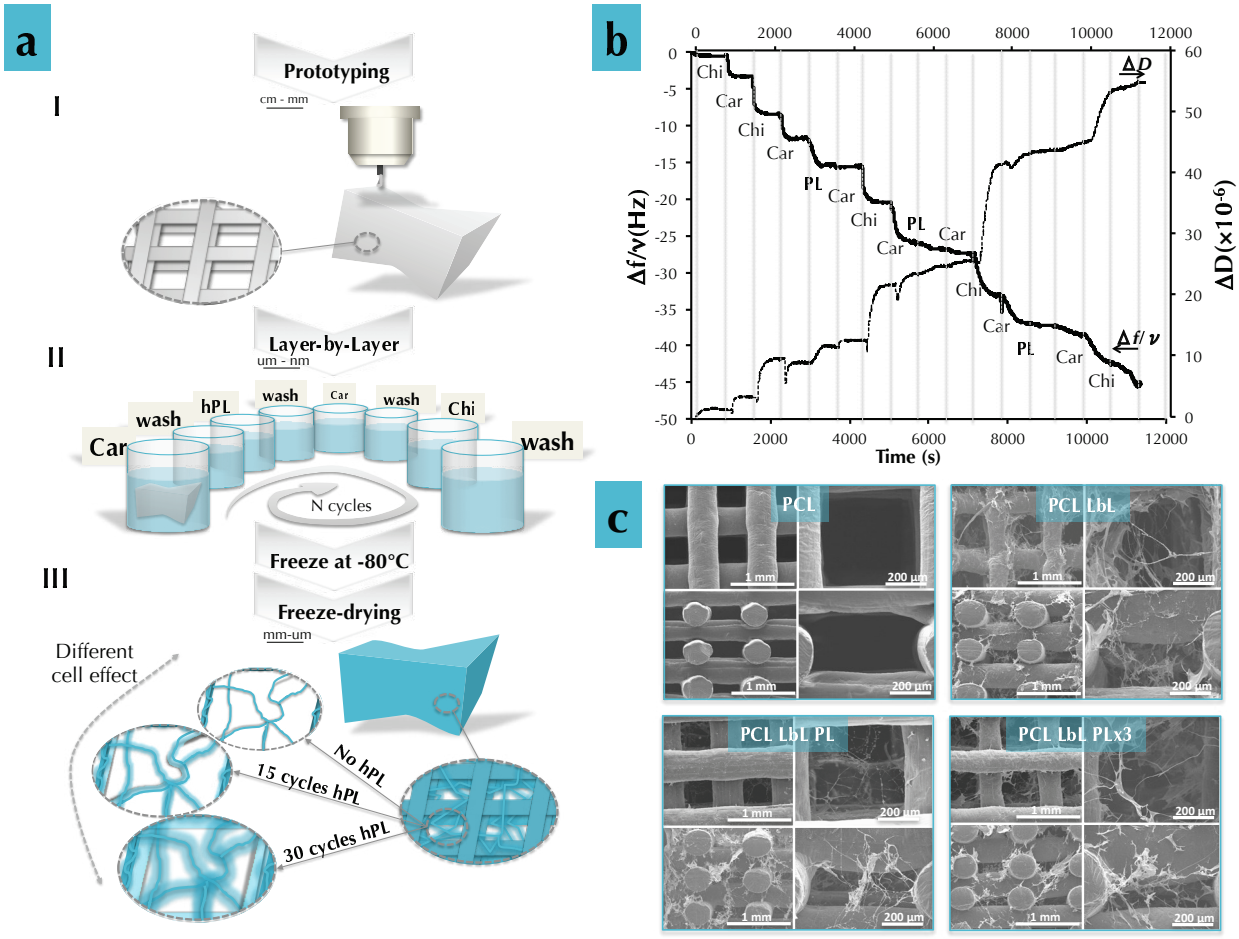

Figure VII.1. a) Sequential approach used: macro/micro scaffolds prepared by Bioplotter™ (I); nano/submicro modification with PL by LbL (II) and freeze-drying (III). b) QCM-D monitoring of the normalized frequency ($\Delta f/\nu$) and dissipation (ΔD), obtained for the 7th overtone for the LbL deposition of (PL-ιCar-Chi-ιCar) tetralayers onto (Chi-ιCar)$_2$. c) SEM micrographs of the top and longitudinal sections of the obtained scaffolds: PCL LbL (10 tetralayers, no PL), PCL LbL PL (10 tetralayers), PCL LbL PLx3 (30 tetralayers). Chi: chitosan, Car: carrageenan.

It has been demonstrated that PL has the potential to enhance cell proliferation, bone formation and angiogenesis when mixed with biomaterials or used as a media supplement.[3, 5, 28-30] However, other reports suggest that new approaches are needed so that we can take full advantage of their properties.[10-13] Around neutral pH, PL solutions are composed of a complex mixture of proteins presenting opposing charges. Most of the GFs have an alkaline isoelectric point, being thus positively charged at neutral pH. Consequently, sulfated polysaccharides are good candidates for the attraction and stabilization of GFs. Previously, we reported the enhancement of SaOs-2 cells biomineralization onto middle sulfated ι-carrageenan/chitosan (ιCar/Chi) nanocoatings, as compared to unmodified 2D PCL.[31] Therefore, PL was included within ιCar multilayers, followed by Chi, a positively charged polyelectrolyte, in mild acidic conditions. Each cycle of layers corresponded to a tetralayer with the sequence: $(\text{ιCar-PL-ιCar-Chi})_n$ – with *n* representing the number of tetralayers. Quartz Crystal Microbalance with Dissipation (QCM-D) was used to monitor the assembling of the polyelectrolytes – Figure VII.1.b. The decrease in frequency is attributed to the deposition of material onto the quartz crystal and the increase in dissipation is assigned to the formation of a viscoelastic film, meaning that

the polyelectrolytes interact and new nanolayers are sequentially being deposited during the cyclic passing of the solutions.

Prototyped polycaprolactone (PCL) scaffolds were modified by LbL assembling recurring to a custom-made dipping robot. The prepared samples were: unmodified PL, PCL LbL - (ιCar-Chi-ιCar-Chi)$_{10}$, PCL LbL PL - (ιCar-PL-ιCar-Chi)$_{10}$ and PCL LbL PLx3 - (ιCar-PL-ιCar-Chi)$_{30}$. To induce the formation of the inner fibrillar structures, the scaffolds were freeze-dried. (More details of materials and methods can be consulted in SI.)

Morphology of the final scaffolds was observed by scanning electron microscopy (SEM) – see Figure 1c. The fibrillar and membrane-like structures containing PL, Chi and ιCar were homogenously distributed inside the pores in all the conditions. The stability observed for these elements is consistent with the good handling and mechanical integrity of porous structures prepared previously using LbL with polysaccharides.[32-33]

The ultimate goal was to explore the osteogenic potential of the developed scaffold. Their ability to induce or improve the osteogenic differentiation of human adipose derived stem cells (hASCs) was evaluated after 4 days (basal media) plus 28 days of incubation in osteoconductive (without dexamethasone, -Dex) or osteogenic media (+Dex), respectively. The samples were further characterized using calcium quantification, energy dispersive spectroscopy (EDS), immunocytochemistry, SEM and gene-expression. (More details of cell culture and seeding conditions can be consulted in SI)

After the culture period, samples were observed by SEM and also stained with Alizarin Red S (ARS), which forms reddish complexes with calcium – Figure VII.S1., Figure VII.2.a. The presence of phosphorous and calcium phosphate crystals was confirmed by SEM and both Ca and P elements detected by EDS analysis – Figure VII.S1. For indirect total calcium quantification, ARS was eluted - Figure VII.S4.a. All the conditions +Dex allowed calcium phosphate deposition. As expected, in the absence of Dex, no significant mineralization was observed on Tissue Culture Polystyrene (TCPS), nor in PCL. PCL LbL -Dex constructs showed a light homogenous coloration indicating some, or an earlier stage, of biomineralization, which was not significant ($p<0.05$) – Figure VII.S4.a. With the presence of PL, PCL LbL PL constructs allowed a homogenous and strong deposition of calcium phosphates in free Dex medium according to the staining, EDS and SEM analysis – Figure VII.S1. However, with 3-fold tetralayer (PCL LbL PLx3), the deposition of calcium did not occur – see Figure VII.S3. Additionally, some differences were detected among the conditions regarding the total fat deposited, measured by Oil red O (ORO) staining elution – Figure VII.S4. Oil red O. The deposited amount of fat was significantly lower when PCL LbL PL was cultured without Dex; however, in the absence of both PL and Dex, the fat content was increased. PCL LbL +Dex has also shown an increased ORO concentration ($p<0.05$); the opposite trend was observed on PCL LbL -Dex.

Regarding the Dex free samples, the presence of osteocalcin in the extracellular matrix has shown the same trend as ARS staining – Figure VII.2.b. Only the samples with 10 tetralayers with PL have shown a strong presence of osteocalcin. No osteocalcin was detected in the LbL PL PLx3 samples, corroborating the inhibition of osteogenesis – Figure VII.S3. The induction of hASCs towards the osteogenic lineage appears as being highly influenced by the presence of PL and the number of tetralayers.

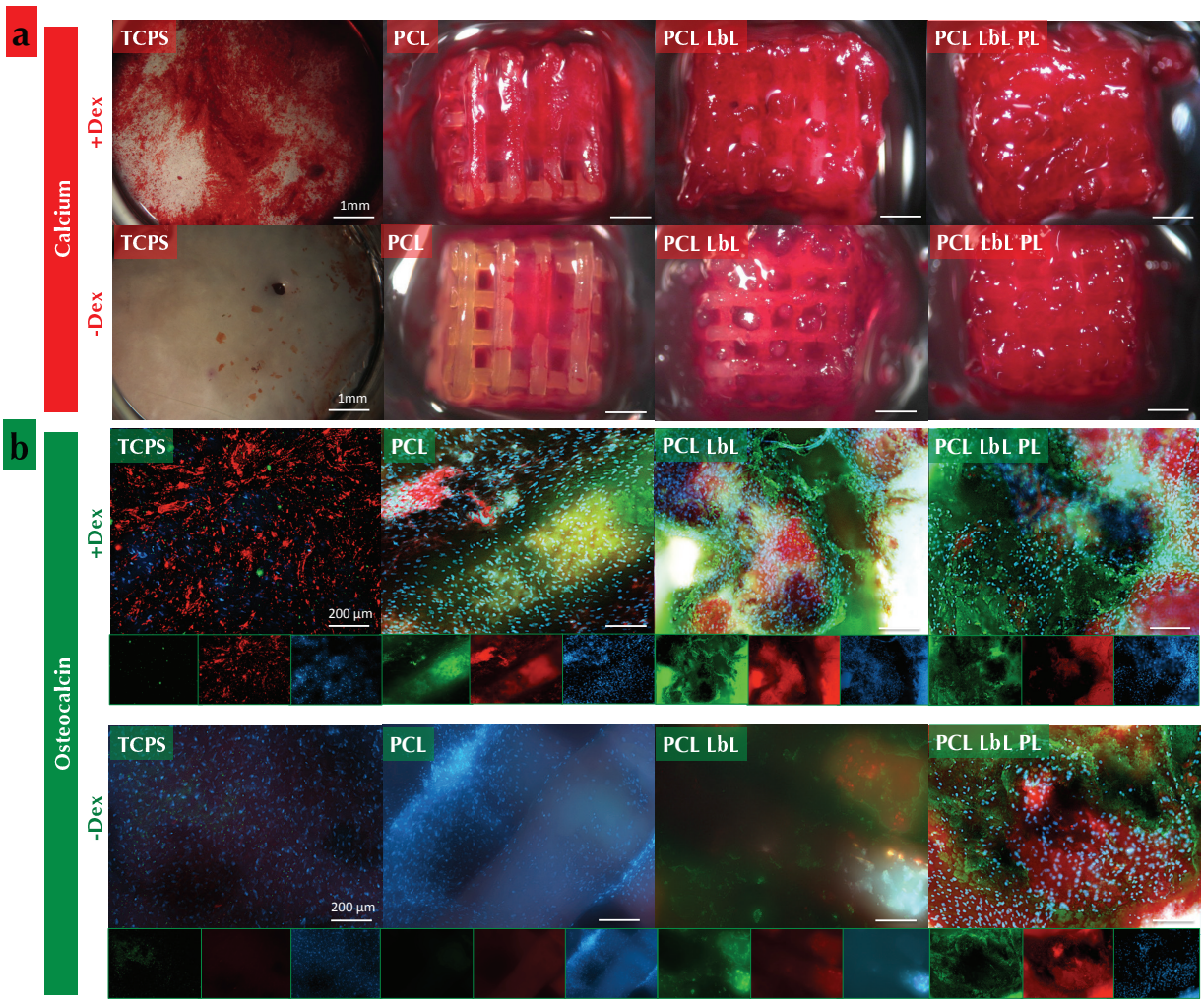

Figure VII.2. Matrix components stained after 32 days in culture. a) Calcium deposits (ARS staining). b) Fluorescence images of staining for human osteocalcin (green), ARS (red) and cell nuclei (blue) on TCPS and scaffolds – below each one are shown the images of each color channel. See Figure S2 for enlarged images of b; and Figure S3 for the PCL LbL PLx3 staining.

The fibrilar structures have provided new cell anchorage points where mineralization has occurred – Figure VII.3. The calcium phosphate deposits were not restricted to the surfaces, but were distributed on the cell aggregates formed in the entire volume of the scaffold.

For the osteogenic differentiation of stem cells the expression of Runx2 is required, since is a crucial early marker of the commitment towards the osteogenic lineage.[34] Runx2 up-regulates the expression of bone sialoprotein, alkaline phosphatase, and osteocalcin, among other proteins synthetized by osteoblasts in the late phase. Mature osteocytes express strong levels of sclerostin (SOST), signaling the mineralization terminal phase.[35-36] Regarding osteogenic differentiation, it has been reported that the use of Dex combined with BMP-2 thins the boundary between osteogenesis and adipogenesis. This combination may simultaneously improve both osteogenesis and adipogenesis.[37-38] As such, the genetic expression of bone and endothelial markers (Runx2, Osteocalcin, Col I, and PECAM-1), hypertrophic chondrocytes (Col X) and adipose tissue markers (PPARγ2 and Leptin) was quantified after 32 days in culture – Figure VII.S4. Regarding the expression of collagenous proteins, all the samples containing LbL structures (with and without PL) showed a decreased expression of Col I and X ($p<0.05$), with exception of PCL LbL PL +Dex in Col type I. Relatively to the control,

there were no superior significant differences in osteocalcin. However, the samples with LbL and 10 tretralayers with PL showed the tendency for a higher expression of osteocalcin even in absence of Dex ($p<0.09$). The sample PCL LbL PL-Dex promoted high osteocalcin gene expression and high osteocalcin, calcium and phosphate levels in the extracellular matrix, demonstrating that it has induced the differentiation of hASCs into mature osteoblasts. The expression of the late osteogenic gene, SOST, was up-regulated in PCL LbL PL +Dex, which was accompanied by a higher expression of Runx2, PPARy2 and PECAM-1. PECAM1 gene codes PECAM-1/CD31 that is found in the endothelial cell intercellular junctions.

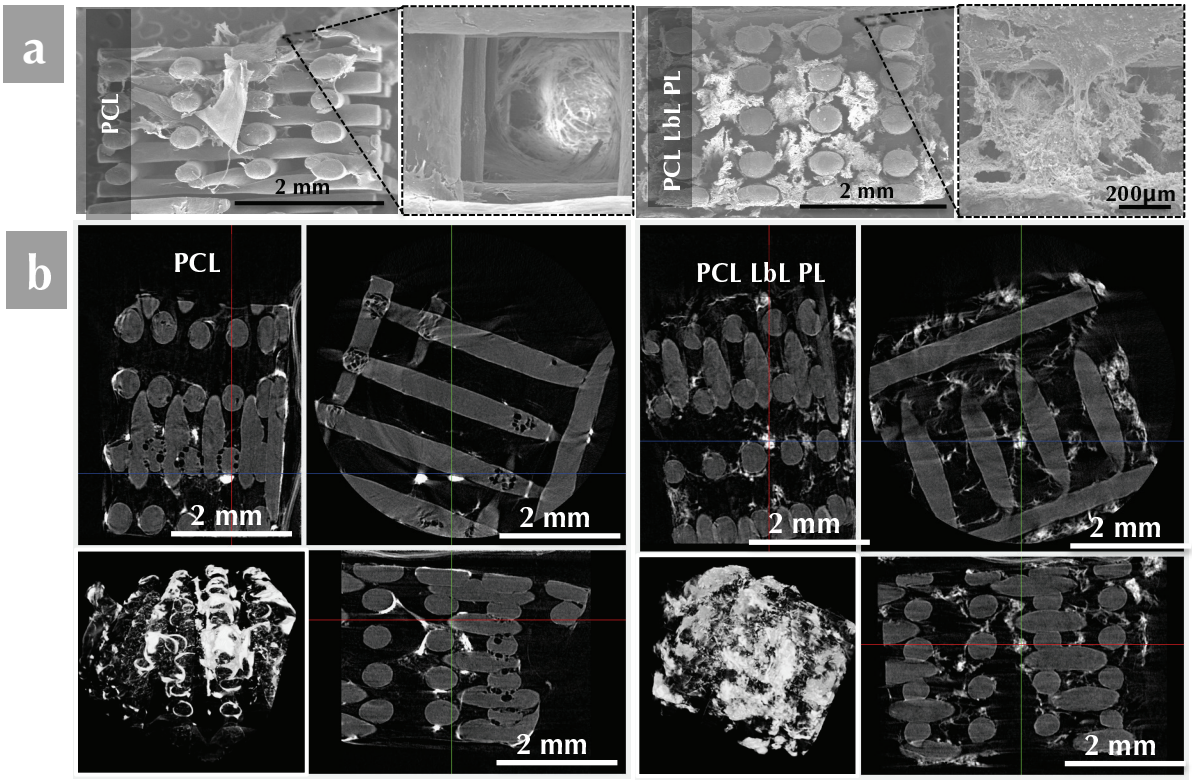

Figure VII. 3. Calcium/phosphates distribution on PCL+Dex and PCL LbL PL+Dex (similar to PCL LbL PL-Dex), after 32 days in culture: a) SEM micrographs of sagittal and top views, respectively; b) 3D reconstruction of the mineral fraction obtained by micro-CT acquisition, and respective sagittal, transverse and coronal plans (from left to right and bottom, respectively).

The simultaneous high expression of such genes may be explained by a higher presence of sub-populations, which suggests that the combination of PL with Dex may give rise to higher cellular heterogenity.[3, 39] In the absence of Dex, the sample with higher calcium content, PCL LbL PL, has shown a lower expression of Runx2 and PECAM-1 than in presence of Dex, though similar to the control. Other genes such as PPARy2, leptin and SOST were also lower than in the control ($p<0.05$). Such a decreases might be indicative that the osteogenesis was not as mature as in presence of Dex. Nevertheless, PCL LbL PL was the only one able to induce osteogenesis in absence of Dex, and with lower evidences of adipogenesis-related genes and fat. The adipocyte-specific PPARy2 showed a tendency to increase on the same samples in which ORO concentration was higher than the control, with exception of PCL LbL PLx3. The expression of Runx2 on PCL LbL PLx3 was down-regulated, together with most of all the other genes assessed. Somehow increasing the number of tetralayers, i.e. PCL LbL PLx3, has led to the inhibition of osteoinduction (-Dex medium). This inhibition might

be mediated by the overexpression of PPARγ2, which is described to inhibit Runx2 and its further dependent expressions.[40-41] Even though, such behavior has not translated into fat deposition.

Controlling the number of tetralayers is then a crucial parameter for the development of free-Dex osteogenic scaffolds when using this methodology.

The results of the present work demonstrate that the proposed method is suitable for the preparation of new 3D hierarchical osteogenic scaffolds. The incorporation of PL, using LbL and freeze-drying induced the differentiation of hASCs into mature osteoblasts with only 10 tetralayers. The fibrillar structures with PL allowed a 3D organization of the mineralization not restricted to the PCL surface. Moreover, this methodology allows to developed tunable scaffolds to instruct stem cells towards the osteogenic lineage.

VII.2. Acknowledgments

The research leading to these results has received funding from the European Union's Seventh Framework Program (FP7/ 2007-2013) under grant agreement no REGPOT-CT2012-316331- POLARIS and FP7-KBBE-2010-4-266033 – SPECIAL. This work was also supported by the European Research Council grant agreement ERC-2012-ADG 20120216-321266 for the project ComplexiTE. Portuguese Foundation for Science and Technology is gratefully acknowledged for fellowships of Sara M. Oliveira. (SFRH/BD/ 70107/2010).

VII.3. Supporting Information

VII.3.1. Supporting Figures

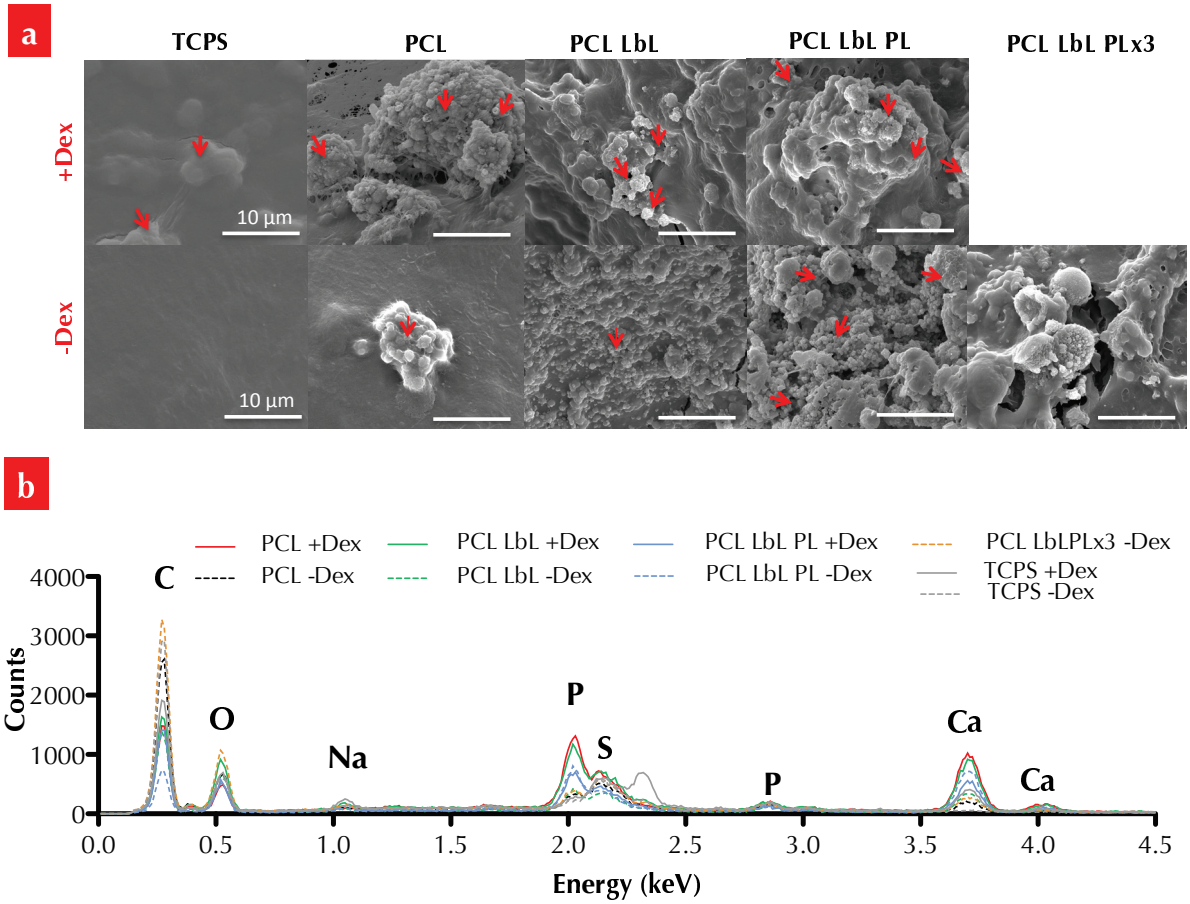

Figure VII.S1. a) SEM micrographs of the hASCs cultured on TCPS, unmodified and modified scaffolds after 4+28 days in culture in absence (-Dex) and presence of Dex (+Dex); the red arrows point the observed CaP deposits. b) EDS spectra of all the samples assessed in this work after the 32 days in culture.

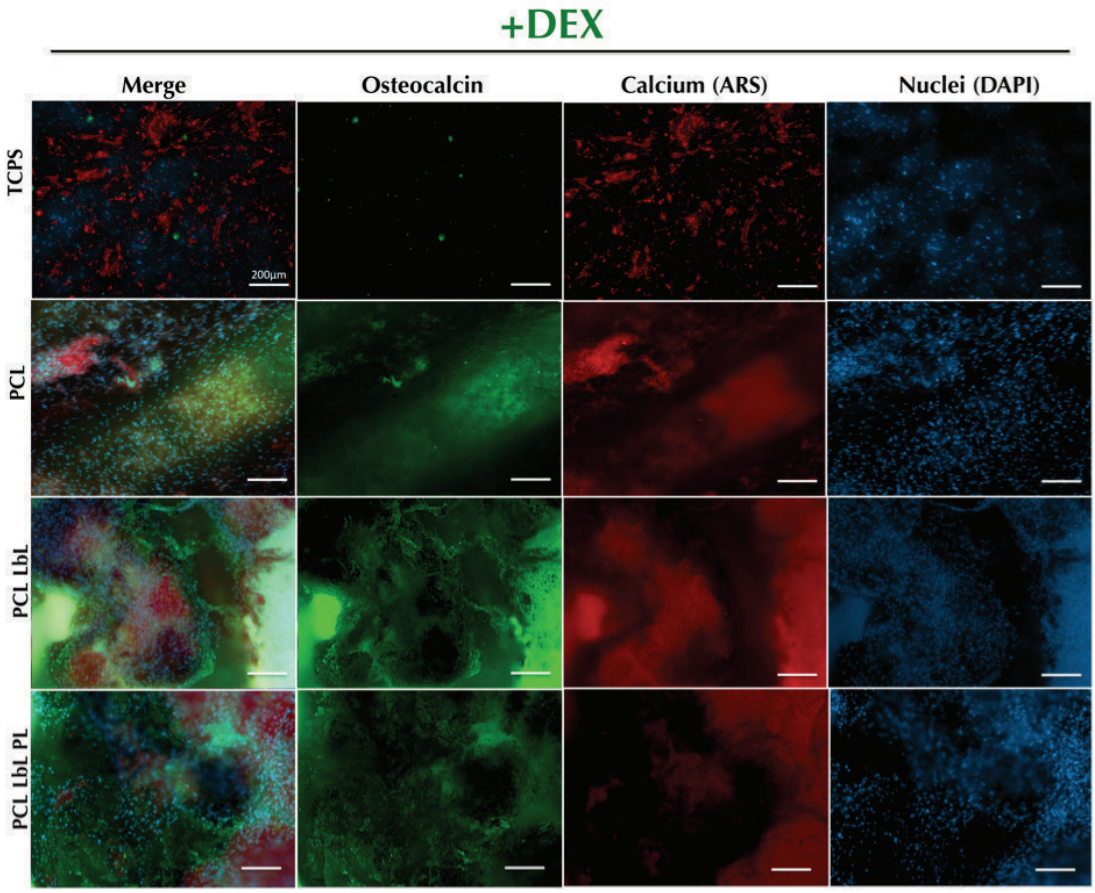

Figure VII.S2. Enlarged version of the images displayed on Figure VII.2. Immunodetection of human osteocalcin (green), ARS staining (red) and cell nuclei (blue) on TCPS, modified and unmodified PCL scaffolds culture for 32 days in presence of Dex.

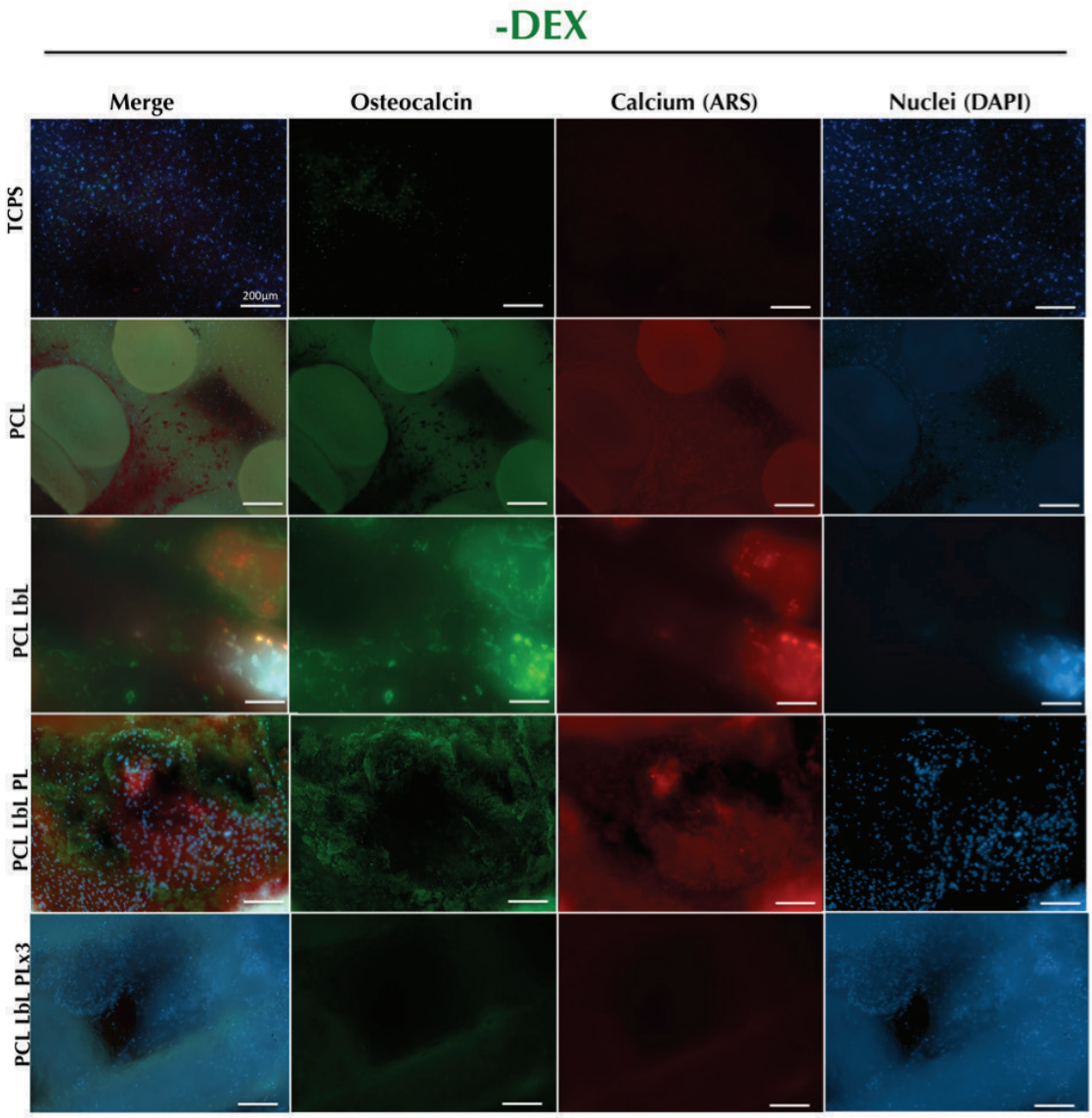

Figure VII.S3. continuation. Immunodetection of human osteocalcin (green), ARS staining (red) and cell nuclei (blue) on TCPS, modified and unmodified PCL scaffolds culture for 32 days in absence of Dex.

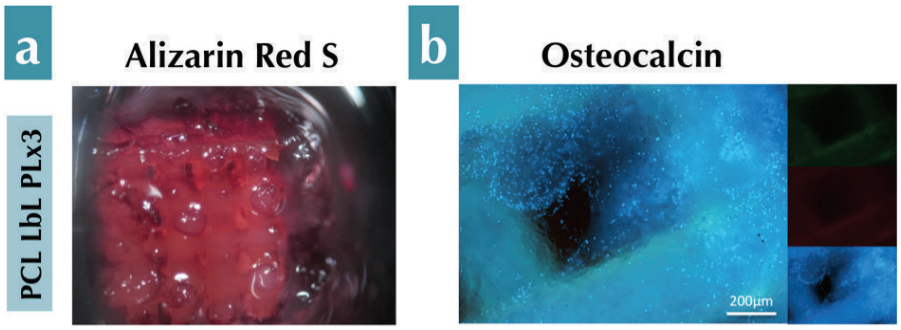

Figure VII.S4. a) PCL LbL PLx3 stained with ARS after 32 days in culture in absence of Dex. b) Osteocalcin immunodetection (green), nuclei (blue), calcium (red). Osteocalcin and ARS just show background signal.

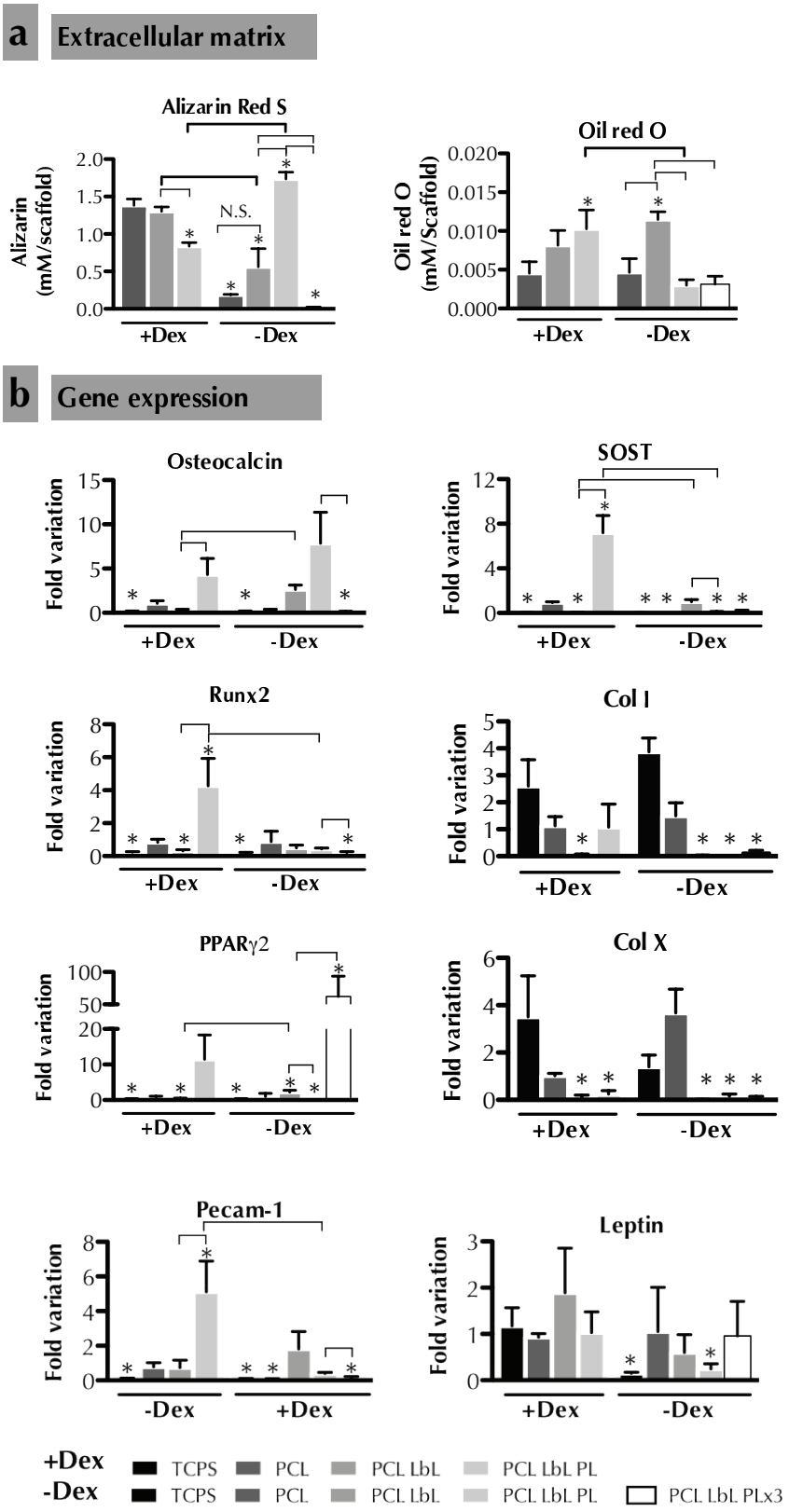

Figure VII.S5. Extracellular calcium, fat and gene expression quantification after 32 days in presence (+Dex) or absence of Dex (-Dex). a) ARS and ORO quantification; b) Osteocalcin, SOST, Runx2, PPARγ2, Col I, Col X, Pexam-1 and Leptin gene expression relatively to PCL+Dex. The expression of these genes was normalized against the housekeeping β-actin gene and calculated by the Livak method ($2^{-\Delta\Delta_{Ct}}$). Results are expressed as average ± standard error with $4 \leq n \leq 8$ for each bar ($p<0.05$). All the significances are identified: bars (the samples are different), * (samples are different comparing to PCL+Dex).

VII.4. Material and Methods

VII.4.1. Materials

PCL (M_w from 70 000 to 90 000), chitosan (Chi, medium Mw, with a degree of deacetylation of 80% - ref. MKBB0566), ethylenediamine were purchased from Sigma-Aldrich. Chi was purified by a re-precipitation method. Briefly, Chi powder was first dissolved in 2% (v/v) acetic acid solution at a 1% (w/v) concentration. The mixture was maintained under stirring overnight at room temperature. The impurities were removed by four filtration cycles. Then, Chi was precipitated by addition of 1 M NaOH while stirring. Final steps consisted of washing Chi with distilled water until reaching a neutral pH and of dehydration by washing with ethanol–water mixtures with increasing ethanol content (20–100% v/v). Chi was freeze- dried for 3 days and ground. ι-Carrageenan (Fluka, 22045) was used as received.

VII.4.2. Methods

VII.4.2.1.Scaffolds Preparation

VII.4.2.2. Human Platelet Lysate Preparation

Platelet rich plasma was obtained from different platelet collections performed at Instituto Português do Sangue (IPS, Porto, Portugal), under a previously established cooperation protocol. The components were obtained using the Trima Accel® Automated Blood Collection System. All the platelet products were biologically qualified according to the Portuguese legislation. The platelet count was performed at the IPS using the COULTER® LH 750 Hematology Analyzer, and the sample's volume was adjusted to 1 million platelets per μL. The collected samples were subject to three repeated temperature cycles (frozen with liquid nitrogen at -196°C and heated at 37°C) and frozen at -20°C until further use. The platelets remaining were eliminated by centrifugation at 1400 × g for 10 min and final human Platelet lysate (PL) aliquots were kept -20°C until final use.

VII.4.2.3. Polyelectrolytes solutions preparations

ι-carrageenan (ιCar) and Chi solutions were prepared in the buffer 1M sodium acetate 40 mM NaCl pH 5.5 with a concentration of 0.5 mg/ml or 4 mg/ml. PL was 10-fold diluted in the same buffer solution.

VII.4.2.4. Polyelectrolytes assembling onto Quartz Crystal microbalance with Dissipation

A Q-Sense E4 quartz crystal microbalance with dissipation (QCM-D, Q-Sense AB, Sweden) was used for the in situ monitoring the polyelectrolytes ιCar, Chi and PL deposition onto the surface of 100 nm gold-coated crystals. Briefly, AT cut quartz crystal can be excited at its fundamental frequency (5 MHz) and at several [illegible] with overtones, respectively). When a thin film is deposited onto the sensor crystal the frequency decreases. If the film is thin and rigid the decrease in frequency (Δf) is

[illegible]

not v[illegible]

the change in the dissipation (Δ*D*[illegible] successively in acetone, ethanol, isopropanol and dried. Adsorption took place at 25°C and at a constant flow rate of 50 ul/min.

First the Chi solution was pumped for 10 minutes, and the weakly bound polyelectrolyte removed by pumping buffer solution for 10 minutes. Using the same frame times, the assembling of (Chi- ιCar)- ιCar-PL-ιCar-Chi was monitored. All solutions were prepared in 1M sodium acetate 40 mM NaCl pH 5.5.

VII.4.2.5. Bare PCL Scaffolds

PCL granules were inserted in the Bioplotter™ cartridge and heated up to 90 °C. Material was extruded by a 22G hypodermic needle with a strand size of 0.5 mm and layer thickness of 0.3-0.4 mm with struts aligned by 90° in 10 consecutive layers.

VII.4.2.6. 3D scaffolds modification by Layer-by-Layer with PL

The LbL was performed in PCL scaffold first modified with ethylediamene (10% in 2-propanol, 1 hour at 37°C) to improve the binding of the first multilayers. All the polyelectrolytes solutions were prepared in 1M sodium acetate with 40 mM NaCl and pH 5.5 with the following concentrations: 10 fold-diluted PL, 4 mg/mL Chi and 4 mg/mL ιCar. A custom-made dipping robot was used to perform the LbL assembling. First a set of two layers of ιCar-Chi were assembled in the PCL scaffold with the sequence: immersion for 5 minutes in ιCar solutions, followed by several washing steps, 5 minutes in Chi solutions and several washing step. The basic sequence used for the structuring LbL was: ιCar (4 min), washx1 (5 min), ιCar (4 min), washx1 (5 min), PL (10 min), washx1 (5 min), Chi (4 min), washx1 (5 min). Different samples were prepared: PL LbL $(\iota Car\text{-}Chi\text{-}\iota Car\text{-}Chi)_{10}$, PCL LbL PL $(\iota Car\text{-}PL\text{-}\iota Car\text{-}Chi)_{10}$, PCL LbL PLx3 $(\iota Car\text{-}PL\text{-}\iota Car\text{-}Chi)_{30}$. To proceed with the fibrillar structures formation, the scaffolds were washed in distilled water, frozen at-80ºC to let ice crystals to growth and freeze-dried for 1-2 days.

VII.4.2.7. hASCs isolation from lipoaspirate

Human subcutaneous adipose tissue samples were obtained from lipoaspiration procedures performed on women with ages between 35 and 50 years under a protocol previously established with the Department of Plastic Surgery of Hospital da Prelada in Porto, Portugal. All the samples were processed within 24 h after the lipoaspiration procedure. Human ASCs were enzymatically isolated from subcutaneous adipose tissue. The lipoaspirate samples were firstly washed with a solution of PBS and 10% Antibiotic/Antimycotic. Liposuction tissue was digested with 0.2% Collagenase Type II solution for 90 min with intermittent shaking, at 37 °C. The digested tissue was filtered using a 100 μm filter mesh (Sigma-Aldrich, Germany). The floating adipocytes were

separated from the precipitation stromal fraction by centrifugation at 1250 rpm for 10 min. The cell pellet was re-suspended in lysis buffer for 10 min to disrupt the erythrocytes. After a centrifugation at 800 rpm for 10 min, cells were again re-suspended and placed in culture flasks with Minimum Essential alpha Medium supplemented with sodium bicarbonate, antibiotic/antimycotic and 10% of FBS. Cells were cultured until confluence at 37°C, 5% CO_2 incubator, changing the medium every 2 days.

VII.4.2.8. hASCs seeding

To proceed with the cell seeding, cells were harvested by trypsinization and filtered with a cell strainer with 100 µm of pore size to remove possible cell aggregates. A cellular suspension with the density of 0.120×10^6 cells/5µL was prepared in Minimum Essential alpha Medium supplemented containing 10% FBS (α-mem). A volume of 5µl of cell suspension was dripped onto each scaffold. Scaffolds were incubated for 2.5 hours in standard conditions (37°C, 5%CO_2) to permit cell attachment and then 2 mL of α-mem was added to each well. After 4 days of incubation, media was changed for osteogenic α-mem (50 mg/mL AA; 10^{-8} M dexamethasone, Dex; 10 mM βGly) or osteoconductive α-mem (50 mg/mL AA, 10 mM βGly). hASCs were obtained from two different donors and used in the second passage. Experiments were performed three times.

VII.4.2.9. SEM-EDS analysis

The constructs were harvested after 4+28 days of culture, rinsed with PBS, fixed with 2.5% glutaraldehyde and dehydrated through a graded series of ethanol (50, 70, 90, 100% v/v; each one for 10 minutes and twice) and dried at room temperature. Morphological analysis of the prepared constructs before and after cell culture was realized in an Ultra-high resolution Field Emission Gun Scanning Electron Microscopy (FEG-SEM; NOVA 200 Nano SEM, FEI Company). Secondary electron images were performed with an acceleration voltage of 5kV. Chemical analyses of samples were performed by Energy Dispersive Spectroscopy (EDS), using an EDAX Si(Li) detector with an acceleration voltage of 15 kV.

VII.4.2.10. X-Ray Microtomography

The new mineral formed in the scaffolds was analyzed by micro-computed tomography (µ-CT) using a desktop µ-CT scanner (1072; SkyScan, Kontich, Belgium) at a voltage of 40 kV and a current of 248 mA, with acquisitions carried out in high-resolution mode of 11µm x/y/z. Isotropic slice data were obtained by the system and reconstructed into 2D XY slice images. Around 600 slice images per sample were compiled and subsequently employed in the rendering of 3D XYZ images to obtain quantitative architectural parameters. A µ-CT analyzer and a µ-CT volume realistic 3D Visualization software (SkyScan) was used as an image processing tool for reconstruction and creation of 3D representation models for the observation of the distribution of the deposited apatite.

VII.4.2.11. Alizarin Red S Staining

ARS, an anthraquinone derivative, can be used to identify calcium in tissue sections. Although the reaction is not strictly specific for calcium, but also occurring with magnesium, manganese, barium, strontium, and iron, these elements usually do not occur in sufficient concentration to interfere with the staining. Calcium forms an ARS-calcium complex in a chelation process. After 4+28 days in culture, scaffolds were rinsed thrice with sterile PBS and cells fixed with 2.5% formalin during 30 minutes. The samples were then rinsed again with distilled water in order to remove any residual ions and 0.5 ml of ARSsolution (2g/100 ml, pH 4.1-4.3 adjusted with ammonium hydroxide) was added to each sample and let to react for around 5 minutes. The excess of dye was removed with distilled water, and samples were observed under stereomicroscopy. The content of calcium will be proportional to the red intensiveness. In order to elute the ARS adsorbed to the scaffolds, 400 μL of 10% (v/v) of acetic acid was added to each sample and incubated at room temperature for 30 min with shaking. Samples were vortexed for 30 seconds. After complete elution, the surfaces were discarded, and the liquid samples heated to 85°C for 10 min. The slurry was then centrifuged at 12,000g for 30 min and 400 μL of the supernatant was removed to a new microcentrifuge tube. Then 150 μL of 10% (v/v) ammonium hydroxide was added to neutralize the acid. The absorbance of triplicates of the samples was read at 405 nm in a microplate reader (Bio-Tek, Synergie HT). A calibration curve made of successive dilutions of an ARS solution with known concentration was used in order to read off the alizarin content of the samples. Experiment was performed for the two hASCs donors with n=6.

VII.4.2.12. Immunolocalization of human Osteocalcin

After 32 days in culture, samples from all the condition were rinsed twice with sterile PBS and fixed with 2.5% formalin for 30 min at room temperature (RT). First the scaffolds were stained with Alizarin Red for detection of Calcium, as described before.

After cells permeabilization with Triton X-100/PBS 0.2% (v/v) for 15 min at RT, proteins were blocked with 3% (w/v) Bovine Serum Albumin (BSA)/PBS for 45 minutes. Samples were incubated overnight at 4°C with the primary antibody anti-osteocalcin (mouse monoclonal anti-Osteocalcin, ab13418, Abcam) diluted 1:50 in 1% BSA/PBS. Afterwards, samples were rinsed with 0.025% Triton X-100/PBS, PBS, followed by 2 hours of incubation with the secondary antibody anti-mouse Alexa Fluor 488 (Invitrogen) with a dilution of 1:100. After the incubation period, samples were rinsed in PBS and stained with 4,6-Diamidino-2-phenyindole dilactate (DAPI, 1:1000, D9564, Sigma-Aldrich). Scaffolds were observed under a microscope (Imager Z1m, Zeiss) and images acquired using a digital camera (AxioCam MRm5).

VII.4.2.13. Oil red O Staining

ORO staining is a lysochrome used for neutral triglycerides and lipids staining with the appearance of a red coloration. A stock solution was prepared by dissolving 300 mg of ORO (Sigma, Aldrich) in 100 mL of 99% isopropanol. The work solution, which is stable for no longer than 2 hours, was prepared by mixing 3 parts (30

mL) of the stock solution with 2 parts (20 ml) of distilled water and allowed to sit at RT for 10 min. After the solution is filtered with a filter paper, 1 mL (5 minutes) of it was added to each construct that had been fixed with 2.5% formalin (30 min), rinsed with distilled water, and with 60% isopropanol (2-5 minutes). Samples were rinsed with distilled water and then 0.5 mL of 100% isopropanol was added to each scaffold (10 minutes) with shaking in order to elute the staining.

The absorbance of triplicates of the samples was read at 500 nm in a microplate reader (Bio-Tek, Synergie HT). A calibration curve made of successive dilutions of the stock solution with known concentration was used in order to read off the alizarin content of the samples.

VII.4.2.14. RT-PCR

The quantification of gene expression of the hASCs which were cultured onto the scaffolds for 4+28 days, it was performed quantitative PCR by a two-step fluorogenic assay using the PerfeCta™ SYBR® Green System (Quanta Biosciences) – see the target genes in Table VII.S1.

The total RNA was extracted using the TRI® Reagent (Sigma-Aldrich), following the manufacture's instruction. Total RNA was quantified using Nanodrop® ND-100 spectrophotometer (thermo Scientific) and first-strand complementary DNA (cDNA) was synthetized using 1 μg RNA of each sample and the qScript™ cDNA Synthesis Kit (Quanta Biosciences) for a 20μL reaction. The obtained cDNA was used as a template for the amplification of the target genes using a MasterCycler EP Gradient detection System (Eppendorf) termocycler and the PerfeCta™ SYBR® Green System kit following the manufactures' instructions. The Livak method, $2^{-\Delta\Delta Ct}$, was used to evaluate the relative expression of each target gene. ΔCt was calculated by the difference between the Ct values of the target gene and the β-actin endogenous housekeeping gene. ΔΔCt was obtained by subtracting the ΔCt of the calibrator sample (PCL+Dex) to the ΔCt of the sample. The results are represented as $2^{-\Delta\Delta Ct}$ and as gene expression relative to PCL+Dex, which value equals to 1.

Table VII.S1. Description of the target genes used in qPCR: name; lineage-related to the target gene; main functions; Forward and Reverse primers; melting temperature used.

Gene	Lineage	Function	Forward (5'-3')	Tm (°C)
Beta-actin	Housekeeping gene	Controls cell growth, migration, and the G-actin pool	ACTGGAACGGTGAAGGTGAC AGAGAAGTGGGGTGGCTTTT	59.5
Osteocalcin	Osteo -late	It is secreted solely by osteoblasts, it can be found in bone and dentin; participates in bone mineralization and calcium ion homeostasis.	GTGCAGAGTCCAGCAAAGG TCAGCCACTCGTCACAGC	59.4
Runx2	Osteo - early	Runt-related transcription factor 2 is a key transcription factor associated with osteoblast differentiation	TTCCAGACCAGCAGCACTC CAGCGTCAACACCATCATTC	58.1
PPARy2	Adipose - late	Peroxisome proliferator-activated receptor is expressed mainly in adipose tissue, in mature osteocytes	TGGGTGAAACTCTGGGAGAT GCGATCTCTGTGTCAACCAT	57.3
Leptin	Adipose - late	It is one of the most important adipose-derived hormones that play a key role in regulating energy intake and expenditure, including appetite and hunger, metabolism, and behavior.	CTCAGGGATCTTGCATTCCC CCATGCATTTGGCTGTTCAG	57.8
PECAM1/	Vascular	Cluster of differentiation 31 is a large portion of the	AAGGCCAGATGCACATCC	57.9

CD31		endothelial cell intercellular junctions	TTCTACCCAACATTAACTTAGCAGG	
SOST	Osteo - late	Produced by mature osteocytes codes Sclerostin proteins that inhibit further mineralization	GTGCCAAGGTCACTTCCAGA CCAGGAGTTTGTCAGCCGTA	57.2
Col I	Osteo	Collagen I is a protein that strengthens and supports several tissue including bone	AAGAACCCCAAGGACAAGAG GTAGGTGATGTTCTGGGAGG	58.4
Col X	Cartilage/ Osteo -middle	Found in hypertrophic chondrocytes undergoing mineralization/osteoblastic differentiation	CAGGCATAAAAGGCCCACTA AGGACTTCCGTAGCCTGGTT	58.4
Adiponectin	Adipose - late	Adiponectin is exclusively secreted by adipose tissue or placenta and it is a hormone that modulates a number of metabolic processes, including glucose regulation and fatty acid oxidation	TGATCTCGGCTTACTGCAAC ACAAGGTCAGGAGTTCGAGA	57.3

VII.4.3. Statistical Analysis

ARS, ORO, and relative gene expression data was statistically analyzed by using a non-parametric test. Non-parametric tests were used once it was verified with Shapiro–Wilk test that the data do not fit the Gaussian distribution profile. The unpaired one-tailed t-test with Welch's correction for non-parametric data was used and considering $p \leq 0.05$ ($4 \leq n \leq 8$). The comparisons tested were: all samples against the control, PCL + Dex; the saffolds +Dex against –Dex; PCL LbL against PCL LbL PL (+Dex; -Dex); PCL LbL –Dex againist PCL LbL PLx3 -Dex; PCL LbL PL - Dex against PCL LbL PLx3 LbL.

VII.5. References

1. S. J. Hollister, Scaffold design and manufacturing: from concept to clinic, Adv Mater, 2009, 21, 3330-3342.
2. W. L. Murphy, M. C. Peters, D. H. Kohn and D. J. Mooney, Sustained release of vascular endothelial growth factor from mineralized poly(lactide-co-glycolide) scaffolds for tissue engineering, Biomaterials, 2000, 21, 2521-2527.
3. V. E. Santo, A. R. C. Duarte, E. G. Popa, M. E. Gomes, J. F. Mano and R. L. Reis, Enhancement of osteogenic differentiation of human adipose derived stem cells by the controlled release of platelet lysates from hybrid scaffolds produced by supercritical fluid foaming, Journal of Controlled Release, 2012, 162, 19-27.
4. E. Anitua, M. Sanchez and G. Orive, Potential of endogenous regenerative technology for in situ regenerative medicine, Adv Drug Deliv Rev, 2010, 62, 741-752.
5. R. E. Marx, E. R. Carlson, R. M. Eichstaedt, S. R. Schimmele, J. E. Strauss and K. R. Georgeff, Platelet-rich plasma: Growth factor enhancement for bone grafts, Oral Surg Oral Med Oral Pathol Oral Radiol Endod, 1998, 85, 638-646.
6. G. Weibrich, W. K. Kleis, G. Hafner and W. E. Hitzler, Growth factor levels in platelet-rich plasma and correlations with donor age, sex, and platelet count, J Craniomaxillofac Surg, 2002, 30, 97-102.
7. L. Chen, X. Yang, G. Huang, D. Song, X. S. Ye, H. Xu and W. Li, Platelet-rich plasma promotes healing of osteoporotic fractures, Orthopedics, 2013, 36, e687-694.
8. M. Kawasumi, H. Kitoh, K. A. Siwicka and N. Ishiguro, The effect of the platelet concentration in platelet-rich plasma gel on the regeneration of bone, J Bone Joint Surg Br, 2008, 90, 966-972.
9. Y. Man, P. Wang, Y. Guo, L. Xiang, Y. Yang, Y. Qu, P. Gong and L. Deng, Angiogenic and osteogenic potential of platelet-rich plasma and adipose-derived stem cell laden alginate microspheres, Biomaterials, 2012, 33, 8802-8811.
10. A. Roffi, G. Filardo, E. Kon and M. Marcacci, Does PRP enhance bone integration with grafts, graft substitutes, or implants? A systematic review, BMC Musculoskelet Disord, 2013, 14, 330.
11. M. R. Sarkar, P. Augat, S. J. Shefelbine, S. Schorlemmer, M. Huber-Lang, L. Claes, L. Kinzl and A. Ignatius, Bone formation in a long bone defect model using a platelet-rich plasma-loaded collagen scaffold, Biomaterials, 2006, 27, 1817-1823.
12. A. S. Plachokova, J. van den Dolder, P. J. Stoelinga and J. A. Jansen, Early effect of platelet-rich plasma on bone healing in combination with an osteoconductive material in rat cranial defects, Clin Oral Implants Res, 2007, 18, 244-251.
13. J. L. Wallace, M. Dicay, W. McKnight and G. K. Dudar, Platelets accelerate gastric ulcer healing through presentation of vascular endothelial growth factor, Br J Pharmacol, 2006, 148, 274-278.
14. E. Saiz, E. A. Zimmermann, J. S. Lee, U. G. Wegst and A. P. Tomsia, Perspectives on the role of nanotechnology in bone tissue engineering, Dent Mater, 2013, 29, 103-115.
15. N. J. Shah, J. Hong, M. N. Hyder and P. T. Hammond, Osteophilic multilayer coatings for accelerated bone tissue growth, Adv Mater, 2012, 24, 1445-1450.
16. N. J. Shah, M. L. Macdonald, Y. M. Beben, R. F. Padera, R. E. Samuel and P. T. Hammond, Tunable dual growth factor delivery from polyelectrolyte multilayer films, Biomaterials, 2011, 32, 6183-6193.
17. T. Crouzier, K. Ren, C. Nicolas, C. Roy and C. Picart, Layer-By-Layer Films as a Biomimetic Reservoir for rhBMP-2 Delivery: Controlled Differentiation of Myoblasts to Osteoblasts, Small, 2009, 5, 598-608.
18. F. Gilde, O. Maniti, R. Guillot, J. F. Mano, D. Logeart-Avramoglou, F. Sailhan and C. Picart, Secondary structure of rhBMP-2 in a protective biopolymeric carrier material, Biomacromolecules, 2012, 13, 3620-3626.
19. I. Vlodavsky, H. Q. Miao, B. Medalion, P. Danagher and D. Ron, Involvement of heparan sulfate and related molecules in sequestration and growth promoting activity of fibroblast growth factor, Cancer Metastasis Rev, 1996, 15, 177-186.
20. D. B. Volkin, P. K. Tsai, J. M. Dabora, J. O. Gress, C. J. Burke, R. J. Linhardt and C. R. Middaugh, Physical stabilization of acidic fibroblast growth factor by polyanions, Arch Biochem Biophys, 1993, 300, 30-41.
21. J. Folkman and Y. Shing, in Heparin and related polysaccharides, Springer, 1992, pp. 355-364.
22. J. R. Bishop, M. Schuksz and J. D. Esko, Heparan sulphate proteoglycans fine-tune mammalian physiology, Nature, 2007, 446, 1030-1037.
23. R. R. Costa and J. F. Mano, Polyelectrolyte multilayered assemblies in biomedical technologies, Chemical Society reviews, 2014, 43, 3453-3479.
24. Y. Yan, M. Björnmalm and F. Caruso, Assembly of layer-by-layer particles and their interactions with biological systems, Chemistry of Materials, 2013, 26, 452-460.
25. V. Gribova, R. Auzely-Velty and C. Picart, Polyelectrolyte multilayer assemblies on materials surfaces: from cell adhesion to tissue engineering, Chemistry of Materials, 2011, 24, 854-869.

26. J. Borges and J. F. Mano, Molecular Interactions Driving the Layer-by-Layer Assembly of Multilayers, Chemical Reviews, 2014.
27. S. M. Oliveira, T. H. Silva, R. L. Reis and J. F. Mano, Hierarchical fibrillar scaffolds obtained by non-conventional layer-by-layer electrostatic self-assembly, Adv Healthc Mater, 2013, 2, 422-427.
28. K.-H. Schuckert, S. Jopp and M. Osadnik, The Use of Platelet Rich Plasma, Bone Morphogenetic Protein-2 and Different Scaffolds in Oral and Maxillofacial Surgery-Literature Review in Comparison with Own Clinical Experience, Journal of oral & maxillofacial research, 2011, 2.
29. N. Chevallier, F. Anagnostou, S. Zilber, G. Bodivit, S. Maurin, A. Barrault, P. Bierling, P. Hernigou, P. Layrolle and H. Rouard, Osteoblastic differentiation of human mesenchymal stem cells with platelet lysate, Biomaterials, 2010, 31, 270-278.
30. J. Leotot, L. Coquelin, G. Bodivit, P. Bierling, P. Hernigou, H. Rouard and N. Chevallier, Platelet lysate coating on scaffolds directly and indirectly enhances cell migration, improving bone and blood vessel formation, Acta Biomater, 2013, 9, 6630-6640.
31. S. M. Oliveira, T. H. Silva, R. L. Reis and J. F. Mano, Nanocoatings containing sulfated polysaccharides prepared by layer-by-layer assembly as models to study cell–material interactions, Journal of Materials Chemistry B, 2013, 1, 4406-4418.
32. P. Sher, C. A. Custódio and J. Mano, Layer-By-Layer Technique for Producing Porous Nanostructured 3D Constructs Using Moldable Freeform Assembly of Spherical Templates, Small, 2010, 6, 2644-2648.
33. J. M. Silva, N. Georgi, R. Costa, P. Sher, R. L. Reis, C. A. Van Blitterswijk, M. Karperien and J. F. Mano, Nanostructured 3D constructs based on chitosan and chondroitin sulphate multilayers for cartilage tissue engineering, PloS one, 2013, 8, e55451.
34. P. Ducy, R. Zhang, V. Geoffroy, A. L. Ridall and G. Karsenty, Osf2/Cbfa1: a transcriptional activator of osteoblast differentiation, Cell, 1997, 89, 747-754.
35. K. E. Poole, R. L. van Bezooijen, N. Loveridge, H. Hamersma, S. E. Papapoulos, C. W. Lowik and J. Reeve, Sclerostin is a delayed secreted product of osteocytes that inhibits bone formation, FASEB J, 2005, 19, 1842-1844.
36. O. Leupin, I. Kramer, N. M. Collette, G. G. Loots, F. Natt, M. Kneissel and H. Keller, Control of the SOST bone enhancer by PTH using MEF2 transcription factors, J Bone Miner Res, 2007, 22, 1957-1967.
37. N. Z. Mostafa, R. Fitzsimmons, P. W. Major, A. Adesida, N. Jomha, H. Jiang and H. Uludag, Osteogenic differentiation of human mesenchymal stem cells cultured with dexamethasone, vitamin D3, basic fibroblast growth factor, and bone morphogenetic protein-2, Connect Tissue Res, 2012, 53, 117-131.
38. Y. Mikami, M. Lee, S. Irie and M. J. Honda, Dexamethasone modulates osteogenesis and adipogenesis with regulation of osterix expression in rat calvaria-derived cells, J Cell Physiol, 2011, 226, 739-748.
39. T. Rada, R. L. Reis and M. E. Gomes, Distinct stem cells subpopulations isolated from human adipose tissue exhibit different chondrogenic and osteogenic differentiation potential, Stem Cell Rev, 2011, 7, 64-76.
40. M. J. Jeon, J. A. Kim, S. H. Kwon, S. W. Kim, K. S. Park, S. W. Park, S. Y. Kim and C. S. Shin, Activation of peroxisome proliferator-activated receptor-gamma inhibits the Runx2-mediated transcription of osteocalcin in osteoblasts, J Biol Chem, 2003, 278, 23270-23277.
41. S. M. Jackson and L. L. Demer, Peroxisome proliferator-activated receptor activators modulate the osteoblastic maturation of MC3T3-E1 preosteoblasts, FEBS Lett, 2000, 471, 119-124.

SECTION 7

GENERAL CONCLUSIONS

CHAPTER VIII

CONCLUSIONS AND FUTURE PERSPECTIVES

CHAPTER VIII

Conclusions and Future Perspectives

The success of a 3D construct relies on the properties defined by its multiscale features: geometry, cell-anchorage, cells, release system, topographical and biochemical cues. The control of such a range of features calls on approaches combining both bottom-up and top-down methods, known as integrative.
In this thesis, an integrative and triple sequential technique was explored to develop 3D constructs for bone tissue engineering: rapid prototyping followed by layer-by-layer and finalized with freeze-drying. This approach may allow control over most of the features required in a 3D construct, namely, geometry, cell-anchorage, cells, release system and biochemical cues.

Modifying the prototyped polycaprolactone (PCL) scaffolds using layer-by-layer and freeze-drying creates new structures (coatings and fibrils) which may have three functions: i) new anchorage points for cells; ii) a strategy for control over surface chemistry; and iii) a way to present instructive cues or include release systems.
The approach was first explored using a pair of polyelectrolytes well known in layer-by-layer assembling: alginate and chitosan. It was observed that assembling parameters such as washing time, number of layers and concentration of the polyelectrolyte affects the density and the distribution of the structures created inside the pores, while not compromising the scaffold micro-porosity nor the mechanical properties.

In order to select a pair of polyelectrolytes with to enhance cell interactions and more suitable for the stabilization an incorporation of platelet lysate (PL), several combinations of sulfated carrageenans and chitosan nanocoatings were studied. The salt concentration and pH for the assembling of the multilayers comprising carrageenan (Car; κ, ι and λ) and chitosan (chi) were optimized. Then, the behavior of an osteoblast-like cell line was studied on these multilayers. Coating PCL membranes with ιCar/Chi allowed a significant increase of calcium phosphate, which highlighted the importance of the surface chemistry in regards to biomeralization.

PL contains several proteins involved in angiogenesis and osteogenesis, and participating throughout the early and maturation phases, which had turned it into a highly investigated autologous source of instructive cues for bone tissue engineering. The type of polyelectrolytes (alginate, chitosan, κCar, ιCar, λCar and heparin) was shown to influence the adsorption of PL, vascular endothelial growth factor (VEGF), basic fibroblast growth factor (FGFb) and platelet derived growth factor (PDGF). ιCar highly adsorbed FGFb, VEGF and PDGF. The low

sulfated polysaccharides could adsorb high PDGF and intermediate VEGF, while Hep showed only high VEGF adsorption. Consequently, by increasing the SD, the VEGF/PDGF and FGF/PDGF adsorption ratios tended to increase. Characterization was limited to the above mentioned growth factors, however, the quantification of other growth factors or cytokines/chemokine should be considered in future work. These differences were thought to possibly translate different cell instructions and motivated the study of the behavior of two different cells relevant for bone tissue engineering: human adipose derived stem cells (hASCs) and human umbilical vein endothelial cells (HUVECs).

In general, the sulfated PL-multilayers promoted morphological changes (reduced cell width and increased length), serum-free cell adhesion and cell proliferation of high passage hASCs (P>5). The observed hASCs behavior suggested that those multilayers might reduce cell senescence associated with: enlargement of morphology (width); increase of alkaline phosphatase activity; and decrease on cell proliferation, during cell culture in basal medium. This interesting observation should be investigated in future work.

Regarding the endothelial cells, the sulfated-PL (ιCar/PL, λCar/PL and hep/PL) nanocoatings activated HUVECs, inducing the formation of tube-like structures and enhancing the expression of pro-angiogenic genes (angiopoietin-1 and VEGF-A) within 20 hours of incubation. Thereby, layer-by-Layer assembling of PL might be a simple methodology to introduce and tune cost-effective pro-angiogenic interfaces in 2D/3D biomaterials. Moreover, the behavior of HUVECs on 3D scaffolds modified with these multilayers should be considered in future studies as a strategy to develop neo-vascularized scaffolds.

Incorporating 10 tetralayers of ιCar/PL/ιCar/Chi, as coatings and fibrillar structures, onto 3D PCL scaffolds has induced hASCs into mature osteoblasts in absence of dexamethasone (common osteogenic inductor). Contrarily, in the absence of PL or with 30 tetralayers with PL, such induction was not observed. This highlighted the importance of a controlled incorporation and stabilization of PL in order to successfully promote the osteogenic differentiation of hASCs. Those behavior variations associated to the number of tetralayers will be further investigated. One plausible reason for such differences could be that, with 30 tetralayers, a high content of mitogenic growth factors, such as bFGF and PDGF, may have induced a high mitogenic stimulation that impeded the osteogenic differentiation. Additionally, in future work, the osteoinductive (*in vivo*) and the angiogenic potential of the developed multiscale scaffolds shall be evaluated in order to pursue a bone tissue engineering application.

The results obtained in this thesis show that layer-by-layer assembling is a suitable method to tune the incorporation of PL onto 2D/3D constructs which can instruct several cell types. The proposed approach promises new autologous osteogenic and multiscale 3D construct, and, possibly, coatings for several tissue engineering applications (e.g., cell expansion and angiogenesis).